PROCEEDINGS OF THE EXPLOSIVES CHEMICAL REACTIONS SEMINAR, HELD AT THE ARMY RESEARCH OFFICE, DURHAM, NORTH CAROLINA, 21-23 OCTOBER 1968

Army Research Office
Durham, North Carolina

1968

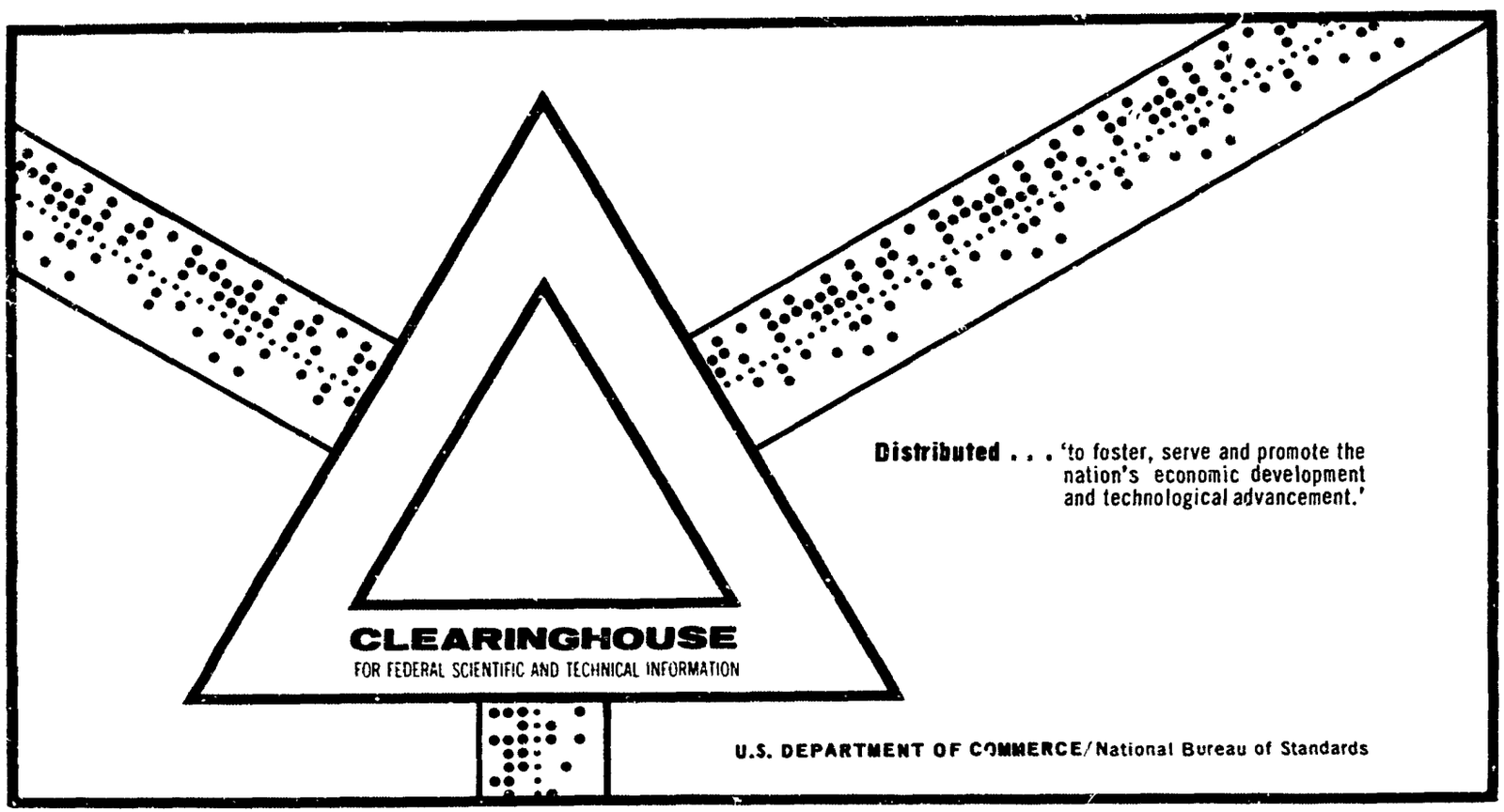

ARO-D Report 70-4

EXPLOSIVE CHEMICAL REACTIONS SEMINAR

BRL

ARO-D

U. S. ARMY BALLISTIC RESEARCH LABORATORIES
and
U. S. ARMY RESEARCH OFFICE - DURHAM

263

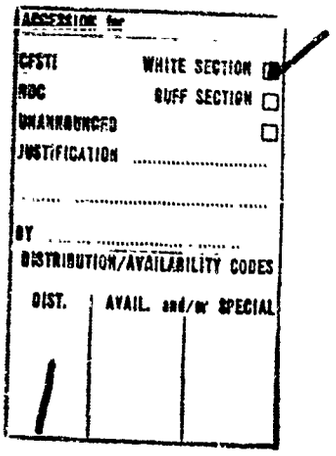
ACCESSION for
CFSTI WHITE SECTION
DDC BUFF SECTION
UNANNOUNCED
JUSTIFICATION
BY
DISTRIBUTION/AVAILABILITY CODES
DIST. AVAIL. and/or SPECIAL

PROCEEDINGS OF THE

EXPLOSIVES CHEMICAL REACTIONS SEMINAR

Sponsored by Panel O-2 (Explosives)

THE TECHNICAL COOPERATION PROGRAM

through

THE BALLISTIC RESEARCH LABORATORIES

and held at

THE ARMY RESEARCH OFFICE - DURHAM
Box CM, Duke Station
Durham, North Carolina

21-23 October 1968

BLANK PAGE

FOREWORD

Dr. R. J. Eichelberger
U.S. Army Ballistic Research Laboratories
Aberdeen Proving Ground, Maryland

The Problems And The Goals For The Seminar On Explosive Reactions

The purpose of this seminar is to explore the feasibility of a more fundamental approach to the reaction rate portion of detonation phenomena. The problems peculiar to military explosives research stem from the fact that military explosives are pure organic compounds, mixtures of organic compounds, or mixtures containing organic molecules plus inorganic oxidizers, or reactive metals, or both. These materials are usually in solid form, cast or pressed to the maximum possible density. During manufacture, storage, and use, they are subjected to a variety of energy stimuli ranging in intensity from levels too low to cause any significant changes, to those sufficient to create initial pressure of several megabars.

Using the principles of hydrodynamics and thermodynamics and some concepts from solid state physics, investigators have made considerable progress in the continuum treatment of initiation and propagation of detonation. This aspect of the problem can be considered at a level of sophistication permitting treatment of interacting, non-steady detonation waves that coalesce into a superficially steady wave. Energy distribution by transport effects can be treated by continuum methods, and the influence of boundary conditions can be taken into account.

The great difficulty lies in providing input data to the continuum models that accurately represent the absorption and distribution of energy received from an external source or evolved by chemical reaction, and the consequent molecular rearrangement and decomposition. No experimental techniques are available or are foreseen that would provide

direct measurement of the needed quantities. New approaches are clearly called for. It appears likely that the new approaches might be found in the areas of lattice dynamics and molecular physics, using the mathematical techniques of statistical mechanics. The manner in which these fields may be joined in the solution of the explosive decomposition problem is suggested in the following hypothetical model of the phenomena.

> For this purpose, we envision a molecular solid, consisting of metastable organic molecules in a crystal lattice, being subjected to an energy stimulus. The stimulus will ordinarily be in the form of mechanical energy, thermal energy, or radiation in the spectral region ranging from infrared to X-ray. Given the nature of the energy source, it would be necessary, first, to accurately predict how the energy is absorbed by the crystal lattice and the molecules. It then becomes necessary to determine with reasonable accuracy how the energy is transported and partitioned between the lattice and the molecules. If decomposition is to occur, the energy imparted to a molecule must be sufficient to break bonds and start a rearrangement forming new molecular species. Some of these reaction processes will liberate energy and lead to other changes in the state of the medium. At some stage, or at some energy density, it will become critical to determine whether the rate of energy evolution due to molecular excitation and decomposition will exceed the rate at which energy can be transported away from a given volume element.
>
> In order to predict the effects of energy partitioning upon the chemical phenomena, it is necessary, first, to know accurately the bond strengths in the molecule.
>
> The changes in bond energies as a result of incorporation of the molecule in a crystal lattice must also be known. The distribution of energy among the bonds as a result of direct stimulation, or interaction with the lattice, and the probability of breakage of each bond, as functions of energy level and time, are the prime objectives of the model. At low energy levels, equilibrium energy distribution, and simple reaction kinetic laws may be satisfactory approximations. At high energy densities, the distribution of energy among the bonds of a molecule may never approach that associated with equilibrium conditions; consequently, the course of decomposition, the chemical species, and the density of species may be quite different at high energies than at lower values. In the extreme case of "steady" detonation, with interacting shock waves providing the energy source to sustain the reaction, temperatures approaching 10,000°K and pressures of several

hundred kilobars are produced. It may be completely erroneous to use the Arrhenius relation, with constants determined under equilibrium conditions, in an analysis of these phenomena.

In the case of mixtures, the diffusion of intermediate products, mixing and subsequent "hybrid" reactions represent additional complicating factors governing the overall "reaction rate."

The pertinent long-term objectives of explosives research can be described as twofold:

- Capability of predicting the chemical behavior of known organic molecular solids with sufficient accuracy to determine the intrinsic sensitivity to initiation, and the magnitude and rate of energy evolution, under arbitrary environmental conditions.
- Capability of predicting the crystal habit and essential physical characteristics of new organic compounds and, as in (a), determining their potential usefulness as explosive materials.

To achieve these objectives, according to the postulated model, we need much more sophisticated treatments of energy absorption, transport and partitioning in molecular crystals, and of nonequilibrium chemical reactions. Statistical mechanics provide the essential mathematical framework.

This seminar provides a means for reviewing the present state and current directions of research in each of the subject areas: lattice dynamics, molecular physics, and statistical mechanics. More important, however, is the opportunity to assess the following (not mutually independent) points with respect to each of the fundamental fields:

a. Will the present state of knowledge in the field permit theoretical treatment of pertinent aspects of the detonation process, with sufficient rigor to yield useful results? If so, have the necessary mathematical models (computer programs?) been developed?

b. If not, what is lacking? What kinds of basic research are needed to attain the required level of knowledge? Does the necessary basic research appear to be feasible, assuming a dedicated, coherent effort?

c. If additional basic research is needed and appears to be feasible, what are the best approaches, to both theoretical and experimental investigation?

d. How can the overall phenomenon be best treated? Should an integrated mathematical model be developed, or should the events be treated in a series of steps? If the latter course is more tractable, are there evident interface problems in proceeding from one stage of the phenomenon to another? What devices for simplification can and should be used, and how much error or uncertainty is likely to result?

It is our hope that, by bringing together experts in the relevant fundamental sciences, a background can be provided against which appropriate plans for future research can be formulated. Answers to the technical problems are not expected to result directly from the conference, but we hope to learn from the discussion how best to proceed to find the answers.

While the emphasis of the seminar is upon explosives and detonation, the same questions are of importance in a number of applied research areas. At the fundamental level of treatment, the detonation process differs in degree, but not in substance, from many other phenomena.

TABLE OF CONTENTS

*Paper is being revised by Dr. Wright

**Dr. Boddington did not submit paper for publication

BLANK PAGE

SESSION I

Monday - 21 October 1968

CHAIRMAN: Dr. James E. Ablard
U.S. Naval Ordnance Laboratory
White Oak, Silver Spring, Maryland

Introduction	Dr. James E. Ablard
Crossed Molecular Beams Research And Connections With Energy Storage Problems	Dr. Robert K. Davis Department of Physics Florida State University Tallahassee, Florida
Electronic Structure And Chemical Instability of Explosives	Dr. Ferd Williams Physics Department University of Delaware Newark, Delaware
Particle Waves and Detonation in Crystalline Solids	Dr. Edwin R. Fitzgerald The Johns Hopkins University Baltimore, Maryland

INTRODUCTION

Dr. James E. Ablard

I was in on what I think was the beginning of this seminar -- by now most of you have had some contacts with the technical cooperation program between England and Canada, Australia and the United States. The Explosives Panel of the Ordnance Subgroup of that diverse body held its fourth meeting in London in May 1966. Panel O-2 is a typical committee from that organization. You've all attended meetings (and the one in London was no exception) where you were like the observer at Northhampton Harbor who was shown the facilities for navigation that had been growing up over the years. He was shown lighted buoys, red buoys, black buoys, but when he was telling about it afterwards, he said the lights flash and the horns blow, bells ring, but the fog rolls in just the same.

Out of the fog in London came a suggestion from Dr. Eichelberger that we sponsor a seminar which would review the new knowledge in instrumentation that has grown up in universities and institutions not usually connected with our explosives program.

In a way we were like the young pilot several years ago who was on his way from New York to Boston. After flying above the forecast for what he thought ought to be long enough, he called down and asked how much farther it was to get to Boston; the reply came: if you keep on going in that direction, its 23,999 miles. We wanted to be sure we were headed towards our objectives in the shortest possible way. We don't want to continue going all the way around the world to get there. On the other hand, we may be like the fellow who was groping around under the street light on the corner. A man came by and asked him what he was looking for -- a quarter, he said. Where did you lose it? Over there. Well, what are you looking for it here for? Because there's more light over here. We may be searching here where it's light and

we can see what we are doing, but over there in what is now dark to us -- may be the pay dirt. So one of the objectives of this seminar is to obtain some advice.

The Panel thought that there was a reasonable chance that some of the new tools and theories of molecular physics could be turned to the solution of some of our problems. The idea, as Dr. Eichelberger pointed out to some of you, was not to have the expert solve the problem but to introduce to us the theories in the fields of their choice and the instruments that are used to get the information in their separate fields. We would expect to take it from there. Getting an idea is like sitting on a tack -- both make you rise to the occasion. We arose to this idea and promptly appointed Dr. Eichelberger as Chairman of the Committee to carry it out. He named the other members of the Committee; I'll do it again. Mr. J. C. Baril was the member from the Canadian Defence Research Staff in Washington. He escaped back to Canada a month or two ago. Dr. Peter Dees was the member from the British Scientific Mission -- he had to rush home and have a brand new first child a few months back. Bill Pheasant is from the office of the Australian Defence Supply Attache; he hasn't escaped yet but his relief is in Washington and he is taking him around this week and couldn't be with us. So the members of the committee who are still about are Dr. Jacobs from NOL and Dr. Ray Walker of the Feltman Research Laboratories at Picatinny.

The Committee was able to secure nine speakers from three countries for this seminar. We are grateful to the speakers who have diverted their attention from their usual interests and have come here this week to brief us. We work in a field quite foreign to their usual pursuits. I hope that a glance at our problems may lead some of them as well as us to the awakening of ideas for our mutual benefit. But before we proceed with this it may be well to make some statements relative to where we are -- from where we think we are in the understanding of high explosives. I borrow here heavily from the writings of Dr. Eichelberger's Committee.

Military high explosives may be pure organic compounds, mixtures of organic compounds, or mixtures containing organic compounds plus inorganic oxidizers, metals, plastics, and so forth. The usual state of the mixtures when ready for use is a cast or pressed charge, pressed to its highest density obtainable in the factories. When this solid detonates, it is traversed by a strong shock which compresses successive layers of the material; the density is considerably higher than the solid density. Under these conditions, essentially complete molecular rearrangement into small stable molecules takes place, in the order of hundred to several microseconds.

Progress has been made in the past 25 years in understanding the physics and chemistry of detonation. We have made use of thermodynamics and hydrodynamics and the equations of state of high pressure physics. We have also made progress in measuring the effects of detonation on the surrounding environment and in so doing have learned how to estimate the action to be expected. From the properties of the shocks created in materials, it is even possible for instance to compute the detonation pressure, but there are two parts of the detonation process for which we have so far only qualitative understanding. They are similar in nature but different.

I refer on the one hand to the description of the process that material undergoes as it is overrun by a detonation and on the other hand to the process that an explosive goes through when a portion of it is energized by some mechanism and the resulting exothermic reaction manages to build up to a detonation. The two processes are similar in that they both involve reaction rates and probably induction theory but they are different in many important ways. Material passing through a steady state detonation is first subject to an extremely high pressure shock -- 300 kilobars and higher. The chemical reaction then begins and continues while the pressure decreases. Completion of the reaction is practically 100 percent certain.

It is not usually necessary to consider more than the small micell of the material to describe the whole process for all micells. That is all micells large enough to contain all the atoms of the mixture. Furthermore, all micells undergo the same reaction in the same time -- not at the same time but in the same time.

In the other case the build-up to detonation -- a small amount of energy may be supplied to a small amount of material at atmospheric pressure. Energy may be sufficient to cause a small portion of the material to decompose. The exothermic reaction may be imparted to neighboring materials which in turn may decompose, or may not. The energy may be dissipated. If the reaction continues, gaseous products may collect until a small pressure is generated -- the small pressure results in a pressure wave length which travels over the unburned material. Continued reaction generates more wavelengths which may coalesce into a larger pressure wave - or they may not. They may escape the solid before they coalesce. This brings in the concept that the size of the solid sample is important for the build-up to detonation and its environment is important -- that means whether it is confined or not. And finally a self-sustaining chemically reacting shock may be generated which rapidly builds up to a detonation. Thus in the build-up to detonation an important part of the process can take place at relatively low pressure -- say, under 1 kilobar.

The success of the reaction is dependent on the size of the sample, on the confinement and other things like the crystal size. Both processes have varying rates depending on the density and some characteristic of the chemical - not very well defined or understood. And finally given the same material in the same state in the same confinement to which sufficient energy has been added to build up to detonation should be successful. Anything less than this we are inclined to think should fail. However there are certainly many cases where the apparent energy required is much less than the normal amount. Success or failure appeared to be statistical. We begin to wonder if a lot less than the usual amount will initiate the detonation some small fraction of the time. The one case in a thousand keeps haunting us.

Now what makes us think that molecular physics and solid state physics might serve to improve the description of these two processes. We hope that statistical dynamics will be able to describe the state of the atoms or molecules when subjected to these extremely high pressures such that their densities are about four-thirds of the solid density. We hope that this description will lead to a prediction of the rates of reaction. The only rate law that has been used to date is the familiar Arrhenius law. It may be the best thing there is. Some recent work tends to show that it leads to reasonable values for the reaction zone length in nitromethane and liquid TNT. This would be the first process referred to above -- that is the steady state detonation. However a look at some of the alternatives might produce other descriptions or might give us more confidence in the Arrhenius expression. And in any case it has not been too successful to date in the build up to detonation process.

The equation of state for the gaseous products which have been used successfully are empirical expressions which describe the Chapman-Jouget conditions at the end of the chemical reaction. They have been arbitrarily fit to what data is available and do not allow much extension beyond the high pressure-high temperature conditions in the Chapman-Jourget situation. Molecular physics of mixtures of gases at high pressures might lead to better more versatile equations of state.

Of considerable current interest is the second process I have mentioned -- the build up to detonation. Our interest is particularly drawn to this because of the instances of prematures in guns and bombs, the one in a thousand cases that I mentioned previously. Considerable progress has been made in the continuum treatment of the build up to detonation process. This has been accomplished using the familiar principles of hydrodynamics and simple kinetics. The great difficulty lies in accurately representing the absorption and distribution of energy in the initial stages. It seems highly probable that the likelihood of chemical decomposition under a given energy absorption is a function of the crystal lattice and imperfections in it. It also seems

probable that a higher density of imperfection should permit the chain reaction process to continue in spite of a given set of difficulties whereas a lesser density of higher chemical potential sites might let the reaction fail. We would have to translate whatever may be learned about the propagation of the wave of a reaction in a pure crystal into a process that jumps from one crystal to another in a conglomerate chart, but this is far down the stream from the current figure.

One bit of specialization we have insisted on -- this particular Panel is concerned with high explosives. While some mixtures which are explosives contain ionic crystals, the pure crystalline high explosive molecules are non-ionic crystals and so we have insisted that we were particularly interested in what the new theories in instrumentation might tell us about non-ionic crystals. This has posed a new problem because we are told that the study of ionic solids is not yet complete and the organic molecules must wait. However we are not content to wait. We prefer to keep our attention on the less familiar - maybe it's in the dark spot -- but that's where the pay dirt is.

I do not know whether the May 1966 decision preceded or followed the initiation of Dr. Walker's work on organic solid states at Feltman Research Laboratories or Mr. Connick's work at the Defense Research Laboratories in Australia and perhaps there is other work in this field that I do not know about. In any event these two installations have made a start in direct application of solid state techniques to non-ionic high explosive crystals. Although they have not been solicited as speakers for this seminar, we will hope that they will make substantial contributions to the discussions through their comments.

In summary I quote from the inclosure to the letter that the Committee mailed to the prospective experts. "In posing the questions to which the speakers would address themselves, they said: Will the present state of knowledge in the field permit theoretical treatment of the detonation process with sufficient rigor to yield useful results? If so, have the necessary mathematical models been developed? If not,

what is lacking? What kind of basic research is needed to attain the required level of knowledge? Does it appear to be feasible, assuming a dedicated coherent effort? What are the best approaches to both experimental and theoretical investigations in this field?" These and other questions were posed. It was really a difficult task. The fact that we were able to have nine speakers on the agenda indicates that we already have some measure of success.

Walt Disney told the story of the boy who knew no such word as "fail," he wanted to march in the circus parade so he offered to take the place of a missing trombonist. He hadn't marched two blocks before the fearful noises from his trombone caused a horse to rear and to create a turmoil. The bandmaster commanded: "Why didn't you tell me you couldn't play the trombone?" The boy said: "How did I know, I hadn't ever tried it before." So far as I know the experiment for setting up a seminar in this fashion on this subject has not been tried before. I hope that it will be a success. At least we will have tried.

CROSSED MOLECULAR BEAMS RESEARCH AND CONNECTIONS WITH ENERGY STORAGE PROBLEMS*

R. H. Davis
Department of Physics, Florida State University

ABSTRACT

Because of recent advances in neutral beam source technology, collisions between a variety of molecules are now subject to detailed experimental investigation. Total cross section measurements provide crude tests of molecular collision models. Early measurements of differential cross sections using alkali beams showed the sensitivity of such measurements to different types of collision partners. High intensity, good resolution nozzle sources extend the domain of feasible differential cross section measurements as functions of energy and angle. An objective of this new field of research is the test of collision models so that they may be more effectively applied to complicated reaction problems such as those which arise in the formation and detonation of explosives.

I. INTRODUCTION

The credit for first thinking about molecular collisions should no doubt go to the several Greek philosophers who invented the concept of a "molecule" more than two thousand years ago. Through the efforts of numerous and much later scientists, many of the properties of gases, liquids, and to some extent solid state matter are now understood in terms of molecules moving more or less freely between collisions with one another. Surprisingly simple assumptions such as billiard ball molecules are adequate to explain many

*Research supported in part by the Air Force Office of Scientific Research; Office of Aerospace Research, U. S. Air Force, under Grant No. AFOSR-440-67.

phenomena. Conversely, measurable quantities are often not sensitive to the details of the collision mechanisms.

In contrast, relatively precise information has been obtained about microscopic collisions in nuclear physics. A sense of perspective is established by considering where nuclear physics would be if observations were restricted to atomic bomb blasts. Accelerators and reactors have been available to nuclear physicists for years while only recently have neutral beam sources suitable for precise collision studies become available to molecular physicists.

In Section II, several facets of the physics of explosives are considered since they point towards the importance of crossed molecular beam research. Section III is a discussion of crossed molecular beam research with effusive sources. Systems with supersonic nozzle sources are described in Section IV. Theoretical considerations in experiment design, data reduction problems, reactions, and scattering are reviewed in Section V. Section VI concludes this paper.

II. CONNECTION WITH PHYSICS OF EXPLOSIVES

A. Potential Energy Storage

An explosive may be defined as a material in which the atoms are arranged in states of high potential energy relative to the states formed in the explosion products. It is a special energy storage system in that the structure and allowed reaction mechanisms will support a detonation. A practical explosive is one in which a compromise is struck between high energy storage density and stability against slow dissipative reactions or accidental detonation during ordinary handling procedures.

While mixtures, such as oxygen-rich chemicals with fuels, continue to find important applications as explosives, the emphasis of current development

work is on new materials in which energy storage is understood in terms of molecular or crystalline properties. Here the problem reduces to an understanding of a stable system of atoms which are held together by "weak" bonds as shown in Figure 1 but which can, through a rearrangement, form "strong" bonds.

The formation process with respect to the natural forms of the atoms is endothermic. It is a process of entropy reduction for the system of atoms making up the explosive material. Of the many systems which may be considered on a basis of energetics alone, only a few have been obtained in practical quantities. Chemical processes of formation generally involve several intermediate steps as schematically shown in Figure 2.

In successive chemical reactions the potential energy of the constituent atoms of the final explosive material are bootstrapped upward until a useful stored energy density is achieved. The problem is to find a series of such reactions which is not abortively terminated by a dissipative reaction channel. Too often the entire procedure is carried out without the benefit of detailed information concerning the reaction mechanisms involved.

B. Stability, Detonation, and Energy of Explosion

In Figure 2, the concept of stability is shown as a local potential minimum in which the explosive as a system resides. While crude, the diagram illustrates a basic problem in that the potential minimum which guarantees stability must be delicately reached without over shooting and precipitating slow decays or catastrophic reactions; i.e., an explosion.

Against the practical requirement of stability for ordinary handling is lodged the equally practical requirement for detonation. Speed of energy release is desired providing it is controlled and free of sympathetic complications.

As a figure of merit for given material the energy of explosion is one of the most important performance ratings. Other practical considerations being satisfied, it should be made as large as possible.

A cursory examination of bonding energy tables will show that a number of arrangements of atoms and molecules in crystals give promise of very high energy densities and correspondingly large energies of explosion. Such a hypothetical energy storage system is shown in Figure 3. A laminar geometry is assumed which immediately raises the question of formation, a point to be taken up later.

The energy of explosion Q_x is obtained from the energy of formation, Q_F, of the explosive and the energy of formation of the explosion products, Q_P.

$$Q_x = Q_P - Q_F \tag{1}$$

To get the energy of formation, consider the periodic array of O-N-H-C as made up of $O\overset{a}{-}(NHC)\overset{b}{-}$. Bond (a) is between the O and N and (b) is between C and O. The bond energies are:

O-C	26 kcal/mole
O-N	-22 kcal/mole

and the average is +2 kcal/mole.

The heat of formation is given by

$$Q_F = \underset{HCN}{-33} \quad \underset{O}{-58} \quad \underset{\substack{\text{Bonds} \\ \text{(a) and (b)}}}{+4} = -87 \text{ kcal/mole} . \tag{2}$$

Several products are possible. To be specific, assume that the products are H_2O, CO, N_2, and C. The energy of formation of the products is

$$Q_P = \underset{H_2O}{1/2} \times 58 + \underset{CO}{1/2} \times 26 + \underset{N_2}{0} + \underset{C}{0} = 42 \text{ kcal/mole} \tag{3}$$

The energy of explosion is the difference

$$Q_x = 42 - (-87) = 129 \text{ kcal/mole}$$

$$= 3{,}000 \text{ kcal/kg}$$

This may be compared with a value given [1] for RDX of 1390 kcal/mole.

Such a calculation immediately raises several questions. First, can this or some other equally interesting system exist? If it does exist, what are the correct bonding energies or taking the system as a whole, what are the details of its structure? Second, if it does exist, is there a formation process which will produce it? Historically, many explosives have been invented by the discovery of a formation process rather than a premeditated design of the system and a subsequent search for ways to make it.

The hypothetical array is laminar in design since it was originally put forward in a discussion of tuned chemical reactions of vapors incident on a solid surface. Momentum control of the reactant beams is assumed to optimize in a controlled fashion weak bond formation.

The third question, which is raised by any proposed energy storage system, is whether or not the system will detonate and if so, under what conditions? How is shock propagated? What are the effects of electromagnetic radiation or nuclear radiation?

In general, these questions are incompletely answered in our applications of atomic and molecular physics and chemistry to explosive materials. In some areas the scientific foundations have not been laid, while in others the application techniques have not been developed.

C. Molecular Collisions

On a microscopic scale the formation of explosive materials is a result of molecular collisions in which chemical reactions produce the explosive material. The control of such collisions is only parametric in conventional chemical processes in that the number and types of atoms or molecules is specified along

with environmental factors such as temperature, pressure and radiation bath. Parameters crucial to the reaction such as the relative momentum of colliding pairs of molecule are not controlled. For a given temperature the spread in relative velocities is comparable to the magnitude of the most probable velocity. The possibility of tuning the reaction to the optimum conditions for the production of the desired substance is lost in a Maxwellian blur.

Conceptionally, the situation is much improved if the resultant is crystalline and if formed by reactions at its surface. Figure 4 illustrates the control effected by a vapor reactant source, not only with respect to the momentum of the reactant molecule but the angle of incidence on the reactive surface as well. The reactant beam may be tuned to maximize the desired reaction rate, which is ultimately determined by microscopic quantum mechanical details. There is not, unfortunately, an extensive literature on crystal growing from the vapor phase which will serve as a basis for the design and investigation of new crystalline explosive formulations. The advantages of surface reactions with regard to energy and momentum balance are apparent and should not be overlooked in future developments.

Chemical reactions in gases offer no special advantages in the control of the reaction mechanism because of the Maxwellian distribution of relative velocities as previously mentioned. The formation of weak bonds between aggregates of atoms which through a rearrangement can form a strong bond is a matter of chance with dissipative reaction processes working to the detriment of high yields of explosive substances. In one form of chemical reaction theory the hazard of forming a given chemical product is introduced by assuming a steric factor.

Between collisions, a gas molecule does have a specific energy and momentum as does the partner in the next collision. Thus, specially prepared gases in the form of jets which are arranged to intersect bring molecules together with

relative momenta limited by the velocity distributions in each of the jets. This is the basic idea of crossed molecular beams research. The objective is to determine as precisely as possible the conditions of molecular collisions so that the details of the mechanisms are manifest.

III. CROSSED MOLECULAR BEAMS-EFFUSIVE SOURCES

A. Early Work

If crossed molecular beam techniques are a powerful tool for the detailed study of molecular collisions, why is the development of the field so belated? There are two related answers. First, sources for the production of well-collimated beams of neutral particles of high energy resolution and high intensity have only recently become available. Second, the detection of low energy neutral particles is a difficult technical problem. This in part accounts for the lead which exists in the study of nuclear collisions. Energies involved in nuclear collisions are considerably larger as suggested by the conventional energy unit 1 MeV = 1,000,000 electron volts. Alpha particles emitted by nuclei can be detected with the assistance of an ordinary microscope as individual scintillation events in a zinc sulfide screen.

The first experiments on reactions with crossed molecular beams are schematically shown in Figure 5. Potassium and halogen compound beams produced in effusive sources intersected in an evacuated chamber with a pressure the order of 10^{-9} Torr. The products of the collision are detected at various angles with respect to the direction of the potassium beam. Effusive sources are ovens with suitable apertures and collimating slits to define the beam. Experiments of these type were chosen by Taylor and Datz[2] for two reasons. First, the alkali atoms and the alkali halide molecules can be detected in a surface ionization device. Second, the beams were readily available.

Several experiments followed their pioneer work on the reaction

$$K + HBr \rightarrow KBr + H \qquad (4)$$

While the yield as a function of angle could be obtained, information relevant to the details of the collisions was limited by the Maxwellian spread of the individual molecular beams.

B. Velocity Selection

By the proper angular shift of vanes mounted on a rotating axis in a turbinelike device, the transmission of molecular beams can be restricted to a predetermined velocity interval. As the velocity resolution is increased, there is a corresponding loss in transmitted intensity since particles of the wrong velocity are removed from the beam. Practically, $\pm$ 5% is a limit on the velocity resolution for many experiments. A system for the measurement of a total cross section is shown in Figure 6.[3] Again, note that an alkali beam is used for ease of detection.

Additional important information[4] can be obtained by the measurement of angular distributions using a system schematically shown in Figure 7.[3] Not only is the velocity of one beam selected, but a further refinement in technique is indicated here by the addition of a state selector. This device provides a multipole electric field which via a coupling with the electric moments of the particle beams defocuses particles in certain states while gathering those in another. A system producing a 10-pole field is described by Waech et al.[5] The use of state selectors is important in beam preparation and yield detection but it will not be further discussed here.

The results of reaction studies with potassium beams vary provocatively for different targets. Qualitative differences in the angular distributions for alkali halide product is shown.* The extreme forward and extreme backward

---

* Figure 8.

peaking of the angular distributions is reminiscent of direct reactions in nuclear physics. The intermediate distributions may be due to long lived compound systems. While such results demonstrate that the yields of chemical reactions may be preferentially concentrated at a given angle with respect to one of the reactant beams, a complete understanding of the anisotropy in terms of molecular structure and collision parameters is not available at this time.

An example of the challenge is dramatically presented by studies of the following reactions

$$\begin{aligned} K + HBr &\rightarrow KBr + H \\ K + DBr &\rightarrow KBr + D \\ K + TBr &\rightarrow KBr + T \end{aligned} \qquad (5)$$

Except for the isotopic differences in the hydrogen atom the three reactions are identical. From a classical chemistry point of view only minor differences should exist. The first two reactions have been carefully studied by Bernstein and his collaborators[6] while the last has been recently investigated by Martin and Kinnsey using a radio-isotope detection technique.[7] The angular distributions are sketched in Figure 9.

Within the uncertainties of the measurement, the results for the hydrogen, bromide and deuterium bromide are very similar. The angular distribution with the tritium bromide target appears, however, to be radically different. At present, this difference is not understood in terms of a reaction mechanism in which only the isotopic state of the hydrogen is changed.

IV. SYSTEMS WITH SUPERSONIC NOZZLE SOURCES

A. Nozzle Sources

The ideal neutral molecule beam source is one which produces mono-energetic, high intensity beams of variable energy for a variety of molecular species. What is desired is a source which will serve molecular collision physics in the way

in which Van de Graaff accelerators have served Nuclear Physics. The effusive sources with velocity selectors have opened the field of research but beam intensities fall far short of the requirements for a general attack. Alkali beams have been used to compensate for this deficiency since alkali atoms and certain of their compounds can be very efficiently detected.

An important step towards an ideal source is the supersonic nozzle, one constructed by J. G. Skofronick[8] is schematically shown in Figure 10. Beams 100 times more intense than those from effusive sources with velocity selectors are produced.

The idea for this type of source was first put forward by Kantrowitz and Gray in 1951.[9] A series of references describing the evolution of the source are given in a recent paper by Skofronick and McArdle,[8] and in an earlier paper by Skofronick.[10]

Structurally simple, the principal of operation can be summarized as follows. The gas to be used in the jet is delivered to the small stagnation volume, one of which is the concave surface of the nozzle. As the gas passes through the nozzle, it is expanded and cooled with a significant fraction of the energy converted into stream kinetic energy of the jet. Immediately downstream from the nozzle is the skimmer which is critically designed to prevent a downstream flow of the laterally expanded gas while transmitting the jet with minimum disturbance due to shock fronts. Mach numbers of ten or larger are readily achieved for the stream velocity.

The velocity distribution function is given by

$$f(v) \propto v^2 \exp - \alpha \ (v/v_s - 1) \qquad (6)$$

where alpha is the constant and v_s is the stream velocity of the beam. The relative shape of the velocity distribution for the nozzle source is compared

with the Maxwellian distribution obtained from effusive sources in Figure 11. Both distributions have been normalized to a peak value of one. Actually, the peak for the nozzle source is a minimum of 100 times larger.

Of special importance experimentally is the success achieved in reducing the pumping requirements and the construction of otherwise compact nozzle sources.[8] Enormous pumps were used in the earlier versions of nozzle sources.

An important feature of these sources, in addition to high intensity and good energy resolution, is the capability for controlled variable energy. This is accomplished by controlling the temperature of the nozzle body which in turn affects the stream kinetic energy. A demonstration of energy variability is shown in Figure 12, in which the most probable kinetic energy of argon atoms is plotted against the nozzle body temperature.

B. Chambers

A conceptually simple experiment is the measurement of total cross sections schematically shown in Figure 13. The beam labelled f(v) enters the scattering cell, which contains the target gas. The attenuated beam is measured in detector (D). Also shown are the relevant formulae and expressions for relating the collision cross section to the observed or effective cross section σ_{eff}. A total cross section measurement for helium on helium is given in Figure 14.[11] Curve A is a total cross section calculated from a PMD potential (see Figure 15). The cross section curves averaged to account for the dispersion in velocity in both the beam and scatterer are shown as curves B and C for the case of scattering gas temperatures of 77K° and 300K°, respectively. The averaging techniques developed by Desloge et al,[12] were used.

Figure 16 illustrates the chamber for crossed beams produced by two nozzle sources. In addition to the two neutral beam sources, a detector is shown which

in this system is positioned for total cross section measurements. By changing the angular position with respect to one beam axis, information about the angular distribution can be obtained. A formula relating the velocity form factors and the collision cross section to the observed effective cross section is given in Figure 17. The importance of differential cross measurements will be taken up in Section V.

C. Data Acquisition and Handling

Even with the intensity improvement gained by the use of nozzle sources, signals at the detector are small. To extract the signals from the noise due to the residual gas and possibly other sources, the beam is chopped as schematically indicated in Figure 10. By a repetitive comparison of the detector signal with beam on to that with beam off statistically significant results are obtained. If the beam burst is of sufficiently short duration, time-of-flight measurements[11] can be used to determine the velocity distribution experimentally.

J. P. Aldridge[13] has designed an economical on-line computer system which serves all of the purposes of conventional signal averaging devices and provides a programmable data handling capability. The system, especially well suited for time-of-flight analysis, is block diagrammed in Figure 18. Suitable small computers are available from several manufacturers.

Once the data is acquired, i.e., the time-of-flight spectrum is stored, the full reach of programmable machine capability is available. The first operation is signal averaging which is readily accomplished. A comparison to a spectrum stored in another part of the computer memory representing the velocity distribution of the beam provides immediate indication of interesting features of the velocity distribution. Because such features may be the result of statistical background fluctuation rather than the real effect, immediate

indication is vital as the run can be promptly repeated and a direct comparison can be made between two or more runs. Real effects will repeat whereas statistical effects should not.

In addition to data acquisition and reduction, certain calculations such as kinematic relations can be performed to guide the experimenter in selecting the most appropriate parameters to improve the quality of the measurements. Further improvements of state selectors, particle detectors and analogue-to-digital converters will further accentuate the advantages of on-line computers in molecular collision physics.

V. DISCUSSION

A. Overview

The study of molecular collisions with crossed molecular beams is a new and rapidly changing field of research. Several topics are discussed in this section to establish a perspective of what has been done and what can be done. The first is a discussion of experiment design criteria with the objective of obtaining the best possible data on molecular collision events under conditions such that quantum mechanical effects are observed. Second, a significant part of the experimentalist's efforts must be devoted to reduction and transformation of the data into a form subject to theoretical interpretation. Graphical techniques have been extensively used but these are tedious as a standard data processing tool. The nature of the problem is illustrated with computed results for coplanar trajectories.

The third topic is that of chemical reaction theory. Most of the molecular collisions involved in the formation, stability and detonation of explosives are of the reactive type. Consequently, the understanding of reactions in terms of molecular collision data deserves special comment. While the paucity of data has rather starved the theoretical developments, several promising approaches

are emerging. Several of these theories require angular distribution measurements of the reaction products.

Fourth, the importance of elastic scattering data to the understanding of reactions and of the gaseous state is pointed out. The scattering of helium by helium is discussed because of the intrinsic interest and as an example.

B. Experiment Design

Since low beam intensities and low detector sensitivity have impeded the study of collisions of neutral atoms and molecules, quantitative comment on the situation with crossed beams from nozzle sources is appropriate. These sources yield approximately 10^{19} neutral particles per sr sec with a velocity resolution as good as $\pm$ 5%. With a flight path of 30 cm from each source and a collision volume of 1 cm^3, the scattering yield for a cross section approximately 10^{-16} cm^2 is in excess of 10^7 particles per cm^2 at a distance of 30 cm from the reaction volume. Isotropy is assumed in this estimate. It should be noted that scattering cross sections which are important of themselves and to reaction models, are found to be typically 10^{-15} cm^2 in test calculations.

Some theoretical predictions are useful in determining to what extent the resolution of the experiment is commensurate with the expected detail of the molecular collision event. Each collision can be characterized in terms of a parameter, alpha, given by

$$\alpha = \mu R^2 \tag{7}$$

where R is the impact parameter and μ is the reduced mass for a system with a projectile mass M_p and target mass N_t. Clearly, alpha represents an effective moment of inertia under consideration, and for the sake of convenience, it is assumed to be a simple function of M_p, M_t, through an approximate (but sufficiently accurate for these purposes) expression for the impact parameter given by

$$R = 10^{-1/2} \left(M_p^{1/3} + M_t^{1/3}\right) \text{ Å} \qquad (8)$$

This expression yields the distance at which the two molecules just touch, if each molecule (or atom) is assumed to have a radius of $10^{-1/2} M^{1/3}$ this approximation gives a reasonable estimate for the size of the molecule or atom provided M is in units of the mass of the hydrogen atom. Figure 19 shows values of alpha plotted against M_t for various projectile masses M_p. Having determined the value of alpha for a given pair of particles the type of phenomena expected can be directly read off Figure 20 which indicates the various regions as a function of relative energy E and the parameter α.

In Figure 20 regions bounded by specific values of the parameter ρ are shown. The parameter ρ is simply given by the equation

$$\rho = kR = [(2\mu E)/\hbar^2]^{1/2} \quad R \simeq \ell_{max} \qquad (9)$$

and this parameter corresponds to the maximum angular momentum ℓ_{max} contributing to the cross section.

The E, α space is approximately divided by the $\rho = 10$ and $\rho = 50$ lines into three physical regions:

1. $0 \leq \rho \leq 10$. In this "resonance" region, the cross section should exhibit rapidly varying values as the energy E is changed due to the expected quantum mechanical phenomena of "compound states" in the continuum. High resolution is needed to study such behavior which is vital to an understanding of the nature of chemical reactions.

2. $10 \leq \rho \leq 50$. This is the "diffraction region" in which the cross sections will tend to be smoother but the angular distributions of reaction products will still show quantum effects such as are well known in electron diffraction. Such angular distributions will be strongly angle-dependent and indicative of the reaction mechanism.

3. $50 \leq \rho \leq \infty$. The "classical region" is a less interesting region where molecules tend to behave more like billiard balls so that the intrinsic structure becomes relatively unimportant.

Finally, the α, E plane is divided by values for the "width" parameter Γ which is given by the equation

$$\Gamma = 2\rho \frac{\hbar^2}{\mu R^2} \cdot = \frac{4E}{\rho} \qquad (10)$$

The parameter Γ is an estimate of width of the state in the compound system which exists during the collision process. It is a criterion for establishing the maximum energy resolution which can be allowed if atomic single particle states are to be experimentally detectable. The value of Γ immediately shows the necessity for high energy resolution. Clearly, a resolution of 10^{-1} Γ is desirable at all energies.

From the discussion of Figure 20, it is apparent that angular resolutions sufficient to reach well into the diffraction region in a given experiment are desirable. In angular acceptance $\Delta\theta = 1°$ is a reasonable choice considering the problems of mechanical construction, desired physical significance, and required threshold for detectable flux.

C. Transformation of Data

Since the center-of-mass motion for the system of colliding particles does not coincide with either beam direction, rather unusual kinematic relationships are found. A CDC 6400 computer program named PUFF-I has been written by Aldridge[14] to quickly establish the kinematic relationships for a given experiment. This program is of immediate use in fixing the design of atomic collision chambers in addition to subsequent use in data reduction.

The computer program to handle the kinematics problem is briefly described here, and results for the elastic scattering of atomic hydrogen by molecular hydrogen are shown by way of illustration. The program works for arbitrary reactant and product pairs and for positive, zero, or negative Q values.

A velocity diagram defining the calculated quantities is shown in Figure 21.

Units: The units to be employed are the convenient set:

energies in eV

masses in amu

velocities in cm/sec

times in seconds

distances in cm

Since the system is over specified, a conversion is necessary.

$$E(eV) = 1.0364084 \times 10^{-12} E(\text{amu cm}^2/\text{sec}^2)$$

This is based on Cohen and Dumont.[15] In the cm-amu-sec system $E = 1/2\ mv^2$.

Let 1 denote the projectile, 2 the target, 3 the light scattered particle, and 4 the heavy scattered particle. This is clearly for convenience as interchange of 1 and 2 or 3 and 4 cannot have an influence on the scattering. In other words, 2 may be used to denote the projectile and 4 may denote the heavy scattered particle depending on what kinematic information is desired.

The kinematic relations are summarized

$$m_1 \vec{v}_1 + m_2 \vec{v}_2 = m_3 \vec{v}_3 + m_4 \vec{v}_4 \tag{11}$$

$$E_1 + E_2 + Q = E_3 + E_4 \tag{12}$$

where Q = reaction Q value adjusted to proper units using Eq. 8. Angles are measured with respect to the direction of particle 1 for convenience from an experimental point of view.

Equations 11 and 12 specify v_3 as a function of θ_3. In particular,

$$v_3^2 \left[\frac{m_3}{m_2}\left(1 + \frac{m_3}{m_4}\right)\right] - v_3 \left[\frac{m_3}{m_4}\left(m_1 v_1 \cos\theta_3 + m_2 v_2 \cos\theta_{23}\right)\right]$$

$$+ \left[\left(\frac{m_1}{m_4} - 1\right)E_1 + \left(\frac{m_2}{m_4} - 1\right)E_2 + \frac{m_1 m_2}{m_4} v_1 v_2 \cos\theta_{2} - Q\right] = 0 \tag{13}$$

$$\cos\theta_{23} = \cos\theta_2 \cos\theta_3 + \sin\theta_2 \sin\theta_3 \cos(\phi_2 - \phi_3)$$

This quadratic form, $Av_3^2 + Bv_3 + C = 0$ can be solved for v_3. There may be 0, 1, or 2 solutions depending on the satisfaction of the conditions (i) $v_3 \geq 0$ and (ii) v_3 real.

$$\text{(i) means } (-B \pm \sqrt{B^2 - 4AC}\ )/2A \geq 0$$

$$\text{(ii) means } B^2 - 4AC \geq 0$$

Then $\vec{v}_4$ follows from Eq. 11.

Center of mass velocity:

$$\vec{V}_{CM} = \frac{m_1}{m_1+m_2}\ \vec{V}_1 + \frac{m_2}{m_1+m_2}\ \vec{V}_2 \tag{14}$$

$$\vec{V}_i = \vec{V}_{CM} + \vec{V}_i' \qquad i = 1, 2, 3, 4 \tag{15}$$

It, therefore, follows that

$$d\sigma_{LAB} = \frac{V_3}{V_3'}\ d\sigma_{CM} \tag{16}$$

Scattering angle: The initial velocity of relative motion is given by the equation

$$\vec{q}_o = \vec{V}_1 - \vec{V}_2 = \vec{V}_1' - \vec{V}_2' \tag{17}$$

The final velocity of relative motion is given by the relation

$$\vec{q}_f = \vec{V}_3 - \vec{V}_4 = \vec{V}_3' - \vec{V}_4' \tag{18}$$

The scattering angle is defined by the expression

$$\cos\theta_{sc} = \vec{q}_o \cdot \vec{q}_f/(1\vec{q}_o|| \vec{q}_f1) \tag{19}$$

Note that it is convenient to ascribe an orientation to these angles. The orientations such that $\vec{V}_4 \times \vec{V}_1$, $\vec{V}_3 \times \vec{V}_1$, and $\vec{q}_f \times \vec{q}_i$ are up define positive angles. Using a similar convention, θ_2 and θ_{cm} should be negative. At present, these are read in and printed out as positive angles.

As an example, the scattering angle θ_{sc}, the differential cross section transformation $\sigma_{lab}/\sigma_{c.m.}$, and the velocity of the scattered projectile are plotted as functions of the laboratory scattering angle θ_3 in Figures 22, 23, and 24. Each of the plots are divided into three segments which are labeled according to the appropriate value of ϕ_{sc} or ϕ_3. The angle ϕ is measured in a counterclockwise sense along the beam 1 direction.

In this example, the relative angle between the beams is 90° which prevents the observation of the scattered yield at 90° (and 270°) in the laboratory. In Figure 22, it is seen that the scattering angle θ_{sc} of 150° cannot be measured at θ_3 = 90° because of the beam 2 position, but it can be observed at θ_3 approximately equal to 132°.

For the regions labeled 1, 2, and 3 the transformation of the differential cross section from the center-of-mass frame to the laboratory frame given as a ratio is plotted in Figure 23. An expansion or reduction of the angular resolution results depending on whether the observation point lies below or above $\sigma_{lab}/\sigma_{c.m.}=1$.

In Figure 24, the velocity of the scattered particle is plotted against the observation angle θ_3. Again, there are 3 segments in the plot depending on the choice of the values of ϕ_3 and ϕ_{sc}.

In this discussion the trajectories of the reactants and the products are assumed to be coplanar. The three dimensional case can be, of course, programmed. Recently, Desloge[16] derived an analytic form for the transformation which permits the calculation for given starting conditions without resort to diagrammatic techniques.

D. Reactions

While several reactions involving heavy collision partners have been studied, it is apparent from the discussion of experiment design that collisions

between light particles promise the more thorough interpretation. Simplicity requires low center-of-mass collision energies corresponding to room temperature or below in order to limit the number of partial waves involved in the collision and to reduce internal excitation to a minimum. These restrictions direct attention to the understanding of the simplest collisions, an accomplishment not extant at this time. Once simple elastic scattering is understood at least in terms of improved molecular particles, rearrangement reactions can be considered as the next step. This basis is needed for a "state of the art" investigation of more complicated chemical reactions such as those responsible for the formation, stability (or absence thereof) and detonation of explosives.

The problem is to understand, in terms of individual events, the mechanisms which control bulk chemical reactions. These mechanisms are usually discussed in terms of classical or semi-classical approximations.[17,18] Recently, Micha[19] has discussed compound state resonances in atom-diatomic-molecule collisions in terms of a modified Feshback theory. His work reinforces the approach developed here in two ways. First, as a result of a detailed quantum mechanical discussion of the collision mechanism, resonance states are computed for the system Xe + H_2 and the system Xe + D_2. Second, in order to precisely fix the parameters of this collision analysis, the need for experimentally determined potentials is pointed out.

Another extreme type of reaction has been discussed by Karplus, Porter, and Sharma[20] for the collision of a hydrogen atom with a hydrogen molecule. Their analysis indicates that a direct reaction mechanism is dominant. That is, the collision time is comparable to the transit time of the projectile across the diameter of the target. Such extreme situations are well known in nuclear physics and it is only a careful measurement of the differential cross section as a function of both angle and energy which generally provides a proper

estimate of the relative contributions of resonance mechanisms and direct reaction mechanisms. Here again the need for precision scattering data is a principal requirement for the next step towards understanding the reaction mechanism.

Perhaps the most richly developed theory for collisions between microscopic particles is that built on the R-matrix. For example, see the recent application of R-matrix theory to nuclear physics by Lane and Robson.[21] Several authors have applied the R-matrix theory to chemical reaction problems,[22,23] but the full power of this approach has not been brought to bear on the problem because of the lack of suitable data and sufficiently extensive theoretical investigation.

An objective of the R-matrix theory is the separation of the energy dependent parts of the cross section from energy independent (or nearly so) parameters which characterize the reaction mechanism. Mathematically, the essential feature of the analysis is the separation of space into an "internal volume" in which the interaction forces are large and an "external volume" in which the forces between the particles are small or nonpolarizing. The distinction between several types of forces involved in molecular collision mechanisms is important here and influences the choice of internal and external regions. A variety of reaction mechanisms may be parameterized, such as long lived intermediate systems, direct reactions, and step-wise reactions which involve more than one identifiable intermediate stage.

E. Scattering

Scattering data and the molecular potential parameters derived from such data are the raw material for several models for chemical reaction mechanisms. They are also of intrinsic importance. Consider the collision between two low energy neutral helium atoms. While the collision partners are among the simplest available, the experimental investigation of this collision can, at best, be

described as inadequate. For the most part, data consists of total cross sections rather than the far more sensitive differential cross sections.

From detailed differential cross section measurements come more precise determinations of the intermolecular potential.[24] As pointed out by Aldridge and Davis[25] provocative results are obtained with the PMD (See Figure 15) when calculations for the total cross section and phase shifts are carried down to very low energies. They find that the conditions for the Ramsauer-Townsend effect in the collision between two helium atoms are satisfied at a temperature corresponding to the lambda point for liquid helium II. A plot of the phase shifts and the total cross section is shown in Figure 25. In collisions where the Ramsauer-Townsend effect operates, one particle, in this case a helium atom, passes through the other with no change. This looks like microscopic superfluidity. Its relation to the dramatic bulk superfluidity property of liquid helium II has not been worked out. Confirmation of this possible insight into quantum fluids must await further experimental investigation, in particular the measurement of angular distributions over a wide range of energy, and a detailed theoretical analysis of the results.

VI. CONCLUSIONS

Both in energy and in beam species molecular collisions between helium atoms for which the conditions of the Ramsauer-Townsend effects are satisfied are rather different from the molecular collisions of the formation and detonation processes in explosives. Current research interests in the collisions between simple particles is motivated by the absence of previous research, molecular collision physics as described here is a new field, and the power of such investigations in the development of collision models. At present, reliable differential cross sections as functions of energy and angle have not been measured over a wide range of parameters for simple collision partners.

From an understanding of the collisions between light atoms and molecules under conditions such that quantum mechanical details are apparent will come appropriate models and theories for the analysis of more complicated collisions. The first in the hierarchy of increasing complexity are the rearrangement collisions. The rich and diverse reaction theory worked out for nuclear collisions can be adopted to such molecular collisions.

Because of the rapid increase in orbital angular momentum, complexity of internal excitation, and the number of both incoming and outgoing channels which results when complex molecules interact, it is difficult to extract mechanism details from such interaction data. Certain systematics will, of course, emerge. For example, it appears that several of the alkali beam experiments can be explained by a direct reaction mechanism.

The technology is now available to investigate the quantum mechanical details of many molecular collisions. The equipment is, as Saul Wexler of the Argonne National Laboratory put it, "at the point where nuclear physics equipment was during the 1920's." Development should be no less rapid.

VII. ACKNOWLEDGEMENTS

The author is indebted to his colleagues in the molecular collision physics group at the Florida State University for numerous discussions and the use of research results prior to publication. The members of the group are the following:

Experimentalists	Theorists
J. P. Aldridge	E. A. Desloge
R. H. Davis	D. Robson
J. W. Sheldon	
W. N. Shelton	
J. G. Skofronick	

REFERENCES

1. F. A. Baum, K. P. Stanyukovick, and B. I. Shekhtev, Physics of an Explosion (translated from Fiz Matgiz, Moscow by Research Information Services, New York), (1959).

2. E. H. Taylor and S. Dtaz, J. Chem. Phys. 23, 1711 (1955).

3. E. F. Greene and J. Ross, Science 159, 587 (1968) (a popular review paper.)

4. J. P. Toennies, Chemische Elementarprozesse edited by H. Hartmann, published by Springer-Verlag, Heidelberg (1968).

5. T. G. Waech, K. H. Kramer, and R. B. Bernstein, WIS-TCI-248X Theoretical Chemistry Institute, University of Wisconsin (1967).

6. A. E. Grosser, A. R. Blythe, and R. B. Bernstein, J. Chem. Phys. 42, 1268 (1965).

7. L. R. Martin and J. L. Kinsey, J. Chem. Phys. 46, 4834 (1967).

8. J. G. Skofronick and K. T. McArdle, (submitted to Rev. Sci. Inst.).

9. A. Kantrowitz and J. Grey, Rev. Sci. Inst. 22, 328 (1951).

10. J. G. Skofronick, Rev. Sci. Inst. 38, 1628 (1968).

11. K. T. McArdle and J. G. Skofronick (to be submitted).

12. E. A. Desloge, R. S. Grace and J. G. Skofronick (submitted to J. Chem. Phys.).

13. J. P. Aldridge (to be submitted).

14. J. P. Aldridge, Computer Program PUFF-I (unpublished).

15. E. R. Cohen and J. W. M. DuMond, Rev. Mod. Phys. 37, 537 (1965).

16. E. A. Desloge (in preparation).

17. D. L. Bunker, Theory of Elementary Gas Reaction Rates, (Pergamon Press, Oxford, 1966).

18. H. S. Johnston, Gas Phase Reaction Rate Theory, (Ronald Press, New York, 1966).

19. D. A. Micha, Phys. Rev. 162, 88 (1967).

20. M. Karplus, N. R. Porter, and R. D. Sharma, J. Chem. Phys. 43, 325A (1965).

21. A. M. Lane and D. Robson, Phys. Rev. 151, 989 (1967): D. Robson and A. M. Lane, Phys. Rev. 161, 982 (1967).

22. B. C. Eu and J. Ross, J. Chem Phys. 44, 2467 (1966).

23. L. Blum, Molecular Physics 11, 63 (1966).

24. R. B. Bernstein and F. A. Morse, J. Chem. Phys. 40, 917 (1964).

25. J. P. Aldridge and R. H. Davis, Phys. Rev. Letts. 19, 1001 (1967).

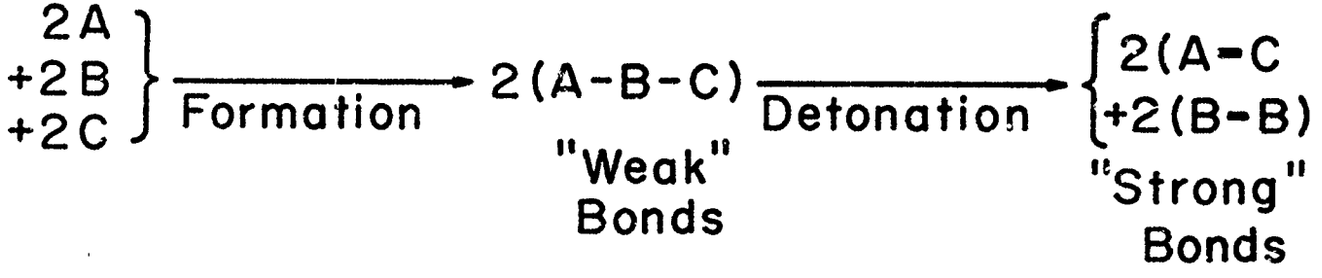

Schematic of an explosive

Fig. 1

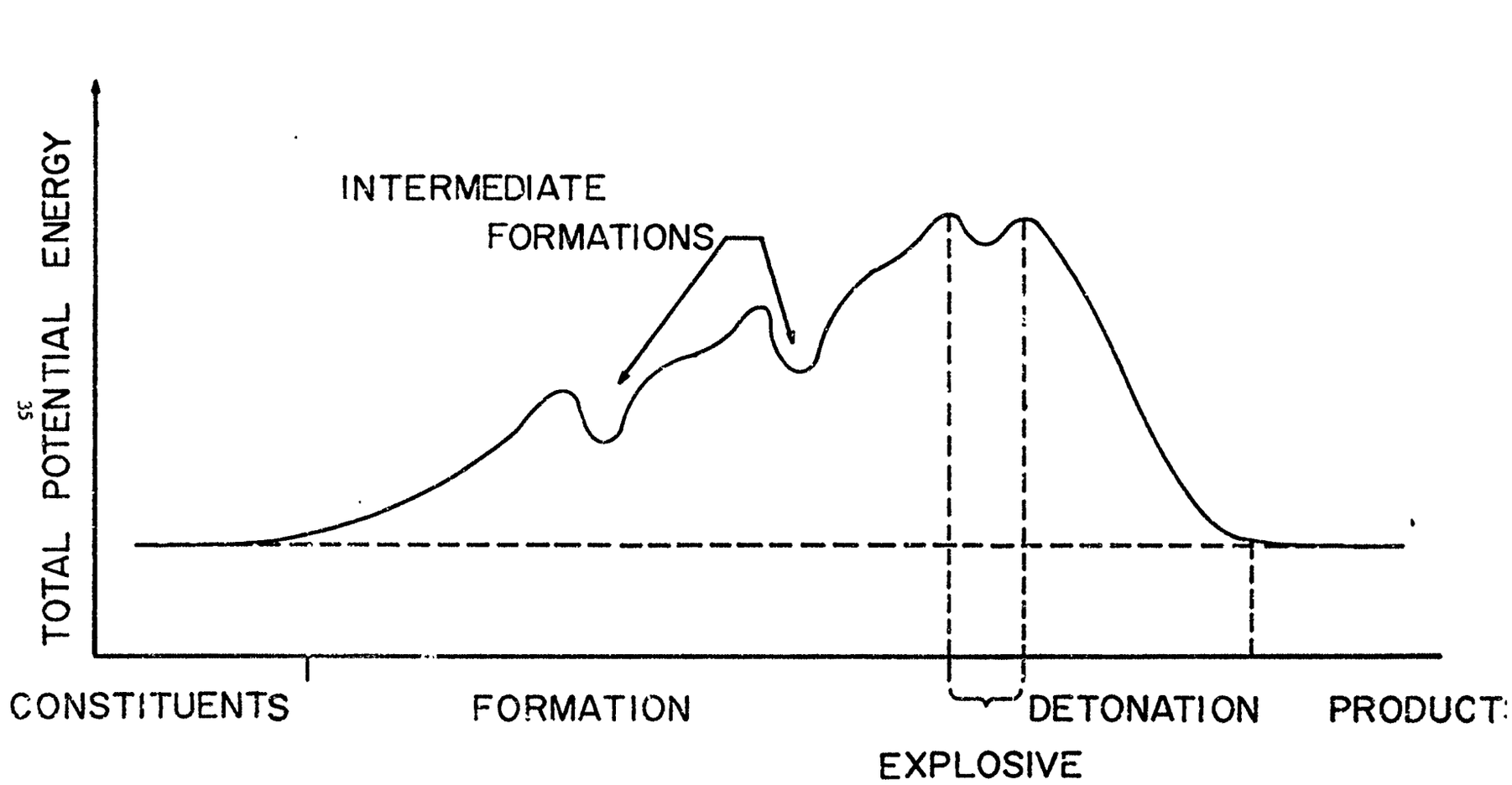

Potential diagram for constituents of an explosive

Fig. 2

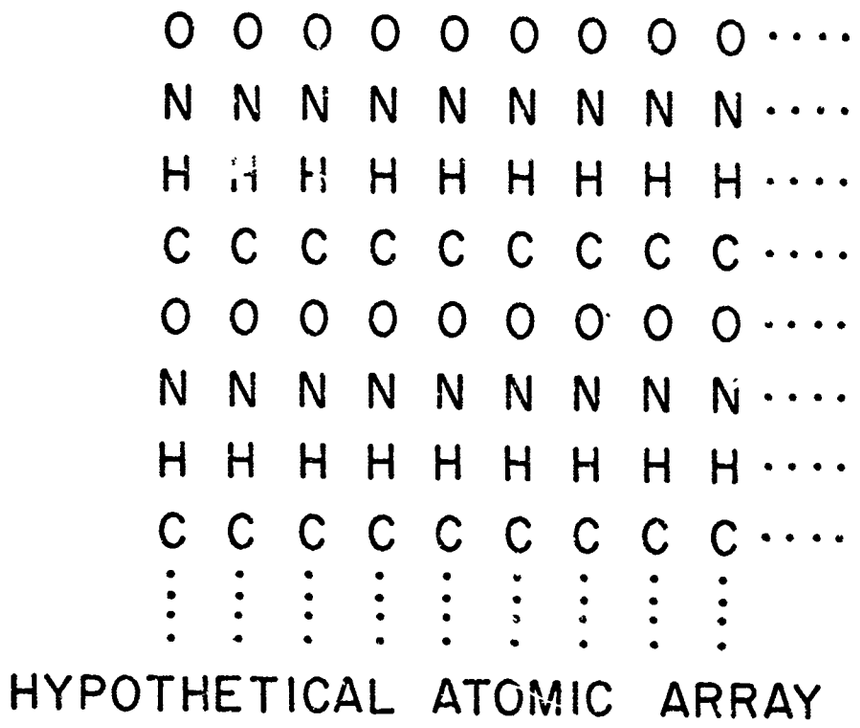

Hypothetical energy storage system

Fig. 3

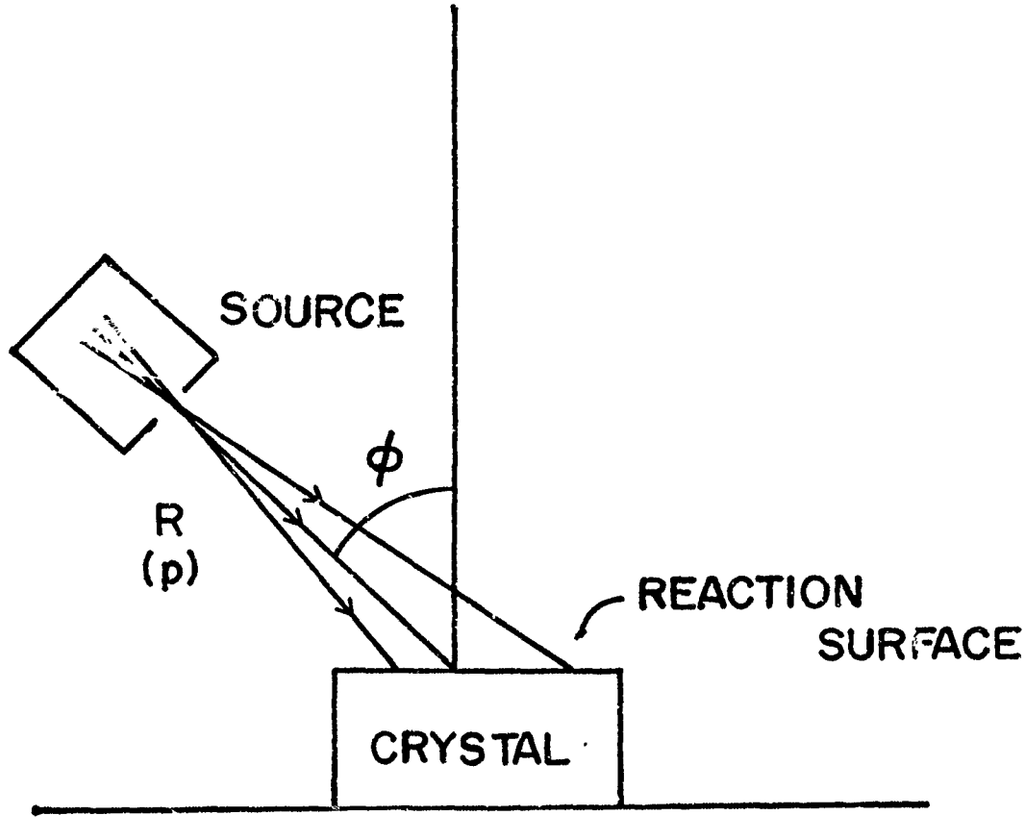

Diagram of system for surface reactions

Fig. 4

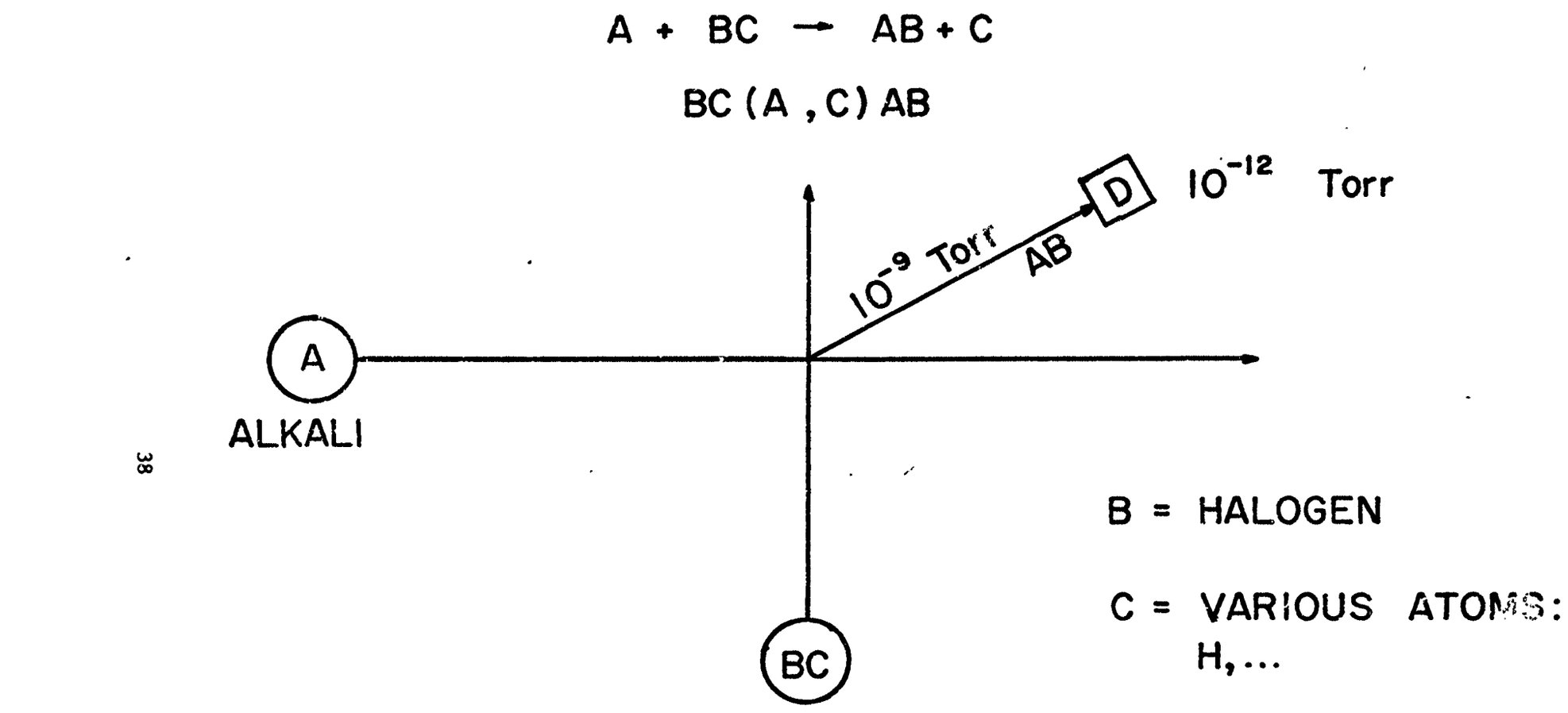

Crossed molecular beams from effusive sources.
Alkali atoms are used in one beam to improve detection effeciency

Fig. 5

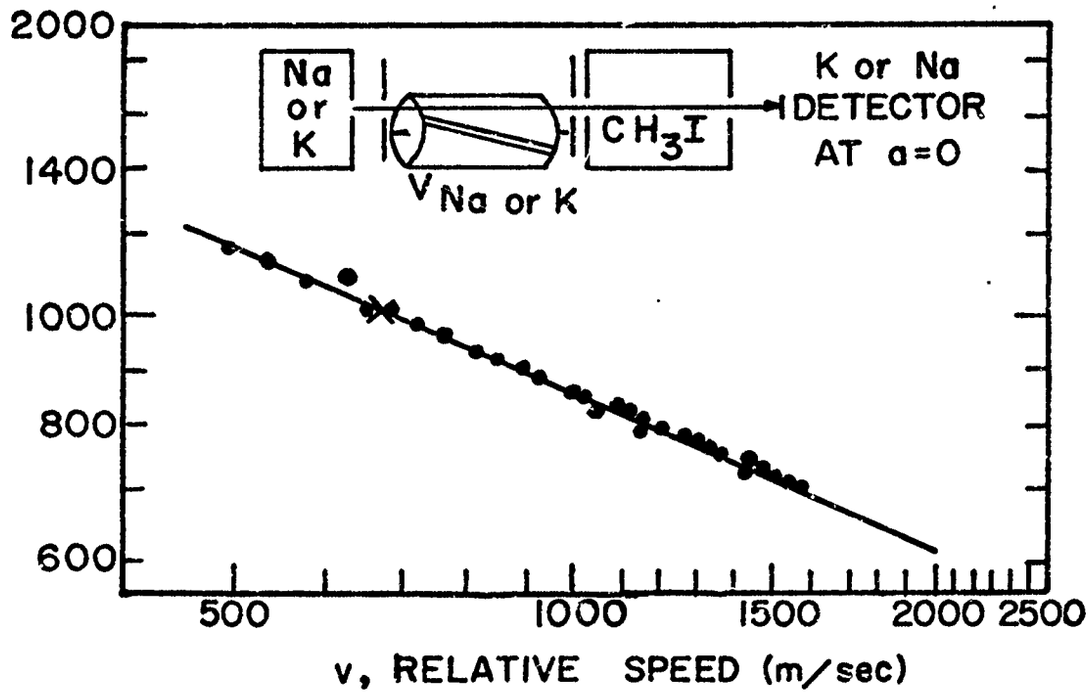

System for total cross section measurement with velocity selection

Fig. 6

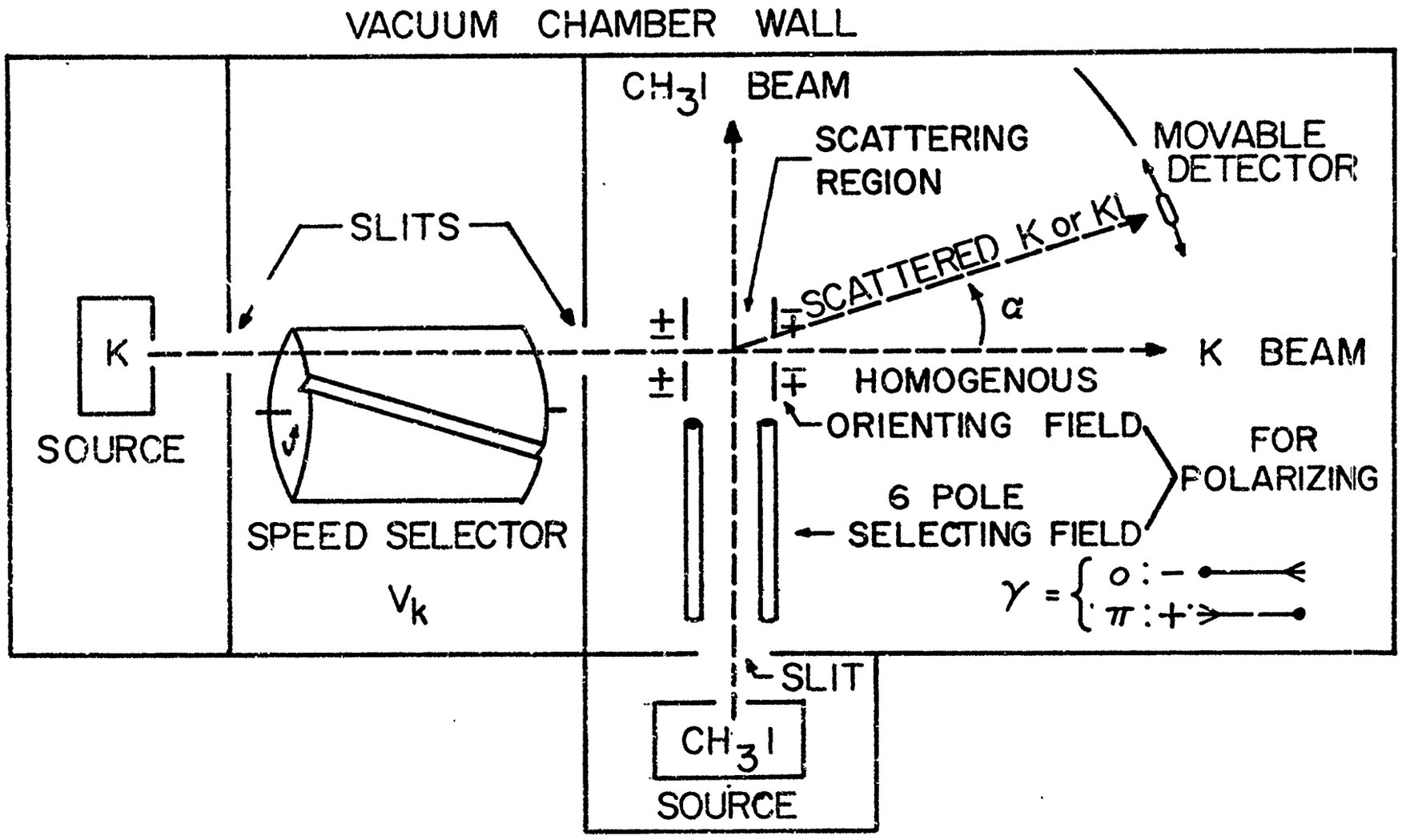

System for differential cross section measurement with velocity selection

Fig. 7

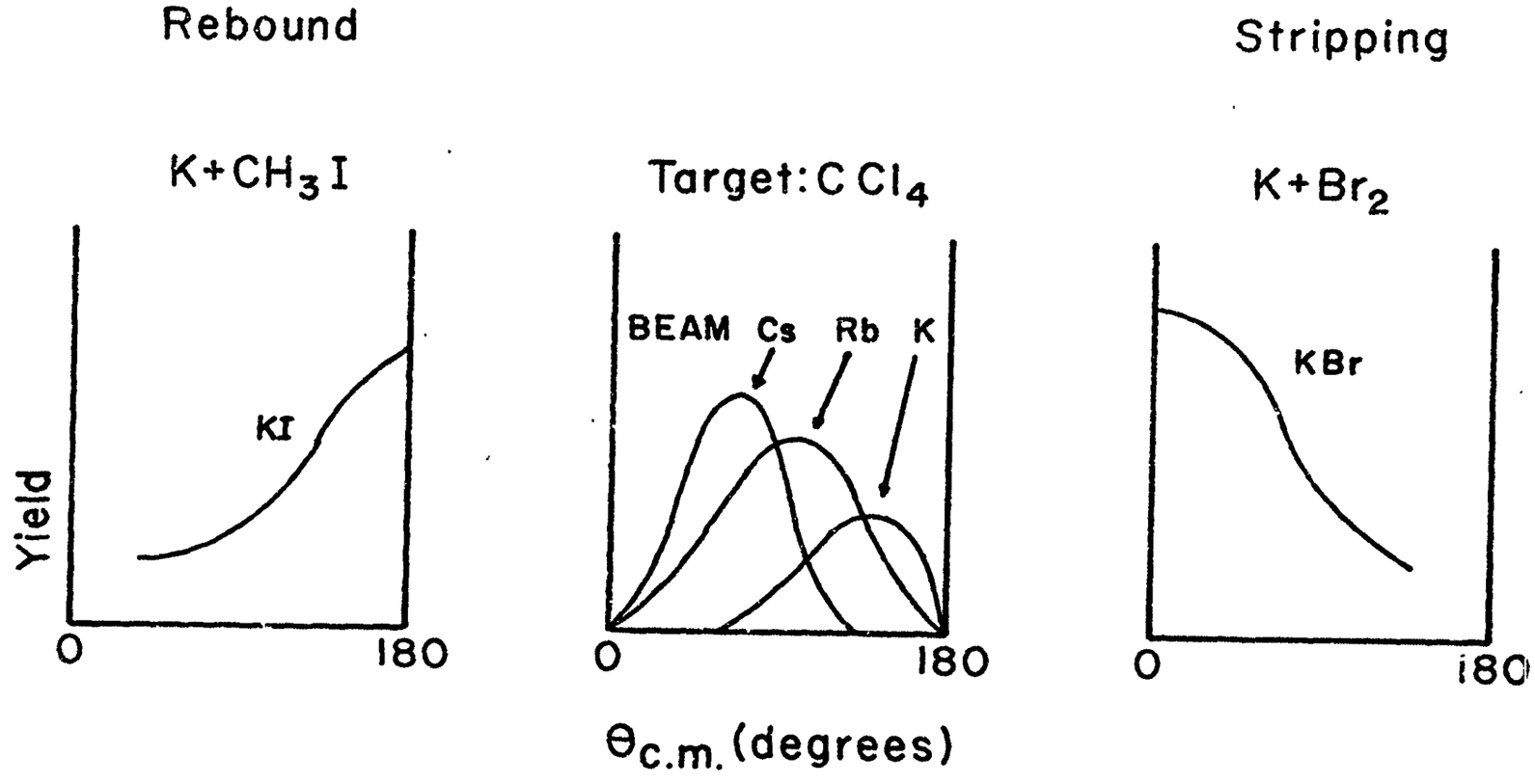

Comparison of reaction studies with potassium atoms and various target molecules

Fig. 8

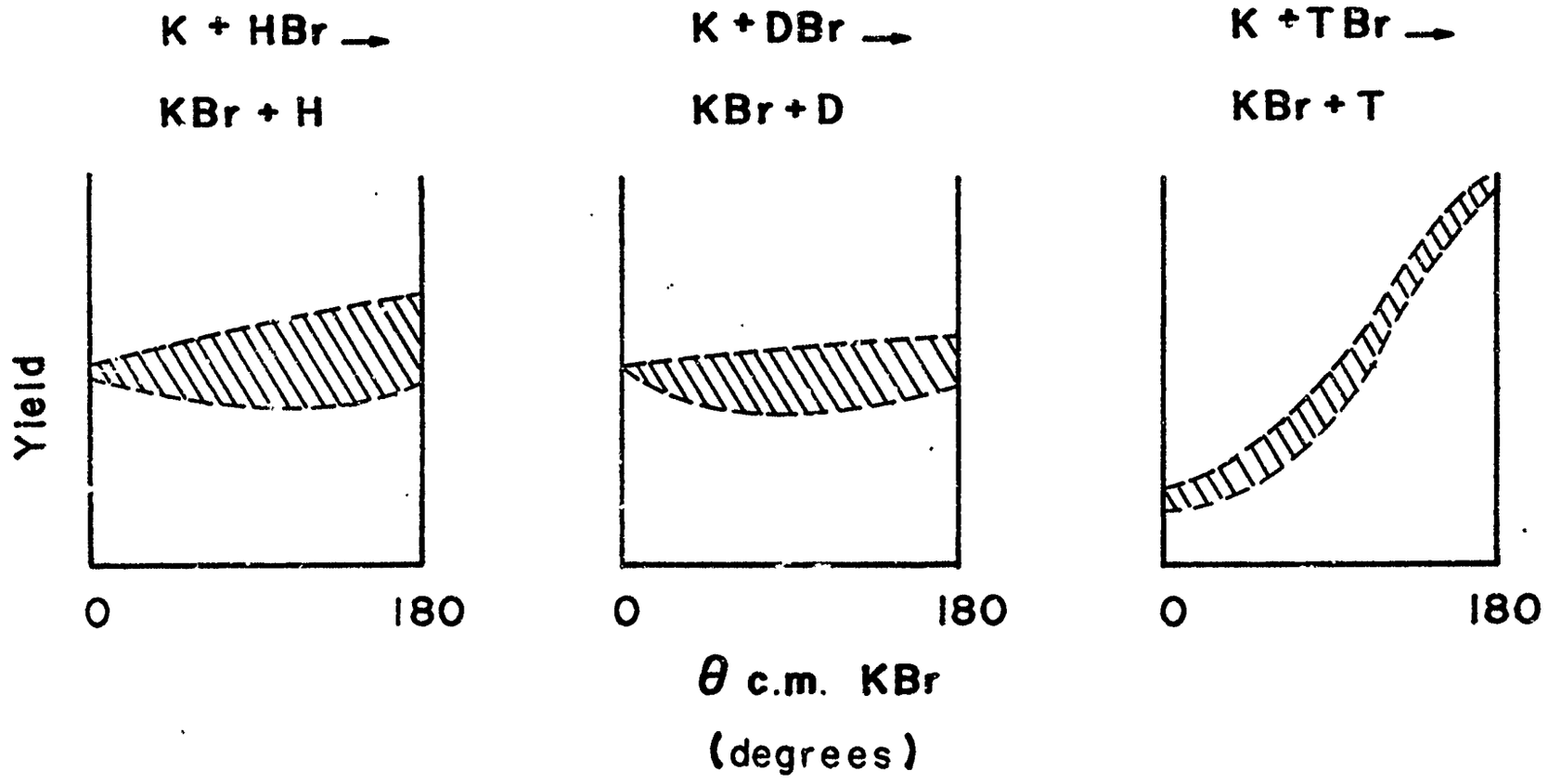

Potassium atom reactions with hydrogen bromide, deuterium bromide, and tritium bromide

Fig. 9

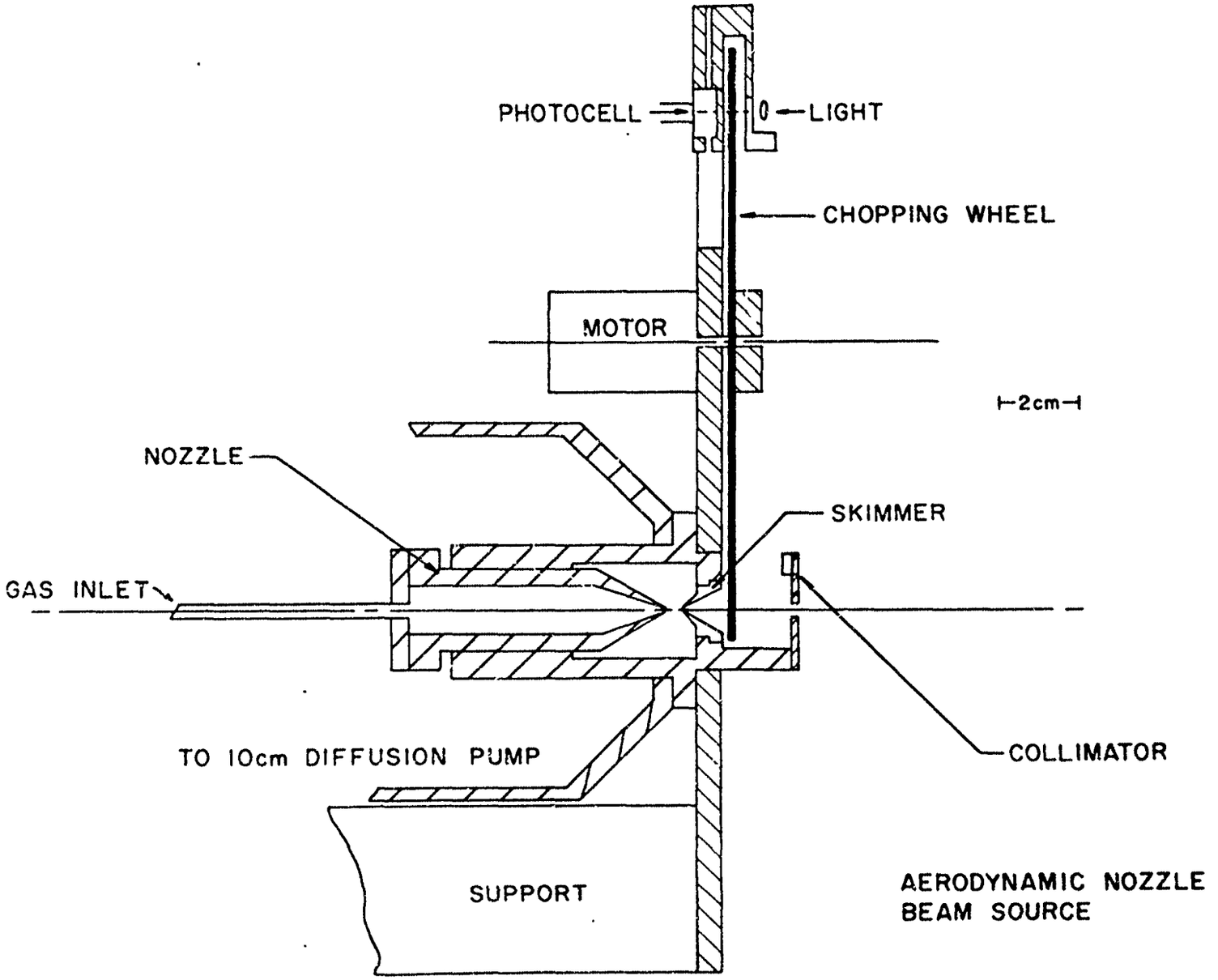

Fig. 10
Schematic of nozzle source

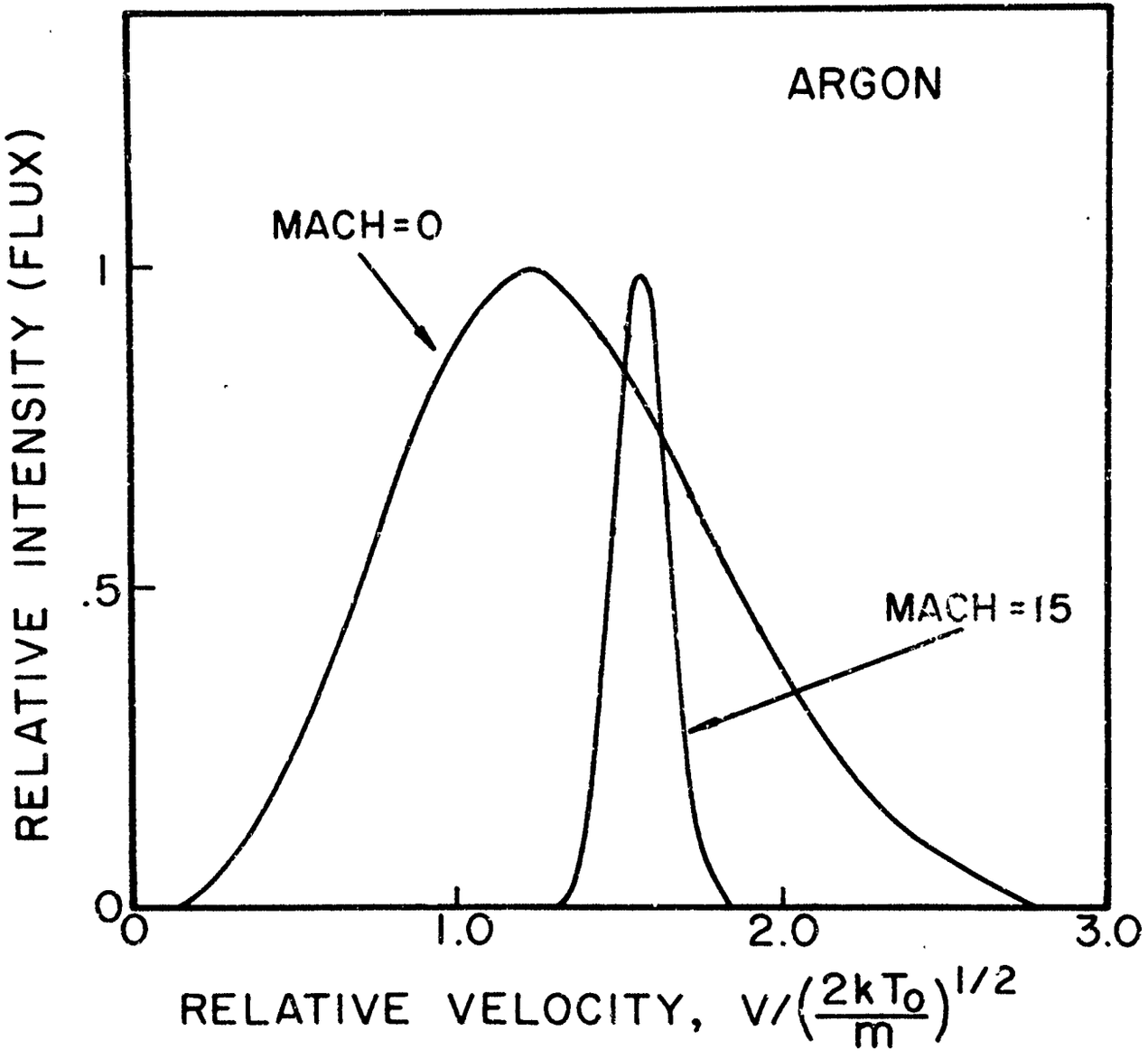

Fig. 11

Velocity distribution for nozzle source

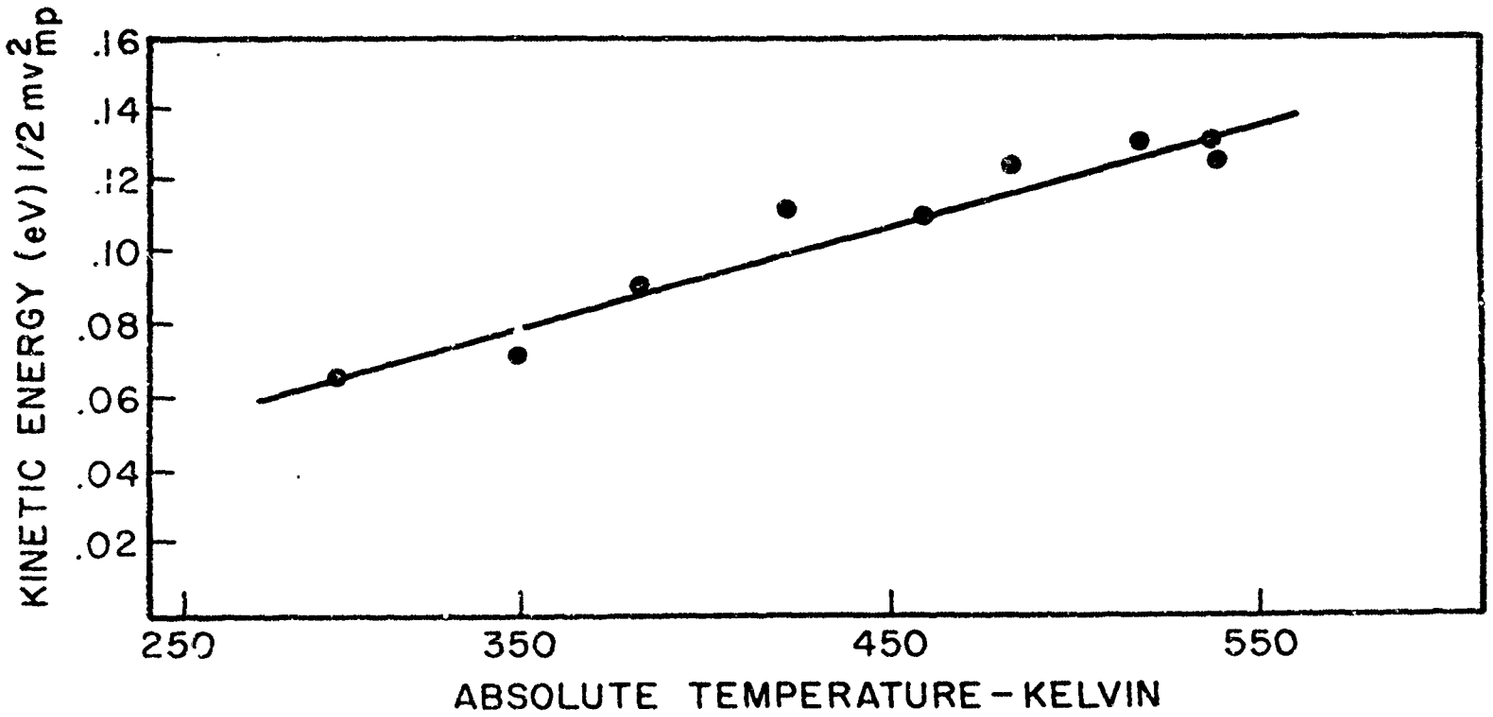

Most probable velocity as a function of nozzle body temperature

Fig. 12

$$\sigma_{eff} = A \int_0^\infty u^2 \sigma(u) \{\exp[-b(u-c)^2] - \exp[-b(u+c)^2]\}\, du$$

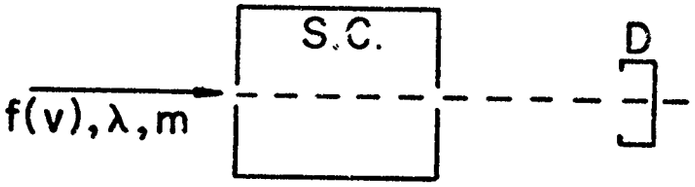

$f(v) \sim v \exp[-\lambda(v-v_s)^2]$

$F(V) = N \left(\frac{\Lambda}{\pi}\right)^{3/2} \exp(-\Lambda V^2)$

$\Lambda = \frac{M}{2kT}$

v_s = stream velocity of beam

λ = velocity dispersion of beam

$u = |\vec{v}-\vec{V}|$

$\sigma(u)$ = cross section in relative coordinates

A,b,c = Constants that depend on v_s, λ and Λ

Total cross section schematic

Fig. 13

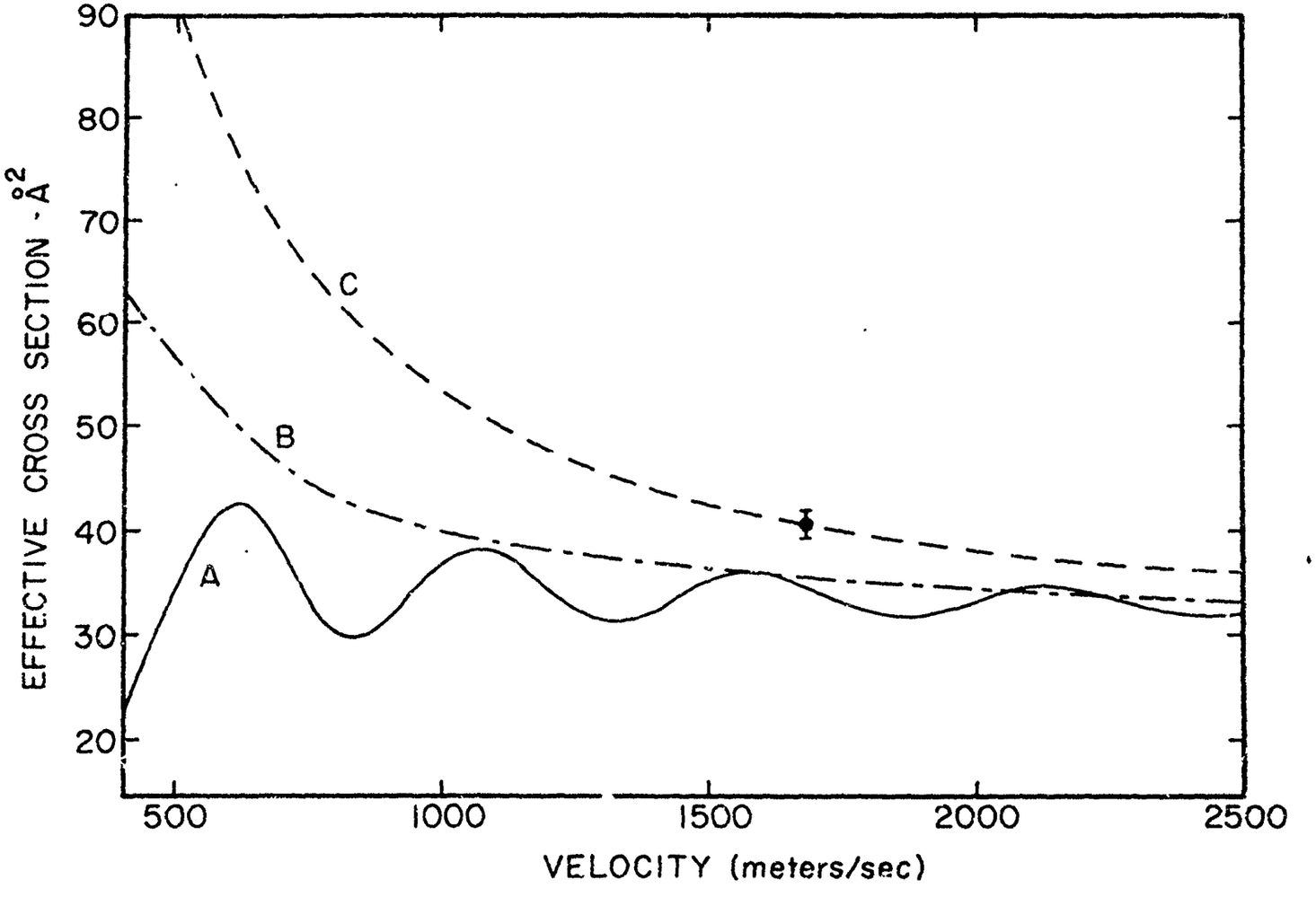

Fig. 14

Total cross section for helium on helium

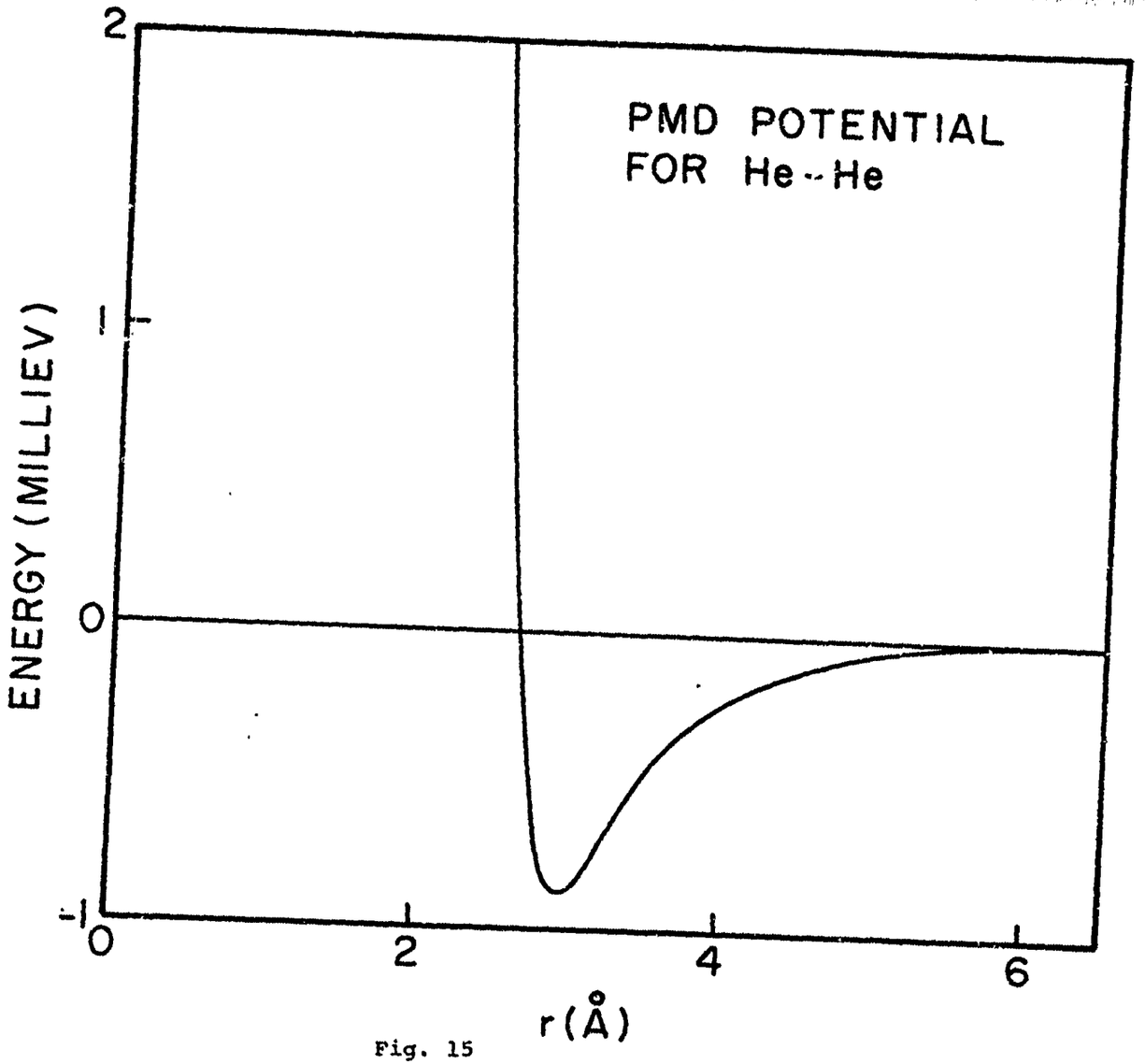

Fig. 15

PMD potential

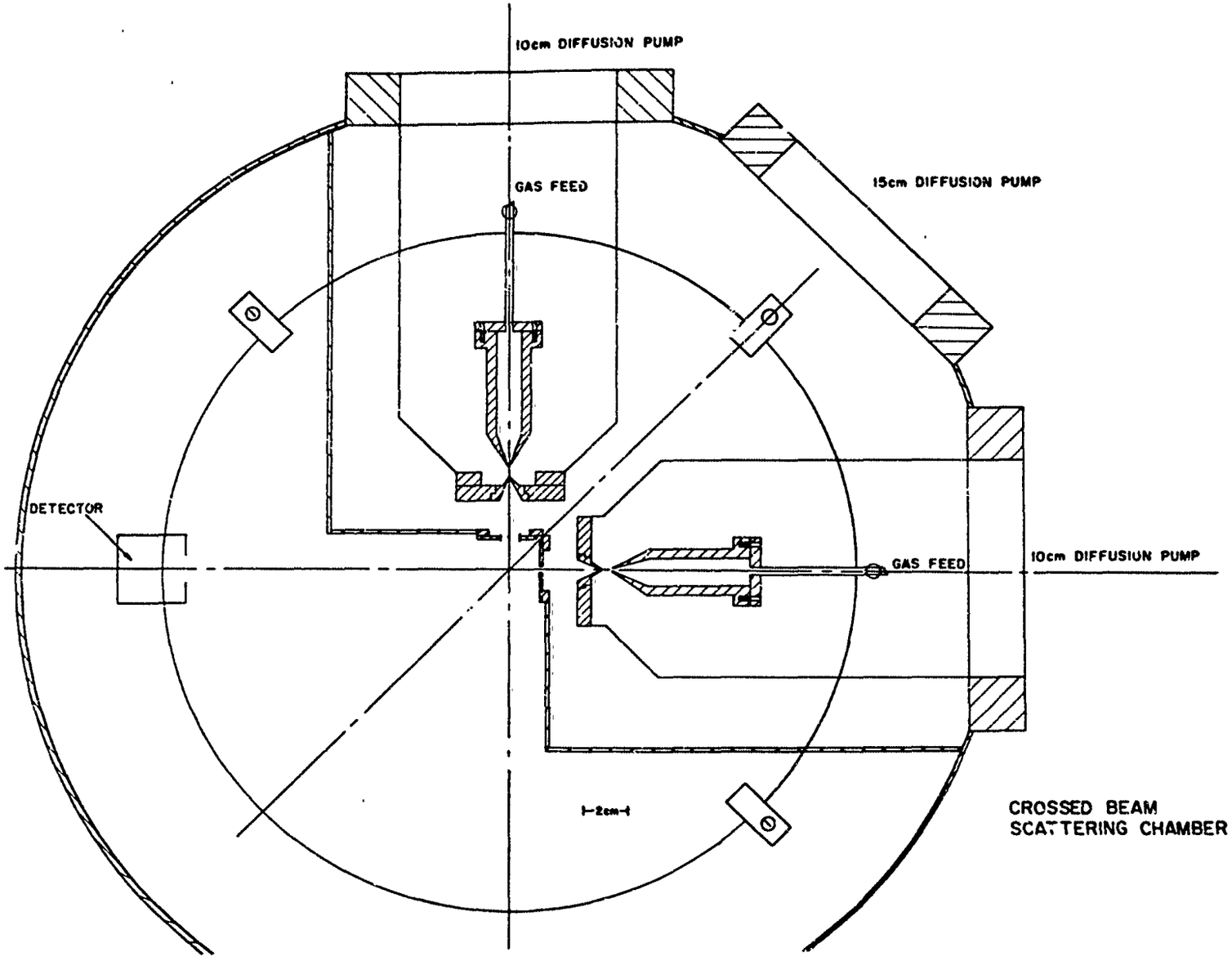

Fig. 16

Chamber for crossed molecular beams

$$\sigma_{eff} = \frac{u_0 \sigma(u_0)}{v_s} \left\{ 1 + \frac{1}{2\Lambda u_0^2} \left[1 + \frac{u_0 \sigma'(u_0)}{\sigma(u_0)} \right) \right\}$$

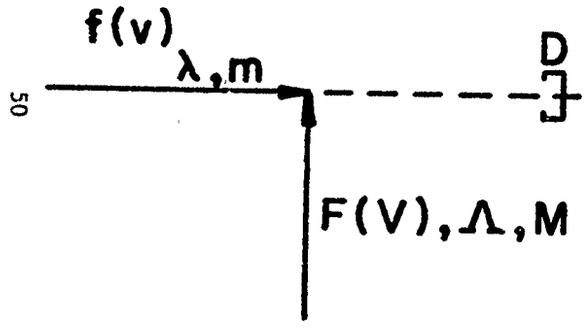

$f(v) \simeq v \exp[-\lambda(v-v_s)^2]$

$F(V) \sim V \exp[-\Lambda(V-V_s)^2]$

v_s = stream velocity of beam 1

V_s = stream velocity of beam 2

λ = velocity dispersion of beam 1

Λ = velocity dispersion of beam 2

u = relative velocity = $|\vec{v}-\vec{V}|$

$u_0 = (v_s^2 + V_s^2)^{1/2}$

$\sigma(u_0)$ = cross section in relative coordinates

Fig. 17

Schematic for crossed molecular beam experiment

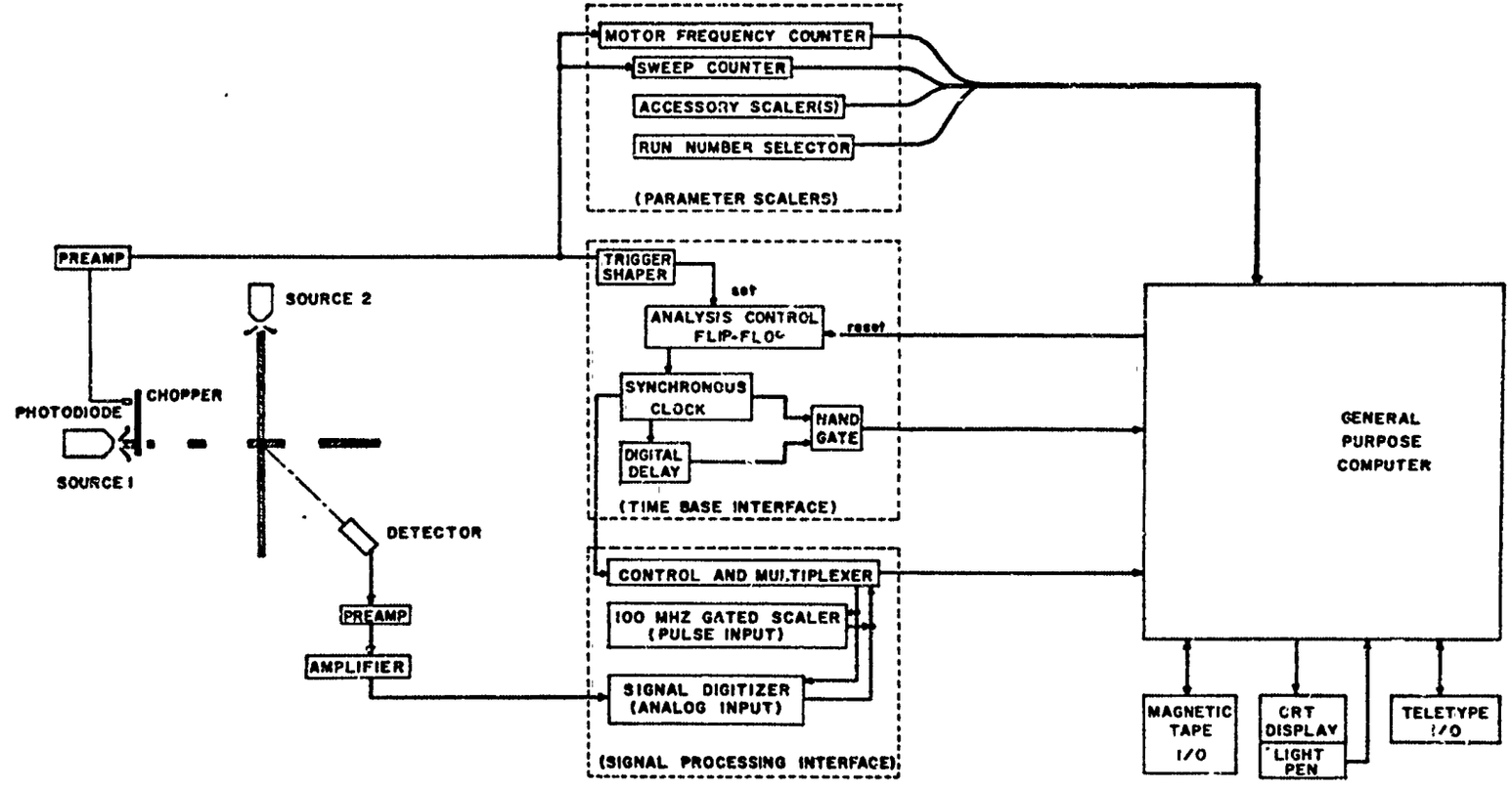

Fig. 18

On-line computer system for molecular collision physics research

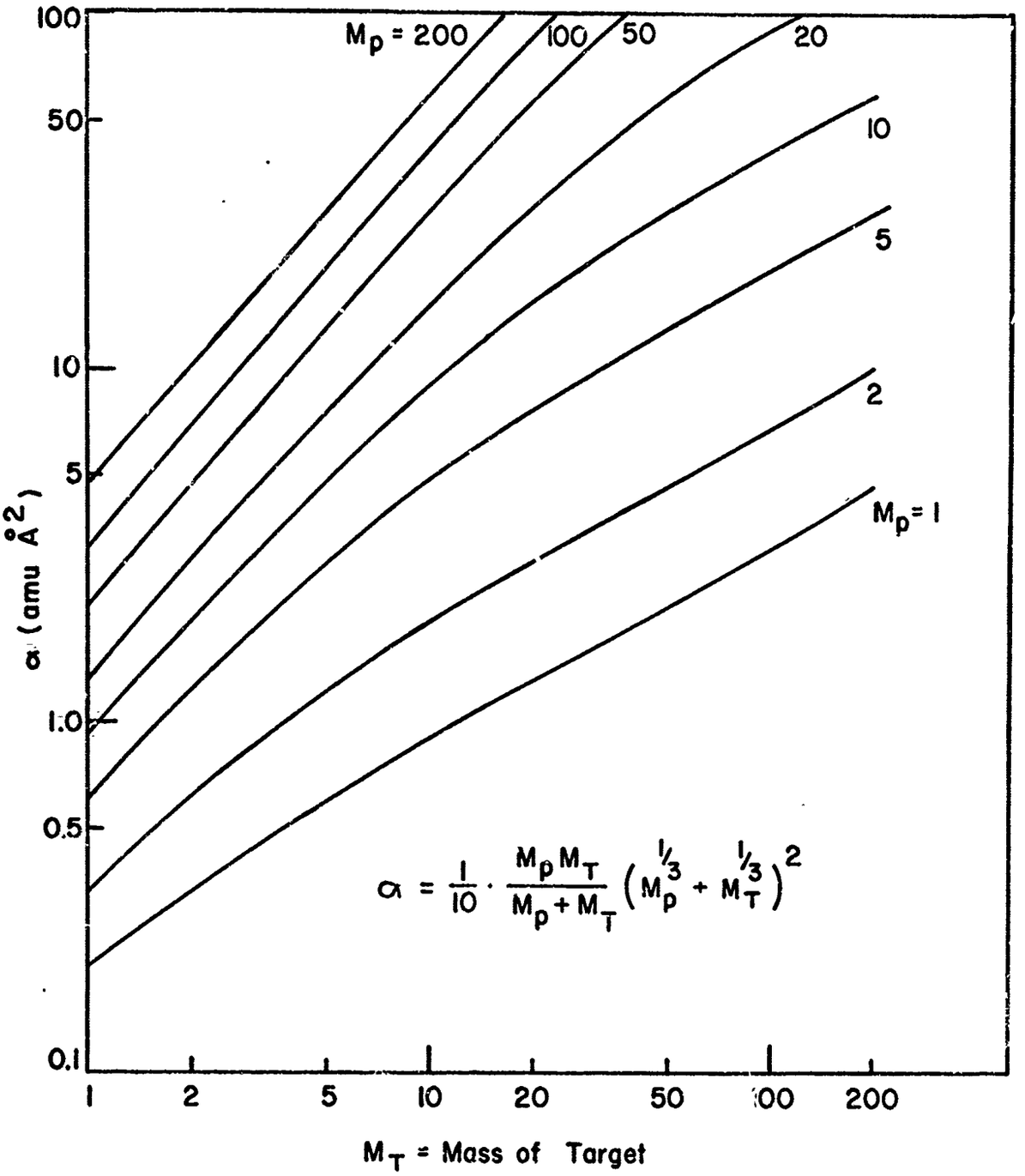

Plot of α against M_t and M_p

Fig. 19

$$\alpha = \frac{M_1 M_2}{(M_1 + M_2)} (M_1^{1/3} + M_2^{1/3}) \times 10^{-1} \quad (\text{Å}^2 \times \text{hydrogen mass units})$$

$\alpha = .209\ E^{-1}\ (\rho = 10)$ $\qquad \alpha = 30E/\Gamma^2$

$= 20.9\ E^{-1}\ (\rho = 100)$ $\qquad \Gamma = 2\rho\gamma^2$

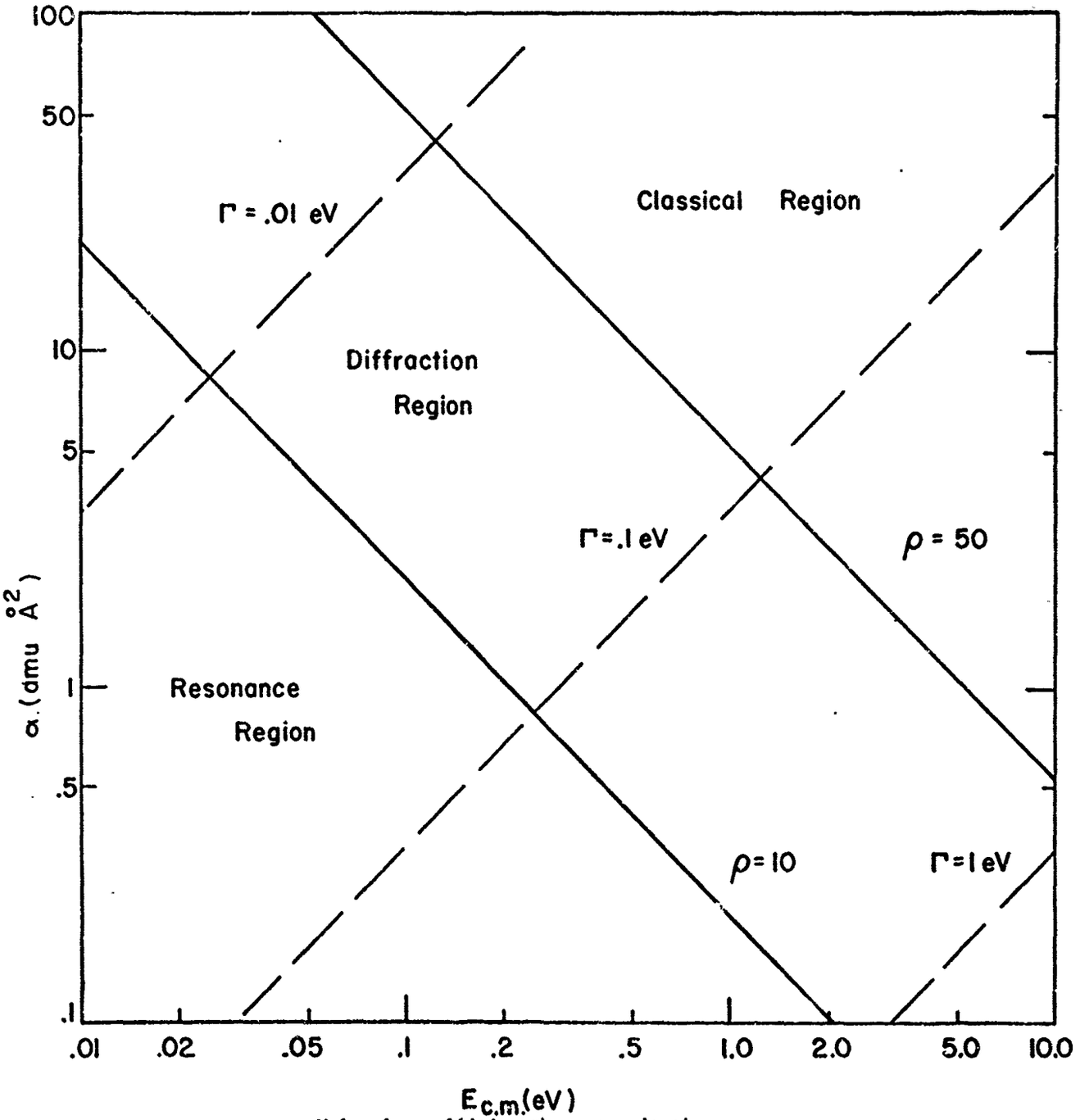

Molecular collision phenomena domains

Fig 20

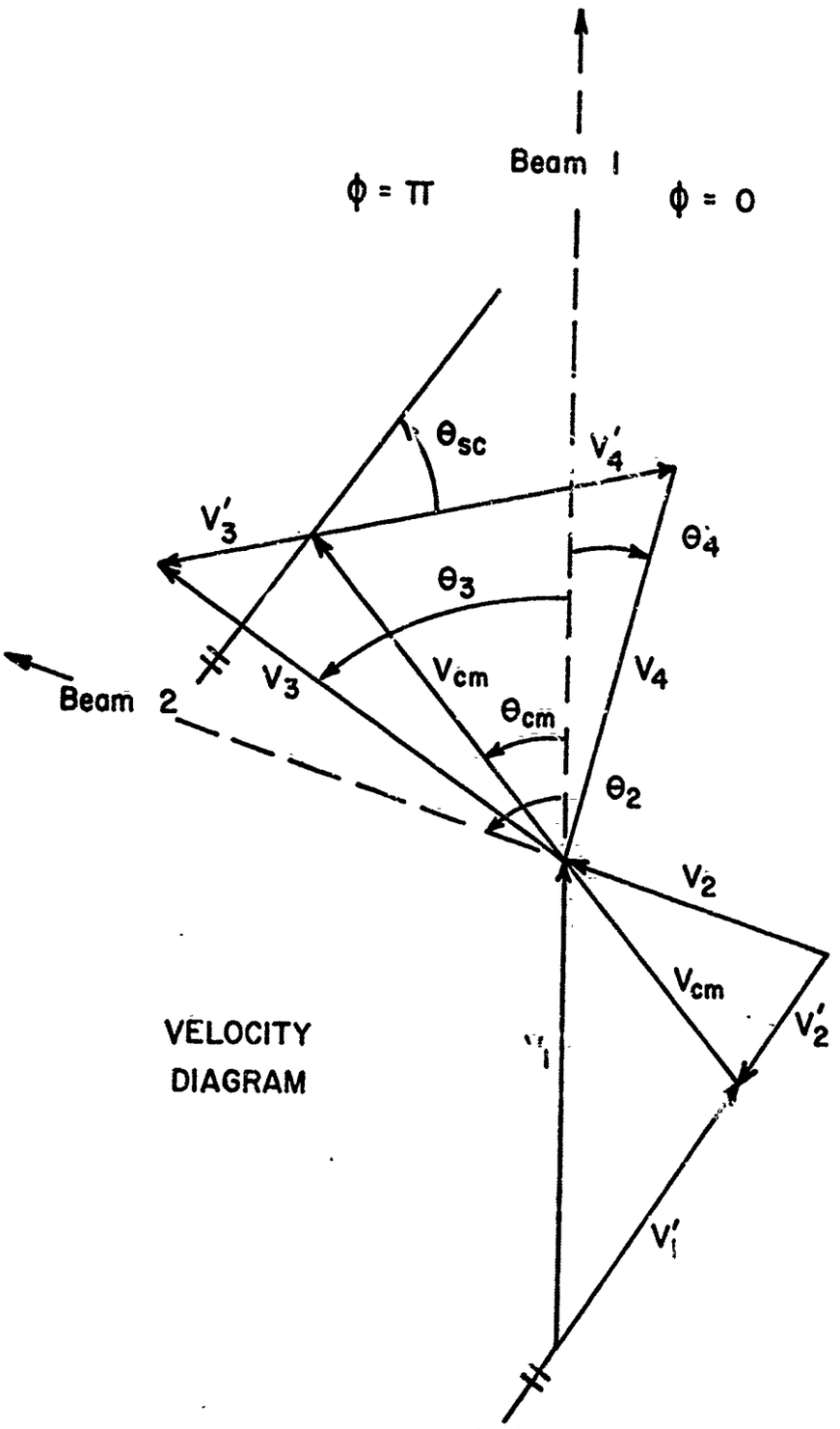

Velocity diagram

Fig. 21

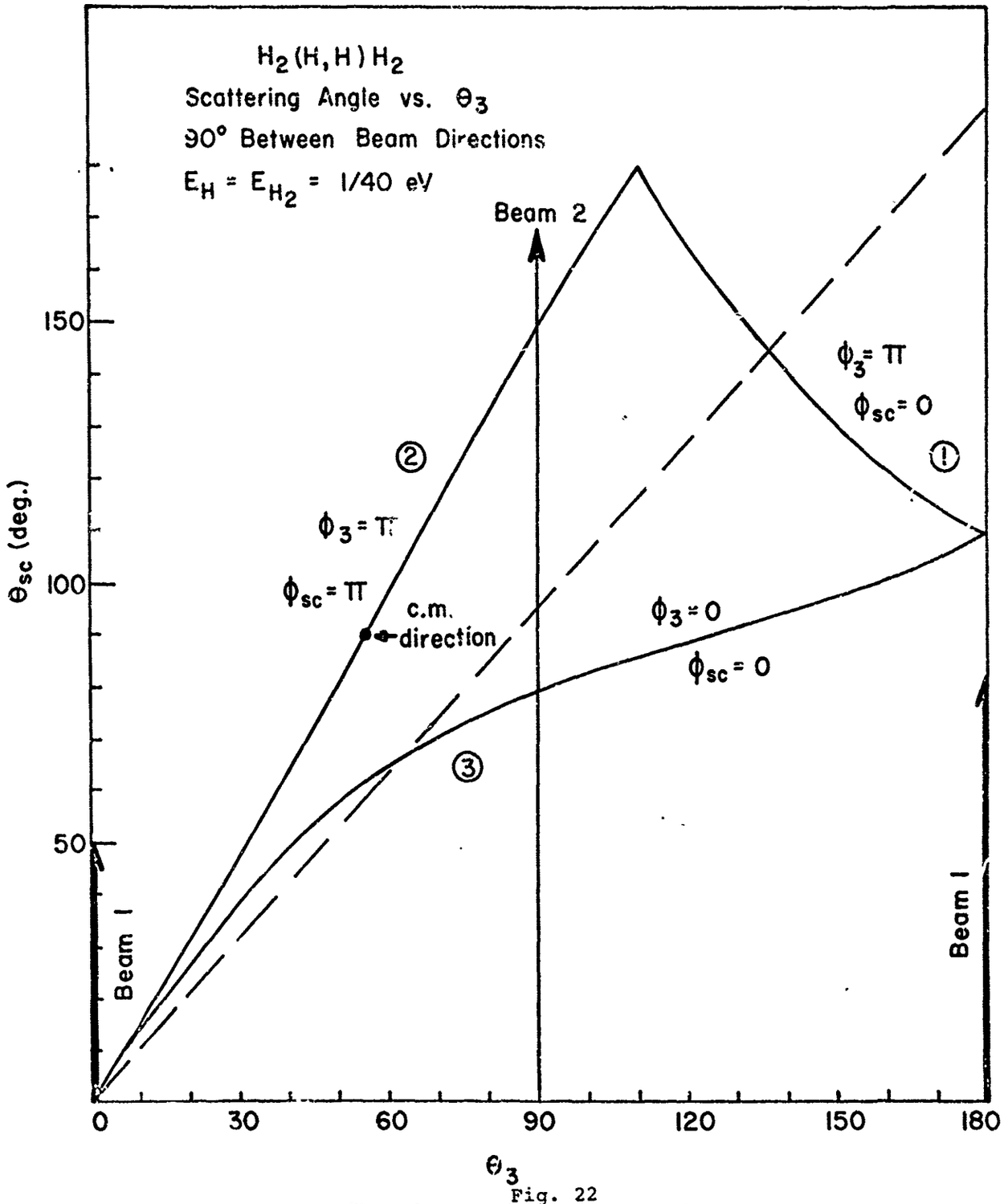

Fig. 22
Plot of scattering angle versus θ_3

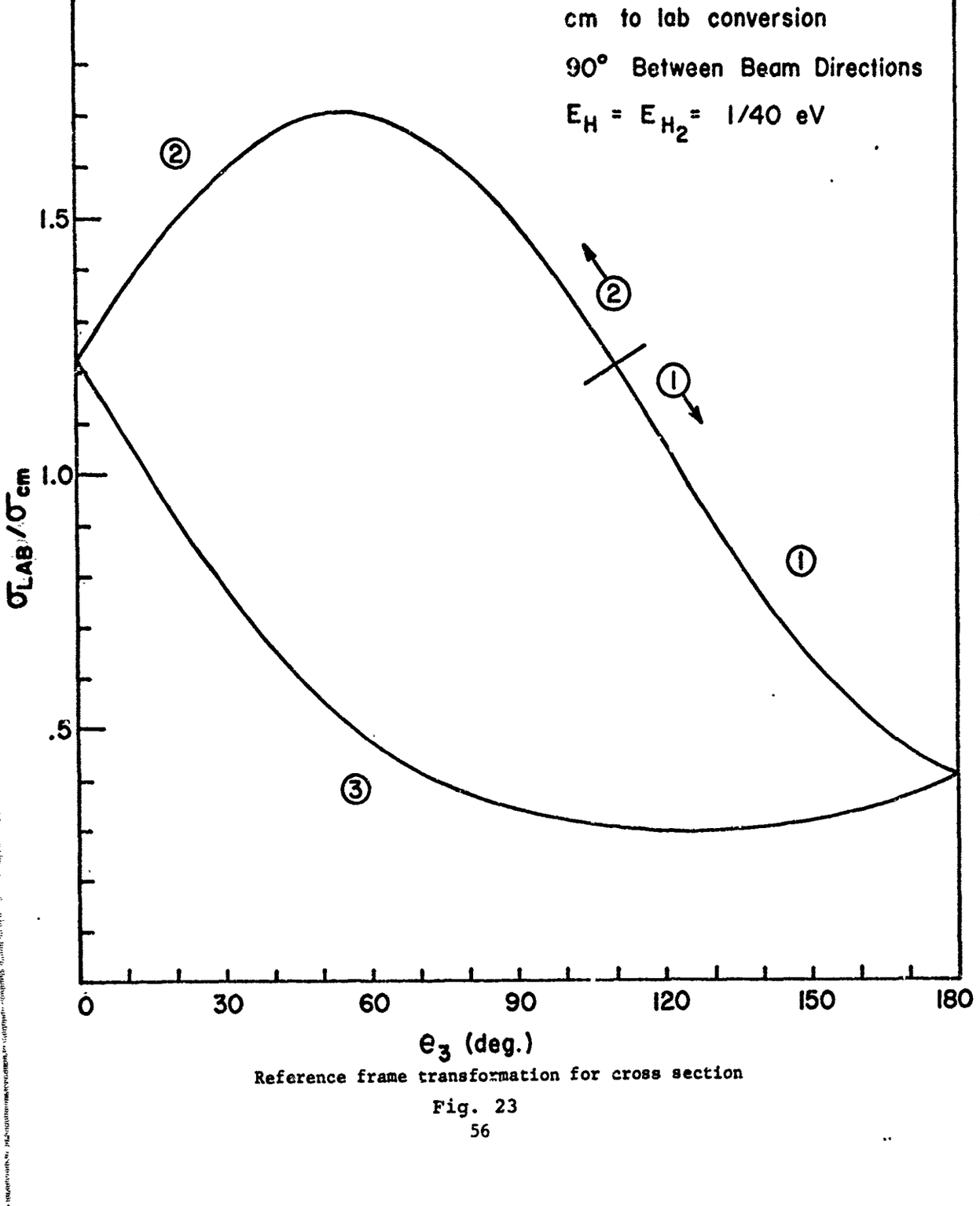

Reference frame transformation for cross section

Fig. 23

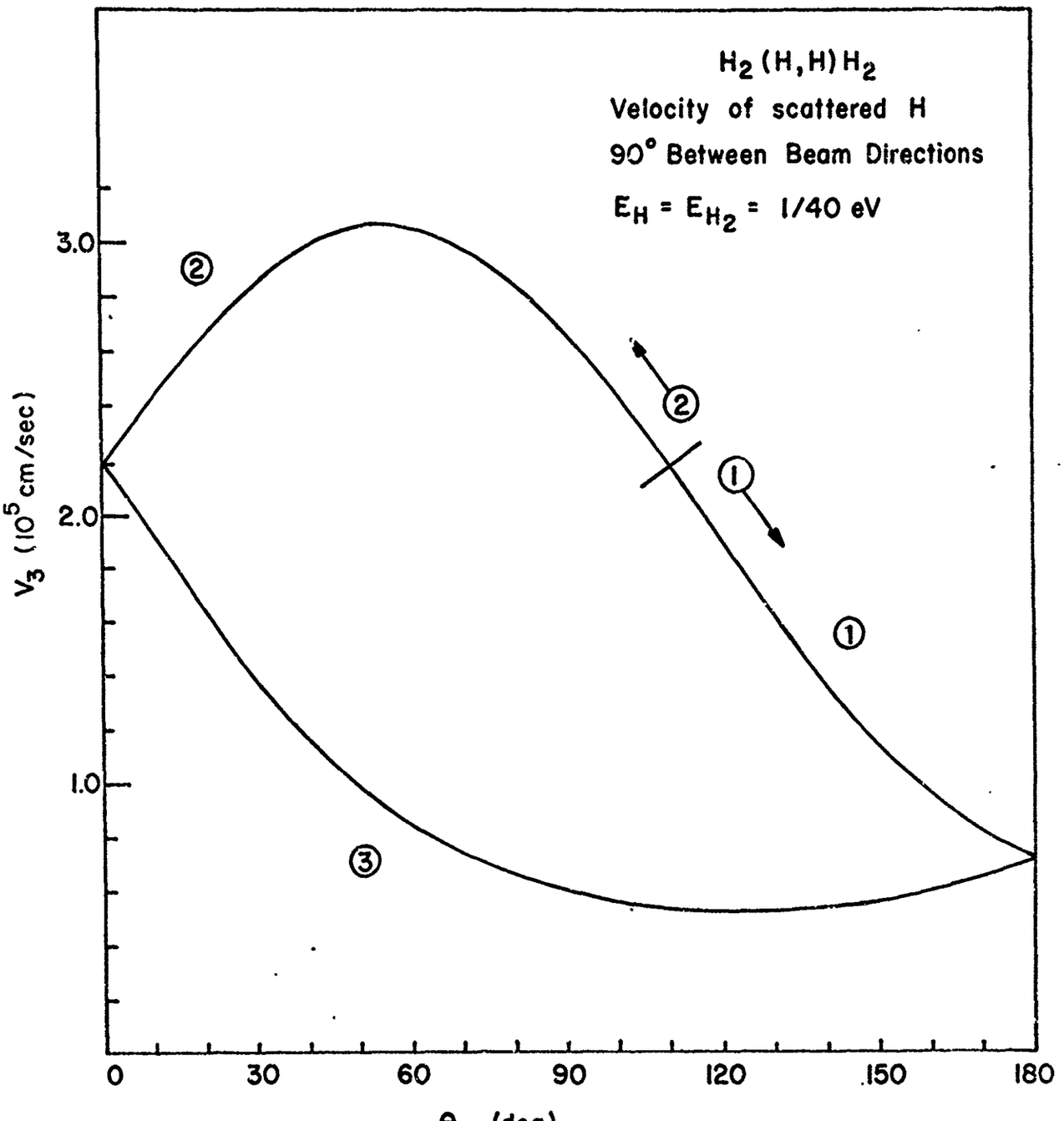

Velocity of scattered H as a function of θ_3

Fig. 24

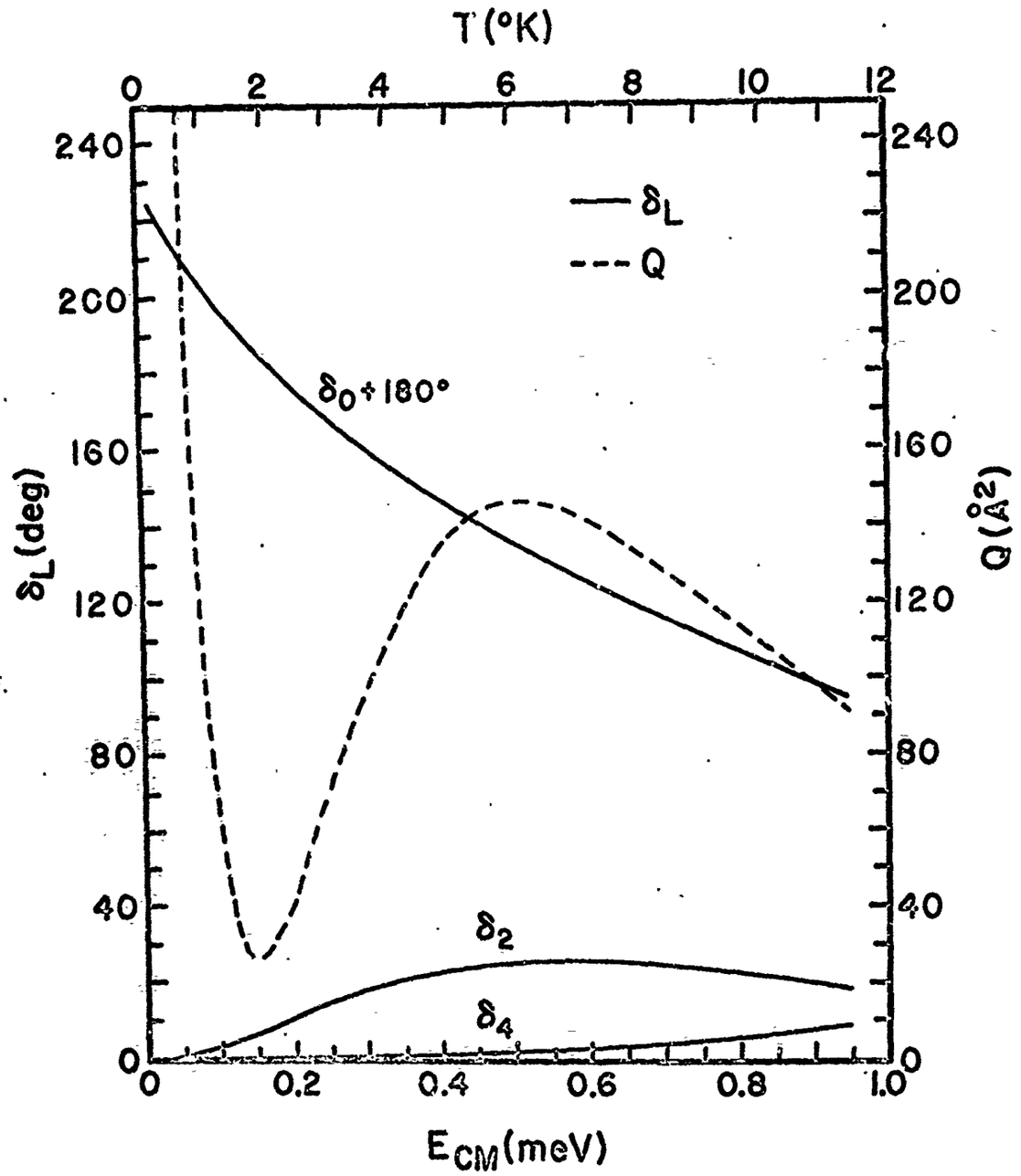

Computed total cross section and phase shifts for helium-helium scattering at low energies

Fig. 25

Electronic Structure and Chemical Instability of Explosives*

Ferd Williams
Physics Department, University of Delaware

ABSTRACT

After briefly reviewing some experimental results which indicate that electronic states and electronic mechanisms have an influence on chemical instability, we consider the problem theoretically and find that, in an extension of the quantum mechanical adiabatic approximation, the dynamics of atomic motion during a detonation are governed by an effective potential whose dominant term is the electronic energy eigenvalues which are dependent on the atomic coordinates. The range of validity of the approximations used in thus establishing a relation between electronic structure and chemical instability is discussed. We consider the electronic states, and electron and exciton transport, in the region of the detonation front and conclude that the gradient in the energy bands arising from the large pressure gradient and the resulting anisotropic electronic transport may have, in some materials, appreciable effects on initiation. Representative primary and secondary explosives are then considered from the point of view of modifications of their electronic states or of their Fermi levels in order to alter explosive characteristics. Finally, we suggest the following: single crystal explosives detonated by electronic mechanisms, homogeneous mixed crystals with intermediate detonation characteristics, and inhomogeneous graded mixed crystals with nonsteady state and unidirectional characteristics.

---

* Prepared for Explosives Chemical Seminar at Army Research Office-Durham, October 21, 1968.

I. Introduction

In this paper we shall consider the possible effects of the electronic structure of molecules and crystals on the chemical instability, and actually the detonation, of explosives. The analysis will be necessarily preliminary rather than rigorous and thorough, and will be sometimes superficial and occasionally speculative. This is perhaps appropriate for someone whose specialization is electronic structure of crystals and who has been invited to explore possible relevance to explosive phenomena. It also seems appropriate because of the lack of published works relating electronic structure to initiation and detonation.

The lack of published works on this subject arises for two reasons. First, the theory of the electronic structure and electronic transport has only recently become anywhere near adequate to cope with materials as complex as lead azide on one hand and 1, 3, 5, 7-tetranitro-1, 3, 5, 7-tetrazacyclooctane (HMX) on the other hand. Second, the hydrodynamic theory of detonations has been remarkably successful in explaining the velocities of detonations,[1] and initiation has been reasonably well explained in most cases as ultimately thermal in origin.[2]

II. Experimental Evidence for the Inter-relation of Electronic Structure and Chemical Instability

Nevertheless, there does appear to be experimental evidence that the electronic states, transitions and occupational probabilities of these states may be involved in the chemical decomposition of inorganic and organic materials, including explosives.

---

[1] Evans, M. W. and Ablow, C. M., Chem. Rev. 61, 129 (1961)

[2] Macek, A., Chem. Rev. 62, 41 (1961)

A classical example of chemical changes arising from electronic processes is the radiation damage of alkali halide crystals. Ionizing radiation generates atomic defects in these crystals, specifically halogen vacancies and halogen molecule negative ions, by electronic mechanisms.[3] These are genuine chemical changes in the sense of creating different molecular or structural entities. The generation of crystal defects by electronic mechanisms may occur in materials whose band gap E_g is large compared to the energy of formation of the defects E_d, because E_g is the maximum energy which is storable in electronic modes before atomic relaxation to form the defect. This requirement is not severe for explosives, in which E_d is negative for those defects involved in the decomposition. More immediately relevant to explosives than the radiation damage of alkali halides is the photo-decomposition of alkali and other metallic azides to form defects such as N_4^- and N_2^- observed in electron spin resonance by King et al,[4] Gilliam and co-workers,[5] Marinkas and Bartram,[6] and others. The photo-decomposition of silver halides and of organic dyes also involves electronic transitions.

The electronic states of crystals are dependent on crystal structure. Some inorganic explosives, for example, lead azide and many organic explosives, for example, TNT and HMX exist in several structures. The initiation

---

[3]Crawford, J. H., Advances in Physics 17, 93 (1968)

[4]King, G. J., et al, J. Chem. Phys. 32, 940 (1960); 34, 1499 (1961); 35, 1442 (1961)

[5]Gilliam, O. R., et al, J. Chem. Phys. 33, 622(1960); Phys. Rev. 125, 451 (1961)

[6]Marinkas, P. L. and Bartram, R. H., J. Chem. Phys. 48, 927 (1968)

characteristics for each of the polymorphs are found to be different. This may be explainable in terms of the differences in electronic states for the different crystal structures.

Finally, the effect of doping with charged impurities on the decomposition of explosives either through changes in the electronic energy levels or through changes in their occupational probability, i.e. Fermi level, is of interest. Fair and Forsyth[7] have reported changes in the photolytic decomposition of lead azide by doping with iron. They have correlated the decomposition with exciton and impurity absorption and photoconductivity, all three of which are purely electronic processes.

We shall, therefore, be concerned with relating electronic structure with chemical instability in the most general theoretical analyses, and with the following: the energy transport during detonation by electronic mechanisms, the possibility of initiation by nonthermal mechanisms, the origin of the difference in stability of organic and inorganic explosives, and electronic means for the possible more efficient use of the energy of explosives.

III. General Theory Relating Electronic Structure to Chemical Instability

Matter consists of electrons and atomic nuclei. We specify the spatial and spin coordinates of the i-electron by $\underline{\xi}_i$ and the spatial coordinates of the j-nucleus by $\underline{R}_j$. According to quantum mechanics a system in a state is described as completely as is possible by a wave function which is a function of the coordinates of all the particles. In general the wave

---

[7] Fair, H. D., Jr. and Forsyth, A. C. Sixth International Symposium on Reactivity of Solids, August, 1968, Schenectady (To be published).

function is also time-dependent, however, we shall be concerned in this analysis with stationary states and with the solutions of the time-independent Schrodinger equation. The time-dependence of the chemical reaction will be taken care of through transitions between stationary states. For a system of n electrons and N nuclei we have the many particle wave function:

$$\psi(\underline{\xi}_1,\underline{\xi}_2,\cdots \underline{\xi}_n,\underline{R}_1,\underline{R}_2,\cdots\cdot\underline{R}_N) \equiv \psi(\underline{\xi},\underline{R}), \qquad (1)$$

where the dependence on $\underline{\xi}$ and $\underline{R}$ indicates the dependence on all electronic and nuclear coordinates, a notation we shall now follow. The many particle wave function satisfies the Schrodinger equation:

$$\hat{H}\ \psi\ (\underline{\xi},\underline{R}) = E\ \psi\ (\underline{\xi},\underline{R}), \qquad (2)$$

where $\hat{H}$ is the Hamiltonian operator involving terms for the kinetic energies of all particles and for all electrostatic interactions, and E are the energy eigenvalues.

From the difference in mass of the electrons m and of the nuclei M_j and from equipartition of energy, it is evident that the electrons move rapidly compared to the nuclei and, therefore, will exist in separable, approximate stationary states which are smoothly modified by the motion of the nuclei. This is of course the well-known adiabatic approximation of Born and Oppenheimer.[8] In order to solve for these electronic stationary states we consider the nuclei fixed in the following Schrodinger equation:

$$\hat{H}_{el}\ \ \Phi_{\underline{R}}(\underline{\xi}) = E_{el}(\underline{R})\ \Phi_{\underline{R}}(\underline{\xi}), \qquad (3)$$

---

[8]Born, M. and Oppenheimer, R., Ann. of Phys. 84, 457 (1927)

where $\hat{H}_{el}$ is the part of $\hat{H}$ which involves electronic coordinates, $\underline{R}$ specifies the fixed $\underline{R}_1 \ldots \underline{R}_n$, and $E_{el}(\underline{R})$ are the electronic eigenvalues or electronic structure which are of course dependent on $\underline{R}$. Again, in accordance with the adiabatic approximation we take ψ to be the following form:

$$\psi(\underline{\xi},\underline{R}) = \phi_{\underline{R}}(\underline{\xi})\ \chi(\underline{R}). \tag{4}$$

Substituting Eq. 4 in Eq. 2 and using Eq. 3, we obtain the following for the Schrodinger equation which governs the motion of the nuclei, if we neglect two terms to be discussed later:

$$\left\{ -\sum_j \frac{\hbar^2}{2M_j} \Delta_{\underline{R}_j} + V(\underline{R}) + E_{el}(\underline{R}) \right\} \chi(\underline{R}) = E\chi(\underline{R}) \tag{5}$$

where $\Delta_{\underline{R}}$ is the Laplacian and $V(\underline{R})$ is the direct interaction between nuclei. The important conclusion, however, is that the electronic structure $E_{el}(\underline{R})$ is a major term in the effective potential which governs the motion of the nuclei. In the usual application of Eq. 5 only displacements in $\underline{R}$ about equilibrium sites are involved. For the large excursions in $\underline{R}$ occurring during chemical reactions, the approximations must be re-examined. It is expected, however, that $E_{el}(\underline{R})$ will persist in the effective potential for the motion of nuclei even during detonations. We believe that the initial assumption of the slow motion of nuclei versus rapid motion of electrons remains approximately valid for detonations. For typical electronic states of molecules and solids, $E_{el} \geq 1$ eV, and therefore the orbital time for electronic motion $\tau_0 \leq 10^{-15}$ sec, which is shorter than any process occurring in a detonation. For example, for shock velocities $v_s = 10^6$ cm/sec the time to transverse an atomic layer $\tau \approx 10^{-14}$ sec. The departure from stationary electronic states is actually one of the terms neglected in obtaining Eq. 5, and this term can be shown to be of order $\frac{m}{M}$ compared to terms retained.

The other term neglected in obtaining Eq. 5 is the following:

$$\sum_j \frac{\hbar^2}{M_j} \{\nabla_{\underline{R}} \phi_{\underline{R}}(\xi) \nabla_{\underline{R}} \chi(\underline{R})\}. \qquad (6)$$

The diagonal elements in the matrix formulation of this term vanish if the number of electrons is conserved, as is the case for non-nuclear reactions. The off-diagonal elements correspond to electron-phonon interaction. Further analysis is necessary to determine whether phonons remain a valid concept or whether Eq. 6 diverges in the chaos of the detonation.

We shall continue, assuming Eq. 5 to be approximately valid as the basis for Fig. 1. The effective potential

$$V_{eff} = V(\underline{R}) + E_{el}(\underline{R}) \qquad (7)$$

is plotted versus the nuclear coordinates or reaction coordinates $\underline{R}$. Because of the double minima the eigenstates $\chi(\underline{R})$ for the system are not in general simple oscillator functions. They are however bound states because $V_{eff} \to \infty$ at the extrema of $\underline{R}$. The reaction is visualized as proceeding from an initial "clamped" state to the final equilibrium state by the perturbation from electron-phonon interaction. The initial and final states are describable as linear combinations of the complete set of $\chi(\underline{R})$. The electronic states $E_{el}(\underline{R})$ at all intermediate configurations $\underline{R}$ between the initial and final configurations are of course involved in determining the $\chi(\underline{R})$. To reduce somewhat the complexity of the problem, the core electrons which survive the reaction unchanged can be grouped on their respective nuclei and $V(\underline{R})$ taken as the ion-ion interaction. In any case, it is evident from Eq. 5 and Fig. 1 that the electronic structure $E_{el}(\underline{R})$ plays an important role in chemical reactions, including detonations.

IV. Electronic States and Electronic Transport in the Region of the Shock Front

The classic theory of detonations of Doering, von Neumann and Zeldovich (see footnote 1 for original references) considered the shock and chemical reaction zones separate; the pressure wave heating the unreacted explosive so that the reaction occurs thermally after an induction period. Hirschfelder and co-workers[9] and Wood[10] investigated the effects of coupling of the shock and reaction zones. We are concerned with the electronic structure in the region of the shock front and with possible electronic transport getting ahead of the shock and contributing to initiation.

We therefore look at the details fore and aft of the shock front in condensed explosives. Ilynkhin and co-workers[11] give the shock velocities v_s, the pressure behind the shock front P, and the ratio of specific volumes after and before shock compression V/V_0 for cast TNT, crystalline RDX and nitromethane. These quantities are approximately 5×10^5 cm/sec, 10^5 atm and 0.7 for these explosives. The important observation to be made is that the electronic structure $E_{el}(\underline{R})$ in the region of shock compression is in general quite different than for the uncompressed explosive. As noted earlier, the electronic states are approximately stationary at shock velocities. The initial predictions for most explosives are that the allowed electronic bands are wider, the forbidden energy gap narrower and all states

---

[9] Hirschfelder, J. et al, J. Chem. Phys. 28, 1130, 1147 (1958); 30, 470 (1959)

[10] Wood, W. W., Phys. Fluids 4, 46 (1961)

[11] Ilynkhin et al, Dokl. Akad. Nauk 13, 793 (1966)

are perturbed towards the vacuum level in the high pressure region. The first prediction is evident for organic explosives because the overlap of the molecular wave functions is increased by compression; the last, from consideration of the increase in kinetic energy of the electrons confined to the smaller volume.

The second feature of the region of the shock front with which we are concerned is the spatial dependence of the electronic structure. If the pressure gradient is only over one or two molecular distances, then we are dealing with an abrupt semiconductor heterojunction whose electronic transport properties are largely determined by space charge effects; if the pressure gradient at the shock front extends over at least 100 molecular distance then, as was shown by Gora and Williams[12] for graded mixed crystals, the concept of a graded band gap is valid. Craig[13] estimated the reaction zone length for nitromethane at 10^{-5} cm from extrapolation of the equation of state for the unreacted material and from thermodynamic adiabatic (not quantum mechanical) explosion theory. The shock front is probably thinner, therefore, we take $\ell \approx 10^{-6}$ cm as an estimate of the length of the pressure gradient and consider the system as having graded band edges. More quantitative determinations of the width of the pressure gradient and of the electronic structure in the high pressure region are needed for typical solid explosives. Fig. 2 includes estimates of these two features of the electronic states in the region of the shock front.

---

[12]Gora, T. and Williams, F. II-VI Compound Semiconductors (Benjamin Press, 1967) p. 639

[13]Craig, B. G. Tenth Symposium on Combustion (1965) p. 863

We now consider electronic transport in the region of the detonation front. The following analysis applies to conduction electrons or to positive holes in the valence band and with straightforward modifications to coupled electrons and positive holes (excitons). The component of the current density arising from ordinary diffusion is:

$$J_D = nv_D = -D \frac{dn}{dx}, \tag{8}$$

where n is the carrier concentration, v_D is the diffusion velocity and D is the diffusion constant. Our primary concern is with the order of magnitude of velocities compared to shock velocities v_s, therefore:

$$v_D \simeq - D \frac{n-n_o}{n} \cdot \frac{1}{\ell}, \tag{9}$$

and for negligible charge carriers in front of the shock we have $n_o << n$. Using the Einstein relation $D = \frac{kT}{e} \mu$, Eq. 9 can be solved in terms of the mobility μ. For an order of magnitude calculation we take $\mu \approx 1$ cm^2/Vsec, typical for a very poor inorganic semiconductor and for a good organic semiconductor, $\ell \approx 10^{-6}$ cm as estimated previously and $T \approx 3000°K$, and obtain $v_D \sim 2 \times 10^5$ cm/sec which is the magnitude of but less than v_s. Incidentally, μ is reduced by the high temperature but increased by the high pressure (10^5 atmospheres); the latter is particularly pronounced for organic semiconductors. A value of μ for the conditions at the shock front of the magnitude observed at ordinary temperatures and pressures for good inorganic semiconductors, i.e. 10^4 cm^2/Vsec, would obviously result in the electronic excitation outrunning the shock wave.

In addition to the ordinary diffusion current, there is an additional anisotropic current arising from diffusional effects in systems with graded

band edges such as shown in Fig. 2. Van Ruyven and Williams[14] derived this anisotropic diffusional component of the current density:

$$J_A = nv_A = -\frac{D}{kT} n \frac{dE(x)}{dx} \qquad (10)$$

where E(x) is the position-dependent band edge for the n electronic carriers. For the same hypothetical system just analyzed for v_D and with $E - E_o$ estimated as 2 eV from considering the change in energy levels of an electron in a box of molecular dimension on compression ($V/V_o \approx 0.7$), we find $v_A \sim 2 \times 10^6$ cm/sec. This exceeds v_s. In general, for $n_o << n$, v_A exceeds v_D by the factor $\frac{E-E_o}{kT}$.

In order to have the electrons, positive holes or excitons, which are generated in the detonation region, precede the shock front and conceivably contribute to initiation, it is also necessary that their lifetime τ_e exceed the threshold value $\ell/v_A \approx 10^{-12}$ sec. This requirement does not appear to be severe.

The anisotropic diffusion of electrons or positive holes in advance of the shock front will yield a space charge and result in an electric field traveling with the shock front. This effect which arises from the graded band edges may explain the voltages measured in shocks. For example, the observations of Eichelberger and Hauver[15] of shock-induced electrical polarization in distilled water may originate from graded band edges, probably for the states involved in protonic conduction.

---

[14] Van Ruyven, L. J. and Williams, F. E., Am. J. Phys. 35, 705 (1967)

[15] Eichelberger, R. J. and Hauver, G. E., Les Ondes de Detonation, Paris CNRS, p. 363 (1962)

In general, any theory of electronic effects in a detonation must include the effects of the graded band edges such as shown in Fig. 2. In addition to band edge transport, electron tunneling is also shown and would be included in a more complete analysis.

V. Electronic States, Fermi Levels and Decomposition of Representative Explosives

As a representative primary explosive, we shall consider lead azide; as a representative secondary, HMX. Both are important militarily; both are challenging scientifically. It now seems that single crystals of both materials can be prepared and used for measurements of electronic properties. We shall consider in a preliminary way a few aspects of their electronic states and the occupational probability of these states, as described by the Fermi level, relevant to the decomposition of these materials.

Perhaps the most striking feature of a preliminary consideration of the electronic states of lead azide is the diversity of types of excitons which it may have. In addition to the charge transfer excitons, well-known in alkali halides, and effective mass excitons, well-known in elemental semiconductors, one predicts for PbN_6: intracation excitons (excited states of Pb^{+2}, ^1P and ^3P of the $1s^2 \ldots 5d^{10}6sGP$ configuration, modified by the complex crystal field of the PbN_6 structure) and intra-anion excitons (excited states of N_3^-). These offer possibilities for the transport of electronic energy.

Slow decomposition or initiation is predicted from Eq. 5 and illustrated in Fig. 1 to depend on occupied electronic states. The Fermi level is the energy of the state at the top of the electron distribution, or more

precisely, the energy for which the occupation probability is one-half. If we assume that during the early stages of decomposition, or during initiation, PbN_6 undergoes the following reaction:

$$2N_3^- \rightarrow 3N_2 + 2e^-, \qquad (11)$$

and that lead metal is not precipitated, then the electrons ($2e^-$) of Eq. 11 will be in the conduction band, perturbed, however, by the field of the [N_3^-] vacancies. The electrons will be in F-center bound states, the Fermi level will have risen, and the n-type electronic conductivity increased. The electronic states $E_{el}(\underline{R})$ in the effective potential V_{eff} of Eq. 7 which governs the motion of the nuclei in Eq. 5 will have changed. Higher $V_{eff}(\underline{R})$ functions on Fig. 1 should now dominate the chemical reaction. It is tempting to predict that initiation occurs rather generally by a rising Fermi level. The well-known memory effect in explosives subjected to repeated partial decomposition may be explainable by accumulated changes in the Fermi level.

Similarly, if both positive holes p^+ and electrons are electrically injected into PbN_6 (double injection), the Fermi level will also rise if the positive holes are removed by the reaction:

$$2N_3^- + 2p^+ \rightarrow 3N_2, \qquad (12)$$

and the compensating electrons occupy perturbed conduction band states. In other words, appropriate electronic injection can in principle achieve the same Fermi level change which may be essential to initiation.

HMX or 1, 3, 5, 7-tetranitro-1, 3, 5, 7-tetrazacyclooctane exists in four polymorphic forms. These are molecular crystals. Both intramolecular

excitons and intermolecular (charge transfer) excitons are predicted. Electronic charge transport depends on overlap of the molecular wavefunctions and is therefore enhanced by the pressures (10^5 atmospheres) in the shock wave during detonation. The mobilities of both types of excitons are also enhanced by pressure.

Surya Bulusu, et al[16] have determined with isotopes that the thermal degradation of HMX proceeds by breakage of C-N bonds. It is important to determine whether charged intermediates are formed during decomposition, and even during detonation, because these would change the Fermi level.

VI. Homogeneous and Graded Mixed Crystals

It is well known in semiconductor physics that most homogeneous mixed crystals of semiconductors have electronic bands intermediate between those of the pure components. This can be explained theoretically on the basis of the virtual crystal approximation, in which the statistical distributions of unit cells in the random alloy are replaced by an average unit cell. Because the de Broglie wavelength for the electron is large compared to unit cell dimensions, the electron responds to the field of the average cell and has the corresponding band structure. To the extent, therefore, that the electronic states influence initiation or detonation, mixed crystal explosives may offer interesting intermediate characteristics. For example, within the constraints of solubility limitations due to differences in crystal structures of copper azide and sodium azide, $Cu_fNa_{1-f}N_3$ may warrant experimental studies.

---

[16] Bulusu, Surya, et al, West Point Conference on Army Materiel Command

In addition, mixed semiconductors with graded compositions have, as described earlier relevant to gradations due to pressure, graded electronic properties, for example, graded band gaps.[14] A graded mixed crystal explosive should have predictable, nonsteady state, detonation characteristics. The nonsteady time dependence and partial directionality of the detonation may permit greater utilization of the energy of the reaction.

VII. Concluding Remarks

In conclusion we emphasize that there are two points of view that can be taken regarding the impact that investigations of electronic structure and transport may have on explosives research. The first which is emphasized in this paper concerns the understanding of phenomena well-known for conventional explosives; the second which is quite speculative concerns the investigation of qualitatively different phenomena and materials relevant to initiation and detonation as a consequence of detailed consideration of electronic processes.

VIII. Acknowledgements

I am indebted to Dr. R. S. Eichelberger for stimulating my interest in preparing this paper, to Drs. J. Hershkowitz, S. J. Jacobs, and R. F. Walker for bringing to my attention many of the references used in preparing this paper, and to Drs. H. Fair and J. Hershkowitz for helpful and critical observations of an early version of the presentation. Helpful discussions with Professor A. Halprin on the adiabatic approximation and with Mr. R. B. Hall on transport are acknowledged.

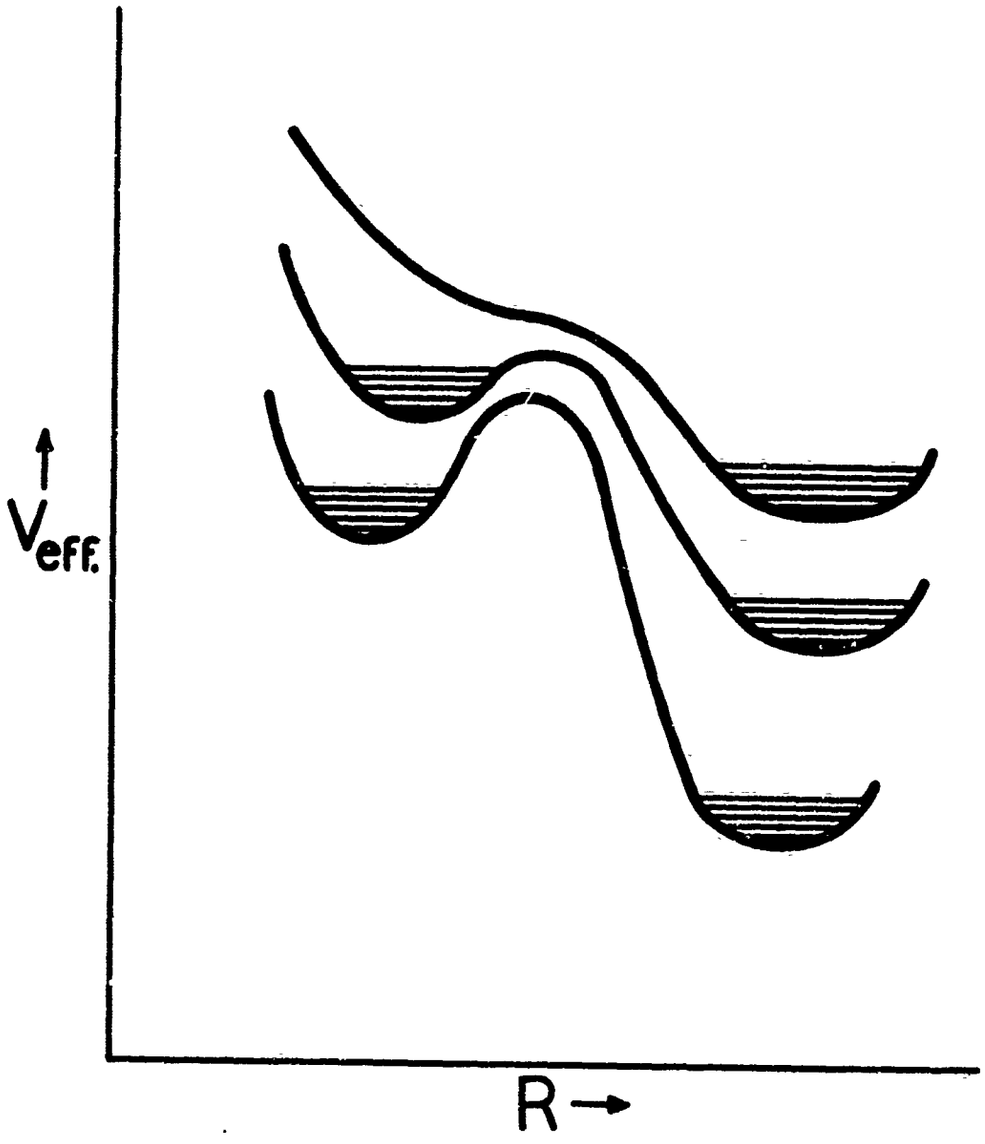

Figure 1

Effective potential for atomic motion during detonation versus generalized reaction coordinate. Different curves correspond to different electronic states; vibrational levels for initial and final configurations are also shown.

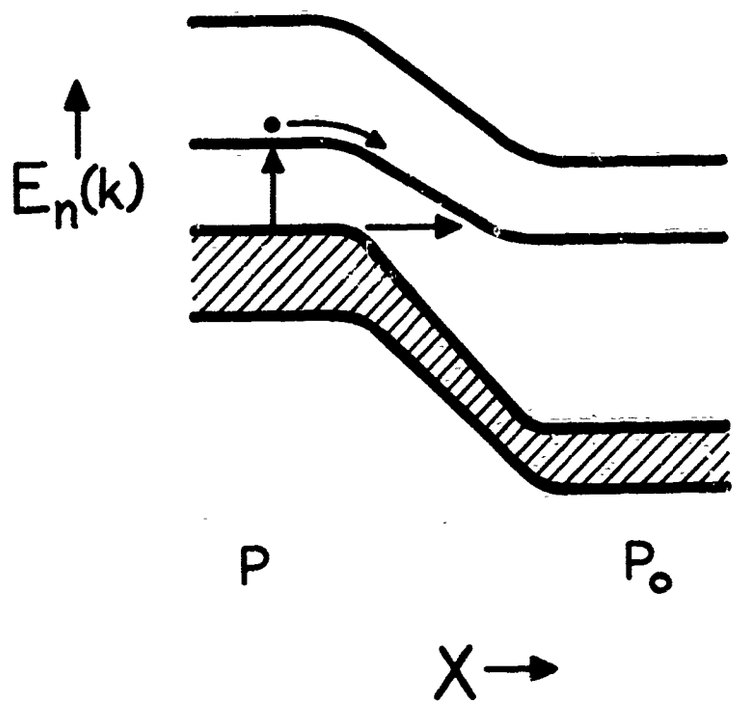

Figure 2

Probable electronic structure of unreacted explosive versus direction through shock front. The pressure fore and aft the front are respectively p_o and p; electronic transitions, transport and tunneling are also shown.

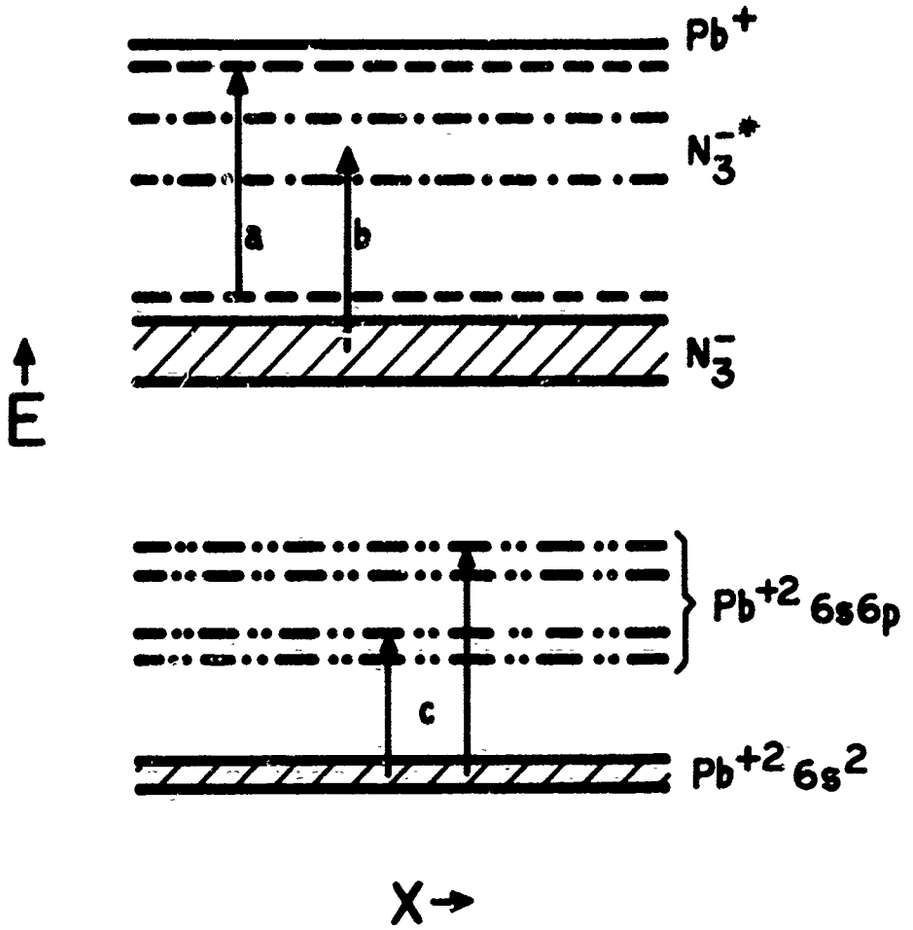

Figure 3

Approximate electronic energy level structure of lead azide. Transitions for creation of the following excitons are included: Effective mass excitons, a; intra-anion excitons, b; and intracation, c.

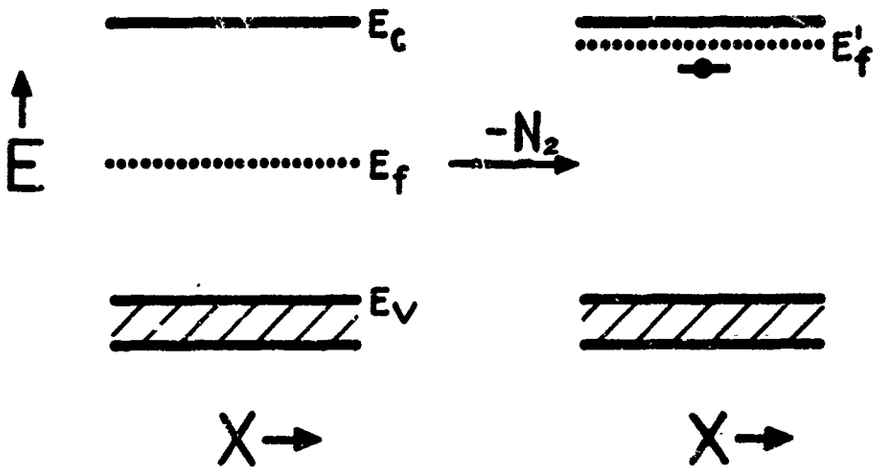

Figure 4

Change in Fermi level of lead azide accompanying decomposition:

$2N_3^- \rightarrow 3N_2 + 2e^-$.

PARTICLE WAVES AND DETONATION IN CRYSTALLINE SOLIDS

Particle Waves

and

Detonation in Crystalline Solids

(A wave-mechanical explanation of detonation)

by

Edwin R. Fitzgerald

Walnut Hill Farms
Baltimore County, Maryland

Introduction

1. Particle waves and momentum transfer

2. High-velocity impact in monatomic crystals

   a) The effect of lattice motion

   b) Phonon fission

3. Momentum transfer and impact in diatomic crystals

4. Detonation by impact

5. Comparison with some experimental results

   a) Non-elastic deformation

   b) Detonation

Conclusions

Introduction

A connection between the propagation of particle waves and deformation in crystalline solids has been presented in earlier publications[1,2]. In general the nonelastic deformations of such solids are considered to result from the motion of certain initially field-free or "free" atoms in a solid in very loose analogy with the free electron theory of conduction. These atoms, moreover, are supposed to move through a crystal as particle momentum waves with wave lengths calculated from the de Broglie relation $\lambda = h/mv_i$; v_i is the final velocity acquired by the free atoms just before they pass beyond their initial field-free regions, h is Planck's constant, and m is the atomic mass. A schematic representation of both external and internal field-free atoms in relation to a crystal lattice is shown in Fig. 1. The internal field-free atom of Fig. 1b is, of course, no longer field-free if a stress, Y_o, is produced in the crystal by an external load. Instead such an atom will now be subjected to a force, $F_i = Y_o/\zeta$, where ζ is the number of atoms per cross sectional area in the region of the stress.

An atom located in an initial field-free region of width pd in the direction of the force will then be accelerated as a particle until it reaches the end of the field-free region; after this it (or its momentum) propagates through the crystal as a particle wave with a wavelength determined by the final velocity as already stated. By equating the work done, by the force F_i through the distance pd , to the final kinetic energy of the particle and using the de Broglie relation for a free particle, a relation between the external stress applied to a crystal and the wavelength of the resulting particle momentum wave is obtained[2],

$$\lambda = h\sqrt{\frac{\zeta}{2pmdY_o}} \qquad \ldots\ (1)$$

The parameter, p, which defines a particular initially field-free region ($s = pd$) is the only new atomic constant introduced in Eq. 1; its value is generally taken to be less than one as indicated in Fig. 1. Moreover, in some cases, final expressions for macroscopic mechanical quantities are independent of p, and the quantities are functions only of known atomic constants[2].

These ideas on the propagation of particle momentum waves and their role in nonelastic deformation are made more specific by the assumption of a differential equation for momentum transfer. For example, in a one-dimensional monatomic row lattice (cf. Fig. 2) conservation of momentum among any three adjacent masses requires that[2]

$$\frac{\partial(mv_n)}{\partial t} = \frac{i\hbar}{2d^2}(v_{n+1} + v_{n-1} - 2v_n) \qquad \ldots\ (2)$$

where mv_n is the momentum of a general nth mass, m, in the lattice of spacing d, $\hbar = h/2\pi$ and $i = \sqrt{-1}$. Eq 2 also results from writing the time-dependent Schroedinger equation for one of the masses (atoms) of such a periodic structure provided that real-property waves (i.e., momentum waves) are associated with moving particles in place of (or in addition to) the Born probability waves of orthodox wave mechanics[3,4]. From Eq. 2 and its solutions a number of macroscopic mechanical properties of crystalline solids have been described and some mechanical quantities calculated directly from atomic constants. These have included transition velocities observed in impact experiments,

threshold velocities for cratering in hypervelocity impact, nonelastic audio frequency resonances, characteristic stresses of plastic deformation, and coefficients of sliding friction[2]. A stress-strain law in close agreement with the experimental results for cubic crystals has been formulated, the velocity dependence of sliding friction and other frictional phenomena accounted for, and the cross-sectional shapes of hypervelocity craters formed at oblique impact explained[2].

The success with which some hypervelocity impact and high-speed frictional phenomena are explained by the particle-wave view of nonelastic deformation suggested that the means by which high explosive reactions are initiated might also be clarified if considered in a similar fashion. In particular, detonation by impact has proved susceptible to a particle-wave explanation by extension of the ideas used for monatomic crystals to diatomic or polyatomic crystals. This explanation is accordingly presented here after a brief review of momentum transfer and impact in monatomic crystals.

1. Particle waves and momentum transfer.

The concepts used to account for momentum transfer and detonation in polyatomic crystals are to a large extent direct extensions of ideas used in describing the behavior of monatomic crystals; therefore it is appropriate to review some of these results. Consider first the infinitely long, one-dimensional row lattice of Fig. 2 with identical point masses, m, spaced a distance d apart. A continuity equation for momentum transfer or flow along this lattice can be written as

$$\frac{\partial(mv_n)}{\partial t} = \underset{\sim}{K}_p(v_{n-1} - v_n) - \underset{\sim}{K}_p(v_n - v_{n+1}) \qquad \ldots\ (3)$$

where

$\frac{\partial(mv_n)}{\partial t}$ represents the net time rate of change of momentum of the nth lattice mass

$\underset{\sim}{K}_p(v_{n-1} - v_n)$ is the rate of momentum transfer from the mass at $n-1$ to that at n

$\underset{\sim}{K}_p(v_n - v_{n+1})$ is the rate of momentum transfer from the mass at n to the mass at $n+1$

$\underset{\sim}{K}_p$ is a momentum transfer constant for the lattice

That is, according to Eq. 3 above we postulate that as a result of an applied force (as discussed in the introduction) some type of momentum transfer occurs in the lattice for which the rate of momentum transfer depends on the velocity differences between adjacent masses. From the conservation of momentum Eq. 3 then follows directly. The exact nature and/or value of $\underset{\sim}{K}_p$ is clearly of great importance. Fortunately it is possible to obtain an exact expression for $\underset{\sim}{K}_p$ by writing a wave solution for v_n in Eq. 3 of the form

$$v_n = Be^{-i(2\pi\nu_p t - knd)} \qquad \ldots\ (4)$$

where $k = 2\pi/\lambda$ is the wave vector, d is the lattice spacing, B is a constant and the frequency ν_p is given by

$$\nu_p = \frac{-i2\underset{\sim}{K}_p}{\pi m} \sin^2 \frac{kd}{2} \qquad \ldots\ (5)$$

According to the particle-wave view of deformation[1,2] Eq. 5 gives the frequency of a particle (momentum) wave in the lattice and in the limit of long wave lengths (small k) this expression must reduce to that for a free particle, i.e.,

$$\lim_{k\to 0} \frac{-i2K_p}{\pi m} \sin^2 \frac{kd}{2} = \frac{\hbar}{4\pi m} k^2 \qquad \ldots\ (6)$$

where $\hbar k^2/4\pi m$ is the free-particle frequency. For small values of k the sine can be replaced by its argument in Eq. 6 so that

$$K_p = i\hbar/2d^2 \qquad \ldots\ (7)$$

and substitution of this value for K_p in Eq. 3 yields Eq. 2 of the introduction

$$\frac{\partial(mv_n)}{\partial t} = \frac{i\hbar}{2d^2} (v_{n+1} + v_{n-1} - 2v_n) , \qquad \ldots\ (2)$$

while Eq. 5 for the frequency becomes,

$$\nu_p = \frac{\hbar}{\pi m d^2} \sin^2 \frac{kd}{2} . \qquad \ldots\ (5a)$$

If instead of the infinite lattice of Fig. 2 we turn our attention to a finite lattice of length $S = Nd$ with fixed ends, a standing wave solution to Eq. 3 is necessary[1,2], but again the same expressions for K_p and ν_p are obtained. Now, however, discrete values of the wave vector, k, are demanded such that

$$k = \left(\frac{q\pi}{Nd}\right) \quad ; \quad q = 1, 2, 3 \ldots (N-1) \qquad \ldots (8)$$

Minimum and maximum values of k in this case are π/Nd and π/d corresponding to respective minimum and maximum values of ν_p,

$$\nu_p(\text{min.}) = \frac{h}{8mS^2} \qquad (\text{for } S = Nd)$$

$$\nu_p(\text{max.}) \cong \frac{h}{\pi md^2} \qquad (\text{for N large}) \qquad \ldots (9)$$

The prevalence of mosaic structures in real crystals indicates that finite lattice segments with lengths of a few microns will be encountered in momentum transfer through crystals[2,5]. Characteristic values of ν_p hence range from 10^2 to 10^{10} cps with accumulations of these particle-wave modes near the ends of the frequency spectrum[1,2]. Considerable experimental evidence exists[1,2] for the presence of such nonelastic modes at the audiofrequency end of the spectrum where from Eqs. 5a and 8 the successive modes are to a very good approximation supposed to occur according to

$$\nu_{pq} \cong \frac{h}{8mS^2} q^2 \qquad \ldots (10)$$

In speaking of wave propagation and assuming a wave solution for the velocity of a general nth mass in a discontinuous medium such as the periodic lattice of point masses shown in Fig. 2, a clear definition of wave motion is needed. We adopt here and apply to the preceding discussion the definition advanced, for example, by Brillouin[6]. That is, let ψ_n be some measurable property of the nth lattice mass which can be defined in the vicinity of the

mass site, but not elsewhere. ψ_n is then said to be propagated as a wave if a differential equation for ψ_n can be set up (on a physical basis) with a solution of the form $\psi_n = Ae^{-i(2\pi\nu t - knd)}$ where $k = 2\pi/\lambda$, ν is the wave frequency, and nd is the equilibrium position of the nth mass relative to the origin. A real property commonly treated in this way is the atomic displacement from equilibrium (x_n) in dealing with elastic displacement waves, but we have chosen instead the momentum (mv_n) to account for nonelastic deformation. Since the displacement and the momentum can only be measured at the positions of the masses in the lattice, we expect to be able to know nothing of such wave properties between lattice masses. Hence it follows that $\lambda = 2d$ is the smallest measurable wave length for real-property waves in a lattice of spacing d. Further, in principle real-property waves such as the momentum waves discussed cannot exist in the lattice at wavelengths less than 2d. Then, from the de Broglie relation, there will be a limiting free-particle velocity (for both external and internal field-free atoms) above which the associated momentum wave will not propagate through a lattice,

$$v_p(\text{max.}) = \frac{h}{m\,\lambda_{(\text{min.})}} = \frac{h}{2md} \qquad \ldots\ (11)$$

The existence of this velocity limit (for stationary lattices) provides a basis for explanations of high velocity impact behavior of crystals in general and the low-velocity impact behavior (detonation!) of some crystals in particular.

Finally it must be mentioned that, although all of the preceding discussion has been confined to momentum transfer in one-dimensional (row) lattices, the results are easily extended to three-dimensional crystals[2] and lead to no

major changes. This follows partly from the fact that the x,y,z components of momentum are independently conserved and partly from the assumption of in-line or central momentum transfer between masses (atoms) in a three-dimensional lattice. The practical outcome is that the results obtained for row lattices apply directly to three-dimensional lattices when the periodic spacing d_j between lattice masses in a particular direction in the crystal is used. Thus the momentum transfer constant in a direction with spacing, d_j, is $K_{Amp} = i\hbar/2d_j^2$ which predicts that the momentum transfer constant will be largest for directions of closest spacing in a crystal. Thus nonelastic deformation of a crystal should occur most readily in the directions of closest spacing, and this is in accord with all experimental evidence. Similarily the maximum values of limiting velocities for field-free particles given by Eq. 11 can be calculated for a particular crystal in terms of the distance of closest approach, d_1, by $v_1 = h/2md_1$. Values for cubic metal crystals calculated in this way range from 9.46×10^3 cm/sec for lithium to 0.238×10^3 cm/sec for thorium[2].

2. High-velocity impact in monatomic crystals.

The existence of limiting velocities (well below the speed of sound) for the free particles supposed to be generating momentum waves suggests, at first, that such waves can not account for high speed deformation of crystals. It turns out, however[2], that there is a way in which waves generated by free particles with velocities above $v_1 = h/2md_1$ can be propagated in a crystal lattice. It is only necessary for a crystal lattice, or parts of it, to move against the incident free-particle wave. Such reverse motion requires, of course, a source of energy, and it is evident that this source can only be the

vibrational (phonon) energy of the crystal lattice itself. In fact, as we shall demonstrate, the proposed mechanism eventually results in destruction of the crystal lattice when the free-particle impact velocity is such as to demand a translational lattice energy per atom equal to the lattice binding energy.

a) The effect of lattice motion

The review discussion in Section 1 was in terms of a fixed or stationary lattice, but we now consider a row lattice of fixed spacing d_1 moving with a translational velocity v_ℓ toward an incoming free-particle of velocity v_i as indicated schematically in Fig. 3a. All velocities are measured with respect to the same system of laboratory coordinates. The distance moved by the field-free particle in reaching the lattice can be expressed in terms of the lattice spacing as pd_1 in accordance with previous notation. The time required for the field-free particle to travel up to a stationary lattice is

$$t = pd_1/v_i \qquad \ldots. (12)$$

while for a lattice (or lattice section) moving toward the incident free particle with velocity v_ℓ this time is reduced to

$$t' = (pd_1 - v_\ell t')/v_i \qquad \ldots. (13)$$

$$= pd_1' \text{ , where } pd_1' = pd_1 - v_\ell t' \qquad \ldots. (13a)$$

Eq. 13 can be solved for t' to give

$$t = \frac{pd_1}{v_i + v_\ell} \qquad \ldots. (14)$$

From Eqs. 12 and 13a it follows that $d_1'/d_1 = t'/t$ and from Eqs. 12 and 14 the ratio t'/t can be written in terms of the velocities as $v_i/(v_i + v_\ell)$ so that

$$d_1'(\text{contracted}) = d_1 \frac{v_i}{v_i + v_\ell} \quad \ldots\ (15)$$

The variation of d_1' with translational lattice velocity is shown in Fig. 3. The apparent lattice spacing clearly decreases as the lattice moves toward the incident particle with increasing velocity; therefore momentum waves of decreasing wavelengths below $2d_1$ can be propagated through the moving lattice. In an entirely similar way it can be shown that the apparent lattice spacing d_1' increases with lattice velocity for a lattice moving away from the incident particle, and a single expression written for both cases (cf. Fig. 3b)

$$d_1'(\text{apparent}) = d_1 \cdot \frac{v_i}{v_i \pm v_\ell} \quad \ldots\ (16)$$

where positive values of v_ℓ denote lattice motion <u>toward</u> the incident field-free particle and negative values correspond to lattice motion <u>away from</u> the incoming particle. Finally, from Eq. 16 a new value for the limiting free-particle velocity allowing momentum wave propagation in a moving lattice can be calculated as $v_i(\text{max}) = v_1' = h/2md_1'$ or, from Eq. 16,

$$v_i(\text{max}) = v_1' = v_1 \frac{v_1' \pm v_\ell}{v_1'} \quad \ldots\ (17)$$

It is instructive to consider the limiting free-particle velocity, v_1', in Eq. 17 as the independent variable and then determine from Eq. 17 the required values of translational lattice velocity, v_ℓ, as in Eq. 18 below.

$$v_\ell = v_1'(1 - v_1'/v_1) \qquad \ldots\ (18)$$

where now negative values of v_ℓ indicate velocities opposite to the incident free-particle velocity, v_1', taken as reference. A plot of v_ℓ vs. v_1' reveals an inverted parabola with vertex at $(v_1/2, v_1/4)$ as shown in Fig. 4. From this figure it is clear that at incident free-particle velocities above v_1 the lattice must move with negative velocities (against the incident particle) in order to allow propagation of the momentum wave associated with the incident particle.

According to our previous discussion it is not necessary for any translational lattice motion to occur for free-particle velocities below v_1. All particle waves generated by velocities below v_1 are propagated in an infinite lattice, and a series of waves at discrete wave lengths are propagated in a finite lattice. For a lattice segment of length $S = Nd$ values of incident free-particle velocities generating such allowed wave lengths are

$$v_{iq} = \frac{\hbar}{m}\frac{q\pi}{Nd} ,$$

$$= v_1 \frac{q}{N} \; ; \; q = 1, 2, 3 \ldots (N - 1) \qquad \ldots\ (19)$$

There will therefore be a series of evenly spaced allowed velocities along the abscissa ($v_\ell = 0$) between 0 and v_1 as indicated in Fig. 4 (branch ODC), as well as the continuous allowed velocity values for forward lattice motion given by the positive branch (OBC) of the curve. Thus there is a choice of lattice behavior for free-particle incident velocities below v_1: (1) the lattice remains stationary and propagates only particle waves of certain discrete wave lengths; or (2) the lattice moves forward at varying velocities, v_ℓ, and

propagates particle waves of any wavelengths between ∞ and $2d_1$. Above v_1 there is only one possibility; i.e., the lattice must reverse and move against an incident field-free particle to propagate waves of wavelengths less than $2d_1$.

As discussed in detail elsewhere[2], the conditions under which the lattice moves or remains stationary represent the difference between transient and equilibrium behavior, respectively. From Eq. 5a the phase velocity, c_p, $(2\pi\nu/k)$ can be calculated in terms of the incident velocity, and be shown to have a maximum value of $v_1/m\sqrt{2}$ when $v_i = 3v_1/4$. The duration times for transient behavior can then be estimated for a given lattice segment length in terms of the time needed for a standing wave to be set up in the segment; for a segment length of 10^{-4} cm. these times are usually of the order of 10^{-6} sec. or greater. Of course there will also be incident velocities below v_1 between the discrete stationary allowed values where only forward lattice motion will allow propagation.

It is also possible to demonstrate[2] the existence of a region of instability between incident velocities of $v_1/2$ and $3v_1/4$ where a sudden jump to the reverse lattice motion required beyond v_1 takes place. The exact location of the instability point on the upper branch, OBC, of the curve in Fig. 4 depends on the number of lattice atoms in a particular segment which are moving with the translational velocity v_ℓ. This number can never be less than two since at least two atoms are needed to define an apparent lattice spacing, but three, four, or many more atoms may eventually share the translational velocity (and energy) as the momentum wave propagation proceeds along the lattice. As each lattice atom moves forward it can, in fact, be expected to "push" along the atoms ahead of it so that additional atoms share in the translational motion

(with a corresponding decrease in the amount of translational energy and momentum of each atom). Because of the existence of these instability conditions for incident velocities above $v_1/2$, as a practical matter the reverse flow will start at some velocity beyond $v_1/2$ instead of at v_1. That is, an incoming particle with velocity greater than the instability value will sooner or later jump to a velocity just above v_1, and the lattice will move in the reverse direction. The extra energy for this jump to a higher velocity is supplied to the particle by the lattice since a point just beyond v_1 corresponds to a lower absolute value of translational lattice velocity, v_ℓ, than a point near $v_1/2$. Finally, above an incident velocity of $2v_1$ we expect the results of reverse flow to become unusually severe as each lattice atom moves in the reverse direction with an energy greater than the initial energy of the incident atom. As mentioned before, such energy can only be supplied by the crystal itself. For the case where two-atom segments are broken loose, the value of translational velocity demanded of each lattice atom will reach a final value, $v_{\ell f}$, when the corresponding energy $(mv_{\ell f}^2/2)$ equals one-half the dissociation energy per atom (D/2) of the crystal lattice. That is,

$$v_{\ell f} = \sqrt{D/m} \qquad \ldots\ (20)$$

The final value of incident particle velocity, v_f, will be that which requires the final translational lattice velocity or, from Eq. 17

$$v_1'(\text{final}) = v_f = \frac{v_1 + \sqrt{v_1^2 + 4v_1 v_{\ell f}}}{2}$$

$$= \frac{v_1}{2}\left(1 + \sqrt{1 + 4v_{\ell f}/v_1}\right) \qquad \ldots\ (21)$$

For $v_{\ell f} \gg v_1$ and $2\sqrt{v_{\ell f}/v_1} \gg 1$ Eq. 21 becomes the approximation

$$v_f \cong \sqrt{v_1 v_{\ell f}}$$

$$\cong v_1^{1/2}(D/m)^{1/4} \qquad \ldots\ (22)$$

which is accurate to within 5% if $v_{\ell f}/v_1 \geq 100$. Values of v_f necessary to produce lattice disintegration or fracture can be calculated from a knowledge of $v_1 = h/2md_1$ and the lattice dissociation energy, D, for a crystal. Eq. 22 also results if we consider a four-atom projectile incident against a three-dimensional crystal where eight-atom chunks now break loose because four adjacent two-atom segments are required to move at velocities greater than $v_{\ell f}$. These ideas on lattice disintegration are depicted schematically in Fig. 5. A threshold velocity, v_f, is thus predicted above which lattice break-up and "cratering" begins, for example, in high-velocity impact.

The previous discussion applies to impact between similar atoms, but is easily extended to provide for a particle of mass m_p with velocity, v_i, striking a lattice with different masses m_t, for example. The momentum of the striking particle is $m_p v_i$ with an associated de Broglie wavelength $\lambda = h/m_p v_i$. In our view this is equivalent to, and can be replaced by, a particle with the lattice mass, m_t, and velocity v_i' provided only that $m_t v_i' = m_p v_i$. That is, an incident atom with mass greater than the lattice masses is equivalent to the smaller lattice mass incident with greater velocity, while the reverse is true for an incident atom with mass smaller than the lattice masses. For dissimilar projectile-target materials, for example, the final velocity of Eq. 22 becomes

$$v_f' = \frac{m_t}{m_p} v_f \qquad \ldots\ (22a)$$

b) Phonon fission

The preceding ideas about conversion of lattice energy into translational energy of lattice segments and ultimate lattice disintegration can also be discussed in terms of the mass-energy equivalence of atoms in a crystal lattice[2,7]. We recall that the vibrational energy of a crystal containing N atoms can be taken as equal to the energy of a system of 3N quantized harmonic oscillators when attention is confined to linear elastic interactions between atoms. For a Boltzman distribution of oscillators among the available energy levels the <u>average</u> energy per oscillator at any temperature T is[8]

$$\langle U_q \rangle = \frac{h\nu_e}{2} + \frac{h\nu_e}{e^{h\nu_e/kT-1}} \qquad \ldots\ (23)$$

where ν_e is the frequency of oscillation of a particular harmonic oscillator of the system and k is Boltzman's constant. The first term of Eq. 23 represents the average zero-point energy of the oscillators (atoms) since it remains when T = 0. With each vibrational mode of frequency ν_e a certain number of sound quanta or <u>phonons</u> can be associated and if $h\nu_e$ is taken as the energy of each, then the number of phonons, n_e, to be associated with any vibrational frequency, ν_e can be determined from Eq. 23,

$$n_e = \frac{\langle U_q \rangle}{h\nu_e} = \frac{1}{2} + \frac{1}{e^{h\nu_e/kt-1}} \qquad \ldots\ (24)$$

From Eq. 24 it is at once clear that phonons of two types occur, viz. intrinsic (non-thermal) phonons and thermal phonons. The intrinsic phonons are present

at all temperatures in a constant amount of 1/2 phonon per mode. Thus each lattice atom (with three vibrational modes) corresponds to 3/2 intrinsic phonons. In the same way there will be <u>three</u> intrinsic phonons associated with every <u>two</u> lattice atoms as indicated in Fig. 6. Hence any two lattice atoms can be characterized by one longitudinal and two transverse intrinsic phonons with sound propagation velocities respectively of c_ℓ, c_{ta}, and c_{tb}. Although two lattice atoms are associated with three phonons only <u>one</u> atomic mass is involved since one half of each lattice mass is assigned to the adjoining atom pair.

Three intrinsic phonons are insufficient, of course, to describe an arbitrary anisotropic solid. Instead three mutually orthogonal three-phonon sets are needed[7] or a total of nine intrinsic phonons; three longitudinal and six transverse. These correspond to 18 vibrational modes of 6 lattice atoms.

In any case it is possible to obtain a quantitative mass-energy equivalence for lattice atoms in general, but consider first a cubic crystal needing only three intrinsic phonons for characterization. If any two atoms of a crystal are sufficiently separated by removal from the lattice or otherwise, three phonons will be destroyed. A mean squared sound velocity for the crystal can be written as

$$\bar{c}_s^{\,2} = \frac{c_\ell^{\,2} + c_{ta}^{\,2} + c_{tb}^{\,2}}{3} \qquad \ldots\ (25)$$

and the "phonon" mass involved is $m/2$ per atom. Accordingly, the annihilation of three phonons with mean sound velocity $\bar{c}_s$ might be expected to result in the release of a vibrational energy per atom of $m\bar{c}_s^{\,2}/2$ or $mc_s^{\,2}$ (where $c_s^{\,2} = \bar{c}_s^{\,2}/2$). Now if a solid lattice is vaporized by supplying heat energy equal to D per atom the final result is also the destruction of all intrinsic

lattice phonons. The separated atoms in the vapor will have an energy of D per atom above their original energy at 0°K in the lattice. Thus we infer that the destruction of intrinsic (zero-point) lattice phonons, by any means, will result in the release of a vibrational energy per atom equal to the dissociation energy, D, per atom such that

$$D = mc_s^2 \qquad \ldots\ (26)$$

where c_s^2 is the mean sound velocity defined above for a cubic lattice in terms of three sound velocities. In the most general case the value of c_s^2 will depend on nine sound velocities corresponding to the three sets of three phonons needed to describe a crystal[7]; for hexagonal crystals four measured sound velocities or elastic modulii are needed to determine c_s^2, etc. We also note another implication of Eq. 26; if the average dissociation energy per atom, D, is to be constant then c_s^2 must also be a constant of the crystal. Therefore the sound velocity sums defining c_s^2 must be invariant and this has been shown to be the case according to classical elasticity theory[7].

From Eqs. 20 and 26 it is at once apparent that $v_{\ell f} = c_s$ so that the final or "fission" velocity for an incident atom to cause disintegration of a lattice can be written as

$$v_f \cong \sqrt{v_1 \cdot c_s} \qquad \ldots\ (27)$$

We now refer to this as the phonon-fission velocity since a particle incident at such velocity will cause a crystal lattice to break up and thus produce phonon splitting or fission. Values of v_1 are of the order of 10^2 to 10^3 cm/sec. while c_s is often about 10^5 cm/sec yielding values of v_f from 10^3 to 10^4 cm/sec. The energy required by an incident particle to produce

fission is therefore less than one-hundreth of that released for incident and lattice particles of the same mass.

$$\frac{m}{2} v_f^2 \leq 0.01\, mc_s^2 \qquad \ldots\ (28)$$

For heavy atoms incident against lattices with light masses the difference between the striking energy and the released energy will be even greater. Self-sustained phonon fission consequently is possible if somehow fragments of the fissioned lattice fly off in such a way as to strike other sections of the lattice to produce more fission, etc.

3. Momentum transfer and impact in diatomic crystals

In order to explain detonation it is necessary to extend the ideas on momentum transfer and impact to diatomic and polyatomic crystal structures. A diatomic row lattice with masses m_2, m_1 is shown in Fig. 7a with a distance d_a between atoms in each molecule and d_m between molecules in the lattice. A field-free atom of mass m_2 incident at velocity v_i on such a lattice is also depicted in Fig. 7b. The question immediately arises as to the manner in which the momentum wave associated with the incident particle is propagated along this diatomic lattice.

Following the general physical principle that the simplest assumption is often the most useful (or even most valid)[9] we assume that the actual momentum transfer process is equivalent to momentum waves of different frequencies travelling independently along the two sets of masses, m_2 and m_1. The notation adopted in Fig. 7 is such that all even numbered lattice sites are occupied by m_2 masses and odd sites by m_1 masses. From the assumption of independent momentum

waves the differential equations for momentum transfer are accordingly:

$$m_2 \frac{\partial v_{2n}}{\partial t} = \frac{i\hbar}{2d^2} (v_{2n+2} + v_{2n-2} - 2v_{2n}) \quad \ldots\ (29)$$

and

$$m_1 \frac{\partial v_{2n+1}}{\partial t} = \frac{i\hbar}{2d^2} (v_{2n+3} + v_{2n-1} - 2v_{2n+1}) \quad \ldots\ (30)$$

where $d = d_a + d_m$ is the periodic spacing between like masses (atoms) in the lattice. Traveling-wave solutions to Eqs. 29, 30 are

$$v_{2n} = B_2 e^{-i[2\pi\nu_2 t - knd]} \quad \ldots\ (31)$$

$$v_{2n+1} = B_1 e^{-i[\pi\nu_1 t - k(nd + d_a)]} \quad \ldots\ (32)$$

where

$$\nu_2 = \frac{\hbar}{\pi m_2 d^2} \sin^2 \frac{kd}{2} \quad \ldots\ (33)$$

$$\nu_1 = \frac{\hbar}{\pi m_1 d^2} \sin^2 \frac{kd}{2} \quad \ldots\ (34)$$

and so that $\nu_2/\nu_1 = m_1/m_2$.

The separate differential equations (Eqs. 29, 30) likewise result from writing the time-dependent Schroedinger equation for one molecule (i.e., two atoms of mass m_2, m_1) and considering the total wave function for the two atoms to be $\psi_T = \psi_2 + \psi_1$ where $\psi_2 = m_2 v_2$ and $\psi_1 = m_1 v_1$ in accordance with the idea that ψ is a momentum wave. Eqs. 29, 30 are also equivalent to the

assumption that momentum transfer between the molecules of Fig. 7 takes place as if point masses $M = m_1 + m_2$ were located at the center of mass of each molecule to form a monatomic row lattice of spacing, d.

In any event, such separate momentum waves will have different limiting velocities, $v_2 = h/2m_2d$ and $v_1 = h/2m_1d$, beyond which reverse lattice motion of each separate set of atoms (i.e. each of the interpenetrating row lattices) is required. Furthermore, the effective incident velocity of a mass m_2 will be different for the "lattice" of masses m_1 and given by $v_i'' = (m_2/m_1)v_i$ where v_i is the actual velocity of a m_2 mass. In order to describe the required translational lattice motion of a diatomic lattice under impact as previously shown for a monatomic lattice in Fig. 4, two curves of v_ℓ vs. v_i' are now needed as drawn in Fig. 8.

The curves in Fig. 8 are for a mass ratio $m_2/m_1 = 107.9/14.0 = 7.70$. Then, for example, an atom of mass m_2, incident with velocity v_2' has that effective velocity for the m_2 lattice, but has a higher effective velocity $v_i'' = v_1' = 7.70\ v_2'$ against the m_1 lattice. A mass m_2 incident at velocity $v_2' \cong v_2/2$ may thus require momentarily that the m_2 masses move forward at velocities $v_2/4 = 0.25\ v_2$ while the m_1 masses move forward at the same time with velocities $v_1/4 = 1.925\ v_2$. The required translational velocity difference between atoms in the same molecule hence would be $1.675\ v_2$.

For the smaller mass, m_1, incident at a velocity $v_1' \cong v_2/2$, on the other hand, the transient response of the m_1 lattice requires a forward velocity of $v_{\ell 1} \cong 0.4\ v_2$ while the m_2 lattice has to move as if hit by a mass m_2 at velocity $v_2' \cong 0.065\ v_2$, or with translational velocity $v_{\ell 2} \cong 0.06\ v_2$. The required intramolecular velocity difference in this case amounts to only

about $0.34\ v_2$.

For incident velocities of a mass m_2 above v_2 (or a mass m_1 above v_1) the separate requirements of the two interpenetrating lattices become alarmingly different in that a large steady state or equilibrium translational velocity difference is demanded for the atoms of each molecule. Thus at $v_2' = 1.2\ v_2$ a reverse velocity of $v_{\ell 2} \cong -0.2\ v_2$ is required for the m_2 masses along with a reverse velocity of $v_{\ell 1} = -1.75\ v_2$ (corresponding to $v_1' = 9.25\ v_2$) or a translational velocity difference of $\Delta v_\ell \cong 1.55\ v_2$. At $v_2' = 1.5\ v_2$, $\Delta v_\ell \cong 4.50\ v_2$; at $v_2' = 2v_2$, $\Delta v_\ell \cong 13.4\ v_2$, etc.

Just as in the case of a monatomic lattice we expect that final values of the "lattice" velocities will be reached beyond which disintegration or fracture of the crystal will occur. Now, however, there are two possibilities for such a crystal break up: 1) breaking of the lattice bonds between molecules in the crystal or 2) breaking of the chemical bonds between the atoms forming the molecules. In the first case lattice disintegration will occur when

$$m_1 v_{\ell 1 f}^2 + m_2 v_{\ell 2 f}^2 = D \qquad \ldots\ (35)$$

where D is the lattice dissociation energy per molecule and $v_{\ell 1 f}$, $v_{\ell 2 f}$ are the final values of translational velocity demanded of each set of lattice atoms; again to define an effective spacing d' at least two atoms of each lattice (a total of four) must move as indicated schematically in Fig. 7b. In the second case molecular dissociation into component atoms will occur when

$$m_1 v_{\ell 1 f}^2 + m_2 v_{\ell 2 f}^2 = 2D_b \qquad \ldots\ (36)$$

where now D_b is the chemical bond dissociation energy per molecule.

Values of D and D_b range from 1 to 10 ev/molecule so that values of $v_{\ell 1f}$, $v_{\ell 2f}$ are expected to be of the order of 2×10^5 cm/sec. Since values of v_1 and v_2 range from 10^2 to 10^3 cm/sec for most crystals, final or fission velocities of about 10^4 cm/sec are again expected for incident atoms of mass m_2 or m_1

$$v_{f2} \cong \sqrt{v_2 \cdot v_{\ell 2f}} \quad ; \quad v_{f1} \cong \sqrt{v_1 \cdot v_{\ell 1f}} \qquad \ldots\ (37)$$

The choice between breaking of intramolecular chemical bonds and breaking of intermolecular lattice bonds obviously depends greatly on the relative values of D_b, D. If $2D_b < D$ chemical bonds will be broken before lattice dissociation occurs. For $2D_b > D$ there will be lattice bond rupture before the chemical bonds within the molecule break, etc.

The general idea that in nonelastic deformation diatomic crystals may act as separate or interpenetrating lattices of identical atoms, is, moreover, extremely useful in accounting for many properties. Thus NaCl can be considered to behave as two interpenetrating fcc monatomic lattices of sodium and chlorine respectively[2]. The distance of closest approach between like atoms in NaCl is in the $< 110 >$ directions so that the momentum transfer constant $(\hbar/2d_j^2)$ is greatest and plastic flow or slip is expected to occur most readily in such directions, as is indeed the case. Similarily from Eqs. 33, 34 and the results presented in section 1 for finite lattices, a series of discrete audiofrequency modes or resonances for each type of atom in a polyatomic finite lattice is expected for a given segment length, S where

$$\nu_{1q} = \frac{\hbar}{8m_1 S^2} q^2$$

$$\nu_{2q} = \frac{\hbar}{8m_2 S^2} q^2$$

. . . . . .

$$\nu_{kq} = \frac{\hbar}{8m_k S^2} q^2 \quad ; \quad q = 1, 2, 3 \ldots N - 1 \quad \text{and} \quad S = Nd.$$

or

$$\nu_{11} : \nu_{21} : \ldots : \nu_{k1} = 1/m_1 : 1/m_2 : \ldots : 1/m_k \qquad \ldots . (38)$$

As we shall see in the final section, there are cases where the observed (nonelastic) resonance frequency ratios are in very close agreement with reciprocal atomic mass ratios as expected from Eq. 39. The identification of two sets of curves in average dislocation velocity v.s. stress data[2,10,11] for NaCl, LiF, etc. also supports the idea that momentum waves may travel independently through each set of identical atoms in a crystal.

4. Detonation by impact

From these general ideas on momentum transfer and the consequent breaking or disintegration of a crystal lattice we turn finally to an attempt to describe the process of detonation in a solid. There is general agreement on the definition of an explosion as a fast chemical reaction forming gases at high pressures from a small amount of a solid, liquid or gas, but some variation seems to exist among various authors as to just what constitutes detonation. Robinson[12] says that detonation is a term applied to the brisant explosion of

high explosives while Bowdon[13] defines detonation as any reaction propagated at speeds greater than the sound velocity in the detonating medium. Everyone seems to agree, however, that detonation can be initiated by impact and we shall first consider such initiation.

The breaking of chemical bonds between atoms in a molecule when the required translational velocity of the atoms results in a kinetic energy in excess of the bond dissociation energy has already been discussed. Impact velocities of 10^3 to 10^4 cm/sec are sufficient (depending on the incident atomic mass) and, as mentioned for phonon fission, the separated atoms will have energies (and velocities) in excess of that initially required to break the bonds. A separated or "dissociated" atom in the row lattice of Fig. 7 may then strike the remaining undissociated lattice with a velocity equal to or greater than that of the original incident free-particle (atom) and cause additional bond breaking, etc.

The chemical bond breaking process may be initiated also by free particles (atoms) incident at velocities below the fission values, v_{f1}, v_{f2} if the required translational velocity difference Δv_ℓ is sufficient to cause a rapid increase or decrease $\pm\Delta d_a$ in the equilibrium bond distance between the atoms in a molecule. The interaction potential V_{12} between atoms in the molecules of Fig. 7 can be represented by the curve shown in Fig. 9 where the mass m_1 is at an equilibrium distance d_a from mass m_2 at absolute zero. If now an incident mass m_2 approaches the lattice at some velocity $v_2' < v_2/2$ the required transient response will result in a forward velocity difference Δv_ℓ between atoms in at least the first two molecules as previously discussed. As a result the bond distance, d_a, will be increased with time (against the attractive force between the atoms) until finally a new distance d_a' is reached corresponding to a potential energy equal to the bond energy D_b.

That is

$$d'_a = d_a + \Delta d_a$$

where

$$\Delta d_a = \Delta v_\ell t_b \quad \ldots\ldots (39)$$

and t_b can be defined as the time necessary for mass m_1 to obtain a potential energy (relative to m_2) equal to the bond energy. Equilibrium bond distances vary but are most often between 1 to 4 x 10^{-8} cm; the exact shape of the interaction potential curve will determine Δd_a, but it can be taken as $d_a/2$. Thus the required time, t_b, can be estimated from a knowledge of Δv_ℓ in terms of the characteristic velocity $v_2 = h/2m_2 d$. For Δd_a = 1.5 x 10^{-8} cm and Δv_ℓ = 1 x 10^2 cm/sec, $t_b = \Delta d_a/\Delta v_\ell \cong 1.5 \times 10^{-10}$ seconds which is well below the transient duration time for most lattice segments. The attainment of a potential energy equal to the chemical bond energy can, of course, occur only by an energy conversion from the intrinsic (zero-point) phonon or vibrational energy of the molecule. Once separated the atoms of each molecule can be expected to share the bond energy in the form of increased translational kinetic energy according to

$$\tfrac{1}{2} m_1 v_{1i}^2 \therefore \tfrac{1}{2} m_2 v_{2i}^2 = D_b \quad \ldots\ldots (40)$$

For typical values of D_b (1 to 10 ev/atom) Eq. 40 requires that at least one of the separated atomic masses will have a translational velocity which may be equal to or greater than the velocity of sound in the crystal. For example, if $v_{2i} \cong 0$ the freed light mass m_1 will have a forward velocity of $v_{1i} = \sqrt{2D_b/m}$ whereas the mean sound velocity in the crystal is $c_s = \sqrt{(D_b + D)/2m} = \sqrt{D_b/m}$ for $D_b = D$.

The released mass m_1 in the second molecule then becomes an internal incident free particle against the rest of the lattice and may require, because of its high velocity, reverse lattice motion of the next two molecules in the lattice. This will result in a decrease in the bond distance between atoms in these molecules until again a distance is reached where the potential energy of mass m_1 (relative to m_2) is greater than the bond energy (cf. Fig. 9b). In this case, however,

$$d'_a = d_a - \Delta d_a \qquad \ldots\ (41)$$

where d_a can again be calculated from $\Delta d_a = \Delta v_\ell t_b$ and for $\Delta d_a \cong d_a/2$, t_b will be about 10^{-10} sec as before. Actually, because of the nonsymmetrical shape of the potential curve, the decrease in bond length required to reach a distance corresponding to a potential energy equal to the bond dissociation energy will be less for contraction than for extension. The freed atoms of mass m_1 in this case will be repelled back against the unbroken lattice once again as incident free particles, and further bond breaking produced in the next two molecules, etc.

Detonation by heat can evidently be explained along the lines just discussed if we note that a rise of temperature in a crystal may correspond to an increase in the mean vibrational energy level of the atoms within a molecule as well as the mean vibrational energy of molecules in the crystal lattice. At any temperature there will be a distribution of both the vibrational energy levels within the molecules and vibrational energy levels of molecules in the crystal lattice. If in one molecule (or a few) the rise in temperature results in raising the vibrational energy level to a value D_b, dissociation may occur for that particular molecule with the consequent creation of an internal high

velocity free particle (atom). Such a free particle will in turn cause bond breaking in the two adjacent molecules, and so on to initiate detonation as previously described.

In general any process which imparts energy in excess of the chemical bond dissociation energy to one or a few molecules (e.g. a spark discharge, an intense light beam, local heating or creation of a hot spot, etc.) may result in initiation of bond breaking or detonation by the creation of an internal high-velocity free particle in a crystal. Bombardment of a crystal with sub-atomic sized particles can also initiate detonation if the velocities are high enough so that the momentum imparted to the crystal atoms requires appreciable lattice motion.

According to these ideas initiation of bond breaking will occur at lower incident velocities when the lattice is at a higher temperature since the bond dissociation energy decreases as the temperature increases (cf. Fig. 9).

One further rather unusual feature (among many) of the proposed explanation of detonation must be mentioned. From Fig. 8 it is evident that a particle of mass m_2 incident on the lattice at <u>exactly</u> the limiting velocity v_2 will require no lattice motion of either set of atoms. This is true since the incident mass m_2 at velocity v_2 is exactly equivalent to an incident mass m_1 at velocity, v_1. Hence no relative motion between atoms in a molecule (or molecules in the lattice) is required, $\Delta v_\ell = 0$, and no chemical or lattice bonds are broken. This is true even though m_2 atoms incident at <u>lower</u> (as well as higher) velocities may initiate bond breaking as previously described. For dissimilar atoms, m_d, nondetonation velocities, v_d, will be those for which $m_2 v_2 = m_d v_d$ or $v_d = m_2 v_2 / m_d$. Thus for an incident mass, m_1, the "dud" velocity, $v_d = m_2 v_2 / m_1 = v_1$, etc.

5. Comparison with some experimental results.

Many of the concepts introduced in this explanation of detonation in terms of particle waves are somewhat novel, and it is therefore appropriate to look for experimental verification of the ideas where possible. Some experimental evidence in support of this general view of deformation in crystalline solids will be presented first and then more particular reference to detonation made.

a) Nonelastic deformation

One of the immediate consequences of the particle wave description of deformation is the prediction of the existence of nonelastic audiofrequency modes dependent on the mosaic structure of crystals. For finite lattice segment lengths around 10^{-4} cm such modes should be observable in the audio-range, and, in fact have been extensively reported[2]. The existence of such modes can be readily observed, for example, in lightly vulcanized rubber (hevea) where reversible changes from a completely amorphous state to an ordered crystalline state can be produced by stretching. This stretch-induced crystallinity has been studied by x-ray diffraction, and crystallization found to appear first at an elongation of 300% at 25°C. Furthermore Yau and Stein[14] have investigated stretched rubber by means of low-angle light scattering using a laser photographic technique. They report evidence for a crystalline superstructure which is pronounced above 300% elongation and of the order of 2×10^{-4} cm in size. These data allow a direct calculation of the lowest particle-wave mode, q = 1, in terms of the carbon atom, taking $S = 2 \times 10^{-4}$ cm. From Eq. 10

$$\nu_{p1} = \frac{h}{8mS^2} \cdot 1 = \frac{6.62 \times 10^{-27}}{8 \times 1.99 \times 10^{-23}(2 \times 10^{-4})^2} = 1040 \text{ cps.}$$

This resonance should appear in the stretched rubber at an elongation just above 300%, and the prediction compares well with the experimental dynamic shear compliance data of Fig. 10 in which a resonance at 1020 cps appears at an elongation of 310%.

The existence of critical velocities in impact experiments has long been recognized. Bell[15], for example, has identified hydrodynamic transition velocities above which "excessive mushrooming in the first diameter is experimentally observed." From our description of impact this transition velocity corresponds to $2v_1$ (i.e, twice the limiting or "reverse flow" velocity), and calculated values of $2v_1$ for aluminum and copper are compared with the Bell transition velocity below:

	Al	Cu
Hydrodynamic transition velocity measured by Bell.	2050 in/sec (± 50 in/sec)	980 in/sec (± 20 in/sec)
$2v_1$	2039 in/sec (5179 cm/sec)	968 in/sec (2458 cm/sec)

In addition Bell has reported[15] another critical velocity in aluminum of 582 in/sec <u>below</u> which there is no mushrooming, delay in strain development, and poor reproducibility near the impact face. In terms of the ideas presented here, unstable behavior and the mushrooming threshold (due to reverse lattice flow) should occur between $0.5v_1$ and $0.75v_1$ or between 508 in/sec and 765 in/sec for aluminum.

The idea of reversed lattice motion taking place against an incoming projectile is also supported by observations on impact at so-called hyper-velocities. That is, according to the ideas presented here, above a certain characteristic velocity v_1 (or in practice above $v_1/2$) sections of a target

will tend to move toward an incoming projectile. Further above another characteristic value, v_f, the target will actually disintegrate or break up; sections of the target will fly off against the incident projectile and in so doing will maintain their crystallographic integrity (i.e., "melting" is not supposed to occur). The reverse motion is not imagined to result from reflection or rebounds from some depth (or back surface) of the target, but, on the contrary, above v_f pieces of the target in the impact region should peel off from the front surface in groups of two atoms or more. Another, quantitative test of these ideas is possible from data on crater depth vs. incident velocity in high-velocity impact experiments. A threshold velocity, v_f, (v_f') is predicted by Eq. 22 in terms of Planck's constant, the closest lattice spacing, a measured lattice dissociation energy, and the atomic mass,

$$v_f \cong \sqrt{v_1 \cdot v_{\ell f}}$$

$$\cong (h/2md_1)^{1/2}(D/m)^{1/4} \quad \ldots\ldots (22a)$$

In using crater depth as a measure of the lattice disintegration process a distinction between a crater and an indentation must be maintained, of course. This is most easily done with data for a soft projectile against a similar or harder target material. Pit-depth data reported by Olive G. Engel[16] for 0.1 and 0.285-cm mercury drops against lead targets is shown in Fig. 11, and the calculated threshold value of $v_f' = 0.54 \times 10^4$ cm/sec agrees well with these experimental results. Similar data given by Partridge[17] for 0.483-cm iron spheres fired into iron targets are shown in Fig. 12. Again the calculated value of $v_f = 2.36 \times 10^4$ cm/sec compares well with the extrapolated zero-

depth value from these somewhat scattered points.

Finally, in connection with the remarks on impact in monatomic crystals a connection between a mean elastic sound velocity and the lattice dissociation energy was developed, i.e. $D = mc_s^2$. Measured values of sound velocities and dissociation energies again afford a means of checking the supposed relation. This "Einstein" relation, indeed, seems to be well verified for 18 cubic metals as shown in Table I, and is also true for a number of hexagonal metal crystals.

In more direct support of the ideas presented on detonation some data on the independent existence of particle waves in like sets of atoms in a polyatomic solid are shown in Table II. Here are tabulated some observed resonances or modes from dynamic shear compliance measurements on a butadiene-acrylonitrile terpolymer (Hycar 1072). According to Eqs. 38 there should be sets of frequencies present for each type of atom or each mass value in the solid lattice. Further, the frequency ratios of a particular mode (e.g., $q = 2$) should be equal to the reciprocal atomic mass ratios for the same segment length (S). This does appear to be the case for this terpolymer as it is also for some other materials.

All of these comparisons, and the more extensive correlations published elsewhere[2] as discussed in the introduction lend support to the general idea that nonelastic deformation may be described in terms of momentum wave propagation in crystalline solids. However, no detailed confirmation of the corresponding explanation of the detonation process has yet been attempted. Such confirmation may require new experiments, modification of present testing methods, or in fact may not be possible. We can, however, examine some of the existing data on detonation and attempt to explain it in terms of the mechanism proposed in the preceding section.

b) Detonation

To begin with we expect that for a given crystal structure, the same spacing between unlike atoms, and comparable bond dissociation energies, the impact sensitivity should increase as the atomic mass ratio of the bonded atoms increases. This follows since the limiting incident velocity at which reverse motion of the metal "lattice" is demanded, decreases as the metallic mass increases ($v_2 = h/2m_2d$), and also because the required translational velocity difference, Δv_ℓ, leading to rapid bond shortening increases as the atomic mass ratios increase in a particular crystal structure. Therefore mercury fulminate (Hg, 200.6) should be more sensitive to impact than silver fulminate (Ag, 107.9) which, in turn, should be more sensitive than sodium fulminate (Na, 23). According to Marshall[18] this is true. In the same way the azides should be increasingly sensitive to impact as the mass of the metallic atom increases, provided the relevant bond lengths, lattice spacings, etc. are unchanged. Accordingly we would suppose the sensitivity to shock or impact to increase for the azides in the order KN_3, CuN_3, AgN_3, $Hg_2(N_3)_2$, $T\ell N_3$, $Pb(N_3)_2$. Bowden[13], however has listed the azides of increasing sensitivity or decreasing stability to heat, light, and shock in a somewhat different order as shown in Table III (see footnote, b). In particular, according to Bowden $T\ell N_3$ is next to KN_3 in stability while CuN_3 is more sensitive than AgN_3. From our point of view $T\ell N_3$ and CuN_3 are out of place, at least insofar as sensitivity to impact is concerned. Bowden has not listed separately the sensitivities to shock, heat, and light for the azides and therefore exact measures or criteria of his sensitivity scale are lacking; differences in bond and lattice dissociation energies could perhaps result in a different ordering of the azide sensitivities to heat and light than for shock or impact. From the data of

Gray and Waddington[19], in fact, it is possible to calculate the difference between the lattice and bond dissociation energies, $\Delta D = D - D_a$, for some of the azides listed in Table III. This difference, ΔD, does increase in the order of increasing sensitivity as given by Bowden (cf. Table III); thus in terms of the supposed atomic potential interaction curve of Fig. 9 a localized increase in energy of the crystal lattice (resulting from heat or light energy) can initiate detonation by producing dissociation of a chemical bond (in preference to dissociation of a lattice bond which causes "melting"). The occurrence of heat or light produced interatomic bond dissociation prior to interlattice bond dissociation (melting) is more likely as ΔD increases and therefore sensitivity to heat and light might be expected to follow ΔD, while sensitivity to impact depends on increasing atomic mass ratios as predicted. Of course a large decrease in spacing between like atoms in the Tℓ-N bond direction could also produce a decrease in impact sensitivity (increase v_2) but this does not seem likely. Rather it appears from our point of view that "sensitivity" by itself or a collective sensitivity may be meaningless and that one should always specify sensitivity to something (heat, light, impact, etc.) when speaking of detonation!

A numerical estimate of what might be called the "falling weight sensitivity" can also be calculated in terms of the diatomic linear lattice of Fig. 7 for specific materials where the crystal structure in a particular direction resembles that of Fig. 7. For example, silver azide (AgN_3) is orthorhombic with rows of alternating silver and nitrogen atoms in line along the Ag-N bond direction in [201] directions on (010) planes[20]. The Ag-N distance is 3.33 Å and hence the limiting velocity, v_2, of an incident silver atom beyond which reverse flow of the "silver lattice" is required is

$$v_2(Ag) = h/2m_2d$$

$$= 6.625 \times 10^{-27}/2(17.89 \times 10^{-23})(6.66 \times 10^{-8})$$

$$= 2.78 \times 10^2 \text{ cm/sec}$$

The limiting velocity for a nitrogen atom against the "nitrogen lattice" is, in the same way, found to be

$$v_1(N) = 2.14 \times 10^3 \text{ cm/sec}$$

The velocity $v_2 = 2.78 \times 10^2$ cm/sec would be attained by a silver bullet (weight) dropped from a height $H = 39.3$ cm ($H = v^2/2g$), for example. Because of the instability cited in section 2, reverse lattice motion (and the consequent initiation of detonation) will in practice occur at velocities between $v_2/2$ and $3v_2/4$ or between 1.39×10^2 and 2.08×10^2 cm/sec.

This predicted range of striking velocities needed to initiate detonation in AgN_3 crystals of a particular orientation can be compared to experimental determinations of the falling weight sensitivity for polycrystalline AgN_3 made by Wohler in 1911 and reported by Marshall[18]. The tests were performed according to specifications set forth by the International Committee on Explosive Testing[18] and consisted of a hardened steel weight of 500 grams falling against a hardened steel striking pin of 12.55 grams in contact with the AgN_3 which was backed by a large steel anvil. Under these conditions the actual striking velocity of the hardened steel pin can only be estimated for an assumed coefficient of restitution. The minimum height of fall for the 500-gram weight to initiate detonation was found to be 31.5 cm corresponding to a final velocity of 2.46×10^2 cm/sec for the weight. This results in a

calculated striking velocity for the steel pin against the AgN_3 of 4.42×10^2 cm/sec if the coefficient of restitution is taken as 0.90. The equivalent incident or "striking" velocity for a silver pin can these be determined from the atomic mass ratio as

$$v_{Ag} \simeq \frac{55.85}{107.9} v_{Fe}$$

$$\cong 0.51 \times 4.42 \times 10^2 \text{ cm/sec}$$

$$\cong 2.25 \times 10^2 \text{ cm/sec}$$

which compares well with the upper limit of 2.08×10^2 for the predicted initiation detonation velocity of silver against silver azide. In fact, since the texture or preferred orientation of the polycrystalline sample used by Wohler is not known, this is an entirely plausible result. The difference between the predicted initiation velocity of 2.08×10^2 cm/sec and that observed could be accounted for in a single crystal sample by an angle, θ, between the incident mass or striking pin and the aligned Ag-N bond directions in the crystal such that $\cos\theta = 2.08/2.25 = .924$ or $\theta \cong 22.5°$. The uncertainties surrounding the actual incident velocity of the striking pin against the sample in this falling weight test, however, are too great to justify any definite conclusions in this regard. The most we can say is that the predicted initiation velocity for silver against silver azide (or iron against silver azide) is in reasonable agreement with the experimental data cited in this instance.

Any falling weight or "drop" test in which a separate striking pin must be put in motion to produce detonation will always create doubt as to the actual incident or impact velocity of the pin against the sample since assumptions about the collision between the falling weight and the striking pin must

be made. On the other hand, Cushman[21] has reported more recent experiments (1918) in which the minimum height of fall of a 3-oz weight with steel firing pin attached is determined for the onset of misfires (nondetonation). Compounds tested were iron disulfide (pyrite, FeS_2), antimony trisulfide (stibnite, Sb ' and lead sulfide (galena, PbS). Extreme precautions were also taken to prepare samples of the same fineness or grain size distribution in each case; equal quantities of three sieve sizes being used for the test samples of each material. Calculation of the initiation velocity is particularly easy for PbS which has the (cubic) sodium chloride structure with a lattice spacing[22] between like atoms in the [100] direction of $d = 5.936 \times 10^{-8}$ cm. Hence the limiting velocity for a lead atom ($m = 34.39 \times 10^{-23}$ g) incident against the "lead lattice" of PbS is

$$v_2(Pb) = h/2m_2d$$

$$\cong 1.62 \times 10^2 \text{ cm/sec}$$

while that for a sulfur atom against the "sulfur lattice" is

$$v_1(S) \cong 1.05 \times 10^3 \text{ cm/sec.}$$

According to our idea that reversed lattice flow results in initiation of detonation, for a lead pin incident against PbS this should occur for incident velocities between 0.81×10^2 cm/sec and 1.21×10^2 cm/sec. Cushman gives 21.0 in. as the minimum experimental drop height producing detonation (100% of the time) for a steel firing pin, corresponding to a striking velocity of 3.24×10^2 cm/sec for a steel pin against PbS. The equivalent striking velocity for a lead pin is then

$$v_{Pb} = \frac{55.85}{207.2} v_{Fe}$$

$$\cong 0.269 \times 3.24 \times 10^2$$

$$\cong 0.871 \times 10^2 \text{ cm/sec}$$

which falls very nicely within the predicted initiation velocity range of 0.81×10^2 cm/sec to 1.21×10^2 cm/sec.

The expectation of a range of incident velocities within which firing or detonation may occur is in our view a direct result of the presence of an instability region between $v_2/2$ and $3v_2/4$ as already described (cf. section 2a and reference 2). Such a range of sensitivities is, indeed, found in the usual falling weight or drop tests. Taylor and Weale[23] describe drop tests on a mercury fulminate mixture using a 2-ounce weight and 0.4 cm diameter steel balls as the striking pins. Some of their data, reproduced in Table IV, suggested to them a statistical distribution "...governed by some probability law." However we expect an incident velocity range for initiation of detonation, Δv_2, equal to $(3v_2/4 - v_2/2)$ or $v_2/4$ in every case; this being the velocity range or difference between the highest velocity $(3v_2/4)$ and the lowest velocity $(v_2/2)$ which, in practice, result in reverse lattice motion. Further, the ratio of the lowest initiation velocity to the highest initiation velocity should be exactly 2/3. This ratio can evidently be determined in a falling weight test (for a constant mass ratio of the falling weight to the striking pin) from the height for 100% initiation, H_{100}, and the height for 0% initiation H_0 as

$$\frac{v_i(\min)}{v_i(\max)} = \sqrt{\frac{H_0}{H_{100}}}$$

and compared with the predicted value of 2/3. The experimental values reported by Taylor and Weale in Table IV give $\sqrt{1.5/4.0}$ or 0.62 which is in only fair agreement with the expected value of 0.67. More extensive tests were subsequently carried out by Taylor and Weale in which 100 samples were tested at each of eight heights of fall. These gave a ratio of $\sqrt{H_o/H_{100}} \cong \sqrt{3.7/8.0}$ or 0.68 which is in good agreement with the predicted ratio of 0.67 (i.e., 2/3) for the initiation velocities. As mentioned above it is important in this calculation that all tests be carried out with the same falling weight for a given mass and type of striking pin so that the actual incident velocity of the striking pin against the explosive will vary only with the height of fall. In some cases[24,25] the percentage ignition (0 to 100%) vs. height of fall is reported for several values of falling weights and the corresponding striking-pin velocities are therefore not proportional to the falling heights alone, but instead depend on the different falling weight to striking pin mass ratios, coefficients of restitution, rigidity of the anvil on which the explosive is placed, etc.

The foregoing comparisons of predicted and experimental results for the initiation of detonation in crystalline solids are far from extensive as stated in the beginning. However, the agreement between the calculations and the observations is sufficiently close to encourage further investigation of the general ideas used to account for the initiation of detonation. Further, it must be emphasized that the critical incident velocities are calculated entirely in terms of fundamental microscopic constants (Planck's constant, atomic mass, and crystal spacing) without the aid of assumed values for any new parameters.

Conclusions

With many unanswered or even unasked questions about detonation, there are still a few general conclusions that can be stated in terms of the simple model discussed. First, it is proposed that in order for repeated bond-breaking to proceed in a solid there must be atoms of different mass bonded together with their bond directions in line for an appreciable distance in a crystal. Second, for a given bond length, lattice spacing, and bond dissociation energy the instability of a crystal should increase as the mass ratios of the bonded atoms increase. This results from the difference in the required reverse translational lattice velocities for each atom and the separate dependence of each translational velocity on the reciprocal atomic masses. That is, for an external or internal incident free atom of velocity, v_i, against a lattice of masses, m_1, the required translational "m_1 lattice" velocity, v_ℓ, is

$$v_{\ell 1} = v_i(1 - v_i/v_1) \qquad \ldots\ (42)$$

where $v_1 = h/2m_1d$. For values of $v_i > v_1$ negative (reverse) lattice velocities, $v_{\ell 1}$, are required. If a second type of atom with mass m_2 is present, the corresponding equation for the translational "m_2 lattice" velocity is

$$v_{\ell 2} = v_i(1 - v_i/v_2) \qquad \ldots\ (43)$$

where $v_2 = h/2m_2d$ and values of $v_i > v_2$ again require reverse lattice motion. From Eqs. 42 and 43 the translational lattice velocity difference $\Delta v_\ell = v_{\ell 1} - v_{\ell 2}$ is clearly a function of the mass ratio m_2/m_1. This

difference in translational velocity results in bond rupture or dissociation in a very short time as discussed in section 4.

A third conclusion is that the impact sensitivity will be a function of the incident velocity requiring reverse lattice motion; in practice this incident velocity for the initiation of detonation will be between $v_2/2$ and $3v_2/4$ for an incident mass, m_2, identical to one set of lattice masses (or between $v_1/2$ and $3v_1/4$ for an incident mass, m_1, identical to the other set of lattice masses in a diatomic lattice, for example). The initiation (initiation of detonation) velocity for any atom of mass, m_k, can always be calculated in terms of one of the lattice masses by determining the equivalent limiting velocity,

$$v_k = \frac{m_k}{m_2} v_2 \qquad \text{or} \qquad v_k = \frac{m_k}{m_1} v_1 \quad , \text{ etc.} \qquad \ldots\ (44)$$

where m_2, m_1 are masses of lattice atoms. Accordingly the initiation velocity for a lead striking pin should be less than that for a steel striking pin against the same explosive; that for a steel striking pin less than that for an aluminum striking pin, etc. It also follows that the actual impact velocity of the striking pin against the explosive is the relevant quantity, and not the velocity (or momentum) of a falling weight against a striking pin.

Finally, it is necessary to explain why <u>all</u> solids with large atomic mass ratios do not explode! Ice, for example, has a mass ratio of 16:1, but is not a high explosive under usual conditions. In terms of the simple "in-line" model of Fig. 7 this can be attributed to the lack of any long-range alignment of the O-H bonds in ice where, in fact, the positions of the hydrogens in the lattice do not seem to be well defined[26]. In other cases recombination of the broken interatomic bonds may take place after the momentum wave has passed,

provided that the products of the broken bond are not subject to sudden expansion (gaseous), or react violently with their environment. Thus the presence in crystals of chemical bonds between atoms of different masses is proposed as a necessary, but far from sufficient condition for a detonation wave to be initiated.

It is further possible that rows of adjacent atoms with different periodic spacings will have different limiting or critical velocities for reverse lattice motion even when the atoms are of comparable masses. Then chemical bonds between atoms in adjoining rows could be broken as a result of some type of microscopic shearing process resulting from the required translational velocity difference between rows. Such bonds would have to have identical orientations over some distance in the crystal, but would not necessarily have to be "in line" as supposed from our simple one-dimensional model.

The eventual success of this attempt to apply to the detonation process some of the ideas on particle waves and momentum transfer in crystals previously used to describe non-elastic deformation remains to be determined. At this stage, however, we are in complete agreement with Willoughby Walke's conclusions[27] of 1897:

> "....According to this view, detonation is the result of a combination of true chemical and dynamical reactions, neither of which alone suffices to explain the attending phenomena...."

Further understanding of the initiation process for detonation will therefore depend on the acquisition of more information on the crystal structures of explosives together with their chemical bond strengths, and, in particular, on the design and performance of more meaningful experiments where the truely relevant physical quantities (e.g. velocities) can be and are directly observed.

Acknowledgement

The suggestion that some of the ideas previously used[2] to describe nonelastic deformation of solids in terms of particle momentum waves might prove useful in understanding the initiation of detonation was made by Dr. R. J. Eichelberger of the U.S. Army Ballistics Research Laboratory. I am grateful to him for directing my attention to this, and for his subsequent interest in and encouragement of these initial efforts.

References

1. E. R. Fitzgerald, J. Acoust. Soc. Am. 39, 856-869 (1966).

2. E. R. Fitzgerald, "Particle Waves and Deformation in Crystalline Solids," (Interscience Div., John Wiley and Sons, Inc. New York, 1966).

3. E. R. Fitzgerald and J. Tasi, Int. J. Solids, Structures 3, 927-933 (1967).

4. E. R. Fitzgerald, Int. J. Theoretical Phys. (to be published).

5. P. B. Hirsch, Progr. Metal Phys. 6, 236-339 (1956).

6. L. Brillouin, "Wave Propagation in Periodic Structures" (McGraw-Hill, New York, 1946).

7. E. R. Fitzgerald and T. W. Wright, Phys. Stat. Sol. 24, 37-44 (1967).

8. A. J. Dekker, "Solid State Physics" (Prentice Hall, Englewood Cliffs, N. J., 1958).

9. A generalization well-known among physicists--The Law of Least Effort.

10. W. G. Johnston and J. J. Gilman, J. Appl. Phys. 30, 129-144 (1959).

11. E. Y. Gutmanas, E. M. Nadgornyi and A. V. Stepanov, Soviet Phys.-Solid State 5, 743-747 (1963).

12. C. S. Robinson, "Explosions: Their Anatomy and Destructiveness" (McGraw-Hill, New York, 1944).

13. F. P. Bowden and A. D. Yoffee, Endeavour, 21, 125-136 (1962).

14. W. Yau and R. S. Stein, J. Polymer Sci. 132,231 (1964).

15. J. F. Bell, "The Physics of Large Deformation in Crystalline Solids" (Springer-Verlag, Berlin, 1968).

16. Olive G. Engel, J. Res. Natl. Bur. Std. 62, 229-246 (1959); 64A, 61-72 (1960).

17. W. S. Partridge, H. B. Vanfleet, and C. R. Whited, J. Appl. Phys., 29 1332-1336 (1958).

18. A. Marshall, "Explosives", Vol. II (J. A. Churchill, London, 1917).

19. P. Gray and T. C. Waddington, Proc. Royal Soc. London 235, 481-495 (1956).

20. Ralph W. G. Wyckoff, Crystal Structures, Vol. II pp. 280 (Interscience, New York, N. Y. 1963).

21. A. S. Cushman, J. Ind. and Eng. Chem 10, 376-383 (1918).

22. Ralph W. G. Wyckoff, Crystal Structures, Vol. I, p. 89 (Interscience New York, N. Y., 1963).

23. Wilfred Taylor and Alfred Weale, Proc. Royal Soc. London A138, 92-116 (1932).

24. M. P. Murgai and A. K. Ray, British J. Appl. Phys. 10, 132-134 (1959).

25. N. R. S. Hollies, N. R. Legge and J. L. Morrison, Canadian J. Chem. 31, 746-754 (1953).

26. Ralph W. G. Wyckoff, Crystal Sturctures, Vol. I. pp. 322-325 (Interscience, New York, N. Y. 1963).

27. Willoughby Walke, Lectures on Explosives (John Wiley and Sons, New York, N.Y., 1897).

Table I

Characteristic deformation velocities[a] for some cubic metals; verification of the relation $D = mc_s^2$

Metal	$v_1 = h/2md_1$ 10^3 cm/sec	v_f velocity for fission 10^4 cm/sec	D lattice dissociation energy ev/atom	$\sqrt{\frac{D}{m}}$ 10^5 cm/sec	c_s obsv. mean sound velocity 10^5 cm/sec
Al	2.58_5	2.92	3.21	3.3_6	3.19
Ni	1.36_4	2.26	4.94	2.8_5	3.05
Cu	1.22_9	1.89	4.11	2.5_0	2.45
Sr	.528	.85	1.69	1.3_7	-
Pd	.682	1.29	4.28	2.0_7	2.26
Ag	$.641_0$	1.14	3.18	1.7_8	1.81
Pt	$.368_6$	.776	6.45	1.7_8	1.90
Au	$.351_2$	.720	4.67	1.5_1	1.52
Pb	$.275_3$	.559	2.38	1.0_5	1.05
Th	$.238_9$	.695	5.92	1.5_7	1.56
Li	9.46_2	6.55	1.60	4.6_8	-
Na	2.33_6	2.20	1.13	2.1_7	1.93
K	1.10_3	1.39	0.954	1.5_4	1.33
V	1.48_3	2.12	5.20	3.1_4	3.04
Cr	1.53_6	2.49	4.24	2.8_1	3.42
Fe	1.44_0	2.36	4.21	2.7_0	3.10
Mo	$.763_1$	1.67	8.67	3.6_2	3.54
Nb	$.751_0$	1.39	[illegible].59	2.7_9	2.64
Ta	$.385_0$	.920	8.02	2.0_7	2.08
W	$.396_2$	1.05	10.3	2.3_4	2.63

[a] Data taken from reference 2

Table II

Dynamic shear compliance spectrum of Hycar 1072 at 35.7°C

(Butadiene, 66 parts, Acrylonitrile, 28 parts,
Methacrylic acid, 6 parts by wt.)

Frequencies - cps

q^2	O^{16}		N^{14}		CH^{13}		C^{12}	
	Obsv.	Calc.	Obsv.	Calc.	Obsv.	Calc.	Obsv.	Calc.
1	YES	91.8	yes	104.8	yes	111.3	yes	122.4
4*	367	(367)	419	(419)	445	(445)	490	(490)
9	840	826	900	943	985	1000	1060	1101
16	1445	1469	1650	1676	1770	1780	1950	1958
25	2295	2295	-	2620	-	2780	-	3060

(measurements made fom 25 to 2500 cps)

Obsv. frequency ratios = 1.000/1.141/1.212/1.333 (q = 2)

Pred. frequency ratios = 1.000/1.142/1.230/1.332

= (1/16)/(1/14)/(1/13)/(1/12)

*frequency values assigned to $q = 2$ for each of the four mass units listed according to the supposed relation

$$\nu_{k,q} = \frac{\hbar}{8m_k S^2} q^2 \qquad ; q = 1, 2, 3 \ldots N-1$$

when the same segment length $S = Nd$ is assumed (cf. text, section 3).

Table III

Predicted order of sensitivity for some azides

Impact[a] sensitivity (increasing downward)	Atomic weight of metal atom	Heat,[b] light sensitivity (increasing downward)	Lattice[c] dissociation energy D kcal/mole	X-N bond[c] dissociation energy, D_a kcal	ΔD $(D-D_a)$ kcal
KN_3	39.1	KN_3	157	137	20
CuN_3	63.6	$T\ell N_3$	164	104	60
AgN_3	107.9	AgN_3	205	112	93
$Hg_2(N_3)_2$	200.6	CuN_3	227	130	97
$T\ell N_3$	204.3	$Hg_2(N_3)_2$	-	-12	-
$Pb(N_3)_2$	207.2	$Pb(N_3)_2$	516	46	470

[a] Impact by an identical metal pin or projectile, i.e., K against KN_3, Ag against AgN_3, etc. For a steel pin (atomic mass of Fe = 55.85) the impact sensitivity of KN_3 is increased by 55.85/37.1 = 1.428 and that of CuN_3 decreased by 55.85/63.6 = 0.878 in a falling weight test, for example. The relative order between KN_3 and CuN_3 which depends on the Cu/K mass ratio (1.626) remains unchanged.

[b] This is also listed by Bowden and Yoffee as the order of increasing sensitivity to heat, light, and shock, but such a collective ordering needs further explanation (cf. reference 13).

[c] From data of Gray and Waddington (reference 19) using Hess's law.

Table IV

Percentage ignitions (initiations of detonation)
v s. height of falling weight[a]
for a mercury fulminate mixture

Height of fall (inches)	Number of trials	Number of ignitions	% ignitions
6.0	12	12	100
5.5	12	12	100
4.5	20	20	100
4.0	20	20	100
3.5	30	25	83.3
3.0	30	18	60.0
2.7	30	11	36.7
2.5	30	13	43.3
2.0	30	8	26.0
1.5	20	0	0

[a]From Taylor and Weale, reference 23. Falling weight of 2.0 ounces (56.7 g) against striking pins of 0.25 g (0.4 cm diameter steel balls). Weight of charge 0.034 grams, thickness 0.02 inches.

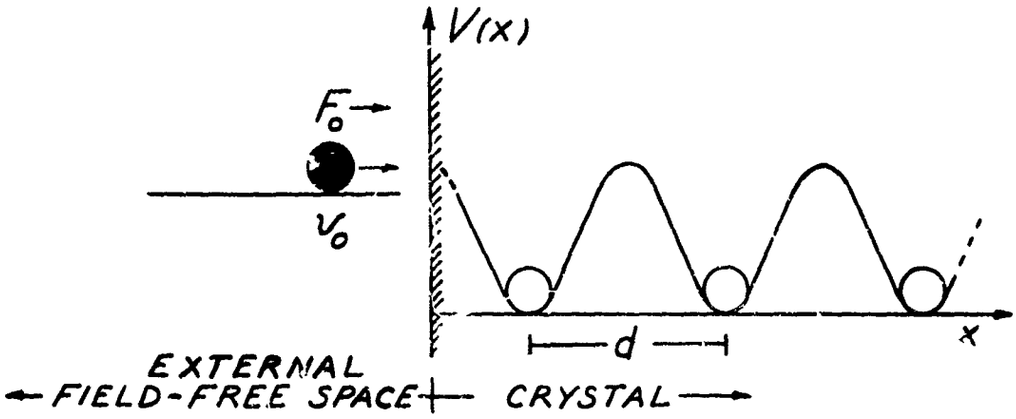

(a)

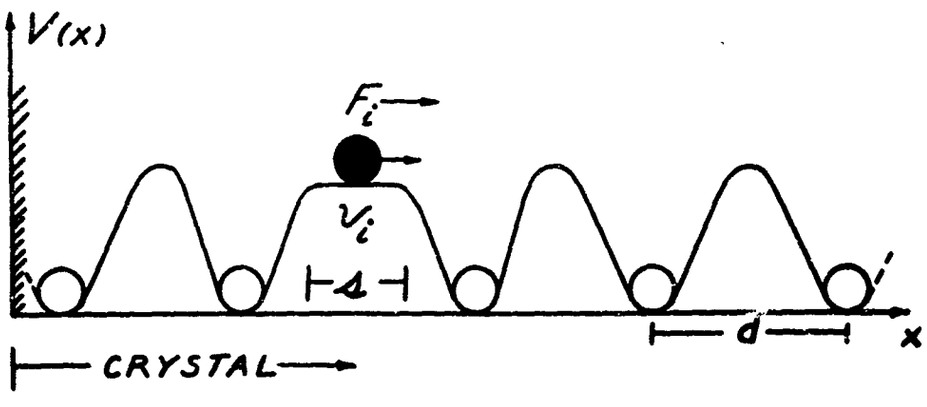

(b)

FIG. 1 (a) Schematic representation of an external field-free atom incident with velocity, v_o, on a crystal with periodic potential variation, v(x), in a lattice of spacing, d. (b) Representation of an internal field-free atom with incident velocity, v_i, in a crystal with periodic potential and spacing, d. The width of the internal field-free region is $s = pd$ (where $p < 1$) as indicated.

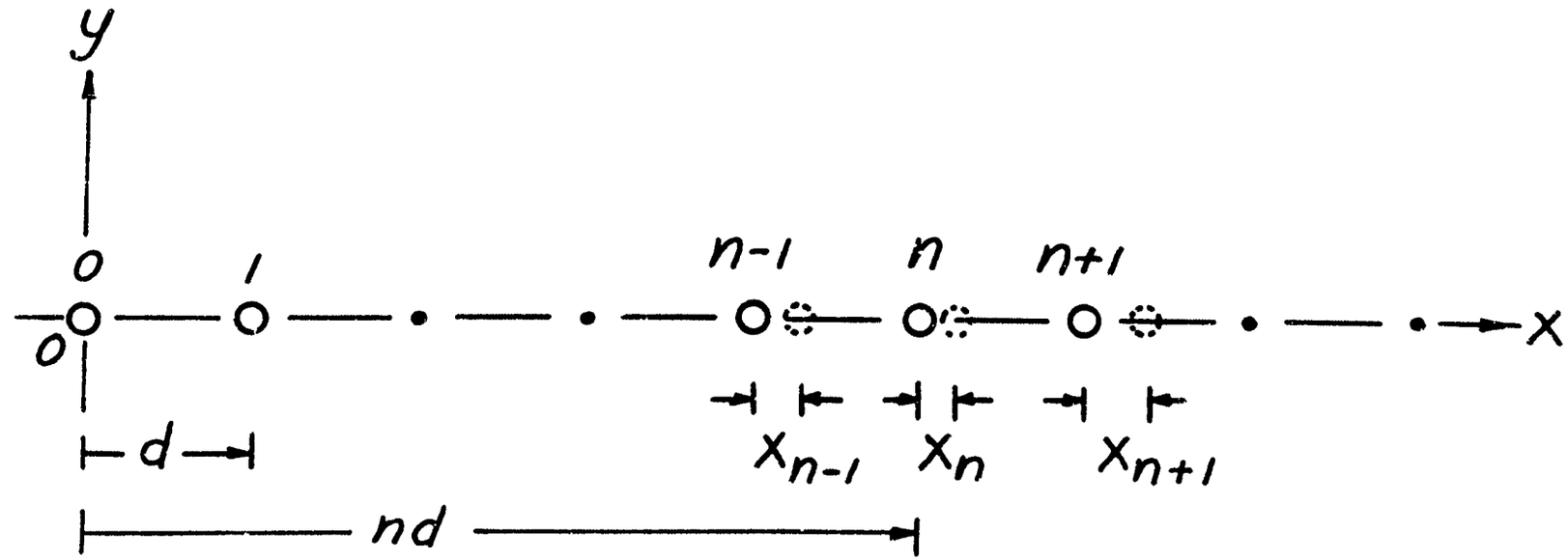

FIG. 2 Schematic drawing of a one-dimensional (row) lattice of identical point masses. Solid circles represent equilibrium positions of masses; the dashed circles represent positions of displaced masses (atoms).

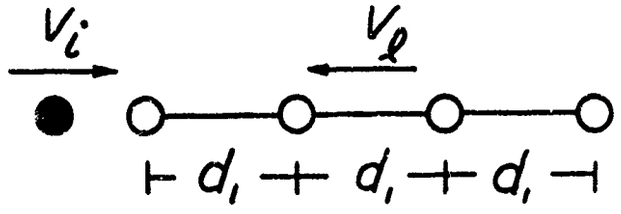

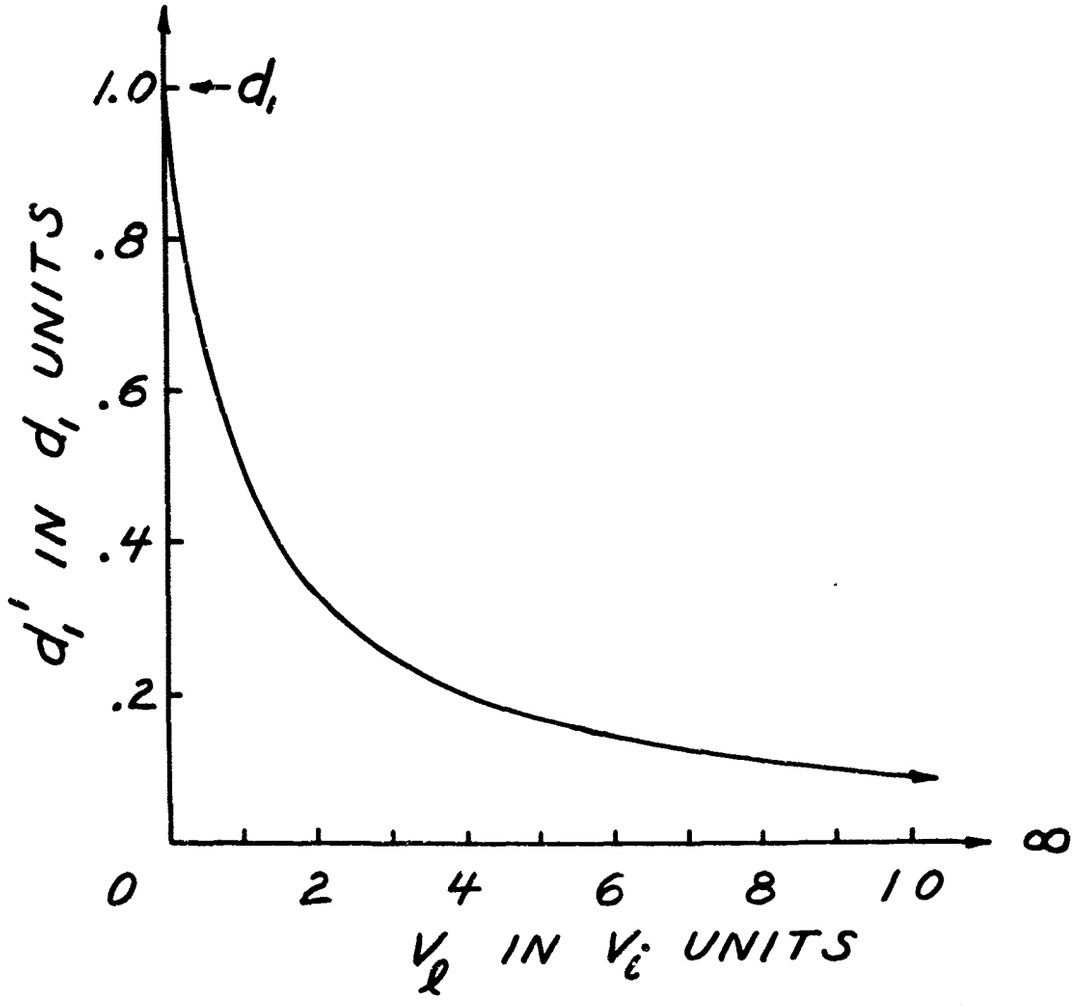

FIG. 3 (a) Effect of translational motion of a lattice segment with velocity, v_ℓ, on the apparent lattice spacing, d_1' seen by an incident free particle (with velocity, v_i) for the lattice moving <u>toward</u> the incident particle.

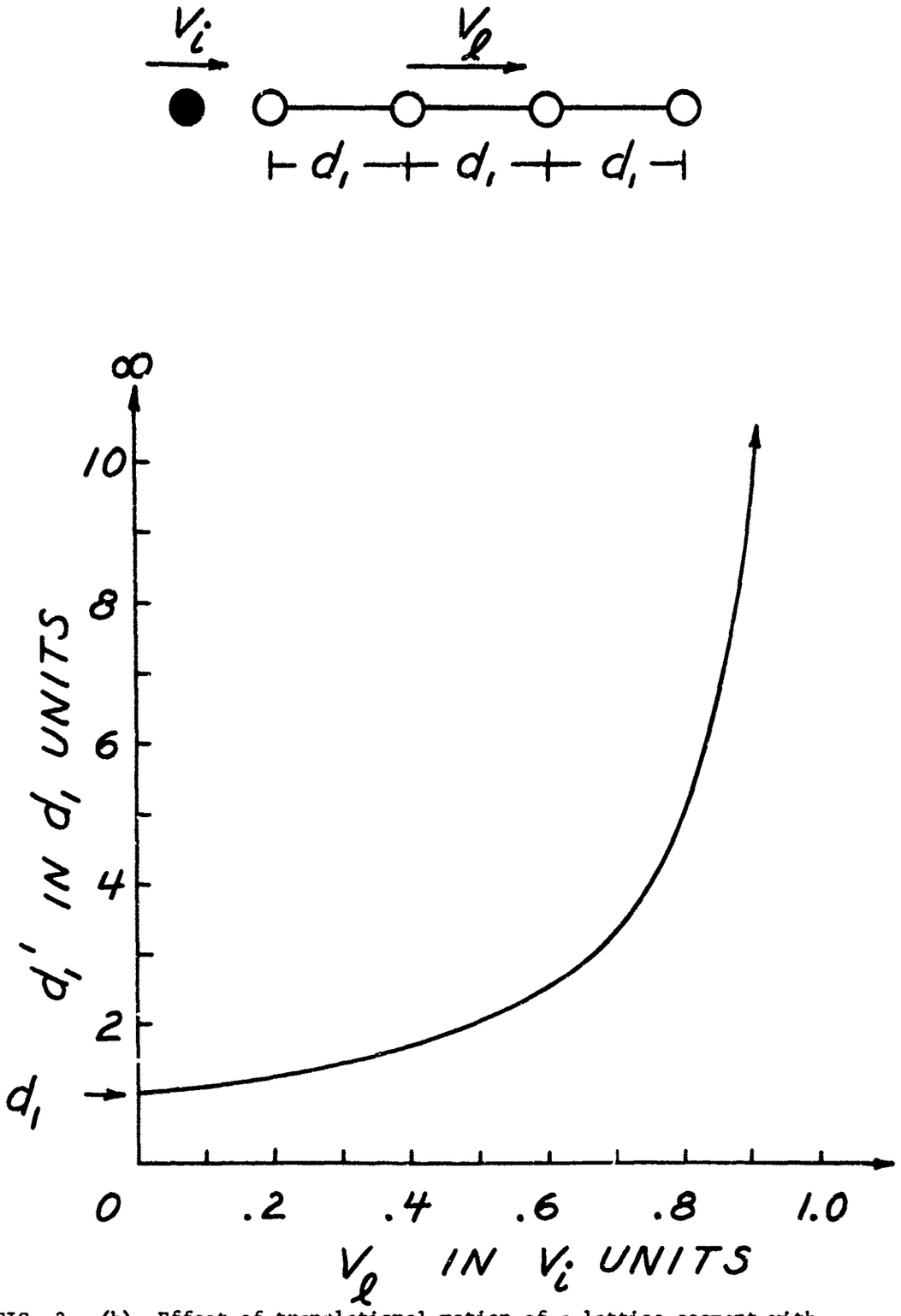

FIG. 3 (b) Effect of translational motion of a lattice segment with velocity, v_ℓ, on the apparent lattice spacing, d_1', seen by an incident free particle (with velocity, v_i) for the lattice moving away from the incident particle.

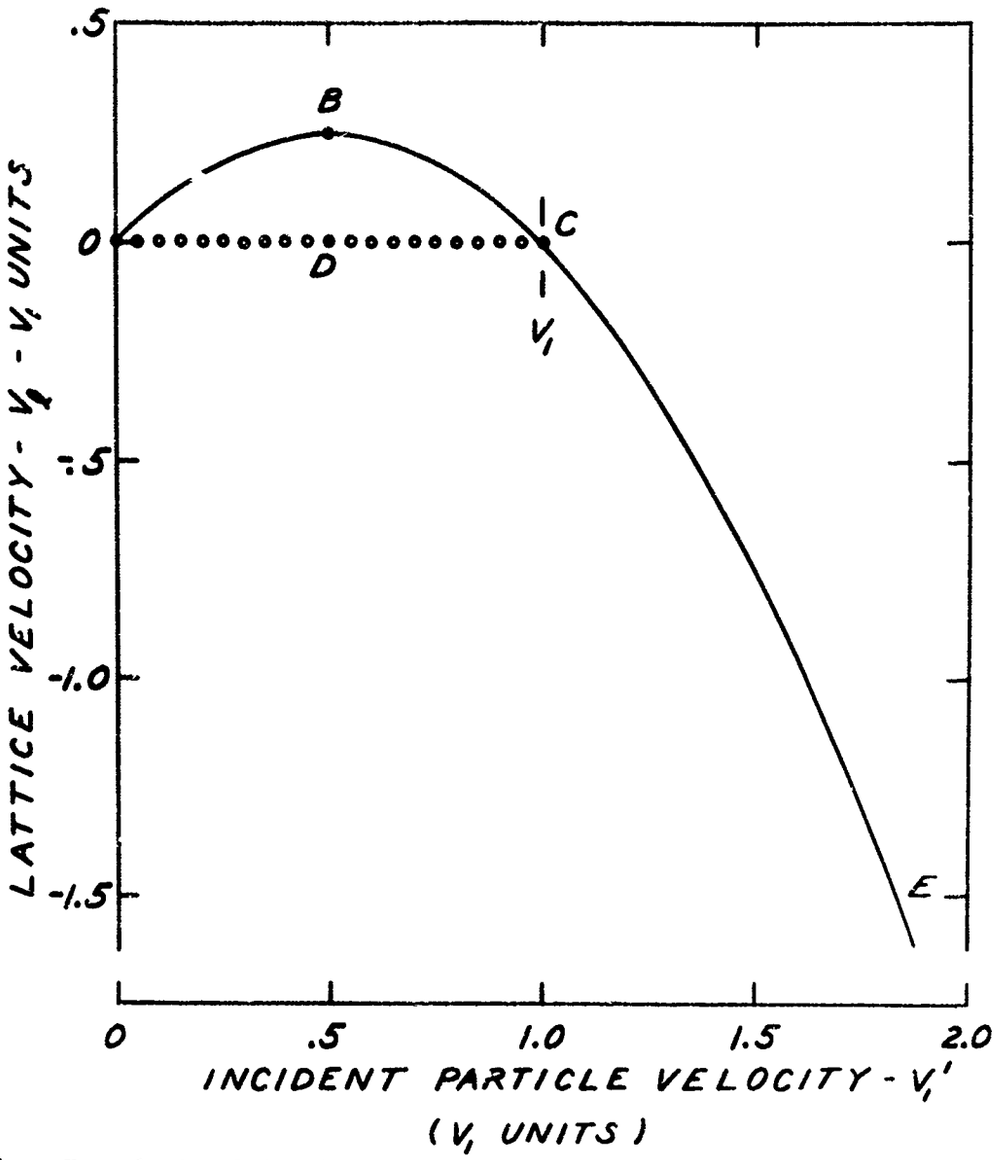

FIG. 4 Translational lattice velocity, v_ℓ, needed to provide an apparent lattice spacing, d_1', for which continuous values of the incident free-particle velocity, $v_i = v_1'$, will be the limiting velocity (branch OBC). Discrete values of v_1' below v_1 also occur for $v_\ell = 0$ as indicated by the points along the abscissa (branch ODC). Above v_1, lattice segments must move <u>against</u> the incoming particle with velocities given by the single, negative branch, CE.

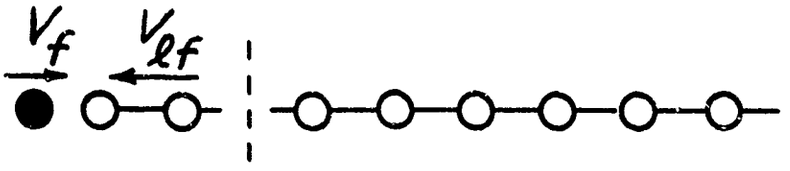

(a)

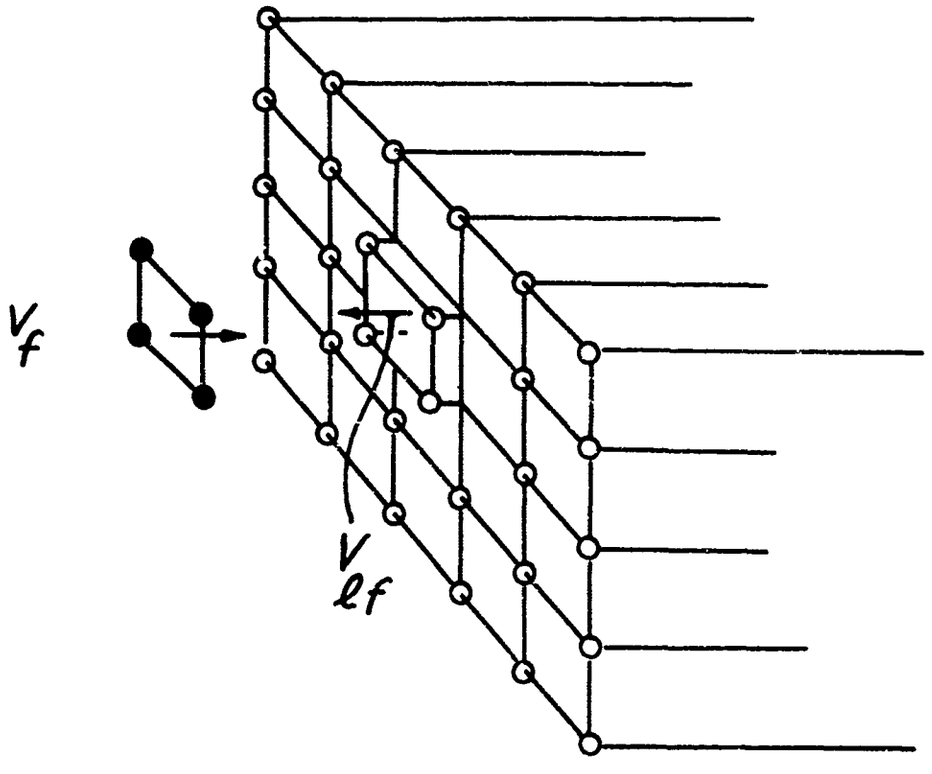

(b)

FIG. 5 (a) Diagram showing how two-atom segments of a row lattice break off to move against an incident particle with velocity, v_f, when the required reverse lattice velocity, $v_{\ell f}$, equals $\sqrt{D/m}$ where D is the dissociation energy per atom and m is the mass of a lattice atom. (b) Diagram showing how an eight-atom piece of a crystal lattice breaks off to move against an incident four-atom "projectile" with velocity, v_f.

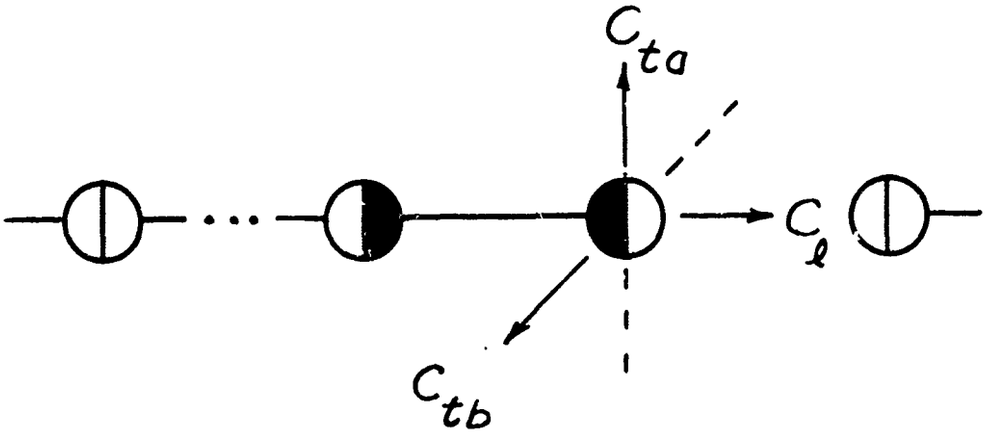

FIG. 6 Diagram showing how two transverse phonons (velocity, c_t) and one longitudinal phonon (velocity, c_ℓ) can be associated with any two-atom combination in a crystal lattice. Each atom in the combination contributes a mass, m/2, to the isolated vibrational mode depicted, so that the equivalent phonon mass of the two-atom system is m.

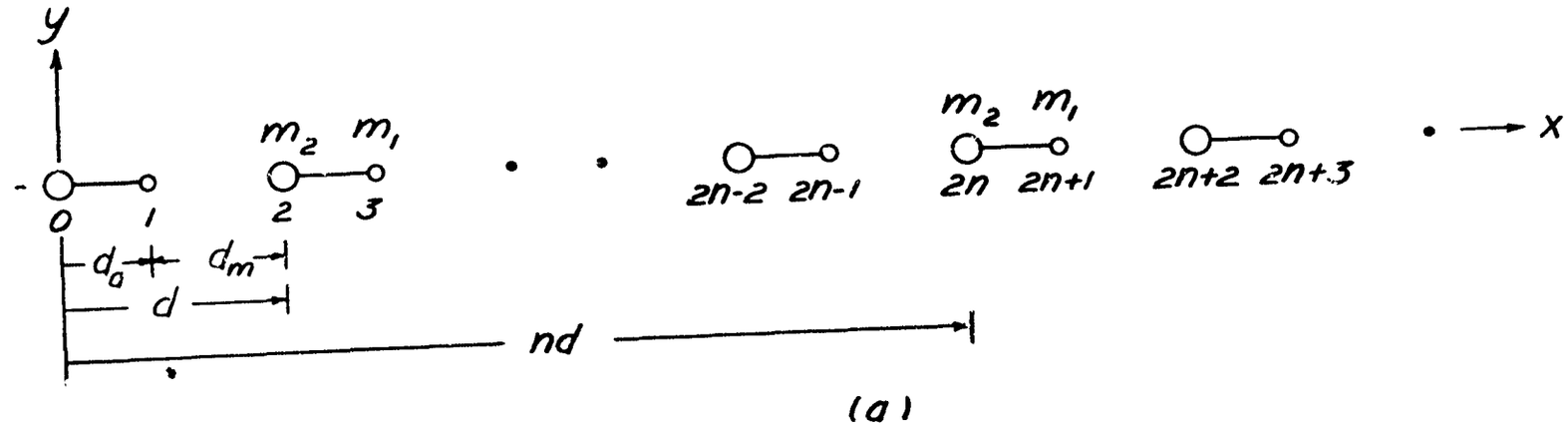

FIG. 7 (a) Schematic drawing of a one-dimensional row lattice with two values of point masses ($m_2 > m_1$) used to represent a diatomic lattice. The notation is chosen so that all even-numbered points have masses, m_2, and odd-numbered points have masses, m_1. The distance between atoms, d_a, is taken to be smaller than the distance between molecules, d_m, in this drawing, but in general any relative values for intra and intermolecular distances can be assumed.

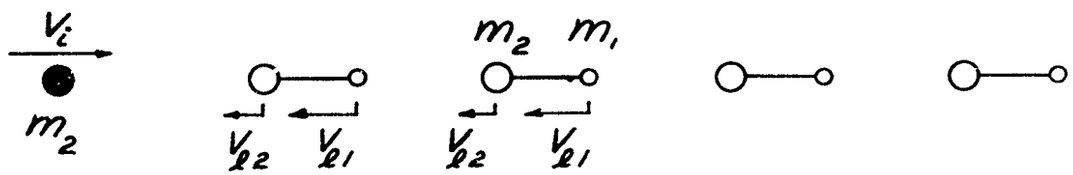

(b)

FIG. 7 (b) Diagram showing the difference in reverse translational velocities ($v_{\ell 2} < v_{\ell 1}$) required by an incident mass m_2 with velocity v_i against the row lattice of (a). The translational velocity difference $\Delta v_\ell = v_{\ell 1} - v_{\ell 2}$ results in a rapid shortening of the interatomic bond distance, d_a, which can initiate detonation as discussed in the text.

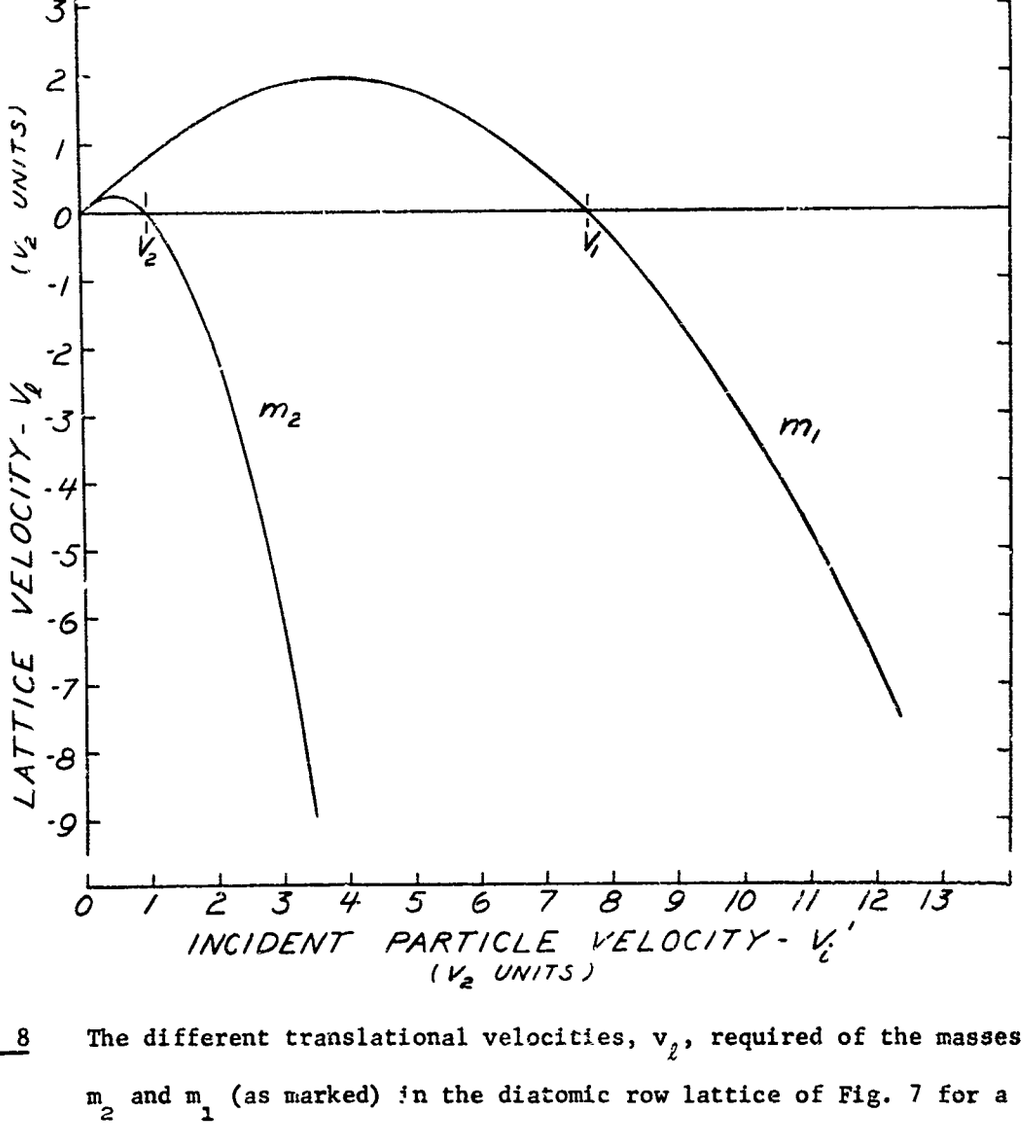

FIG. 8 The different translational velocities, v_ℓ, required of the masses m_2 and m_1 (as marked) in the diatomic row lattice of Fig. 7 for a particle of mass m_2 incident with velocity v_i'. Curves are drawn for a mass ratio $m_2/m_1 = 7.70$ so that $v_1/v_2 = 7.70$. An incident mass m_2 at velocity v_i' is equivalent to a mass m_1 incident at $7.70\ v_i'$ so that the translational velocity difference required for any incident velocity can be found from these curves as discussed in the text.

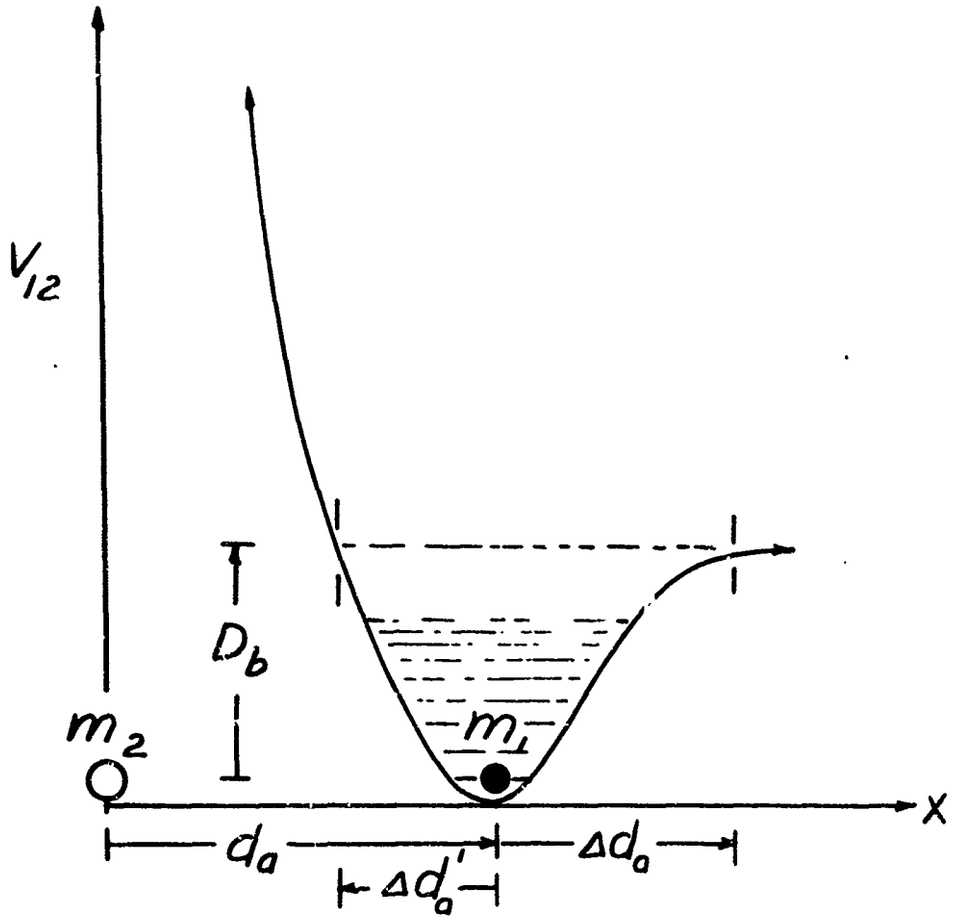

FIG. 9 Representation of the interatomic "pair" interaction potential, V_{12}, between two masses (atoms) of the diatomic row lattice of Fig. 7 as a function of the distance, x, between atoms. If the bond distance is shortened an amount Δd_a the resulting potential energy of m_1 (relative to m_2) may equal the bond dissociation energy, D_b, and bond breaking or rupture can result as discussed in the text.

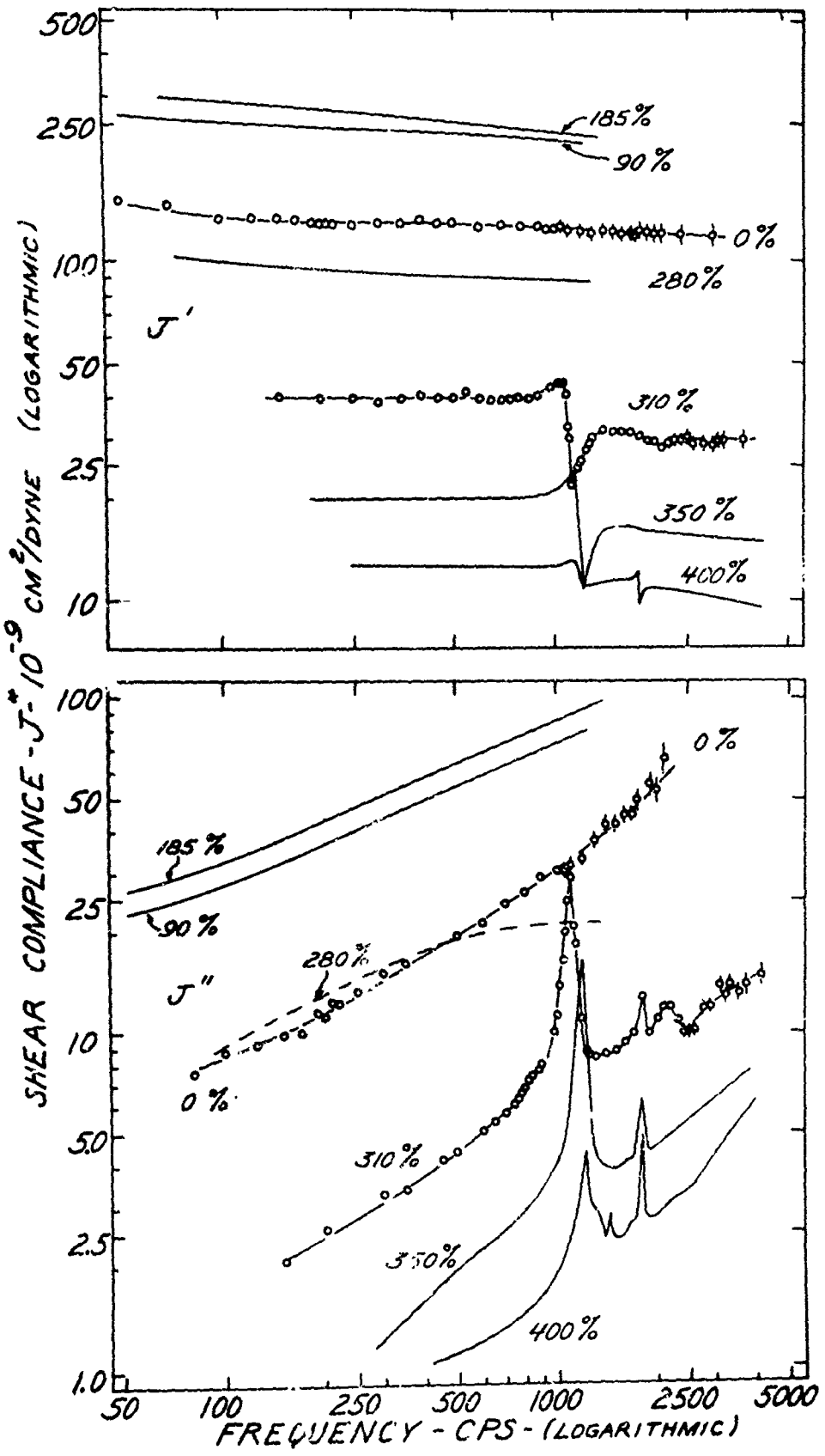
500
250
100
50
25
10
185%
90%
0%
280%
J'
310%
350%
400%
SHEAR COMPLIANCE - J* - 10^-9 CM²/DYNE (LOGARITHMIC)
100
50
25
10
5.0
2.5
1.0
185%
90%
J"
280%
0%
310%
350%
400%
50
100
250
500
1000
2500
5000
FREQUENCY - CPS - (LOGARITHMIC)

Figure 10

BLANK PAGE

FIG. 10 Logarithmic plot of complex shear compliance, $J^* = J' - iJ''$, vs. frequency for natural rubber at various static elongations, as indicated. Results above 300% varied with time; the curves shown are for approximately equilibrium conditions (i.e., after 80 hours). Temperature was 25.1 $\pm$ 0.2 °C. Experimental points are shown for 0 and 310% elongations, but are otherwise omitted to avoid confusion. Note that the sharp peak near 1000 cps appeared first at an elongation of 310%, and thus coincides with the occurrence of both a crystallinity and a superstructure. (cf. reference 2)

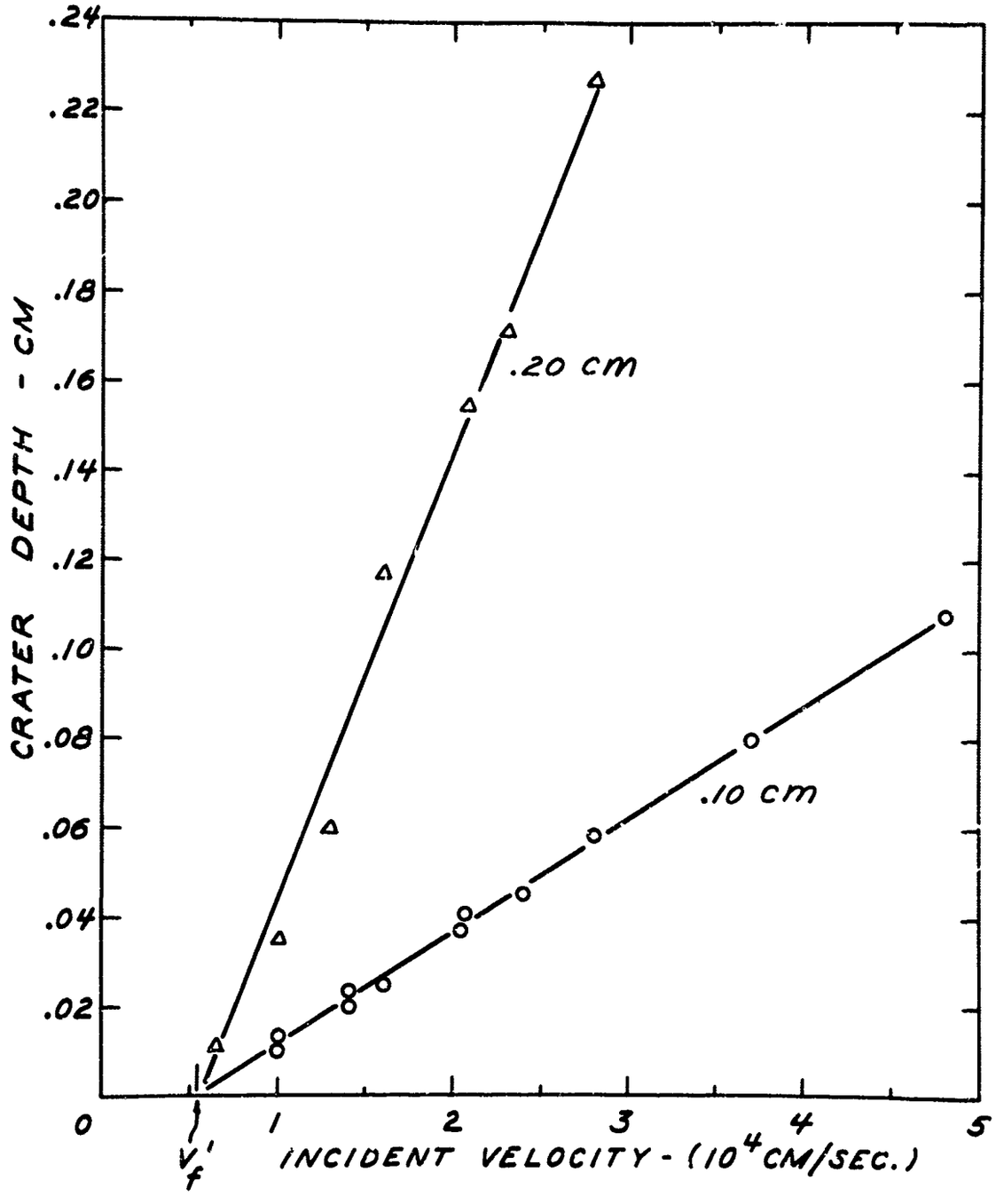

FIG. 11 Crater depth vs. incident velocity for two sizes of mercury drops impacting lead target plates. (Data from Olive G. Engel.[16]) The predicted threshold velocity, v_f', is 0.54×10^4 cm/sec.

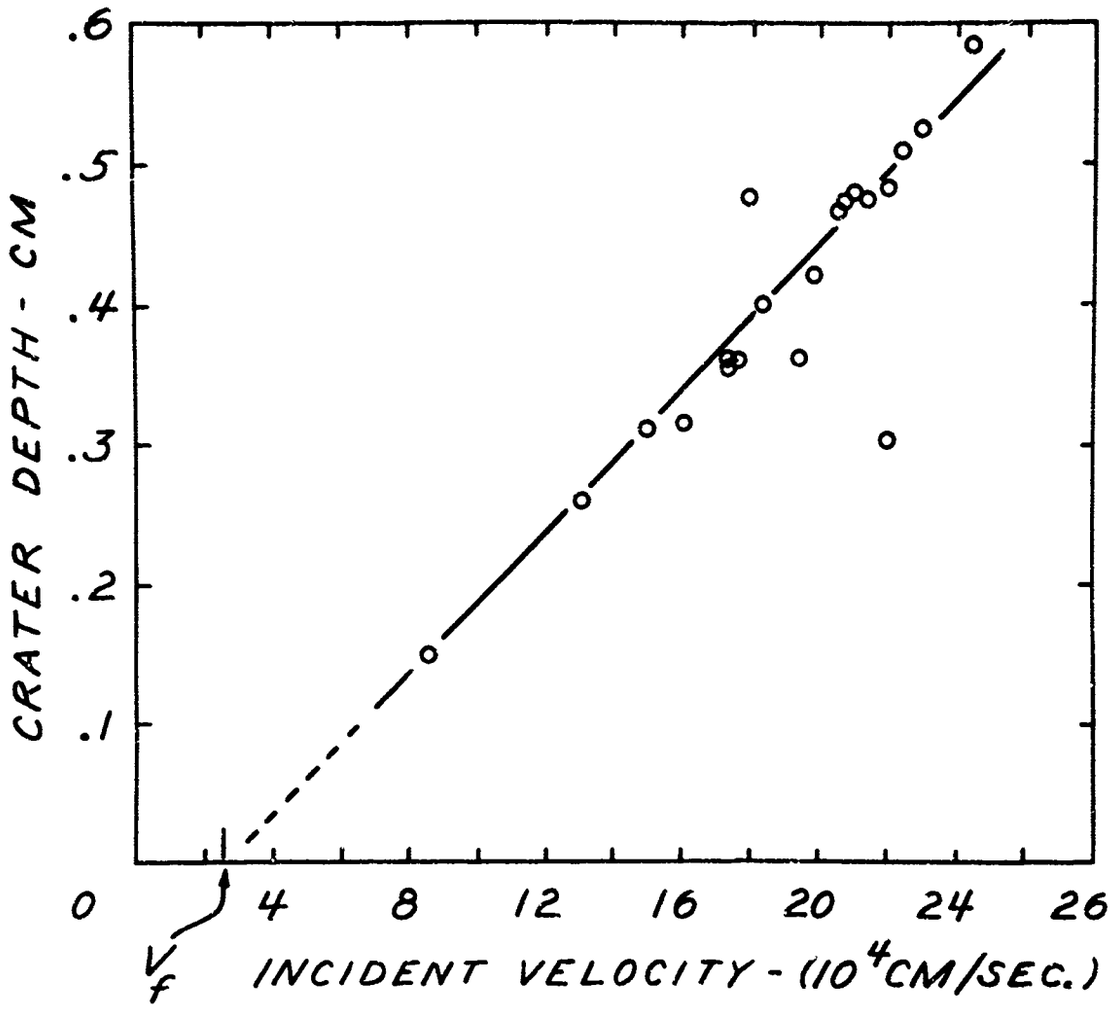

FIG. 12 Crater depth vs. projectile velocity for 0.483-cm iron spheres fired into semi-infinite iron targets. (Data from reference 17.) The predicted value of v_f is 2.36×10^4 cm/sec.

PART II

SESSION II

Tuesday - 22 October 1968

CHAIRMAN: Mr. Gordon R. Adams
Royal Explosives Research and
Defence Establishment
Ministry of Technology
Waltham Abbey, Waltham Cross
Essex, England

Propagation of Waves in Discrete Media, Harmonic, Anharmonic, and Defective	Dr. Elliott W. Montroll Department of Physics and Astronomy University of Rochester Rochester, New York
Dielectric And Lattice Dynamical Properties Of HMX And Related Substances*	Dr. George F. Wright University of Toronto Toronto, Canada
Crystal Lattice Effects On Thermal Initiation**	Dr. Terry Boddington University of Leeds Leeds 2, England
The Significant Structure Theory of Liquids Applied to the Shock Compression of Argon and Detonation of Condensed Explosives	Dr. Sheng Hsiu Lin Department of Chemistry Arizona State University Tempe, Arizona Co-Authors: Dr. Henry Eyring Department of Chemistry University of Utah Salt Lake City, Utah and Dr. D. Tweed Department of Chemistry Arizona State University Tempe, Arizona

* Paper is being revised by Dr. Wright
** Dr. Boddington did not submit paper for publication

SESSION II

PROPAGATION OF WAVES IN DISCRETE MEDIA, HARMONIC, ANHARMONIC, AND DEFECTIVE.

by

Elliott W. Montroll

Department of Physics and Astronomy
The University of Rochester
Rochester, New York

February 1969

The propagation of sound, shock, and detonation waves in continuous media has been investigated in great detail, but theoretical information is sparse on wave propagation in discrete media in the nonlinear regime and in the linear regime in the presence of irregularities. The aim of this lecture is to summarize the difference between the propagation of small amplitude waves in continuous and discrete media and to present some of the features of nonlinear wave propagation in discrete media, and of both linear and nonlinear wave propagation in irregular discrete media.

I. COMPARISON OF PROPAGATION OF SMALL AMPLITUDE WAVES IN CONTINUOUS AND ONE-DIMENSIONAL DISCRETE MEDIA.

The wave equation for the propagation of small amplitude waves in a continuous medium (without an energy dissipation mechanism) is

$$f_{tt} = c^2 f_{xx} \tag{1}$$

(where $f_x \equiv \partial f/\partial x$, etc., c the propagation velocity and f the physical quantity, for example density, whose variation in the medium is determined by the wave propagation). Any function

$$f = f(x \pm ct) \tag{2}$$

is a solution of (1). Hence, any initial disturbance of f from a constant value retains its form while propagating with velocity c either to the left or to the right. Even a very sharp gradient in an initial disturbance retains its shape as it propagates.

A medium composed of springs and masses generally does not allow an arbitrary wave to propagate without a change in form. The one-dimensional discrete analogue of (1) is the

$$d^2f_n/dt^2 = (\gamma/m)[f_{n+1} - 2f_n + f_{n-1}] \tag{3}$$

where f_n is the displacement of the n^{th} mass from its equilibrium position. If both sides of (3) are divided by a^2 (a being the lattice spacing), the resulting equation

$$\frac{m}{\gamma a^2}\frac{d^2f_n}{dt^2} = \frac{1}{a}\left\{\frac{f_{n+1}-f_n}{a} - \frac{f_n-f_{n-1}}{a}\right\} \tag{4a}$$

reduces to (1) as $a \to 0$ if one defines

$$c^{-2} = \lim_{\substack{a\to 0 \\ m/\gamma\to 0}} m/\gamma a^2 \qquad \text{and} \qquad (f_{n+1}-f_n)/a = \partial f/\partial x. \tag{4b}$$

A solution of (3) is

$$f_n = \exp i(n\theta \pm \omega t) \tag{5}$$

if θ and ω are related by the dispersion relation

$$\omega^2 = (2\gamma/m)(1 - \cos\theta)$$

or

$$\omega = \omega_L \sin\theta/2 \qquad \text{if} \qquad \omega_L = (4\gamma/m)^{\frac{1}{2}} \tag{6b}$$

The appropriate values of θ (and, therefore, of the normal mode frequencies ω), depend on the end conditions on the chain. For example, if the chain is composed of N particles and is closed in the form of a ring, then $f_{n+N} \equiv f_n$ so

that one must have

$$\theta = 2\pi k/N \qquad \text{where} \qquad k = 1,2,3,\ldots,N. \tag{7}$$

The wave forms

$$\cos(n\theta \pm \omega t) \qquad \text{and} \qquad \sin(n\theta \pm \omega t)$$

which are obtained by taking linear combinations of (5) and its complex conjugates yield waves which propagate to the left (for + sign) or to the right (for - sign) with velocity (a being the lattice spacing)

$$v = a\, dn/dt = \pm a\omega/\theta$$

$$= \pm \frac{N a \omega_L \sin(\pi k/N)}{2\pi k} \simeq (a\omega_L/2)\{1 - \frac{2}{3}\pi^2 k^2 a^2/L^2 + \ldots\} \tag{8}$$

which depends on k with $L \equiv aN$ being the length of the chain. In the long wavelength regime, $ka << L$, v is constant as in the continuum case.

Since an arbitrary initial condition can be expressed as a linear combination of normal modes of (5), we find that any wave with a sharp wave front, or any wave which is restricted to a limited region of space small compared with the total chain length, contains many k components. The small k components will travel with velocity $a\omega_L/2$ independently of k, while the large k components will travel with a velocity of O(N/k). Hence the wave form will lose some of its sharpness and spread because of the dispersive effect of a discrete medium.[1]

A convenient way of following the development of a wave form as it progresses through a chain is to express the solution of the equation of motion (3) in terms of Bessel functions as was first emphasized by Schrödinger[2]. Let

$$u_{2n} = f_n \qquad \text{and} \qquad u_{2n+1} = \frac{1}{2}\omega_L(f_n - f_{n+1}) \tag{9a}$$

Then the equations of motion (3) in terms of the u_n's become

$$\frac{2du_n}{d\tau} = (u_{n-1} - u_{n+1}) \qquad \text{with} \qquad \tau = t\omega_L \tag{9b}$$

This equation is exactly the same form as the Bessel function equation

$$J_{n-1}(\tau) - J_{n+1}(\tau) = 2dJ_n(\tau)/d\tau \tag{10a}$$

Another useful Bessel function equation is the recurrence formula

$$J_{n-1}(\tau) + J_{n+1}(\tau) = (2n/\tau)J_n(\tau). \tag{10b}$$

We see then that u_n can be expressed as a linear combination of Bessel functions

$$J_{n-r}(t\omega_L) \qquad r = 0,\pm1,\pm2,\ldots \tag{11}$$

If initially all displacements f_n are zero and all velocities except the m^{th} are initially zero, then

$$u_n(t) = f_m(0)J_{n-2m}(\tau) \tag{12}$$

is a solution of (9b). On the other hand, if velocities are initially zero and the m^{th} displacement is initially the only nonvanishing one,

$$u_{2m+i}(0) = \tfrac{1}{2}\omega_L f_m(0) \qquad \text{and} \qquad u_{2m-1}(0) = -\tfrac{1}{2}\omega_L f_m(0) \tag{13}$$

so that

$$\begin{aligned} u_n(t) &= \tfrac{1}{2}\omega_L f_m(0)\{J_{n-2m-1}(\tau) - J_{n-2m+1}(\tau)\} \\ &= \omega_L f_m(0)\, dJ_{n-2m}/d\tau \end{aligned} \tag{14}$$

Since our original equations (9) are linear, a superposition of these special solutions (12) and (14) lead to

$$u_n(t) = \sum_{m=-\infty}^{\infty} \{f_m(0)J_{n-2m}(\tau) + \omega_L f_m(0)\ dJ_{n-2m}/d\tau\}$$

$$= \sum_{m=-\infty}^{\infty} \{f_m(0)J_{n-2m}(\tau) + \tfrac{1}{2}\omega_L[f_m(0)-f_{m+1}(0)]J_{n-2m+1}(\tau)\} \qquad (15)$$

The particle velocities and displacements are then, respectively,

$$\dot{f}_n(t) = u_{2n}(t) \qquad (16a)$$

and

$$f_n(t) = f_n(0) + \int_0^t u_{2n}(\tau)\ dt \qquad (16b)$$

Some interesting special cases[3] are (a) particle at origin displaced by unity at t = 0, all other particles at equilibrium positions, and all particles initially at rest

$$f_n(t) = J_{2n}(t\omega_L) \quad \text{if} \quad f_m(0) = 0 \quad \text{and} \quad f_m(0) = \delta_{m,0} \qquad (17)$$

and (b) particle at origin at equilibrium but moving with velocity unity, all others fixed at equilibrium position

$$f_n(t) = \int^t J_{2n}(t\omega_L)\ dt \text{ if } \dot{f}_m(0) = \delta_{m,0} \quad \text{and} \quad f_m(0) = 0 \qquad (18)$$

so that

$$f_n(t) = \frac{2}{\omega_L} \sum_{\nu=0}^{\infty} J_{2n+2\nu+1}(t\omega_L). \qquad (19)$$

In the case of a semi-infinite chain, the particle "-1" is uncoupled with "0" so that the end condition of the chain is

$$\frac{d^2 f_o}{dt^2} = -\frac{\gamma}{m}(f_o - f_1), \qquad (20)$$

or, in terms of the u's

$$2du_o/d\tau = - u_1 \tag{21}$$

It is easy to verify that if $f_o(0) = 1$ and all else vanishes at $t = 0$,

$$f_n(t) = J_{2n}(t\omega_L) + J_{2n+2}(t\omega_L) \qquad \text{for } n = 0, 1, 2, \ldots \tag{22}$$

while, if $\dot{f}_o(0) = 1$, and all else vanishes at $t = 0$,

$$f_n(t) = \int_0^t dt\{J_{2n}(t\omega_L) + J_{2n+2}(t\omega_L)\} \qquad \text{for } n = 0, 1, 2, \ldots \tag{23}$$

The case in which the end particle, $n = 0$, is driven to the right with a constant velocity u, with all other particles initially at rest at their equilibrium positions, is a simple model of a shock produced by a driving plate on a bar. The solution of our equation of motion is

$$f_n(t) = \frac{2u}{\omega_L} \sum_{\nu=0}^{\infty} (2\nu+1) J_{2n+2\nu+1}(t\omega_L) \tag{24}$$

We have plotted the case of an initial impulse (23) and of a driven first particle in Fig. 1a and 1b. In a nondispersive medium, all particles would have the same trajectory as $f_o(t)$ but lagging it with a time depending on the particle number. However, as is clear from the figure 1, this is not the case for our chain of particles. In general, the wave form broadens and flattens as it propagates and is accompanied by a diminishing train of ripples, both in space and time. It was pointed out by Gilman and Vineyard[4] that the pulse in (17) reaches the n^{th} particle at time

$$t \sim \frac{2n}{\omega_L} + \frac{0.809(2n)^{1/3}}{\omega_L} \qquad \text{if } n >> 1$$

Neither the linear continuous or discrete models exhibit shock wave character. There is no dependence of the wave shape on amplitude and the

characteristic sharpening of the wave form does not occur.

The simplest one-dimensional chain with nonharmonic interactions in which shock waves develop is a chain of hard spheres which interact only through their mutual infinite repulsion at short distances. We discuss[4] this case now. Certain other more complicated models will be presented later.

Consider a one-dimensional gas of hard spheres which are initially equally spaced and at rest so that the distance between the centers of successive spheres is a. Let m be the mass of each ϕ sphere.

The laws ofconservation of momentum and energy between two colliding spheres of mass m_1 and m_2 can be summed up in the equations

$$m_1u_1 + m_2u_2 = m_1v \tag{25a}$$

$$\tfrac{1}{2}m_1u_1^2 + \tfrac{1}{2}m_2u_2^2 = \tfrac{1}{2}m_1v^2 \tag{25b}$$

where u_j is the velocity after collision of the sphere of mass m_j and it is postulated that before collision, that of mass m_2 is at rest while that of mass m_1 has a velocity v. It is easily seen that

$$u_2 = \frac{2v}{1+(m_2/m_1)} \quad \begin{cases} \rightarrow v & \text{as } m_1 \rightarrow m_2 \\ \searrow 2v & \text{as } m_1 \rightarrow \infty \end{cases} \tag{26a}$$

$$u_1 = \frac{v(1-m_2/m_1)}{1+(m_2/m_1)} \quad \begin{cases} \nearrow 0 & \text{as } m_1 \rightarrow m_2 \\ \searrow v & \text{as } m_1 \rightarrow \infty \end{cases} \tag{26b}$$

These formulae can now be applied to the propagation of a disturbance down the line of equal masses which we discussed above to be originally at rest and uniformly spaced. Let us first analyze the case in which the par-

ticle at the left end of the chain moves to the right with velocity v. After it collides with the first particle to its right, we see from the upper arrow cases of eq. (26a) and (26b) that the incident particle stops, giving its velocity to the one with which it collides, which then achieves the velocity v. This continues down the line. If the diameter of each sphere is Δ, the time between collisions is

$$t = (a-\Delta)/v \tag{27}$$

The mean speed at which the disturbance propagates is the ratio of distance it proceeds in each collision to the time required for that propagation,

$$V = a/[(a-\Delta)/v] = v/[1-(\Delta/a)] > v \ . \tag{28}$$

After the disturbance passes, the atoms are again at rest but they have moved a distance $(a-\Delta)$ to the right.

A case which is more interesting is that in which the particle at the left end is driven with a constant velocity v which, through a continually applied driving force, is not affected by collisions. This is equivalent to giving the left end particle an infinite mass and corresponds to the lower arrow case of equations (26a) and (26b). Hence the velocity of the leading edge of the disturbance is, (replacing v in (28) by 2v),

$$\dot{V} = 2v/[1-\Delta/a]. \tag{29}$$

Since the velocity of the trailing edge is v, the average thickness of the pulse is

$$\delta = \left\{ \frac{1+(\Delta/a)}{1-(\Delta/a)} \right\} vt \tag{30}$$

and v is the velocity of particles in the shocked region. The trajectories of both of the cases discussed are plotted[4] in figures (2) and (3).

II. EQUATIONS OF MOTION AND DISPERSION RELATIONS IN 2D AND 3D HARMONIC LATTICES.[5]

We now examine the two- and three-dimensional models which correspond more closely to real solids. The equations of motion of a crystal lattice follow immediately from the crystal Hamiltonian which has the form

$$H = T + \Phi \,, \tag{31a}$$

T being the kinetic energy

$$T = \frac{1}{2} \Sigma\, m_k\, u_\alpha^2(^{\ell}_{\kappa}) \tag{31b}$$

and Φ the potential energy

$$\Phi = \Phi_o + \frac{1}{2} \sum \Phi_{\alpha\beta}(^{\ell\ \ell'}_{\kappa\ \kappa'}) u_\alpha(^{\ell}_{\kappa}) u_\beta(^{\ell'}_{\kappa'}) + O(u^3) \tag{31c}$$

where, in the harmonic approximation terms, cubic and higher order in displacements from equilibrium are neglected.

The quantities

$$u_\alpha(^{\ell}_{\kappa}) \qquad \text{and} \qquad \Phi_{\alpha\beta}(^{\ell\ \ell'}_{\kappa\ \kappa'})$$

represent respectively the displacement from equilibrium of the particle (of mass m_κ) located at the κ^{th} position in the ℓ^{th} unit cell (α running through the set of components, x, y, and z) and the force constant which couples the displacement in the α direction of the κ^{th} atom in the ℓ^{th} cell with that in the α' direction of the κ' atom in the ℓ' cell. The quantity Φ_o is the vibra-

tional potential energy in the equilibrium state with all atoms located at their equilibrium positions and

$$\Phi_{\alpha\beta} = \left[\frac{\partial^2 \Phi}{\partial u_\alpha(\ell_\kappa)\, \partial u_\beta(\ell'_{\kappa'})} \right]_0 \tag{32}$$

The evaluation of these second derivatives is also to be made at the equilibrium state.

The equations of motion of the vibrating lattice can be found from the Hamiltonian (31a). In the small vibration harmonic approximation, the resulting equations are linear in the displacements u. Since boundary effects are generally uninteresting, one usually employs the Born-von Karman periodic boundary conditions in lattice vibration discussions. The periodic nature of the crystal implies that the α^{th} component displacement of particle κ in all ℓ can be written as

$$u_\alpha(\ell_\kappa) = m_\kappa^{-\frac{1}{2}} u_\alpha(\kappa) \exp i[\, t\omega(k) + 2\pi\, k\cdot r(\ell)] \,, \tag{33}$$

When this is substituted into the equations of motion

$$m_\alpha \ddot{u}_\alpha(\ell_\kappa) = \sum_{\beta,\ell',\kappa'} \Phi_{\alpha\beta}(\ell_\kappa\, \ell'_{\kappa'}) u_\beta(\ell'_{\kappa'}) \tag{34}$$

one obtains a set of homogeneous equations whose solution exists only if the determinant of the coefficients of the displacements vanish. The matrix of the determinant is called the "dynamical matrix". The normal mode frequencies $\omega(k)$ associated with the wave vector k are solutions

$$\det \{D_{\alpha\beta}(k_\kappa\, \kappa') - \omega^2(k)\delta_{\alpha\beta}\delta_{\kappa\kappa'}\} = 0 \tag{35a}$$

where

$$D_{\alpha\beta}(k_\kappa\, \kappa') = (m_\kappa m_{\kappa'})^{-\frac{1}{2}} \sum_\ell \Phi_{\alpha\beta}(\ell_\kappa\, \kappa') \exp[2\pi i k\cdot r(\ell)] \tag{35b}$$

The detailed dispersion relations

$$\omega = \omega(k) \tag{36}$$

which are the roots of the characteristic determinants (10a) as a function of k are very sensitive to the detailed choice of force constants Φ. Experiments such as the scattering of slow neutrons by crystals can be used to determine these dispersion curves.[13] The force constants $\Phi_{\alpha\beta}$ can sometimes be obtained from information on the elastic constants of the crystal. By combining both sets of data, a best set of force constants and dispersion curves can be found. Note that there are a number of branches of dispersion relations. For example, in the case of a monatomic cubic crystal, the dynamical matrix is 3x3 and there are three branches.

There is one model which leads to considerable simplification. It is a simple cubic lattice with nearest neighbor forces only,[6-8] both central and noncentral, the noncentral forces being required to keep the lattice stable, relative to shear. This case is simple because the x, y, and z components of the motion do not couple so that the dynamical matrix is diagonal. The equations of motion are those of a lattice with one degree of freedom per lattice point. We let the displacement of the $(\ell,m,n)^{th}$ particle from equilibrium in the x direction be

$$\begin{aligned} M\ddot{x}_{\ell,m,n} = &\gamma_1(x_{\ell+1,m,n} - 2x_{\ell,m,n} + x_{\ell-1,m,n}) \\ &+ \gamma_2(x_{\ell,m+1,n} - 2x_{\ell,m,n} + x_{\ell,m-1,n}) \\ &+ \gamma_3(x_{\ell,m,n+1} - 2x_{\ell,m,n} + x_{\ell,n,n-1}) \end{aligned} \tag{37}$$

where γ_1 is the central force constant and γ_2 and γ_3 the noncentral force constants between nearest neighbors. Two similar sets of equations exist for y and z displacements.

One can express the motions of particles in the lattice as linear combinations of the normal modes,

$$x_{\ell,m,n} = \exp\{i(\omega t+\ell\phi_1+m\phi_2+n\phi_3)\} , \tag{38}$$

the ϕ's being chosen as

$$\phi_j = 2\pi k_j/N, \qquad k_j=0, 1, 2, \ldots, N-1, \tag{39}$$

so that the x's satisfy periodic boundary conditions

$$x_{\ell,m,n} = x_{\ell+N,m,n}, \text{ etc.}, \tag{40}$$

N being the number of lattice points in each direction in the lattice. The points (ϕ_1,ϕ_2,ϕ_2) are points on the reciprocal lattice. The normal mode frequencies are found to be the function $\omega(\phi_1,\phi_2,\phi_3)$ defined by

$$M\omega^2 = \sum_1^3 2\gamma_j(1 - \cos\phi_j), \tag{41}$$

which is triply periodic in reciprocal (ϕ_1,ϕ_2,ϕ_3) space. Equations similar to (37) exist for y and z components of the displacements as well. All yield the same dispersion relation. Each set of frequencies is called a branch of the frequency spectrum. When next nearest neighbor interactions are introduced, these branches become somewhat different. One frequency corresponds to each triple of ϕ's of the form (39).

The thermodynamic properties of a crystal depend on the normal mode frequencies $\{\omega\}$. For example, the specific heat at constant volume is

$$c_v = k \sum_j \left(\frac{\hbar\omega_j}{2kT}\right)^2 / \sinh^2(\hbar\omega_j/2kT) \tag{42}$$

As $N \to \infty$ we see from (41) that the normal mode frequency becomes dense so that the sum (43) can be expressed as an integral over the frequency distribution function $g(\omega)$ which has the property $g(\omega)d\omega$ is the fraction of frequencies between ω and $\omega+d\omega$. Then

$$c_v = Nk \int_0^{\omega_L} g(\omega)\{(\hbar\omega/2kT)^2/\sinh^2(\hbar\omega/2kT)\}\, d\omega \tag{43}$$

where ω_L is the largest frequency, which, in case (41), becomes

$$M\omega_L^2 = 4(\gamma_1+\gamma_2+\gamma_3). \tag{44}$$

Every lattice point $(2\pi k_1/N, 2\pi k_2/N, 2\pi k_3/N)$ corresponds to a frequency ω. In the limit $N \to \infty$ the number of lattice points in the region

$(0 < \phi_j < 2\pi)$, j=1,2,3, becomes dense and one can construct surfaces of constant frequency. In two dimensional cases, there are only two ϕ's, ϕ_1 and ϕ_2, and one has curves of constant frequency. These are exhibited in Fig. 4 as obtained from (41) with $\gamma_3 \equiv 0$, the dispersion relation obtained from the 2D equations of motion

$$M\ddot{x}_{\ell,m} = \gamma_1(x_{\ell+1,m} - 2x_{\ell,m} + x_{\ell-1,m}) + \gamma_2(x_{\ell,m+1} - 2x_{\ell,m} + x_{\ell,m-1}). \tag{44a}$$

If $G(\omega^2)$ is defined as the fraction of square frequencies between ω^2 and $\omega^2+d\omega^2$, then it is clear that $G(\omega^2)$ is proportional to the rate at which (ϕ_1,ϕ_2,ϕ_3) space is swept out by a surface of constant frequency as the frequency increases. Since

$$g(\omega)d\omega = 2\omega G(\omega^2)\, d\omega\ , \tag{45}$$

$g(\omega) = 2\omega G(\omega^2)$, and the distribution function $g(\omega)$ can be expressed (for a single branch of the spectrum) as the volume integral

$$g(\omega) = \frac{1}{8\pi^3}\frac{\partial}{\partial\omega}\int\int\int_{0<\omega(\phi_1\phi_2\phi_3)<\omega} d\phi_1\, d\phi_2\, d\phi_3 \tag{46a}$$

or the surface integral

$$g(\omega) = \frac{1}{(2\pi)^2}\iint \frac{ds}{|\text{grad }\omega|} \tag{46b}$$

where the integration proceeds over the entire surface ω = constant.

The frequency spectrum is easily obtained in the 2D case. One finds from the 2D analogue of (41) that

$$M^2\omega - 2(\gamma_1+\gamma_2) = -2\gamma_1\cos\phi_1 - 2\gamma_2\cos\phi_2 \quad \text{and} \quad M\omega_L^2 = 4(\gamma_1+\gamma_2) \tag{47}$$

The lines of constant frequency are plotted in fig. 4. If, when $\omega^2 < \frac{1}{2}\omega_L^2$, we multiply by 4 the fraction of frequencies in the first quadrant whose square is between ω^2 and $\omega^2+d\omega^2$, we find

$$G(\omega^2) = \frac{4}{4\pi^2}\,\frac{\partial}{\partial\omega^2}\int_0^{\phi} d\phi_1 \int_0^{\phi_2} d\phi_2 \tag{48}$$

where ϕ_2 is to be expressed in terms of ϕ_1 through (47) and ϕ is the value of ϕ_1 when $\phi_2 = 0$, i.e.,

$$2\gamma_1\cos\phi = 2\gamma_1 - M\omega^2$$

or

$$\phi = \cos^{-1}\left(1 - \frac{M\omega^2}{2\gamma_1}\right)$$

Then

$$G(\omega^2) = \frac{1}{\pi^2}\int_0^{\phi} d\phi_1 \left\{1 - \left[\frac{2(\gamma_1+\gamma_2) - M\omega^2 - 2\gamma_1\cos\phi_1}{2\gamma_2}\right]^2\right\}^{-\frac{1}{2}}$$

so that if we define a new variable of integration, x, by

$$(x-1)(M\omega^2/4\gamma_1) = \cos\phi_1 - 1$$

we see that

$$G(\omega^2) = \frac{1}{(\pi\omega)^2}\int_{-1}^{1} \left\{(1-x^2)\left[\left(\frac{8\gamma_1}{M\omega^2} - 1\right) + x\right]\left[\left(\frac{8\gamma_2}{M\omega^2} - 2\right) - x\right]\right\}^{-\frac{1}{2}} \tag{49a}$$

which is a complete elliptic integral of the second kind. This is defined by

$$K(k) = \int_C^{\pi/2} (1 - k^2\sin^2\theta)^{-\frac{1}{2}}\, d\theta \tag{49b}$$

One finds that

$$G(\omega^2) = \frac{M}{2\pi^2(\gamma_1\gamma_2)^{\frac{1}{2}}} K\left(\frac{M\omega(\omega_L^2-\omega^2)^{\frac{1}{2}}}{4(\gamma_1\gamma_2)^{\frac{1}{2}}}\right) \quad \text{if } 0 < M^2\omega^2(\omega_L^2-\omega^2) < 16\gamma_1\gamma_2 \qquad (50a)$$

In a similar manner it can be shown that

$$G(\omega^2) = \frac{2}{\omega\pi^2(\omega_L^2-\omega^2)^{\frac{1}{2}}} K\left(\frac{2(\gamma_1\gamma_2)^{\frac{1}{2}}}{\omega(\omega_L^2-\omega^2)^{\frac{1}{2}}}\right) \quad \text{if } \omega^2(\omega_L^2-\omega^2) > 16\gamma_1\gamma_2 \qquad (50b)$$

where throughout $M\omega_L^2 = 4(\gamma_1+\gamma_2)$. There are two logarithmic singularities in $G(\omega^2)$, one at $M\omega^2 = 4\gamma_1$ and the other at $M\omega^2 = 4\gamma_2$. The functions $G(\omega^2)$ and $g(\omega)$ are plotted in Fig. 5.

While one cannot obtain simple formulae such as (50) for $G(\omega^2)$ in the 3D case, a representation as a single integral can be found and $G(\omega^2)$ can be easily calculated numerically. The graph of the function $g(\omega)$ for the simple cubic lattice model discussed above is given in Fig. 6. Fig. 7 is that for a more realistic model of sodium which is constructed to fit data on neutron scattering. The singularities are of the form $(|\omega-\omega_c|)^{\frac{1}{2}}$ as ω approaches certain critical values ω_c. A considerable literature exists on the nature of these singularities and the reason for their existence.[5,6,9-12]

A considerable literature also exists on the experimental determination of dispersion curves for various crystals[13].

The frequency spectrum and dispersion curves for polyatomic crystals is somewhat more complicated than that for monatomic ones[1,5]. In a simple cubic lattice in which the two atomic species alternate along the lattice points (for example, an NaCl type lattice), a generalization of (41) can be found for the squares of normal mode frequencies[14]. If the light and heavy masses are, respectively, M_1 and M_2, there are two branches to the frequency spectrum. The high frequency branch, which is known as the optical branch, is

$$\omega_+^2 = \tfrac{1}{2}(\omega_1^2+\omega_2^2) + \tfrac{1}{2}[(\omega_2^2-\omega_1^2)^2 + 16X^2/M_1M_2]^{\frac{1}{2}} \qquad (51a)$$

and the low frequency branch, which is known as the acoustical branch, is

$$\omega_-^2 = \tfrac{1}{2}(\omega_1^2+\omega_2^2) - \tfrac{1}{2}[(\omega_2^2-\omega_1^2)^2 + 16X^2/M_1M_2]^{\frac{1}{2}} \qquad (51b)$$

where

$$X = \sum_{j=1}^{3} \gamma_j \cos\phi_j \qquad (52)$$

and the ϕ_j's run through the set of values (39).

Also

$$M_j\omega_j^2 = 2(\gamma_1 + \gamma_2 + \gamma_3) \qquad \text{with } j = 1,2\ . \qquad (53)$$

The frequency distribution in this case is plotted in Fig. 8. Note the band gap between the two bands.

III. PROPAGATION OF A PULSE IN A 2D ANHARMONIC LATTICE.

Considerable insight on the propagation of a disturbance in two- and three-dimensional lattices can be obtained from machine calculations recently made by Payton, Rich, and Visscher[15] on 2D square lattices with linear and nonlinear force laws in the special case in which all interactions are between nearest neighbors only (with both central and non-central forces). The linear case is the model which we have discussed above. In the nonlinear case, the force law chosen was an expansion to fourth order of the Lennard-Jones potential

$$\phi_o(r) = \varepsilon_o[(r/r_o)^{12} - 2(r_o/r)^6]$$

$$= -\varepsilon_o + \frac{1}{2}\gamma(r-r_o)^2 - \frac{1}{3}\mu(r-r_o)^3 + \frac{1}{4}\nu(r-r_o)^4 \qquad (54)$$

The magnitudes of μ and ν relative to γ were taken to be appropriate for noble gas solids in the anharmonic case, and zero in the harmonic one. With arbitrary units such that $\gamma = 1$, the potentials used were

$$\Phi(x) = \frac{1}{2}x^2 - \frac{1}{3}\mu x^3 + \frac{1}{4}\nu x^4 \qquad (55)$$

Periodic boundary conditions were chosen in the direction normal to that of the propagation of the input disturbance and reflecting boundary conditions were set at the end of the lattice in the direction of propagation of the disturbance so that it could be reflected from the ends.

The feature that has made the calculations especially interesting is that they have been exhibited on a movie film. The 2D lattice is represented by a grid and the energy at a lattice point is shown by the raising of the grid at that lattice point by an amount proportional to the energy

(c.f. Fig. 9). The initial disturbance was the same at all lattice points along lines normal to the direction of propagation. The initial energy pulse had a kinetic energy per atom corresponding to 3 K and extended over several lattice rows.

Two typical film frames are shown in Figs. 9a and 9b; 9a represents a stage in the propagation of an energy pulse through a monatomic harmonic lattice. The initial pulse diminishes in amplitude as it progresses and, due to the dispersive character of the lattice, a trail of smaller amplitude waves develops behind it. Fig. 9b represents the situation as the wave propagates through the anharmonic lattice postulated above. Figs. 9a and 9b correspond to the states of development at the same time on the two lattices. Notice that a shock wave with a sharp front appears in the anharmonic case. As expected, its propagation velocity exceeds that of the small amplitude wave which trails it. The small amplitude trailing part behaves in essentially the way that a wave would propagate in the harmonic lattice. Payton, Rich, and Visscher have also made movies of the propagation of waves in lattices with defects. These are discussed in Section IV.

Similar calculations can also be made in 3D lattices but a film presentation is not possible.

A fundamental difficulty arises in the development of a theory of the propagation of large amplitude or shock waves in a 3D lattice. When large amplitude displacements from equilibrium occur, atoms exchange positions and lattice imperfections appear. These are very hard to program into a calculation.

A strong shock in a real solid has a front of only a few atomic layers. The mechanism of the rearrangement of the atoms from a lower to a higher density

state is unclear as is the dissipation mechanism after the shock passes. Cyril Smith has proposed that a shock front contains an array of edge dislocations which move with the shock front and which acccunt for the increase in density in the shock without the destruction of the lattice. A schematic picture of an edge dislocation is shown in Fig. 10 and the type of array of edge dislocations which might appear in the shock front is given in Fig. 11. Gilman and Vineyard[4] have discussed this model to some extent. The molecular motions in the shock front are probably similar to those experienced in melting.

IV. EFFECT OF DEFECTS ON LATTICE VIBRATIONS.

Let us now investigate the effect of defects on lattice vibrations and on the manner in which waves propagate through a defective lattice. Impurities are an important class of defects as are dislocations. The replacement of an atom in a lattice by an impurity corresponds to a local variation in mass and force constants, while a dislocation is essentially an extended variation in force constants.

Even without introducing a detailed model for the impurity, several effects can be deduced on general grounds by applying certain theorems (first due to Rayleigh) concerning systems of springs and masses. Let us suppose that the normal mode frequencies of an unperturbed lattice are

$$\omega_1^{(0)} < \omega_2^{(0)} < \omega_3^{(0)} < \omega_4^{(0)} < \ldots < \omega_n^{(0)} \tag{56}$$

Then, if one mass in the system is reduced, all frequencies are increased; however, the j^{th}, $\omega_j^{(1)}$, is bounded between the unperturbed j^{th} and $(j+1)^{st}$ so that

$$\omega_j^{(0)} < \omega_j^{(1)} < \omega_{j+1}^{(0)} \qquad j = 1,2,3\ldots,n-1 \tag{57a}$$

$$\omega_n^{(0)} < \omega_n^{(1)} \tag{57b}$$

If, instead, one mass is increased, one obtains the new set of frequencies $\omega_j^{(2)}$ such that

$$\omega_j^{(0)} > \omega_j^{(2)} > \omega_{j-i}^{(0)} \qquad j = 1,2\ldots,n-1 \tag{58a}$$

$$\omega_1^{(0)} > \omega_1^{(2)} \tag{58b}$$

The increase in a force constant has the same effect as the decrease of a mass (and vice versa). These results are, of course, in qualitative agreement with those involving a mass tied to a rigid wall by a spring in that a decrease in mass increases the frequency of vibration as does an increase in spring constant, and vice versa.

As we observed in the last section, a crystal contains a large number of degrees of freedom and, therefore, a large number of normal mode frequencies. These were shown to appear in dense bands. The inequalities (57) and (58) then imply that the frequencies of the perturbed lattice are essentially the same as those of the unperturbed one except that frequencies at the band edge might be displaced a considerable distance from the band. For example, if the lattice contains a light defect, the frequency $\omega_n^{(1)}$ (see inequality 57b) is not bounded from above so that it might become separated from the band. Indeed, if a linear chain which has no imperfections has a highest frequency ω_L, it can be shown that the defect frequency which escapes from the band and which is due to the light mass defect, is[16]

$$\omega = \omega_L [Q(2-Q)]^{-1/2} \qquad \text{with} \qquad Q = m'/m, \tag{59}$$

m' being the light defect mass and m the mass of a host lattice atom.

An observation first made by Lord Kelvin is useful for the interpretation of the nature of the normal mode of vibration associated with a frequency that is separated from the band. He found that if one tries to drive a wave into a periodic structure from one end with a frequency that is not in the frequency band, the wave damps out in a distance that depends on the displacement of the driven frequencies from the band edge, the penetration depth decreasing as the displacement from the band edge increases.

At a given temperature, thermal motion drives the various normal modes. One whose frequency lies out of the band remains localized because from Kelvin's theorem it cannot propagate far in the crystal. Hence in a monatomic crystal, localized modes develop around defects which involve light masses or force constants larger than those associated with pairs of atoms in an unperturbed crystal.

If two mass defects are far from each other, a localized mode develops around each and both modes have the same frequency. However, as the two are brought closer to each other until the ranges of localization overlap, the two modes interact with each other and the frequency degeneracy is split, one frequency going up and the other down. An impurity generally corresponds to a change in mass and several force constants; six in the case of a simple cubic lattice, with nearest neighbor interaction only. Since the splitting of the degeneracy by variation of several force constants is analogous to that by change of several masses, under favorable conditions one local mode might appear for the mass change and six with similar frequencies for the force constant change in a simple cubic lattice. As the concentration of impurities increases, impurity bands of frequencies develop.

As was mentioned in Section II, in the case of ordered diatomic and polyatomic lattices, the frequency spectrum contains optical (high frequency) and acoustical (low frequency) bands. A typical defect in such lattices is an interchange of two atoms, which corresponds to a local disorder. The change in frequency spectrum due to interchanging A and B atoms in an ordered AB lattice can be seen from a consideration of Rayleigh's theorem.[14] Let the mass of an A atom be M_A and that of the B atom be M_B with $M_A < M_B$. Then the act of replacing a heavy B atom by a lighter A atom causes a localized mode to emerge from the top of the optical and another from the top of the acousti-

cal band. The completion of the interchange by replacing the light A with a heavier B causes a mode to emerge from the bottom of the optical band. Similar remarks can be made about the influence of a change in force constants. The various frequencies of the localized modes and their sources are sketched in Fig. 12 for the case of $\gamma_{AA} > \gamma_{AB}$ and $\gamma_{BB} < \gamma_{AB}$. The diagram corresponds to our simple cubic lattice model which possesses one degree of freedom per lattice point. All degrees of freedom are taken into account by multiplying each mode by a degeneracy factor of three. This degeneracy is split by considering next nearest neighbor interactions. If two force constants are changed at widely separated points in a lattice, the associated localized mode frequencies are degenerate. The degeneracy is split as the two anomalous force constants are brought closer together. If it is assumed that only central force constants are changed when an A atom is replaced by a B atom in our ordered diatomic lattice, two new force constants are associated with the substituted B atom. The pairs of closely lying frequencies in Fig. 12 are drawn to correspond to the resulting splitting of pairs of anomalous force constant localized mode frequencies.

Some of the localized modes shown in Fig. 12 might be suppressed for the following reason. Suppose a small decrease in a mass is made so that frequencies barely rise from the bands. A large decrease in the force constants which reduce all frequencies might return these modes to the bands. This interplay between changes of masses and force constants has been discussed for one-dimensional systems elsewhere. Situations exist in which a frequency does not emerge from the bands until a parameter is changed by more than a certain critical amount.

Now consider a two- or three-dimensional lattice with a low concentration of randomly distributed mass defects. Let a disturbance propagate

through the lattice and suppose that the disturbance extends over the complete line, (or plane, in the 3D case), normal to the direction of propagation while the depth of the disturbance is of the order of five to twenty-five lattice spacings. One would expect the following events to occur.

In the neighborhood of a light impurity, a localized mode would be generated. However, since the frequency of vibration of the light particle is higher than that of its neighbors, they would tend to be in phase with the pulse for a long time while the light impurity would be sometimes in phase and sometimes out of phase with the pulse. Hence the light impurity would not couple to and pick up energy from the pulse as well as its heavier neighbors would. If, for example, one plotted the energy associated with each particle, the light mass would have less than its neighbors. On the other hand, a heavy defect has greater inertia than its neighbors so that it remains in phase with the driving pulse for a longer time and can pick up more energy leading to a spike in an energy curve. The motion of the heavy atom is called a resonance mode. It has a finite lifetime which is the time required to transmit its energy to the rest of the crystal. Changes in force constants yield similar results--an increase in force constant corresponding to a decrease in mass, and vice versa.

Defects act as scatterers so that part of the pulse is reflected backward by them and, indeed, at a fixed concentration in a sufficiently long sample, one would expect little of the pulse to continue through it without being reflected back.

The mathematical theory of the effect of defects has been developed in a number of papers, including those in References 16 and 17. Several reviews exist, (see, for example, References 5, 18, and 19). Recent experimental work is reported in Reference 20.

Payton, Rich, and Visscher[15] in their film program discussed in the last section, have given an excellent visual presentation of the propagation of a disturbance in a lattice with defects. The atoms of the host lattice were given a mass three, and light and heavy defects were given masses one and nine, respectively.

The first cases considered were an isolated light and an isolated heavy defect in an otherwise perfect two-dimensional lattice. The quantity exhibited in Fig. 13 which summarizes their results is the energy at each lattice point.

The difference between the passage of a wave through a light and a heavy impurity is shown in Fig. 13. The dip in energy in the light impurity case and the spike in the heavy one are as described above.

Figures 14a and 14b give an equal time comparison of energy penetration into a harmonic lattice containing 15% heavy atoms with that into a 15%-light impurity region. The impurity sites are the same in both cases. The pulse seems to propagate further in the lattice with light impurities than in the one with heavy. Apparently the heavy impurities reflect the incident wave better than do the light ones.

Finally, Figures 14a and 14c show the effect of 15% heavy impurities on both harmonic and anharmonic lattices. Clearly the pulse propagates through defects in the anharmonic lattice (case c) more easily than through the harmonic one.

All the figures were taken from reference 15. The movies exist in the Los Alamos film library.

V. ERGODICITY AND PERMANENT WAVES IN ANHARMONIC ONE-DIMENSIONAL CHAINS.

One of the basic ideas in the classical statistical mechanics of systems undergoing small vibrations is that, at equilibrium at a given temperature, the energy of the system becomes equally divided into the various normal modes of vibration. This is the so-called equipartition theorem which states that the energy in every mode is (1/2kT).

Of course some mechanism has to be provided for the weak coupling of the various modes since, if a system is completely harmonic, energy can never be transferred between modes. A weak anharmonicity, a radiation field, or contact with some kind of heat bath are considered to be sufficient to make the mode mixing possible.

The equipartition theorem is deduced from equilibrium statistical mechanics and not from an investigation of the asymptotic behavior of its dynamics. Hence one could imagine (but not many did seriously) that equilibrium might never be achieved, in which case the theorem would not be applicable. A number of calculations have been made recently, investigating this point.

i) Fermi, Pasta, and Ulam calculations.[21]

In the early days of high speed computers, E. Fermi became interested in their employment for the solution of nonlinear problems. He felt that future fundamental theories in physics may involve nonlinear operations and equations and that it would be useful to develop some experience in this field. As a test problem, he thought that the dynamics of the approach to equipartition would be interesting to investigate.

A problem which Fermi, Pasta, and Ulam investigated with MANIAC I at Los Alamos was the ergodic behavior of a linear chain of particles which interacted through a nonlinear interparticle force. The interaction laws studied

were respectively quadratic, cubic, and certain broken line interactions so that the equations of motion were successively

$$\ddot{x}_i = (x_{i+1} + x_{i-1} - 2x_i) + \alpha[(x_{i+1} - x_i)^2 - (x_i - x_{i-1})^2] \qquad (60a)$$

$$\ddot{x}_i = (x_{i+1} + x_{i-1} - 2x_i) + \beta[(x_{i+1} - x_j)^3 - (x_i - x_{i-1})^3] \qquad (60b)$$

$$\ddot{x}_j = \delta_1(x_{i+1} - x_i) - \delta_2(x_i - x_{i-1}) + c \qquad (60c)$$

$$i = 1, 2, 3, \ldots, N$$

where x_i represents the displacement of the i^{th} atom from its equilibrium position. The constants α and β were chosen so that at maximum displacement the nonlinear terms were only about one-tenth of the linear ones. In the third case, the parameters δ_1, δ_2, and c were not constants but assumed different values depending upon whether or not the quantities in the parentheses were greater or less than a certain value fixed in advance. The values of N used by FPU were 16, 32, and 64.

The total energy of the chain, in the harmonic approximation, is

$$E = \sum_j \{\tfrac{1}{2} x_j^2 + [(x_{j+1} - x_j)^2 + (x_j - x_{j-1})^2]\}$$

$$= \sum_k \{\tfrac{1}{2}\dot{a}_k^2 + 2a_k^2 \sin^2(\pi k/2N)\} \qquad (61)$$

The normal coordinates a_k are defined by

$$a_k(t) = \sum_j x_j(t)\sin(kj\pi/N) \qquad (62)$$

so that

$$x_j(t) = \frac{2}{N} \sum_{k=1}^{N} a_k(t)\sin(jk\pi/N) \qquad (63)$$

Also,

$$\ddot{a}_k + \omega_k^2 a_k = 0 \qquad k = 1,\ldots N \tag{64a}$$

where

$$\omega_k = 2\sin(\pi k/2N). \tag{64b}$$

When anharmonic terms are included their contribution, which in case (60a) is proportional to the sum of $\alpha(x_{j+1}-x_i)^3$ and in case (60b) to sum of $\beta(x_{j+1}-x_j)^4$, must be added to (61). In the FPU calculation, their contribution to E was never more than a few percent. In the presence of anharmonicities, the various a_k's coupled so that the members of the set of equations (64) are all coupled.

If all the energy is initially in the normal mode k = 1, one would expect the coupling to generate a slow flow of energy into the higher modes until equipartition with som small fluctuation is achieved. As $N \to \infty$ these fluctuations should vanish.

In the FPU calculations, the process started as expected, energy flowed into the second, then the third, then the fourth and fifth mode, but, to the surprise of all concerned, most of the energy suddenly flowed back into the second mode and soon into the first mode with this exchange continuing. With N = 32 and $\alpha = 1/4$, the total energy in modes with $k > 5$ never exceeded 8%. The details are shown in Fig. 15.

ii) Some Aspects of Perturbation Theory of Chain with Quadratic Nonlinearity.

While perturbarion theory is not the most effective way of obtaining a clear understanding of nonlinear processes, one can without too much difficulty obtain some ideas from it. The easiest case to discuss is

the quadratic nonlinearity which yields the equations of motion

$$m\ddot{x}_j = \gamma(x_{j-1}-2x_j+x_{j+1}) + \alpha[(x_{j-1}-x_j)^2 - (x_j-x_{j+1})^2]. \tag{65}$$

Let us consider a ring of springs and masses so that $x_{j+N} \equiv x_j$. Then we set

$$x_j = \frac{1}{N}\sum_{k=1}^{N} a_k \exp(2\pi ikj/N \tag{66a}$$

so that

$$(x_{j-1}-x_j) = \frac{1}{N}\sum a_k[-1 + \exp(-2\pi ik/N)]\exp(2\pi ikj/N) \tag{66b}$$

and

$$(x_{j-1}-x_j)^2 = \frac{1}{N}\sum_k\sum_{k'} a_{k'}a_{k-k'}e^{2\pi ijk/N}\left[1-e^{-2\pi ik'/N}\right]\left[1-e^{-2\pi i(k-k')/N}\right] \tag{66c}$$

Similar expressions exist for (x_j-x_{j+1}) and $(x_j-x_{j+1})^2$. If all these equations are substituted into (65) and coefficients of $\exp(2\pi ikj/N)$ on both sides of the resulting equation are equated, one finds that

$$\ddot{a}_k + \omega_k^2 a_k = \frac{2i\alpha}{mN}\sum_{k'} a_{k'}a_{k-k'}\{\sin 2\pi k'/N - \sin 2\pi k/N + \sin 2\pi(k-k')/N\}$$

$$= (8i\alpha/mN)\sum_{k'} a_{k'}a_{k-k'}\sin(\pi k/N)\sin(\pi k'/N)\sin\pi(k'-k)/N \tag{67a}$$

where

$$\omega_k^2 = (2\gamma/m)(1 - \cos 2\pi k/N) \tag{67b}$$

or

$$\omega_k = \omega_L \sin\pi k/N \qquad \text{with} \qquad \omega_L^2 = 4\gamma/m. \tag{67c}$$

Since the solution of

$$\ddot{a}_k + \omega_k^2 a_k = f(t) \tag{68a}$$

is

$$a_k(t) = a_k(0)\cos t\omega_k + \omega_k^{-1}\dot{a}_k(0)\sin t\omega_k + \omega_k^{-1}\int_0^t f(\tau)\sin(t-\tau)\omega_k\, d\tau \tag{68b}$$

we see that the differential equation (68a) is equivalent to the non-linear integral equation

$$a_k(t) = a_k(0)\cos t\omega_k + \omega_k^{-1}\dot{a}_k(0)\sin t\omega_k + (8\pi i\alpha/mN\omega_L)\int_0^t \sin(t-\tau)\omega_k \sum_{k'=1}^{N} a_{k'}(\tau)a_{k-k'}(\tau)\sin\frac{\pi k'}{N}\sin\pi\frac{(k-k')}{N}\,. \tag{69}$$

A systematic but tedious way of solving this equation is to iterate to obtain a power series in the small parameter α. To get some idea of how the mode coupling develops, let us choose the simple example $\dot{a}_k(0) = 0$ for all k and

$$a_k(0) = Nc(\delta_{k,1} - \delta_{k,N-1})/2i \tag{70a}$$

This corresponds to the initial sine distribution

$$x_j(0) = c\sin 2\pi j/N \tag{70b}$$

Note that

$$\omega_k = \omega_{N-k} \tag{71}$$

Then upon iteration we find that

$$a_k(t) = \frac{Nc}{2i}(\delta_{k,1} - \delta_{k,N-1})\cos t\omega_1 - \frac{2\pi i a c^2 N}{m\omega_L}\sin^2\frac{\pi}{N}(\delta_{k,2}+2\delta_{k,N}+\delta_{k,N-2})\int_0^t \cos^2\tau\omega_1 \sin(t-\tau)\omega_k\, d\tau \tag{72}$$

The integral is elementary and one finds

$$a_k(t)/N = (c/2i)(\delta_{k,1} - \delta_{k,N-1}) \cos t\omega_1$$

$$- \frac{i\pi(a/4\gamma)c^2\omega_1^2}{\omega_L\omega_k} (\delta_{k,2}+\delta_{k,N-1})\{(1-\cos t\omega_k)$$

$$+ \frac{\omega_k^2}{\omega_k^2-4\omega_1^2} (\cos 2t\omega_1-\cos t\omega_k)\} + 0(a^2c^4). \qquad (73)$$

We have used the fact that $\omega_1^2 = \omega_L^2\sin^2\pi/N$, and the term proportional to $\delta_{k,N}$ has been dropped because the quantity in the bracket vanishes when k = N (since ω_N=0). The only nonvanishing a_k's are a_1, a_{N-1}, a_2 and a_{N-2}. Hence, first order perturbation only excites the second sine mode, sin $4\pi j/N$. If one iterates again, the terms of order a^2c^4 correspond to excitation of the third sine mode, etc. Higher modes appear with coefficients that are higher powers of a^2c^4.

In the FPU calculation, c was chosen to be of order 1 and a of order 1/10. Hence it would be hard for the higher modes to become excited. On the other hand, they could get excited through resonances. Note the frequency denominator $\omega_k^2-4\omega_1^2$. As one develops perturbation theory to higher and higher order, denominators of the form $n_k^2\omega_k^2-n_\ell^2\omega_\ell^2$ appear where n_k and n_ℓ are integers. Hence, if frequencies are commensurable so that $n_k\omega_k=n_\ell\omega_\ell$, the resonances appear and energy is easily transferred from the k^{th} to the ℓ^{th} mode. Since, as $\beta \to \alpha$

$$\frac{\cos t\beta - \cos t\alpha}{\alpha-\beta} \to t \sin t\alpha$$

This means that when a resonance exists, by waiting long enough the factor t eventually overwhelms the smallness of the factor $(ac^2)^2$.

This observation has been made by Ford[22,23] who also noticed that when N is a prime or a power of 2, no resonances exist in the normal mode frequencies. Since N was chosen to be 16, 32, or 64 in the FPU calculations, this efficient energy transfer mechanism did not exist and the energy spilled back from the second, third, or fourth modes into lower ones before higher ones ever had a chance to become excited.

Incidentally, resonance phenomena have been known for many years in celestial mechanisms. Newton's theory of gravitation and theory of planetary orbits was under attack for many years by astronomers who noted that the orbit parameters of Saturn and Jupiter seemed to vary linearly with the time. The enigma of the "mean motion" of these planets was resolved by Laplace who observed that the small value of $5\omega-2\omega'$ (ω and ω' being the unperturbed frequencies of the orbits of Saturn and Jupiter) led to a resonance. The period of the coupled system was 929 years. An interesting discussion of resonances (especially between asteroids) in the solar system was given by E. W. Brown.[24]

iii) Calculations of Northcote and Potts.[25]

In order to examine the importance of the number of particles in the chain and to check the sensitivity of the FPU results to the nature of the model, Northcote and Potts investigated the model of a line of rigid spheres of diameter D connected by simple harmonic springs. The nonlinearity is apparent only as an infinite repulsion when the spheres are in contact. This is an easy model to program for a computer because, between collisions, the solution of the equations of motion is known. One could start with an initial set of positions and momenta of the rigid spheres and, from the known solution of the harmonic problem, determine the new positions and momenta at some time t_1. If these positions and momenta indicate that no collisions

occurred in this time t_1, a new set is found appropriate for a time t_2. Suppose it is clear that a collision between the ℓ^{th} and $\ell+1^{st}$ spheres has occurred in the interval t_2-t_1. Then one chooses a new time $t_1 < t_2' < t_2$ and determines whether the collision occurs in the interval $t_2'-t_1$ or t_2-t_1'. This process can be continued until the collision time is determined to within any desired accuracy. In terms of the moment of collision, a new set of solutions of the equation of motion is developed with initial conditions obtained by interchanging the momenta of the ℓ^{th} and $\ell+1$'s particles and giving the other variables the values they had at the moment of collision.

The numerical results were quite different from those obtained by FPU (same end conditions, particles at ends kept fixed, were used). Equipartition was achieved slowly when the chain started in the lowest mode and more rapidly when it started in a higher mode. The mixing of modes seemed to start effectively at the chain ends. The first collision of the atoms next to the ends with the end atoms gave a strong localized reflection so that the chain configuration after the collision required higher components of the harmonic normal modes for their description. The mixing does not have to follow a stepwise course through successive modes as it did in the FPU case. After some time, the configuration of the system bore little resemblance to the initial state. By that time, modes began to exchange energy more freely and mode transitions at the chain boundary were no longer the dominant influence.

There seemed to be no evidence of the periodic behavior observed by FPU and others. The only significant difference in the energy sharing process between the weak and strong coupling cases was that the rate of mode mixing was greater in the strong coupling than in the weak coupling examples.

We have chosen three figures from the Northcote and Potts paper to exhibit these results. The first, Fig. 16 represents the energy in the first and second modes as a function of collision number. Notice the rapid drop of energy in the lowest mode after the 37th collision, and also notice that most of the energy in the first mode goes directly into modes higher than the second, especially after the 37th collision, without going into the second mode. The constants of the system were chosen to be N = 15 particles, $M = 3 \times 10^{-23}$ g., $\gamma = 400$ dynes/cur., $\ell = 4.000 \times 10^{-8}$ cm., $a = 3.995 \times 10^{-8}$ cm. and $d = 3.400 \times 10^{-8}$ cm. Figures 17 and 18 compare the manner in which the temperature equilibrates when the chain is initially in the first mode with the energy all initially in the 31st mode. N = 31 and Fig. 17 corresponds to $\varepsilon = E/N = 0.7 \times 10^{-14}$ erg (equilibrium temperature $T = 62.0^{\circ}K$), while Fig. 18 corresponds to $\varepsilon = 0.4 \times 10^{-14}$ erg and an equilibrium temperature $T = 31.7^{\circ}K$.

Now why does the striking difference exist between the FPU and the Northcote and Potts calculation? Ford's remarks on the importance of resonance effects are irrelevant to the NP calculation because perturbation theory as presented above is not appropriate for the strong hard sphere nonlinear model in which the force law cannot be expanded in a power series in the displacements from equilibrium.

iv) Solitons.

A deeper point of view of the problem of energy transfer between modes was taken by Zabusky and Kruskal[26]. By letting the lattice spacing vanish as was done in eq. (4b), they were able to convert the FPU difference-differential equations into a nonlinear partial differential equation. The resulting equation could be transformed into one which has been investigated in connection with water waves, the Korteweg-de Vries equation

$$u_t + uu_x + \delta^2 u_{xxx} = 0.$$

This equation has special solutions which preserve their character as a function of time. These solutions are called solitons and are the analogues of normal modes of linear problems. Let an initial disturbance be a soliton, and let it be decomposed into the normal modes of a related linear problem. When the soliton is reflected from the chain ends, it returns to its initial configuration. In terms of the Fourier coefficients of the normal mode decomposition, it would seem that energy is flowing from one normal mode to another so that when the initial configuration is repeated, the original Fourier components repeat themselves. Zabrusky and Kruskal would then explain the FPU results by saying that the initial state of the chain is close to a soliton state which preserves its character for a long time, making it seem that the chain is not ergodic and that energy gets transferred in and out of the lower modes periodically.

Rather than reproduce the ZK analysis, we demonstrate the existence of solitons by constructing them for a rather general class of nonlinear wave equations.

The continuum wave equation

$$u_{tt}/c^2 = u_{xx} \tag{74}$$

in an unbounded medium has the general solution

$$u = f(x \pm ct) \tag{75}$$

so that if the form f(x) of a wave is given at time t = 0, its form is forever the same and its propagation velocity is c.

On the other hand, if we have a nonlinear wave equation such as

$$u_{tt}/c^2 = [F(u)]_{xx} \tag{76}$$

then we would expect that mode coupling would develop. One can, however, construct special persistent waves or solitons for any function F(u).

We remember that any function u(w) with w ≡ x±ct is a solution of the linear equation (1). Now consider the equation with constants c_1 and c_2:

$$F\{u(w)\} = u(w) + c_1 + c_2 w. \tag{77}$$

For any function F(u) one can solve this (perhaps transcendental) equation for u(w). The u(w) may not be a function which interests us, but, nevertheless, one could generally find a solution. If u(w) is such a solution, then (77) can be substituted into (76) to find (since $\partial^2 w/\partial x^2 = 0$) that $u = u(w)$ is a solution of (76).

Let us construct some examples by working backward. Suppose we are interested in a soliton that looks like a shock wave with

$$u(w) = \tfrac{1}{2}(1 + \tanh w) \tag{78a}$$

Then

$$\tanh^{-1}(2u - 1) = w \tag{78b}$$

and

$$F(u) = u + c_1 + c_2 \tanh^{-1}(2u-1) \tag{78c}$$

so that the nonlinear wave equation which has our shock wave type of soliton solution is

$$u_{tt} / c^2 = u_{xx} + c_2\{\tanh^{-1}(2u-1)\}_{xx}. \tag{79}$$

The Gaussian soliton

$$u(w) = \exp(-w^2/a) \tag{80a}$$

implies that

$$w = \{a \log(1/u)\}^{\frac{1}{2}} \tag{80b}$$

so that

$$F(u) = u + c_1 + c_2\{a \log(1/u)\}^{\frac{1}{2}} \tag{80c}$$

and

$$u_{tt}/c^2 = u_{xx} + c_2[\{a \log(1/u)\}^{\frac{1}{2}}]_{xx}. \tag{81}$$

Other examples can be constructed.

v) Solitons on Discrete Lattices.

It is not so easy to construct solitons for wave propagation in nonlinear discrete lattices. An elegant example, however, was given by Toda.[27] He considered a chain of atoms whose interaction potential was defined by

$$\phi(R) = \text{const.} + a(R-D) + (a/b)c^{-b(R-D)}$$

$$= \text{const.} + \tfrac{1}{2}ab(R-D) - (ab^2/6)(R-D)^2 + \ldots \tag{82}$$

Hence, if ab = const. while $a \to \infty$ and $b \to 0$, then $\phi(R)$ becomes the harmonic potential. However, if $b \to \infty$ for fixed a,

$$\phi(R) \to \begin{cases} \infty & \text{if } r < D \\ 0 & \text{if } r > D \end{cases} \tag{83}$$

which is the defining characteristic of a hard sphere repulsion.

Now consider a chain of atoms with deviations from equilibrium positions $u_1, u_2, \ldots$. Then the kinetic and potential energies of the chain are

$$T = \Sigma\, p_n^2/2m \qquad \text{with} \qquad p_n = m\dot{u}_n \tag{84a}$$

$$\Phi = \Sigma\, \phi(u_n - u_{n-1}) \tag{84b}$$

The equations of motion are, in the usual form,

$$\dot{p}_n = m\ddot{u}_n = -\partial\phi(u_n - u_{n-1})/\partial u_n - \partial\phi(u_{n+1} - u_n)/\partial u_n \tag{85}$$

If we use the interaction law (82)

$$m\ddot{u}_n = a\exp\{-b[u_n - y_{n-1} - D\} - a\exp\{-b[u_{n+1} - u_n - D]\} \tag{86}$$

Let us now subtract the relative coordinates

$$r_n = u_n - u_{n-1} \tag{87}$$

into (85). Then

$$m\ddot{u}_n = f(r_n) - f(r_{n+1}) \tag{88}$$

so that by subtracting the $(n-1)^{st}$ of the equations from the n^{th}, we find

$$-\frac{d}{dt}(\dot{r}_n) = \frac{1}{m}\{f(r_{n+1}) - 2f(r_n) + f(r_{n-1})\} \tag{89}$$

where now

$$u_1 = r_1 \; ; \; u_2 = r_1 + r_2 \; ; \; u_3 = r_1 + r_2 + r_3; \quad \text{etc.} \tag{90}$$

Now define

$$\dot{s}_n = \frac{1}{m}f(r_n) \tag{91a}$$

and suppose this expression can be inverted so that

$$r_n = \chi(\dot{s}_n) \qquad \text{and} \qquad \dot{r}_n = \ddot{s}_n\chi'(\dot{s}_n) \tag{91b}$$

Then (89) is equivalent to

$$-\ddot{s}_n\chi'(\dot{s}_n) = s_{n+1} - 2s_n + s_{n-1} \tag{92a}$$

The specific choice

$$f(r) = -\alpha(1 - e^{-br}) \quad \text{with} \quad \alpha = ae^{bD} \tag{92}$$

yields the connection between (89) and (92). Then

$$b(s_{n+1} - 2s_n + s_{n-1}) = s_n/(\dot{s}_n + \alpha/m) \tag{93}$$

Toda[27] found a special soliton solution of these equations by noticing that this formula resembles one which can be derived from the addition formula for the elliptic function sn u. The following elliptic function identity is well known[28]:

$$sn^2(u+v) - sn^2(u-v) = 2\frac{d}{dv}\left\{\frac{sn\ u\ cn\ u\ dn\ u\ sn^2 v}{1 - k^2 sn^2 u\ sn^2 v}\right\} \tag{94}$$

where k is the modulus of the Jacobi elliptic functions and

$$dn^2 u = 1 - k^2 sn^2 u\ . \tag{95a}$$

Then if one defines

$$\varepsilon(n) = \int_0^u dn^2 u\ dn\ , \tag{95b}$$

$$\varepsilon'(u) = dn^2 u \text{ and } \varepsilon''(u) = -2k^2 sn\ u\ cn\ u\ dn\ u \tag{95c}$$

so that

$$k^2 dn^2(u+v) - k^2 dn^2(u-v) = -\frac{d}{dv}\left\{\frac{\varepsilon''(u)}{sn^{-2} v - 1 + \varepsilon'(u)}\right\} \tag{96a}$$

or

$$\int_0^v dn^2(u-v)\,dv - \int_0^v dn^2(n+v)\ dv = -\frac{\varepsilon''(u)}{sn^{-2} v - 1 + \varepsilon'(u)} \tag{96b}$$

Then

$$\varepsilon(u+v) - 2\varepsilon(u) + \varepsilon(u-v) = \frac{\varepsilon''(u)}{-1 + sn^{-2}v + \varepsilon'(u)} \tag{97}$$

The structure of this formula closely resembles that of (93). It is known that[28]

$$Z(u) \equiv \varepsilon(u) - uE/K = \frac{\partial}{\partial u} \log \Theta_4(u/2K) \tag{98}$$

where E and K are, respectively, complete elliptic integrals of the first and second kind of the variable k, and Θ_4 is the fourth theta function. Then

$$Z(u+v) - 2Z(u) + Z(u+v) = \frac{Z''(u)}{-1 + sn^{-2}v + (E/K) + Z'(u)} \tag{99}$$

The reader, by direct differentiation, can verify that not only do (97) and (93) resemble each other, but that a special solution of (93) is

$$s_n(t) = (2K\nu/b)\, Z\{2K(\nu t \pm n\lambda)\} \tag{100}$$

as seen by setting

$$v = 2K/\lambda \quad , \qquad u = 2K(\nu t \pm n/\lambda) \tag{101a}$$

and observing the dispersion relation between λ and ν

$$-1 + sn^{-2}(2K/\lambda) + (E/K) = \frac{\alpha b}{m(2K\nu)^2}$$

or

$$2K\nu = \{(\alpha b/m)/[-1 + sn^{-2}(\tfrac{2K}{\lambda}) + E/K]\}^{\frac{1}{2}} \tag{101b}$$

The function Z(u) is periodic with Z(u+2K) = Z(u) and ν and λ are, respectively, the frequency and wavelength of the soliton. Finally, by combining

(91ʊ) and (100))

$$r_n = -\frac{1}{b}\log\{\,1+\frac{4(K\nu)^2 m}{\alpha b}[dn^2\{2K(\nu t \pm n/\lambda)\} - \frac{E}{K}\,]\}$$

when the modulus k is very small

$$\text{sn } u \simeq \sin u \;;\; E/K \simeq 1 - \tfrac{1}{2}k^2 \;,\quad Z(u) \simeq (K^2/4)\sin 2u,\quad K \simeq \pi/2.$$

and if $\gamma = \alpha b$

$$s_n \simeq \frac{\omega k^2}{8b}\sin(\omega t \pm 2\,\frac{\pi n}{\lambda}) \qquad \text{with} \qquad \omega = 2(\gamma/m)^{\frac{1}{2}}\sin\pi/\lambda$$

Furthermore

$$r_n \simeq -(\omega^2 k^2/8\alpha b^2)\cos(\omega t \pm 2\pi n/\lambda)$$

which corresponds to a typical wave which propagates in the harmonic lattice.

The function which appears in the soliton formulae,

$$dn^2(2Kx) - (E/K)$$

is plotted in Fig. 19. As $k \to 1$ with $u = 2K/\lambda$ fixed, the various elliptic functions reduce to hyperbolic ones.

While all continuum wave equations of the type (76) have soliton solutions, it seems that more conditions must be satisfied for discrete wave equations. I suspect that the model used by Northcote and Potts does not have one.

vi) Mode Mixing in Two Dimensions.

The first 2D mode mixing calculations have recently been made by Hirooka and Saito[29] who investigated two dimensional lattices with a quartic anharmonic term in the potential, (i.e., the 2D generalization of (60b)). Computer calculations indicate the existence of a critical induction period

after which the energy sharing between modes develops rather rapidly. The induction period increases as the quartic force constant β decreases. There seems to be a critical value of β, say β_0 such that when β exceeds β_0, the system becomes ergodic while, when β is less than β_0, the lattice seems to be almost periodic in the manner exhibited by the FPU 1D calculations.

REFERENCES

1. cf. L. Brillouin, Wave Propagation, (McGraw-Hill, 1946, or Dover Reprint, 1953).
2. E. Schrodinger, Ann. Phys., 44:191(1914).
3. P. M. Morse and K. V. Ingard Theoretical Acoustics, (see, explicitly, p. 89-91), (McGraw-Hill, 1968).
4. J. J. Gilman and G. H. Vineyard, Preprint.
5. cf. A. Maradudin, E. Montroll and G. Weiss, Theory of Lattice Vibrations in the Harmonic Approximation. (Academic Press, 1963.)
6. W. A. Bowers and H. B. Rosenstock, J. Chem. Phys., 18:1056(1950).
7. H. B. Rosenstock and G. F. Newell, J. Chem. Phys., 21:1607(1953).
8. E. W. Montroll, Proc. of 3rd Berkeley Symposium on Mathematical Statistics and Probability, Vol. III, p. 209, 1956.
9. E. Montroll, J. Chem. Phys., 15:575(1947); Am. Math. Monthly LXI:46, (1954).
10. L. van Hove, Phys. Rev., 89:1189(1953).
11. H. B. Rosenstock, Phys. Rev., 97:290(1955).
12. J. C. Phillips, Phys. Rev., 104:1263(1956).
13. cf. W. Cochran, Reports on Progress in Physics 26:1(1963), and, B. N. Brockhouse and A. T. Stewart, Rev. Mod. Phys., 30:236(1958).
14. A. Maradudin, Paul Mazur, E. Montroll and G. Weiss, Rev. Mod. Phys., 30:175(1958).
15. D. N. Payton, III, M. Rich, and W. M. Visscher, Localized Excitations in Solids, p. 657, (Plenum, 1968).
16. E. W. Montroll and R. B. Potts, Phys. Rev., 100:525(1955).

17. I. M. Lifshitz, Nuovo Cimento Suppl. 3,1,591(1956).

18. A. Maradudin, Reports on Progress in Physics 28:331(1965).

19. I. M. Lifshitz and A. M. Kosevich, Reports on Progress in Physics 29:216(1966).

20. Localized Excitations in Solids; Editor, R. Wallis (Plenum, 1968).

21. E. Fermi J. Pasta and S. Ulam, Collected Works of Enrico Fermi, Vol. II, p. 978, (Chicago, 1965).

22. J. Ford, J. Math. Phys., 2:387(1961); J. Ford and J. Waters, J. Math. Phys., 4:1293(1963).

23. E. A. Jackson, J. Math. Phys., 4:551(1963).

24. E. W. Brown, Bull. Am. Math. Soc., 34:265(1928).

25. R. S. Northcote and R. B. Potts, J. Math. Phys., 5:383(1964).

26. N. J. Zabusky and M. D. Kruskal, Phys. Rev. Letters 15:241(1965).

27. M. Toda, J. Phys. Soc. Japan 22:431(1967); 23:501(1968).

28. E. T. Whittaker and G. N. Watson, Modern Analysis, Chapter 22 (Cambridge, 1927).

29. H. Hirooka and N. Saitô, Preprint.

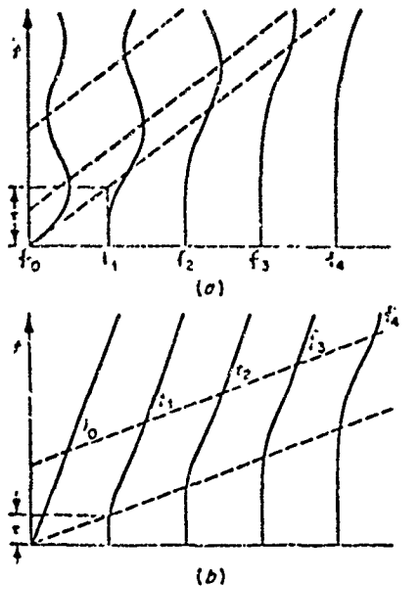

Fig. 1. Curves (a) represent the trajectories of various masses when the end particle is given an initial impulse. Curves (b) represent the situation in which the end particle is driven with a constant velocity[3].

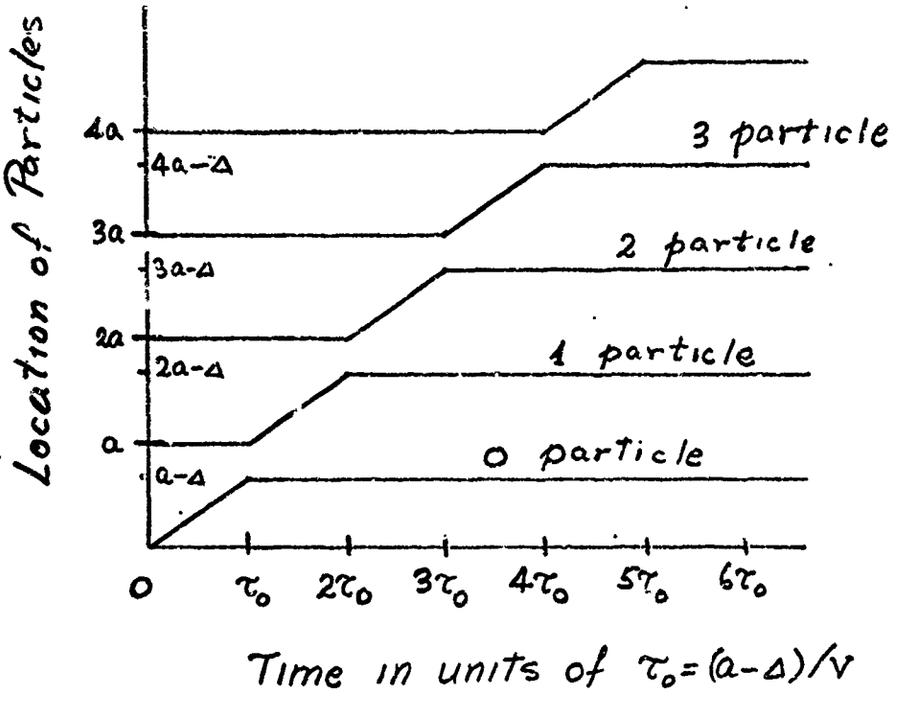

Fig. 2. Trajectories of a line of hard spheres when the left most particle has an initial velocity V and the rest of the spheres are initially stationery.

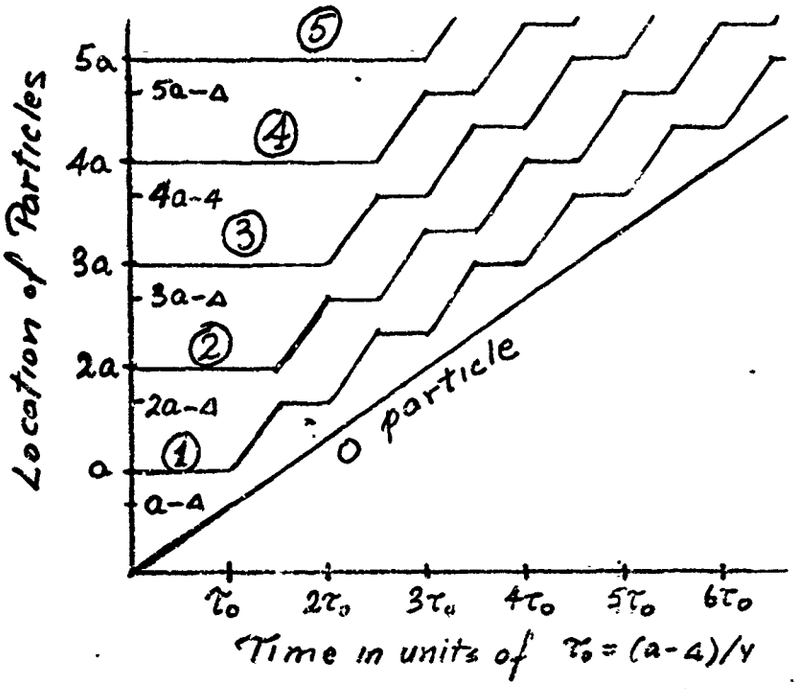

Fig. 3. Trajectories of a line of hard spheres when the left sphere is driven with a constant velocity V.

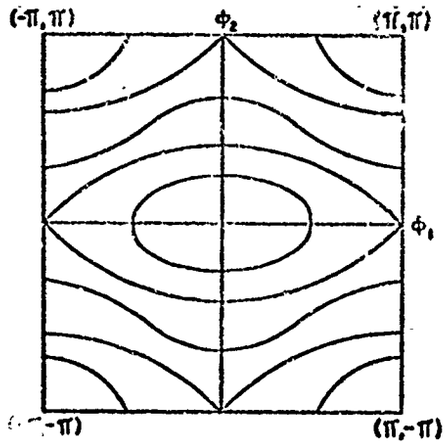

FIG. 4. Schematic curves of constant frequency in the reciprocal lattice of a two dimensional crystal.

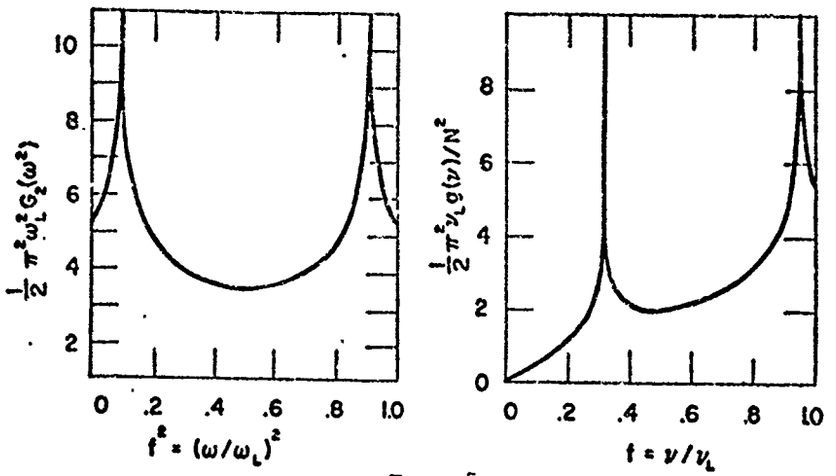

FIGURE 5

Frequency spectrum of a 2-D lattice with $\gamma_2/\gamma_1 = 1/9$. Logarithmic singularities occur at $f = 0.316$ and 0.948.

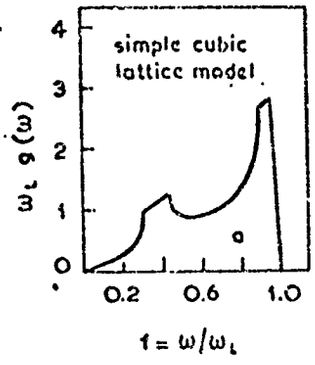

Fig. 6. (a) Frequency spectrum of a simple cubic model lattice with nearest neighbor central and non-central forces. The central forces are 8 times as large as non-central ones.

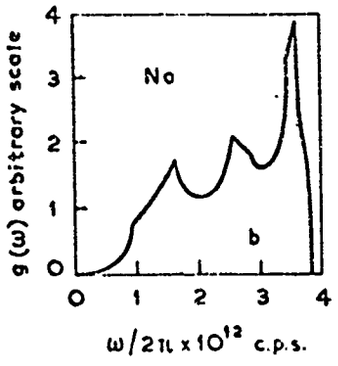

Fig. 7. (b) Experimental frequency spectrum of sodium.

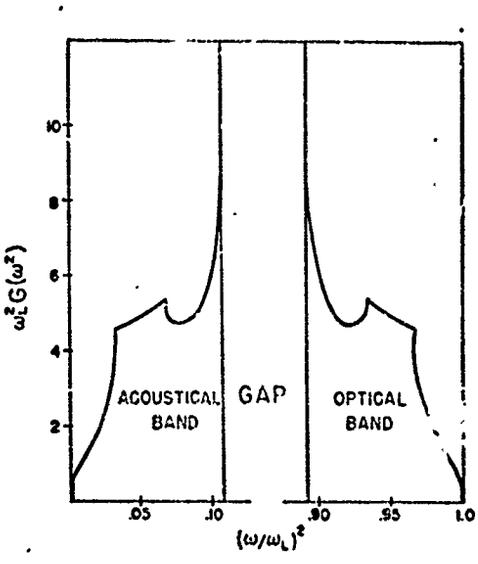

Fig. 8. Distribution of ω^2 for diatomic lattice with $M_2 = 8M_1$ and $\gamma_1/\gamma_2 = 8$.

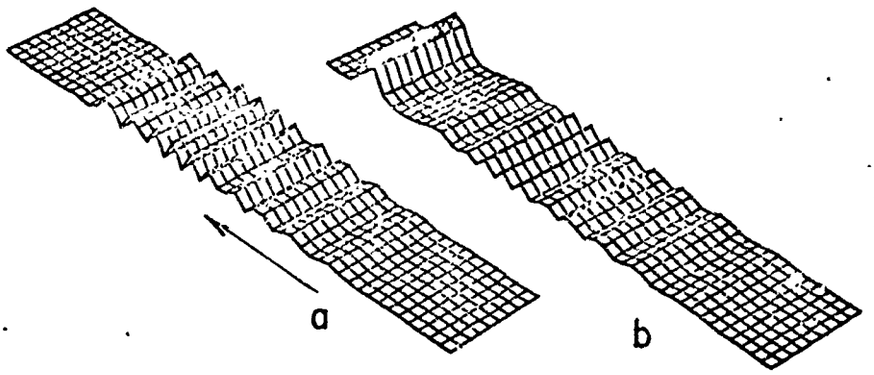

Fig. 9. Comparison of the energy waves at equal times in harmonic (a) and anharmonic (b) monatomic lattices.

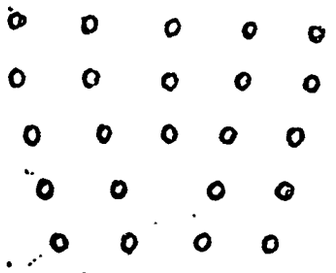

Fig. 10 Edge dislocation . Symbol ⊥

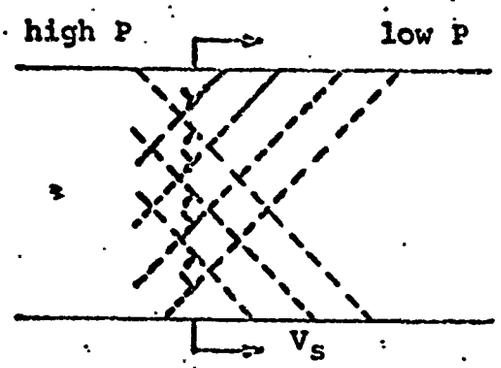

Fig. 11. Development of dislocation lines at shock front. Region 2, left of shock front, is high pressure. Region to the right is low pressure[4].

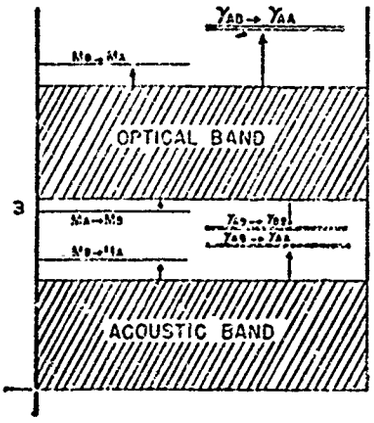

FIG. 12 Sketch of localized mode frequencies in a diatomic lattice which result from a disordered pair of atoms. $M_B \rightarrow M_A$ is used to identify the mode that results from replacing the mass of an atom of kind B by that of one of kind A. $M_A < M_B$.

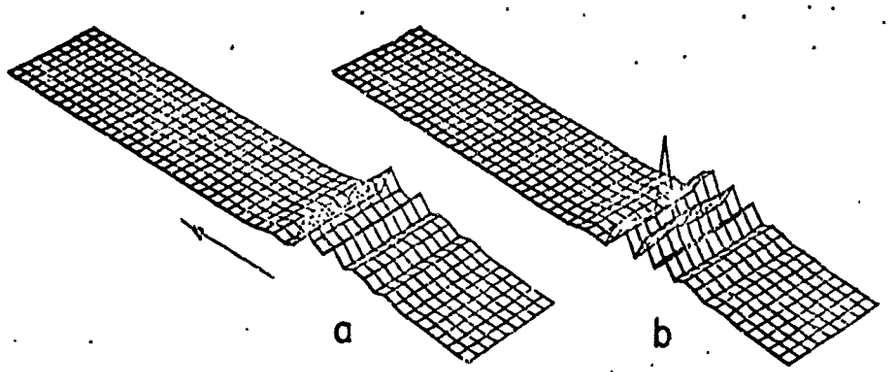

Fig. 13. Illustrations of the dip occurring in the energy wave as it passes over a light impurity (a) and the spike resulting from encounter with a heavy impurity (b).

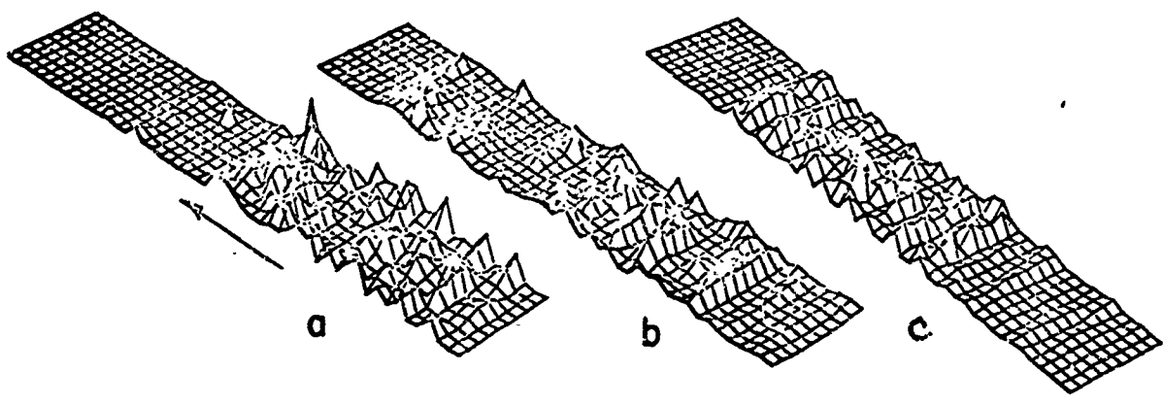

Fig. 14. Equal time comparison of energy penetration into a harmonic lattice containing 15% heavy impurities (a) with that into a 15% light impurity region (b). Impurity sites are identical in the two pictures. (c) corresponds to heavy impurities in anharmonic case.

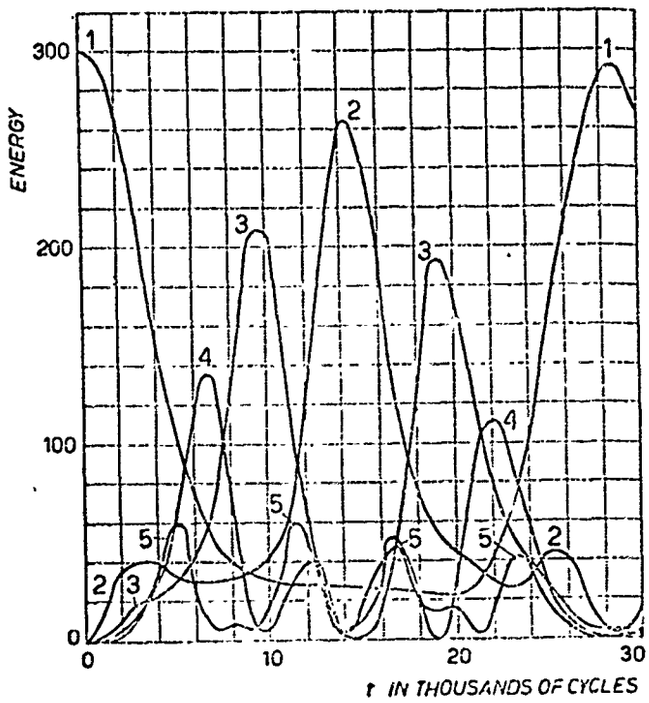

Fig. 15. Variation in energy in various modes as a function of time. The units of energy are arbitrary. N = 32; $\alpha = 1/4$. The initial form of the chain was a single sine wave. Modes higher than the 5th never exceeded 20 units of energy on the scale given here.[21]

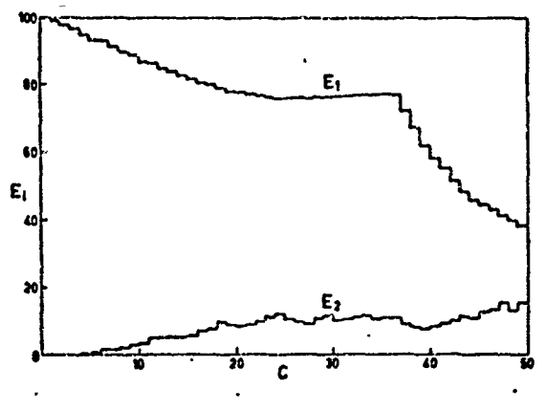

Fig. 16. The energy in the first two modes after C collisions for N = 15 particles. The mean energy/particle is $\varepsilon = 0.7 \times 10^{-14}$ erg. All energy was initially in the first mode[25].

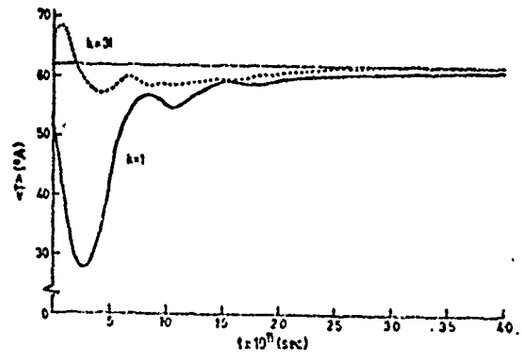

Fig. 17. The mean temperature computed for the systems N = 31, $\varepsilon = 0.7 \times 10^{-14}$ erg, and $E_i = \delta_{ik}E$ at t = 0. The predicted thermodynamic temperature is $T' = 62.07^{\circ}A$.

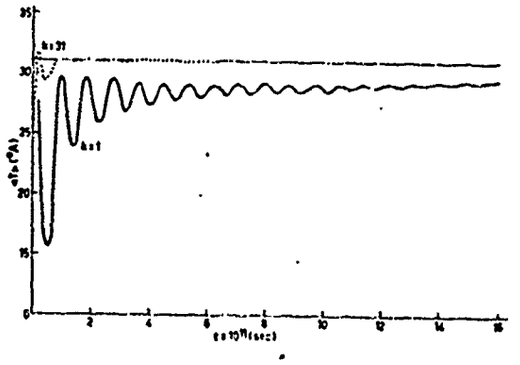

Fig. 18. The mean temperature for the weakly nonlinear systems N = 31, $\varepsilon = 0.4 \times 10^{-14}$erg, $E_i = \delta_{ik}E$ at t = 0. $T' = 31.7^{\circ}A$. The distinctly linear behavior of the system for k = 1 is apparent.

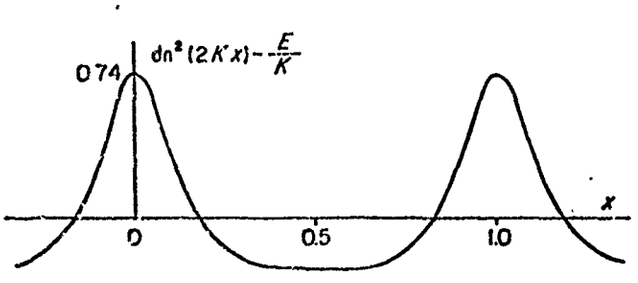

Fig. 1D $f(x)=\mathrm{dn}^2(2Kx)-E/K$ as a function of x, for $k^2=0.992$ where k is the modulus.[27]

THE SIGNIFICANT STRUCTURE THEORY OF LIQUIDS APPLIED TO THE SHOCK COMPRESSION OF ARGON AND DETONATION OF CONDENSED EXPLOSIVES

S. H. Lin* and D. Tweed
Department of Chemistry, Arizona State University

and

H. Eyring
Department of Chemistry, University of Utah

ABSTRACT

The shock compression of argon is reported by van Thiel and Alder for two initial states at 86°K and 2 bar, and 148.2°K and 70 bar. In this investigation, the significant structure theory of liquids is applied to the shock compression of argon. At high pressures, to take into consideration of the pressure effect on the solid-like portion of the partition function of argon, the Lennard-Jones potential and the Gruneison constant have been introduced. The Tait equation is used to correct the pressure effect on V_s, the molar volume of solid. The Hugoniot adiabatics are calculated and are compared with the experimental results. The agreement is satisfactory. The significant structure theory of liquids is also applied to calculate the detonation velocity of condensed explosives like NH_4NO_2 and $C_3H_5(NO_3)_3$. The agreement between calculated results and experimental values is again satisfactory.

---

*Alfred P. Sloan Fellow

1. INTRODUCTION

The significant structure theory of liquids has been developed by Eyring and his co-workers and has been successfully applied to the calculation of various liquids,[1] surface tension,[2] viscosities,[3] thermal conductivities,[4] and diffusion coefficients.[5] In this investigation, we shall apply the significant structure theory of liquids to the shock compression of argon. Shock compression of argon has been reported by van Thiel and Alder.[6] Liquid argon has been shock compressed from two initial states at 86°K and 2 bar, and 148.2°K and 70 bar. The shock compression is well suited to the study of the inert gases at small interatomic distances because of the large pressure and temperature range that can be covered. The pressure range is, of course, high in shock wave experiments on all condensed substances, and it goes up with the normal density of the material.

2. SIGNIFICANT STRUCTURE THEORY

According to the significant structure theory of liquids, a fluid is assumed to consist of a quasi lattice in which mobile holes of molecular size move from site to site. If V_s and V are the molar volumes of the solid and fluid phases, respectively, and a random distribution of holes and molecules is assumed, then the number of holes present in the fluid is given by $N(V-V_s)/V_s$, N being Avogadro's number. Such a hole is assumed to confer gaslike properties on neighboring molecules which jump into it. Thus, there will be effectively $N(V-V_s)/V$ molecules with gaslike degrees of freedom and effectively NV_s/V molecules with solidlike degrees of freedom. Further, these holes provide for a solidlike molecule a positional degeneracy equal to the available neighboring positions, n_h, multiplied by a

Boltzmann-type probability factor involving the necessary energy ε to exclude competing molecules from the available positions. On the basis of these considerations, the partition function, f, say for a monatomic liquid such as inert gases, can be expressed as,[1]

$$f = (f_s f_c)^{V_s/V} \cdot (f_g)^{(V-V_s)/V} \tag{1}$$

where

$$f_s = \left[\frac{e^{Es/RT}}{(1-e^{-\theta/T})^3}\right]^N \tag{2}$$

$$f_c = (1 + n_h e^{-\varepsilon/RT})^N \tag{3}$$

and

$$f_g = \left[\left(\frac{2\pi mkT}{h^2}\right)^{3/2} \cdot \frac{eV}{N}\right]^N \tag{4}$$

f_s stands for the solidlike portion of the partition function, for which the Einstein oscillator model is used. The quantity f_c is the portion of the partition function contributed from the geometrical degeneracy factor. f_g represents the partition function of the gaslike part. E_s is the energy of sublimation. n_h and ε are defined by

$$n_h = n\frac{(V-V_s)}{V_s} \tag{5}$$

and

$$\varepsilon = \frac{a E_s V_s}{V-V_s} \tag{6}$$

For the detailed discussion of the theory, the original papers should be consulted.[1]

At high pressures and temperatures, the pressure effect on V_s and f_s must be taken into account. Thus, knowing the total partition function f as a function of T and V, we can calculate the thermodynamic quantities like the Helmholtz free energy A, internal energy E, and pressure P from

$$A = -kT \ln f = \frac{V_s}{V} (\bar{A}_s + \bar{A}_c) + \frac{(V-V_s)}{V} \bar{A}_g \tag{7}$$

$$E = kT^2 \left(\frac{\partial \ln f}{\partial T} \right)_V = \frac{V_s}{V} (\bar{E}_s + \bar{E}_c) + \frac{(V-V_s)}{V} \bar{E}_g \tag{8}$$

and

$$P = -\left(\frac{\partial A}{\partial V} \right)_T = \frac{V_s}{V} (P_s + P_c) + \frac{(V-V_s)}{V} P_g + \frac{V_s}{V^2} (\bar{A}_g - \bar{A}_s - \bar{A}_c) \left(-1 + \frac{\beta_s}{\beta} \right) \tag{9}$$

where

$$\bar{A}_s = - E_s + 3RT \ln (1 - e^{-\theta/T}) \tag{10}$$

$$\bar{A}_c = - RT \ln (1 + n_h e^{-\varepsilon/RT}) \tag{11}$$

$$\bar{A}_g = - RT \ln \frac{(2 \pi mkT)^{3/2}}{h^2} \frac{eV}{N} \tag{12}$$

$$\bar{E}_s = - E_s + \frac{3R\theta}{e^{\theta/T} - 1} \tag{13}$$

$$\bar{E}_c = \frac{n_h \varepsilon e^{-\varepsilon/RT}}{1 + n_h e^{-\varepsilon/RT}} \tag{14}$$

$$\bar{E}_g = 3/2 \, RT \tag{15}$$

$$P_s = \frac{dE_s}{dV} - \frac{3R}{e^{\theta/T}-1} \left(\frac{\partial\theta}{\partial V}\right)_T \tag{16}$$

$$P_c = \frac{RT\left(\frac{\partial n_h}{\partial V}\right)_T - n_h\left(\frac{\partial \varepsilon}{\partial V}\right)_T}{1 + n_h e^{-\varepsilon/RT}} e^{-\varepsilon/RT} \tag{17}$$

and

$$P_g = \frac{RT}{V} \tag{18}$$

β_s and β in Eq. (9) represent the compressibility of solid and liquid, respectively. From the above equations one notes that the partition function of significant structure theory includes the parametric quantities E_s, V_s, θ, n, and a, which are characteristic of a substance. These quantities have been calculated theoretically by using an intermolecular potential.[7]

When the pressure is very small, the pressure effect on V_s and f_s is small and hence P_s and β_s/β are negligible.[1] At high pressures, for example, one may use the Tait equation [8] to correct the pressure effect on V_s,

$$V_s = V_{so} - C \ln\left(\frac{B + P}{B}\right) \tag{19}$$

and use the Lennard-Jones potential to correct the pressure effect on E_s,[8]

$$E_s = \frac{1}{2} N \tilde{\varepsilon} \left[C_{12}\left(\frac{N\sigma^3}{V_s}\right)^4 - 2 C_6 \left(\frac{N\sigma^3}{V_s}\right)^2\right] - (3/2) R\theta \tag{20}$$

through V_s and θ, where $C_6 = 14.4539$, and $C_{12} = 12.1318$. To correct the pressure effect on the Einstein temperature θ, one may use the Grüneisen constant, which is defined by[9]

$$\gamma = - \left(\frac{d \ln \theta}{d \ln V_s} \right) \tag{21}$$

3. CALCULATION OF THE HUCONIOT ADIABATIC FOR ARGON

The Hugoniot adiabatic can be obtained from the Rankine-Hugoniot jump conditions,[8]

$$E - E_o = 1/2 \ (P + P_o) \ (V_o - V) \tag{22}$$

where P_o and V_o represent the initial pressure and initial volume respectively. If the thermodynamic properties of a substance are known, then it is possible to express the energy E as a function of the pressure and volume, $E = E(P,V)$. Substituting this expression into Eq. (22), we obtain a certain curve in the P, V-plane. The relation between P and V represents the Hugoniot adiabatic curve. The initial pressure and initial volume, P_o and V_o, are parameters of this curve. The problem of finding the Hugoniot adiabatic curve by using the significant structure theory of liquids is straightforward and is equivalent to eliminating both T and E using Eqs. (8), (9) and (22), so that P can be expressed in terms of V only. In principle, the Hugoniot adiabatic curve can be obtained no matter how complicated Eqs. (8) and (9) may be. But in practice, we can accomplish this only by using numerical interation methods.

The parameters of argon are summarized in Table I. To check the applicability of the Einstein model of solid, we rewrite Eq. (16) as follows

$$P_s = \frac{2 \bar{\varepsilon}}{\sigma^3} \left[C_{12} \left(\frac{N\sigma^3}{V_s} \right)^5 - C_6 \left(\frac{N\sigma^3}{V_s} \right)^3 \right] + \frac{\gamma}{V_s} \left(3/2 \ R\theta + \frac{3R\theta}{e^{\theta/T} - 1} \right) \tag{23}$$

by using the Lennard-Jones potential. The isotherm of solid argon at $T = 77°K$ is shown in Fig. 1, and is compared with measurements reported by Stewart.[10] In the pressure range under consideration, the agreement

seems satisfactory. To check the applicability of the Tait equation, Eq. (19) we rewrite Eq. (19) as follows

$$P_s = B + \frac{C}{\beta_s V_s} \tag{24}$$

This means that at a particular temperature, the Tait equation predicts that P_s vs $1/\beta_s V_s$ should be linear. P_s vs $1/\beta_s V_s$ for solid argon is plotted in Fig. 2, using Stewart's data. The linearity holds for the whole range of pressure under consideration.

Next, we turn to the calculation of the Hugoniot adiabatic curve by using the significant structure theory of liquids. The Hugoniot adiabatic exists; adiabats are calculated for P_o = 2 bar ρ_o = 1.405 g/cc and P_o = 70 bar and ρ_o = 0.919 g/cc. In Figs. 3 and 4, the calculated results are compared with experimental values reported by van Thiel and Adler.[6] The agreement is satisfactory.

4. DETONATION OF CONDENSED EXPLOSIVES

According to the significant structure theory of liquids, the partition function of a fluid mixture can be expressed as

$$f = \frac{N!}{\prod_i N_i!} \prod_i \left[f_{si}^{X_i(V_s/V)} \, f_{gi}^{X_i(V-V_s)/V} \right] \left(f_c \, e^{-Es/kT} \right)^{V_s/V} \tag{25}$$

where

$$V_s = \sum_i X_i V_{si} \quad \text{and} \quad E_s = \sum_i X_i^2 E_{si} + 2 \sum_{isj} X_i X_j (E_{si} E_{sj})^{1/2}$$

the quantities E and P are then given by,

$$E = \sum_i X_i \bar{E}_{gi} + V_s/V \left(\bar{E}_c - E_s + \sum_i X_i \bar{E}_{si} - \sum_i X_i \bar{E}_{gi} \right) \tag{26}$$

and

$$P = P_G + \frac{V_s}{V}\left[\sum_i X_i P_{si} - P_G + \left(P_c + \frac{dE_s}{dV}\right)\right] + \left[\sum_i X_i(\bar{A}_{gi} - \bar{A}_{si}) + (E_s - \bar{A}_c)\right](V_s/V^2)(-1+\beta_s/\beta) \quad (27)$$

where

$$\bar{E}_{si} = kT^2\left(\frac{\partial \ell n f_{si}}{\partial T}\right)_V ; \quad \bar{E}_{gi} = kT^2\left(\frac{\partial \ell n f_{gi}}{\partial T}\right) ; \quad \bar{E}_c = kT^2\left(\frac{\partial \ell n f_c}{\partial T}\right)_V ; \quad (28)$$

$$\bar{A}_{si} = -kT\,\ell n f_{si} ; \quad \bar{A}_{gi} = -kT\,\ell n f_{gi} ; \quad \bar{A}_c = -kT\,\ell n f_c \quad (29)$$

and

$$P_g = \frac{NkT}{V}; \quad P_{si} = kT\left(\frac{\partial \ell n f_{gi}}{\partial V}\right)_T ; \quad P_c = kT\left(\frac{\partial \ell n f_c}{\partial V}\right)_T \quad (30)$$

the partition functions f_{gi}, f_{si} of component i for nonlinear triatomic molecules can be written as:

$$f_{gi} = \left[\left(\frac{2\pi m_i kT}{h^2}\right)^{3/2} (eV/N)\frac{8\pi^2(8\pi^3 A_i B_i C_i)^{1/2}(kT)^{3/2}}{\sigma_i h^3}\prod_{v=1}^{3}\frac{1}{1-e^{-\theta_{vi}/T}}\right]^N \quad (31)$$

and

$$f_{si} = \left[\frac{1}{(1-e^{-\theta_i/T})^6}\cdot\prod_{v=1}^{3}\frac{1}{1-e^{-\theta_{vi}/T}}\right]^N \quad (32)$$

and for linear triatomic molecules can be written as:

$$f_{gi} = \left[\left(\frac{2\pi M_i kT}{h^2}\right)^3 (eV/N)\cdot\frac{8\pi^2 I_i kT}{\sigma_i h^2}\cdot\prod_{v=1}^{4}\frac{1}{1-e^{-\theta_{vi}/T}}\right]^N \quad (33)$$

and

$$f_{si} = \left[\frac{1}{(1-e^{-\theta_i/T})^5}\prod_{v=1}^{4}\frac{1}{1-e^{-\theta_{vi}/T}}\right]^N \quad (34)$$

similarly, the partition functions f_{gi}, f_{si} of component i for diatomic molecules are:

$$f_{gi} = \left[\left(\frac{2\pi m_i kT}{h^2}\right)^{3/2} \cdot (eV/N) \cdot \frac{8\pi^2 I_i kT}{\sigma_i h^2} \cdot \frac{1}{1-e^{-\theta_i'/T}}\right]^N \tag{35}$$

and

$$f_{si} = \left[\frac{1}{(1-e^{-\theta_i/T})^5} \cdot \frac{1}{1-e^{-\theta_i/T}}\right]^N \tag{36}$$

The pressure effect on E_s of nonpolar molecules has been discussed in Section 2. To correct the pressure effect on E_s of water, we shall use[11],[8]

$$E_s = -4\bar{\varepsilon}\left[C_{12}'(d/R)^{12} - C_6'(d/R)^6 - C_3'(t_1/\sqrt{2})(d/R)^3 f - C_4'(t_2/\sqrt{2})(d/R)^4 g\right] - E_o^\circ \tag{37}$$

where R is the intermolecular distance and E_o° is the zero-point energy. The quantities in Eq. (37) are given as:

$$t_1 = 1.200;\ t_2 = 0.654;\ d = 2.725\cdot\text{Å};\ \bar{\varepsilon} = 707\ \text{cal/mole}$$

$$C_{12}' = 4.000;\ C_6' = 4.033;\ C_3' = 4.633;\ C_4' = 4.237.$$

f and g in Eq. (37) are functions of the three angles which describe the mutual orientation of two water molecules.

To calculate the detonation velocity, we have to use the Chapman-Jouquet condition, which states that the detonation is sonic with respect to the products at the end of the reaction zone. The Chapman-Jouquet condition can be stated in another way; i.e., the Michelson line

$$P = P_o + D^2/v_o^2\ (v_o - v) \tag{38}$$

is tangent to the Hugoniot adiabatic, Eq. (22), at the end of reaction zone. v_o and V represent the specific volumes. In this way, we can calculate the detonation velocity D, from Eqs. (22), (26), (27), and (33). This has been done for NH_4NO_2 and $C_3H_5(NO_3)_3$. For NH_4NO_2, we obtain D = 4750 m/sec and the conditions at the end of reaction zone, $p = 4.95 \times 10^4$ atm, T = 3030°K, and $v = 0.747$ cm^3/g. For $C_3H_5(NO_3)_3$, we obtain D = 7750 m/sec, and the conditions at end of reaction zone, $p = 1.975 \times 10^5$ atm, T = 5620°K, and $v = 0.511$ cm^3/g, compared with the experimental value[12] of D = 7500 $\pm$ 500 m/sec. The agreement again seems to be satisfactory.

TABLE I

PARAMETERS OF ARGON

n	10.7	σ	3.402 Å
a	0.0052	γ	2.25
V_{so}	24.98 cc/mole	B	1.716×10^{9} dyne/cm^2
θ	60.0°K	C	2.639
$\bar{\varepsilon}$	1.690×10^{-14} dyne/cm^2		

REFERENCES

1. (a) H. Eyring and R. P. Marchi, J. Chem. Educ. 40, 562 (1963).
   (b) T. S. Ree, T. Ree and H. Eyring, J. Chem. Phys. 41, 524 (1964).
   (c) D. Henderson, H. Eyring and D. Felix, J. Phys. Chem. 66, 1128, (1962).
   (d) M. S. Jhon, J. Grosh, T. Ree and H. Eyring, J. Chem. Phys. 44, 1465 (1966).

2. W. C. Lu, M. S. Jhon, T. Ree, and H. Eyring, J. Chem. Phys. 46 1075 (1967).

3. T. S. Ree, T. Ree, and H. Eyring, J. Phys. Chem. 68, 1163 (1964).

4. S. H. Lin, H. Eyring, and W. J. Davis, J. Phys. Chem. 68, 3017 (1964).

5. T. S. Ree, T. Ree and H. Eyring, J. Phys. Chem. 68, 3262 (1964).

6. M. Van Thiel and B. J. Alder, J. Chem. Phys. 44, 1056 (1966).

7. T. S. Ree, T. Ree, H. Eyring and R. Perkins, J. Phys. Chem. 69, 3322 (1965).

8. J. O. Hirschfelder, C. F. Curtiss and R. B. Bird, "Molecular Theory of Gases and Liquids," (John-Wiley, 1954).

9. J. C. Slater, "Introduction of Chemical Physics," (McGraw-Hill, 1939); also E. R. Dobbs and G. O. Jones, Rept. Prog. Phys. 20, 516 (1957).

10. J. W. Stewart, J. Phys. Chem. Solids, 1, 146 (1956).

11. J. S. Rowlinson, Trans. Faraday Soc., 47, 120 (.951).

12. J. Taylor, "Detonationation of Condensed Explosives," (Oxford Press, 1952).

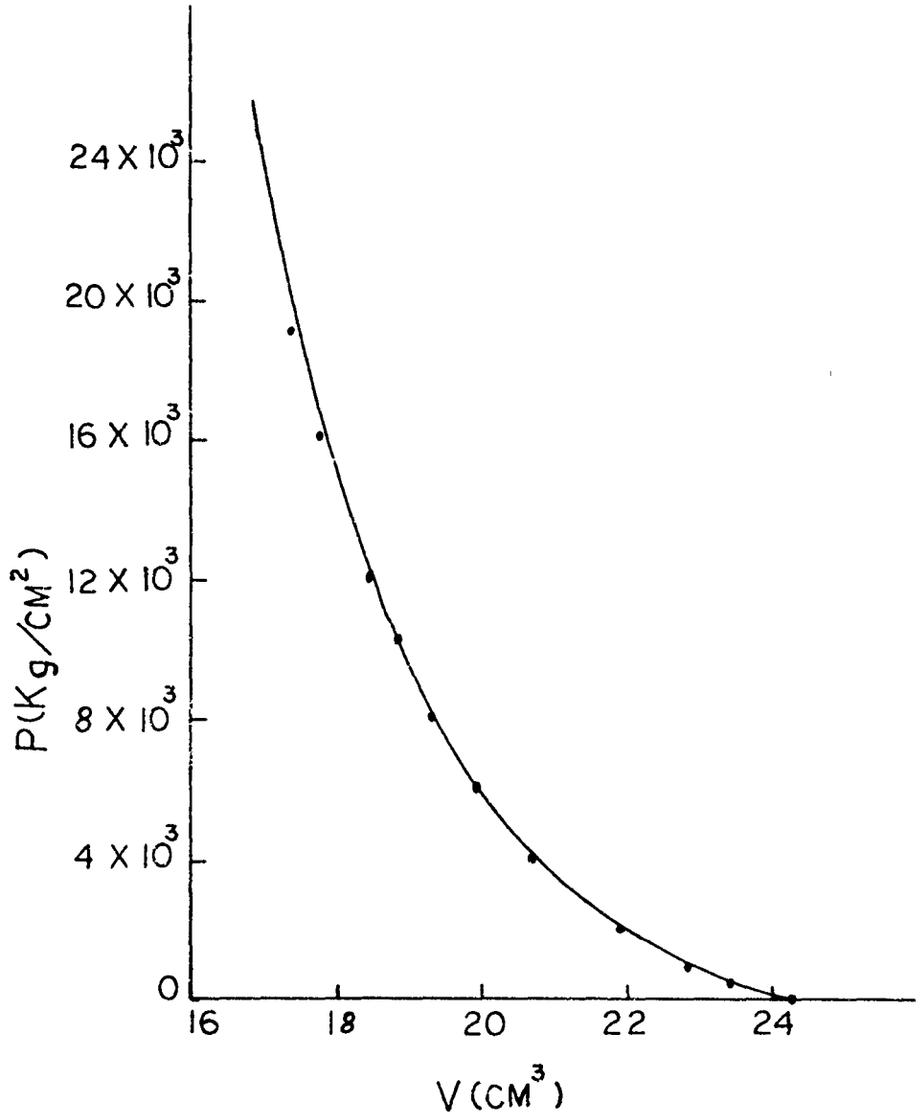

FIG. 1

P_s vs V_s for Solid Argon at T = 77°K (___ calculated; ... experimental)

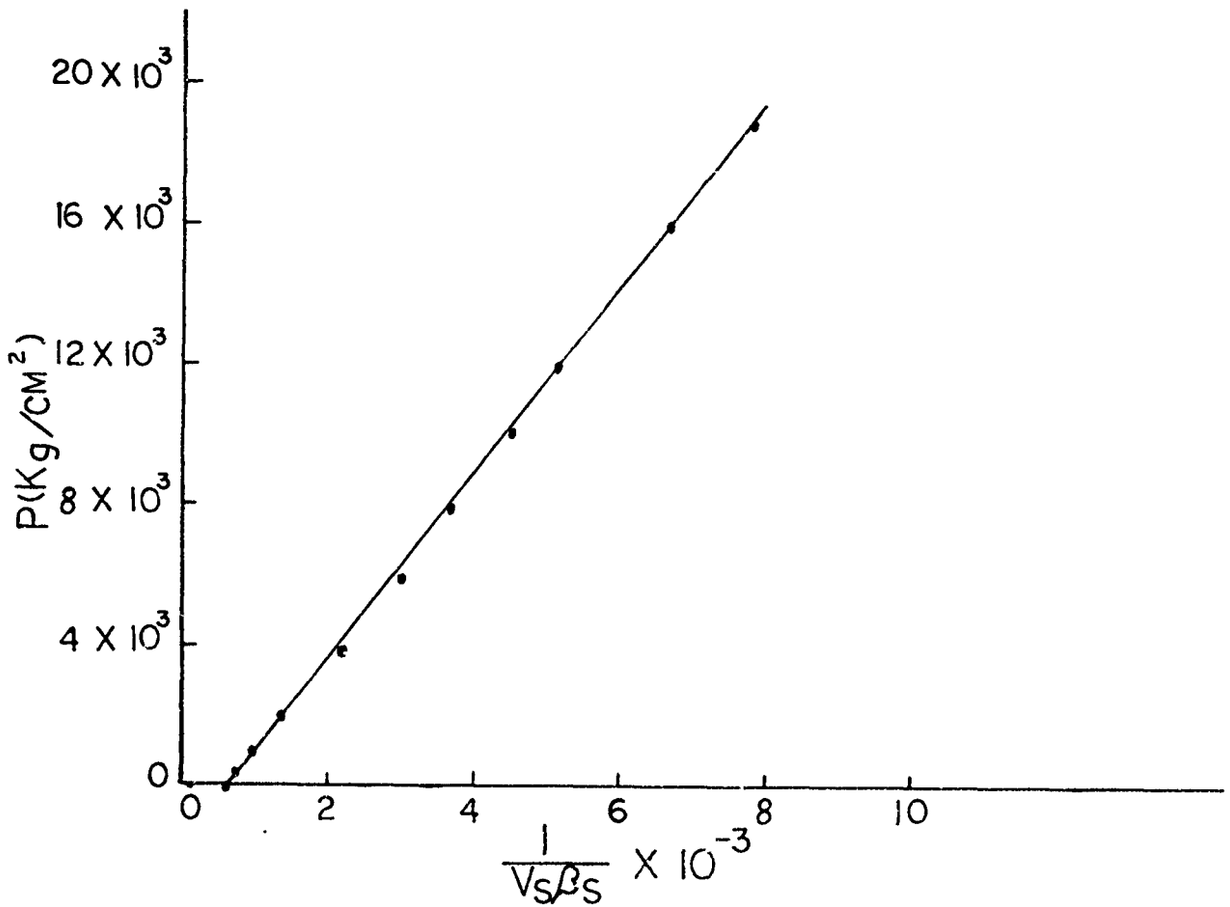

FIG. 2

P_s vs $1/V_s\beta_s$ for Solid Argon at T = 77°K

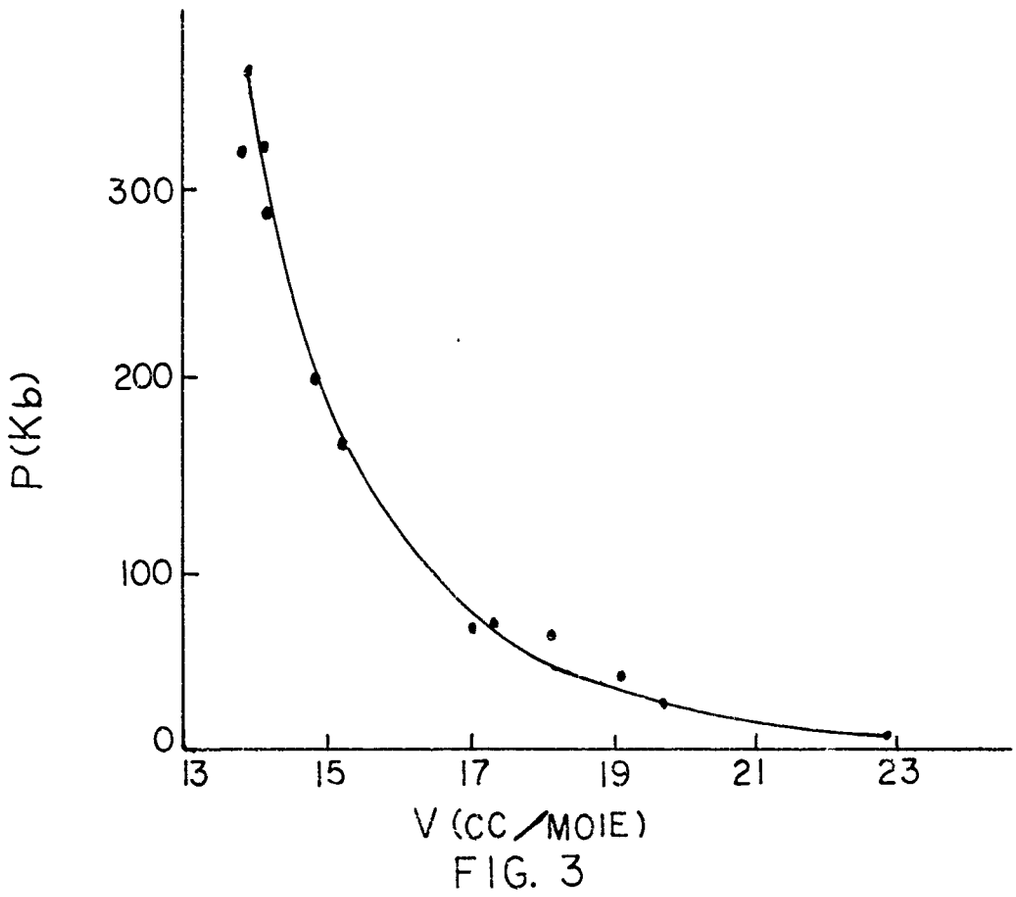

FIG. 3

Shock compression of Argon
(P_o~2 bar ρ_o = 1.405 g/cc)

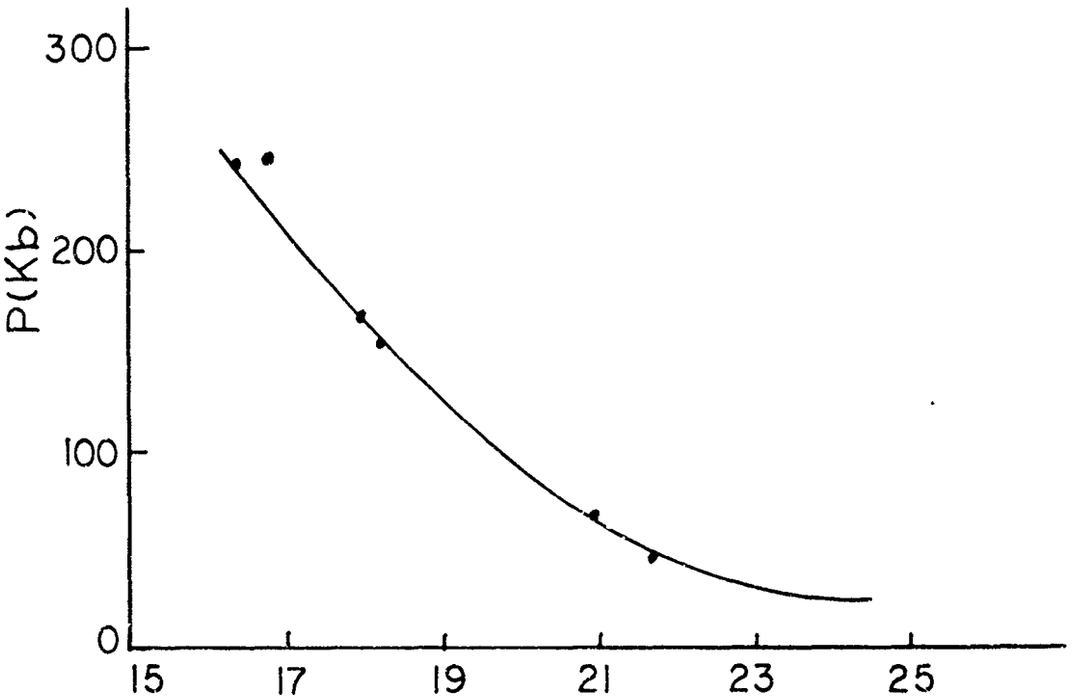

FIG. 4

Shock compression of Argon
(P_o=70 bar ρ_o = 0.919 g/cc)

SESSION III

SESSION III

WEDNESDAY - 23 October 1968

Chairman: Mr. Jean Belanger
Canadian Armament Research and Development Establishment
Defence Research Board
P.O. Box 1427
Quebec, P.Q., Canada

Mechanism of Propagation of Steady Detonation

Dr. Wildon Fickett
Los Alamos Scientific Laboratory
University of California
Los Alamos, New Mexico

MECHANISM OF PROPAGATION OF STEADY DETONATION*

Wildon Fickett
Los Alamos Scientific Laboratory, University of California
Los Alamos, New Mexico

INTRODUCTION

The two classes of self-sustaining waves in explosives have very different characteristics. Deflagrations, or flames, are relatively slow and quiet. Detonations are fast and violent.

A deflagration wave propagates at much less than acoustic velocity. The burned material emerges from the rear of the wave with a higher temperature, but lower pressure and density, than that of the initial state. Momentum changes are relatively unimportant. The equations describing the process have a steady solution at a unique wave-propagation velocity. The calculation of this velocity requires the solution of an eigenvalue problem, in which the most important effects are the rate of the chemical reaction and the rate at which the resulting increased translational energy of the reaction products is transported forward by heat and matter diffusion. The transport coefficients thus play an important part in the process.

A detonation is very different. It may be regarded as a strong shock supported by an immediately-following chemical reaction, triggered by the high temperature produced by the nearly-instantaneous compression and heating in the shock. The rapidity and violence of the process causes the relative importance of transport effects and momentum changes to be completely reversed: here momentum changes are all-important, while transport effects can be neglected for most purposes.

---

*Work performed under the auspices of the U. S. Atomic Energy Commission.

The front of a detonation which has run some distance is observed, over a fixed area of the front, to approach a plane surface of discontinuity (provided one does not look too closely), and the velocity is observed to approach a constant limiting value. Thus, a one-dimensional flow model of the process is suggested. Under this assumption, and the additional one that the flow within the reaction zone is steady in a frame attached to the shock, relatively simple solutions to the flow equations can be found. In this approximation the unique value of the steady propagation velocity or detonation velocity is generally determined not by the solution of an eigenvalue problem containing the details of the flow within the reaction zone, but by the sonic character of the flow at its end. The main consideration is the question of whether a disturbance originating behind the front will overtake it and affect its motion. The calculation of the detonation velocity is thus considerably simplified. It turns out that the final state and its sonic character are determined by the solution of the (algebraic) conservation laws of one-dimensional steady flow. The equation of state of the reaction products must be known, but no information about the reaction kinetics is needed.

Typical examples of the detonation velocity, and of the pressure, density, and temperature at the end of the reaction zone are given in Table I. Here M is the Mach number of the detonation, that is, the detonation velocity divided by the sound speed in the undisturbed material. The temperatures given for the liquid and solid are uncertain to perhaps 20 to 30 percent.

The high velocity of the detonation results in an astonishing power level for the rate of conversion of chemical bond energy to mechanical and heat energy. In a good solid explosive this rate is about 10^{10} watts per

sq. cm. of front, which may be compared with the total U. S. electric generating capacity of about 3×10^{11} watts. The rate at which the earth receives energy from the sun, about 4×10^{16} watts, could be equaled by a detonation wave 20 meters square.

Although condensed (i.e., liquid and solid) explosives are the ones of interest here, they are comparatively difficult to study because of the high pressures generated. The equation of state is too poorly known to be of any use in quantitative testing of theories. Thus, most of the fundamental advances in understanding from the experimental side have come from the study of gaseous systems, where the experiments are cheap and easy by comparison, and the known equation of state (ideal gas with small corrections) makes possible quantitative a priori calculations. To what extent the understanding gained here applies to condensed materials is not always clear.

ELEMENTS OF THE THEORY

In this section, we review briefly the elements of the one-dimensional flow theory, in order to establish a framework and terminology for the subsequent discussion.

We first consider the flow behind the front. As shown in Figure 1, the detonation is supposed to be initiated at one end of a closed tube. The effect of initiation transients is neglected, the detonation being assumed to have run at constant velocity from the point of initiation. Also the reaction zone structure is not shown; only the state at its end appears in the figure. As shown in the first pressure-distance profile, the front is followed by a self-similar rarefaction wave which terminates about halfway back where it has reduced the forward material velocity produced by the front to zero, thus matching the rigid-wall rear boundary condition, and the pressure to about half the value at the front. The detonation velocity suggested by the simple

one-dimensional theory is such that the flow at the end of the reaction zone is sonic with respect to the front; i.e., the sound speed is equal to the material velocity in a coordinate frame attached to the front. Since the head of the rarefaction wave moves at sonic velocity, it just keeps up with the front.

The second profile illustrates what may be more nearly the real case; here the flow at the end of the reaction zone is supersonic with respect to the front. Since the head of the rarefaction now moves more slowly than the front, it is separated from the front by an ever-widening region of constant state.

We now apply the laws of conservation of mass, momentum and energy to the assumed one-dimensional steady flow in the reaction zone. For purposes of illustration, consider a system in which a single reaction takes place described by a progress variable which ranges from 0 for no reaction to 1 for complete reaction. The conservation relations connect any point in the reaction zone with the initial state. They can be written as

$$\rho_o^2 D^2 = (p - p_o) / (v_o - v) \qquad \text{Rayleigh line}$$

$$E(p,v,\lambda) - E(p_o, v_o, \lambda=0) = 1/2(p+p_o)(v_o - v) \qquad \text{Hugoniot}$$

$$u^2 = (p-p_o)(v_o - v)$$

Here ρ, v, p, E, D, and u are the density, specific volume, pressure, specific internal energy, detonation velocity, and material velocity (in the laboratory frame in which the undisturbed material is at rest), and the subscript zero denotes the initial state. The equation of state is written in the form $E = E(p, v, \lambda)$ for convenience.

Curves of constant D and constant u and solutions of the Hugoniot equation in the p - v plane are shown in Figure 2. Curves of constant u are hyperbolas,

with u increasing with pressure along the Hugoniot. Curves of constant D, or Rayleigh lines, are straight lines passing through the initial point, with slope proportional to D^2. The Hugoniot for no reaction (λ=0) is the locus of possible shock states. The Hugoniot for complete reaction (λ=1) is the locus of possible states at the end of the reaction. The effect of the heat release in the reaction is to displace the Hugoniot cut from the origin, so that it no longer passes through the initial point. Possible states immediately behind the shock and at the end of the reaction zone are given by the intersection of a Rayleigh line with the $\lambda = 0$ and $\lambda = 1$ Hugoniots, respectively. In contrast to a shock, which can have any strength, it is seen that the velocity D_{C-J} in the figure, at which the Rayleigh line is tangent to the complete-reaction Hugoniot, is the minimum possible one for a detonation. For any larger velocity there are two possible states at the end of the reaction zone, marked S and W in the figure.

We now state some properties and define some terms:

1. The state immediately behind the shock, point N in Figure 2, will be called the shock state. This is sometimes referred to as the von Neumann point.

2. The state at the end of the reaction zone will be called the final state.

3. On the complete-reaction Hugoniot, or detonation, the entropy is a minimum at the C-J or tangent point and the flow there is sonic with respect to the front. At all points of lower pressure, called weak points, the flow is supersonic, and at all points of higher pressure, called strong points, the flow is subsonic.

4. The detonation pictured in Figure 1 is a self-supporting detonation. If the fixed wall at the rear is replaced by a piston moving with constant velocity, the detonation velocity will be independent of changes in the piston velocity over a certain range. But if the piston is moved forward rapidly enough (faster than u_{C-J}) the detonation velocity is increased and an overdriven detonation wave is produced.

HISTORY

The phenomenon of detonation was first recognized by Berthelot and Vieille (1881) and by Mallard and Le Chatelier (1881) in the course of their studies of flame propagation. The elements of the simplest theory essentially as outlined above were formulated independently by Chapman (1899) and Jouquet (1905, 1906). In their work, it is realized that in the usual experimental situation the front will be followed by some type of rarefaction wave, though this part of the flow is not treated in detail. A detonation whose final state is a strongpoint (at which the flow is subsonic) will be overtaken and slowed down by the rarefaction. This argument suggests the so-called Chapman Jouquet hypothesis: that the steady detonation velocity of the self-supporting wave is the minimum value consistent with the conservation conditions. It is concluded, without satisfactory justification, that the weak points can be ignored.

This simple theory was quite successful. The detonation velocity, the only quantity measured at that time, is predicted within a percent or two, even with the relatively crude thermodynamic functions then available. The first indication that all was not well was the discovery of spinning detonations in the 1920's, in which a bright spot on the front is observed to trace out a helical path as the detonation propagates. This interesting phenomena was largely confined to "marginal" systems with relatively small heat of reaction. It was regarded as a more or less isolated phenomenon and did not give rise to serious questioning of the one-dimensional flow assumption as applied to most detonations.

The next advance in theory came in the early 1940's with the detailed treatment of the reaction zone in the so-called ZND model, put forth independently by Zeldovich (1940) in Russia, von Neumann (1942) in the United States, and

Doering (1943) in Germany. The configuration assumed is a plane shock, treated as a jump discontinuity, followed by a region of one-dimensional steady flow in which the reaction goes to completion. The steady-flow equations for the reaction zone are written down and their properties studied for the case of a single forward reaction proceeding to completion. This study shows that, in the usual case, only strong final states or the CJ state can be reached. The CJ hypothesis is applied as before.

What might be termed the modern era in experimental work on gas detonations begins about 1950. The principal object is the measurement of the pressure, density, and some composition variables of the final state and comparison of these with the nearly exact calculated results based on the ideal gas equation of state and the tabulated thermodynamic functions of the product species. The use of the electronic computer lightens the computational burden considerably. While the results are not entirely consistent, the general conclusion is that the state point lies approximately on the weak branch of the detonation Hugoniot at a pressure of something like 10% below the CJ value. Figure 3 from Schott's review (1965) gives the properties of such a point, in this case arbitrarily chosen for purposes of illustration.

In condensed explosives, about the only properties which can be measured with sufficient accuracy to test the theory are the detonation velocity and, to a lesser extent, the pressure. But the equation of state of the products is so poorly known that an attempt to compare the experimental results with an a priori calculation is of no use. The special properties of the CJ point, however, allow the pressure to be predicted from the measured dependence of velocity on the initial energy and density. Values of pressure obtained in this way by Davis, Craig, and Ramsay (1965) are in disagreement with those obtained by the conventional method of observing the motion of thin metal plates in

contact with the explosive. Petrone (1968) disputes this conclusion, offering an alternative interpretation of the conventional pressure measurements which would, if correct, remove the disagreement. The disputed point is whether the reaction zone is large enough to affect the motion of the metal plates; Petrone believes that it is, while Davis, Craig, and Ramsay believe that it is not. The author's opinion is that Davis, Craig, and Ramsay are correct.

At about this same time, the theoretical work was being directed toward a thorough study of the nature of possible steady solutions under less restrictive assumptions. This work extends to the consideration of an arbitrary number of chemical reactions proceeding in both forward and backward directions, so that the effects of chemical equilibrium must be considered. Also studied in some detail is the inclusion of transport effects, through use of the Navier-Stokes equations. In nearly all cases based on less restrictive assumptions than those of the ZND model, it is found that there may be, for certain values of the physical parameters, a class of solutions terminating at a final weak state. For the other more "normal" class of solutions, the Chapman Jouquet hypothesis, slightly modified to account for the effects of chemical equilibrium, is still proposed. It is unlikely that a solution terminating in a weak state applies to any of the more commonly investigated gaseous systems. The applicability of such a solution would not explain the disagreement in any case, since the entire one-dimensional theory rests on the neglect of motions transverse to the direction of propagation, which, as it turns out, are probably too important to ignore.

As detonations were studied in more detail, it began to be apparent, beginning in the early 1960's, that transverse wave motions are present on the front in nearly all cases, with true one-dimensional flow being generated only in exceptional circumstances. The spacing of these waves is strongly

dependent on the heat release and reaction rate, and varies over a wide range. The phenomenon of spin, originally regarded as a somewhat isolated curiosity, is now recognized as one extreme of this general phenomenon - the lowest-frequency (spatial) mode which will fit into a round tube. The theoretical work of this same recent period has also been much concerned with the question of the effects of non-one-dimensional flow, a much more difficult problem than the study of the steady solution. The main progress to date is the finding that the steady solution is typically unstable to small perturbations, together with the study of the time-dependent replacement for the steady solution when the flow is constrained (by assumption) to be one-dimensional.

STEADY SOLUTIONS

The general framework for the construction of steady solutions is that of the ZND model. At the front of the wave is a shock, treated as a jump discontinuity. Ahead of the shock no reaction occurs, the undisturbed explosive being in a state of metastable equilibrium. Following the shock is a region of steady flow (i.e., independent of time in a coordinate frame attached to the shock) in which the chemical reaction takes place. The steady solution sought is to extend from the shock back to the point of complete reaction or chemical equilibrium (which will make it formally infinite in length for the common types of reaction rates). Some other non-reactive and possibly time-dependent flow, such as a rarefaction wave, is to be appended to the end of the reaction zone in order to match the prescribed rear boundary condition. This is most commonly specified as a following piston of specified constant velocity which, of course, includes the special case of zero velocity; i.e., a rigid wall.

Other assumptions are that the flow is one-dimensional (plane) and laminar, and that the material behind the shock is everywhere in local

thermodynamic equilibrium except for the chemical reaction. This is equivalent to the assertion that the material possesses an equation of state, with the chemical composition included in the set of independent variables. The only entropy-producing process, other than the shock jump itself, is that of chemical reaction. Throughout the following discussion transport processes - viscosity, heat conduction, diffusion - may be taken to be neglected except where specifically mentioned. Work on this problem with more than one reaction, but with neglect of transport effects, has been done by Wood and Kirkwood (1957), Wood and Salsburg (1960) and Erpenbeck (1964). Transport effects have been considered, but with only a single chemical reaction, by Hirschfelder and his group (1961), Wood (1963), and others.

Let us now outline the form of the solution for the case of a single forward reaction. Let the reaction be

$$A \rightarrow B$$

with progress variable λ equal to the mass fraction of species B. The steady flow equations are

$$(\rho u)_x = 0$$

$$(p+\rho u)_x = 0$$

$$(H+\tfrac{1}{2}u^2)_x = 0$$

$$\lambda_x = r/u,$$

where ρ, u, p, H, and r are the density, material velocity, pressure, specific enthalpy, and reaction rate per unit mass, and the subscript x denotes differentiation with respect to the distance x. The reaction rate is assumed to be a function of the local thermodynamic state.

The integrals of the first three equations can be expressed as the three conservation relations given earlier. With an assumed value of D as a parameter, these can be solved for p, v, and u as functions of λ, so that only a single

ordinary differential equation

$$d\lambda/dx = r(\lambda;D),$$

remains. The initial point for the integration is the shock state. The value of λ is zero there by assumption, and the solution of the conservation relations with $\lambda = 0$, of course, gives the complete state.

The assumption of a single forward reaction (restricted also to the case of no decrease in the number of moles with reaction) is too restrictive in that it does not give any solutions of a second type which generally appears under less restrictive assumptions, such as the consideration of more than one reaction, of the possibility of a decrease in the number of moles (more generally, a volume decrement) with reaction, of slight (radial) divergence of the flow, or of transport effects.

In all of these cases, there are two general classes of solution which we will call "normal" and "eigenvalue" solutions. The normal solution is of the type obtained with a single forward reaction. The profiles of Figure 6, presented in the next section, are examples. It always terminates at either a strong point of the detonation Hugoniot or the CJ point, never at a weak point. In the phase space of the ordinary differential equations for the steady flow, such a point is a nodal critical point or is reached through a nodal sector of a higher-order critical point. In determining a value of D for a given rear boundary condition, only the properties of the terminal state at the end of the reaction zone need be known. This can, of course, be calculated from the conservation relations and the equation of state, without knowledge of the reaction rate. In the overdriven case, the rear boundary is matched by the final state having the same material velocity as the piston, plus a region of constant state behind the reaction zone. In the unsupported case, the final state is the CJ point, with a rarefaction wave adjoined.

The eigenvalue solution has an entirely different character. In order for it to occur, there must be some process which is effectively endothermic in its effect on the flow, such as an endothermic reaction (which absorbs instead of releasing energy), or a normally exothermic reaction which is driven past its equilibrium point by the flow and becomes effectively endothermic as it returns. In this type of solution, the integral or solution curve of the differential equations proceeding from the shock state must reach a special point called the pathological point at which the essentially endothermic and essentially exothermic processes are in balance in their effect on the flow. From this point, the integral curve may proceed to either a strong point or a weak point, the weak point being a saddle-type critical point of the differential equations. For a given substance (i.e., for given equation of state and reaction kinetics with parameters fixed), the eigenvalue solution, if it exists at all, can do so only for a unique value of D, and its determination is an eigenvalue problem whose outcome is sensitive to the details of the properties of the material, in particular the reaction kinetics. A steady solution for a profile of this type is diagrammed in Figure 4. It bears some resemblance to that for the nonreactive flow in a convergent-divergent nozzle. The solid curve is the profile for the eigenvalue D, which is the velocity of the self-supporting wave. Point P is sonic, and points S and W are the final strong and weak points. For piston velocities less than u_S the detonation will be followed by a slower-moving second wave. For piston velocities less than u_W this wave will be a rarefaction and for piston velocities between u_W and u_S it will be a shock. At piston velocities above u_S the detonation is overdriven and the profile takes the shape of the dashed curve, subsonic throughout.

HYDRODYNAMIC STABILITY

The existence of these extensively-studied steady, one-dimensional solutions of the flow equations does not, of course, mean that they will necessarily appear as the long-time limit of a flow problem with appropriate boundary conditions. The opposite appears to be the case: the flow in the reaction zone of self-supporting detonations in nature is neither steady nor one-dimensional.

The first step in asking whether this is predicted by the equations chosen to represent the flow is to investigate the hydrodynamic stability of the one-dimensional solutions against small (three-dimensional, time-dependent) perturbations. This is done by linearizing the time-dependent flow equations about the one-dimensional steady solution. The shock is taken into account explicitly, one of the complications in the analysis being the necessity of working in the accelerated coordinate system in which the longitudinal distance is measured from the perturbed shock front. The resulting set of linear partial differential equations then describes the growth or decay of infinitesimal perturbations on the steady solution. Let the space and time variables be x, y, z, t with the steady detonation propagating in the x-direction. The equations are reduced by Fourier transformation on y and z, and Laplace transformation on t to a set of ordinary differential equations in x with variable coefficients depending on the steady solution, and with shock boundary conditions at the front. The solution of these equations contains a sum of terms of the approximate form $\sum_i e^{\tau_i t}$, where the τ_i are the values of the time-transform variable τ at the poles of a certain complex function. For each value of τ_i, the corresponding perturbation grows or decays according to whether the real part of τ is positive or negative.

The necessary calculations have been done by Erpenbeck (1964) for the idealized system represented by a polytropic gas of constant heat capacity reacting according to

$$A \rightarrow B$$

with Arrhenius rate r (per unit mass)

$$r = (1-\lambda)e^{-E^+/RT},$$

with λ the mass fraction of species B, E^+ the activation energy, T the temperature, and R the gas constant.

The parameters are γ (fixed at 1.2), D, E^+ and the heat of reaction Q. Figure 5 shows the stability at $Q = 50\ RT_o$ as a function of transverse spatial wave number of the perturbation for a range of values of D and two values of the activation energy. The stability is increased by decreasing the activation energy. At the larger values of D, the steady solution is unstable only to perturbations whose transverse wavelengths are of the order of the reaction zone length. Interestingly, at values of D not too far above D_{CJ}, the steady solution is unstable to perturbations of zero transverse wave number or infinite wave length; that is, those in which the motion, although time-dependent, is a function of x only and in which the shock front is planar. Thus, a one-dimensional pulsating flow of some type is to be expected as the long-time limit of the self-supporting detonation for this case.

This interesting result suggests a one-dimensional time-dependent numerical finite difference calculation of the flow, a type of computer experiment which can be characterized as based on well-developed numerical or algorithmic technology (with the exception of the non-trivial addition of chemical reaction), and well within the capability of second-generation computers. The calculation uses the method of characteristics. Some results from the paper of Fickett and Wood (1966) are shown in Figures 6 and 7.

The two cases compared in these figures have in common γ=1.2, Q=50RT$_o$, D^2=1.6 D^2_{CJ}, chosen to be typical of gaseous systems. According to Figure 5, the steady solution should be stable for E^+ = 40RT$_o$ and unstable for E^+ = 50RT$_o$. Figure 6 shows profiles of the steady solution for these two cases. Figure 7 shows the shock pressure history for a detonation initiated by a piston whose velocity decreases linearly from the value of the velocity at the shock state of the steady solution to that at the final state (in a time comparable to the reaction time), and then remains constant. As predicted by the linear perturbation analysis, the case E^+=40RT$_o$ is stable, with the flow settling down fairly quickly into the steady solution. The case predicted to be unstable, E^+=50RT$_o$, behaves very differently, with large continuing pulsations. These eventually become periodic; the irregularities in the figure are caused by reflections from the piston. In spite of the large amplitude and nonlinearity of the pulsation, the mean pressure is within one percent of the steady-solution value. The linear theory finds only one value of τ_i with positive real part for this case. The growth rate and period observed in the computer experiment are in qualitative agreement with those suggested by the real and imaginary parts of this τ_i. The linear perturbation analysis was later extended by Erpenbeck (1967) to include higher-order terms. This nonlinear analysis results in a periodic behavior of the shock pressure similar to that described above. Mader (1965) has obtained similar pulsating solutions from a numerical finite-difference calculation for condensed explosives.

The instability of the steady solution extends to quite small values of Q. Figure 8 shows a shock pressure history for the case γ=1.2, Q=RT$_o$, E^+=50RT$_o$, D^2=1.6 D^2_{CJ}. The irregularity of the pattern is consistent with the presence in the linear analysis result of more than one value of τ_i with positive real part.

STRUCTURE OF THE FRONT

A reaction zone consisting of an induction zone followed by a narrow region of rapid reaction and heat release is sensitive to perturbations because a detonation can easily propagate through the almost-unreacted material of the induction zone. A small hot spot at the rear of the reaction zone, for example, could initiate a hemispherical detonation wave which would soon overtake the front. The observed structure of the front can be imagined to arise from the collision of such microdetonations, as they have been called by Dremin (1968). The details of the process are quite complicated but the main features are sketched in Figure 9. The lower line shows three microdetonations which have broken through the original front and begun to collide with each other. The shock reflection at the collision is initially regular. As the angle of collision changes, a Mach stem is formed. In the second line it is shown as having overtaken the original front. Behind the Mach stem, the pressure is high and the reaction zone short. Where the spherical front of the original microdetonation has passed through the original front into unshocked material, the reaction zone is relatively long. The reflected shocks moving approximately perpendicular to the original front initiate reaction as they pass into this region and thus become detonations propagating in the transverse direction. Meanwhile, the speed and strength of the Mach stem is being decreased and its reaction zone lengthened by rarefaction from its sides and rear. By the time the transverse wave reverses its direction by collision with its neighbor, it again finds a region of unreacted material into which to propagate - the now-lengthened reaction zone behind the original Mach stem, and the process is thus able to repeat itself. Clearly the natural spacing of transverse waves will be strongly dependent on the reaction kinetics. It must be large

enough to allow an appreciable induction zone to form behind the transverse waves so that when their direction is reversed by collision they will find sufficient unreacted material to sustain their propagation. It must be small enough so that a new microdetonation does not have time to form from a random perturbation between two transverse waves approaching each other.

Structures of this type are observed in nearly all detonating systems. The wavelength can be made large enough for convenient study by diluting the original gaseous system with an inert gas. The principal means of observation are: (1) study of the tracks left in soot-coated walls of the detonation tube by the Mach stem and other features of the front; (2) photography with the motion stopped by an arc or pulsed laser flash source or by velocity-synchronization of the camera; and, (3) small pressure transducers placed in the walls of the tube.

The main results of the observations are summarized in a recent review by Strehlow (1968). In typical systems the spacing of the transverse waves varies over a range of a few tenths of a centimeter to ten centimeters or more, depending on the amount of diluent and the initial pressure. Quite regular to very irregular patterns may be obtained, depending on the degree of dilution and the system chosen.

It is important to note that this structure is an intrinsic feature of the detonation front, and would be present even in the absence of walls. Similar structure is observed on spherical detonation fronts. The presence of walls of course affects the details of the structure to some extent, but is not at all necessary for its existence.

High speed photographs of the detonation front in liquid explosives, most recently by Mallory (1967), indicate the presence of a similar structure, with spacing increased by dilution with an inert liquid. Because of the relative difficulty of observation, extensive quantitative studies have not been made.

The flow structure in the front is quite complex; the actual transverse wave contains one or more triple-shock interaction points behind the front in addition to the one at the front. The book by Voitsekhovskii, Mitrofanov, and Topchian (1963) gives a detailed account of their intensive study of the details of flow in gases.

The general features of the flow may be illustrated by the case of the single Mach reflection propagating across a detonation front as shown in Figure 10. A nearly one-dimensional detonation front is produced by passing a detonation through a convergent-divergent channel. The transverse structure disappears in the convergent section. Before it has time to reappear in the expansion, reflection at the corner produces the downward propagating three-shock confirguration shown. The diagram shows the streamlines in a coordinate system attached to the triple point. The Mach stem is much stronger than the incident shock and the reaction zone behind it is correspondingly shorter. The exact nature of the flow behind the reflected shock is not clear. Material passing through both the incident and reflected shocks will have a shorter reaction time than that passing through the incident shock only, but not so short as that passing through the stem. Emerging from the rear will be three streams of material with different entropies and velocities: the material passing through the incident shock only, that passing through the incident and reflected shocks, and that passing through the stem only. With many such configurations passing back and forth across the front, the flow behind may well be turbulent.

White (1961) has made an extensive experimental study of the propagation of steady detonation in the mixture of $2H_2+O_2+CO_2$ in which the front structure is of such a size that the apparently turbulent zone behind the front can be easily seen in his spark interferograms. He also offers a qualitative

theoretical analysis showing the effect on the conservation laws of including some terms representing the effect of isotropic turbulence in the flow equations.

Combining White's results with more recent knowledge of the details of the front structure, the following overall picture of the flow can be constructed. As we saw above, different streams of material passing through the structured front experience quite different histories. The reaction is very fast in some and slower in others, but probably on the average more rapid than that in the corresponding hypothetical one-dimensional wave. Large fluctuations in the state occur in the interior. The extreme is reached at the point of collision of two transverse waves, with resulting pressures as large as ten times the one-dimensional CJ pressure. Front velocities may vary as much as twenty percent above and below the one-dimensional CJ value. Emerging from the end of this complex "reaction zone," roughly speaking, is a turbulent flow with space scale comparable to that of the spacing of the transverse waves on the front. The situation is further complicated by the presence of transverse shocks degenerating farther to the rear into acoustic waves. The decay of this turbulence is a much slower process than the chemical reaction and the corresponding "turbulence decay zone" is much longer than the reaction zone. (In White's system at an initial pressure of 0.3 atm., the turbulence decay zone is a few cm. long and the reaction zone is probably less than a tenth of this.)

The final state appears to be approximately on the weak branch of the complete-reaction Hugoniot, at a pressure ten to fifteen percent below the CJ value. The point marked "WEAK" in Figure 3 is typical. The flow at the end of the turbulence decay zone is of course not completely uniform and steady so that the usual one-dimensional conservation laws cannot be applied exactly to this plane. But the closeness of the average pressure to the

steady value in the one-dimensional pulsating detonation gives some reason to hope that the defect averaged over the cross section of the tube is small.

Perhaps the most interesting property of this final state is that the flow there is supersonic with a local Mach number of about 1.15 in a frame attached to the shock. In this flow, a following rarefaction wave head or weak shock would recede from the front at a speed of 8 to 10 percent of the detonation velocity.

REFERENCES

M. Berthelot and P. Vieille, Compt. Rend. 93, 18 (1881).

D. L. Chapman, Phil. Mag. 47, 90 (1899).

W. C. Davis, B. G. Craig, and J. B. Ramsay, Phys. Fluids 8, 2169 (1965).

W. Doering, Ann. Physik 43, 421 (1943).

A. N. Dremin, Twelfth Symposium (International) on Combustion (in press).

J. J. Erpenbeck, Phys. Fluids 7, 684 (1964).

J. J. Erpenbeck, Phys. Fluids 7, 1424 (1964).

J. J. Erpenbeck, Phys. Fluids 10, 274 (1967).

W. Fickett and W. W. Wood, Phys. Fluids 9, 903 (1966).

J. O. Hirschfelder, C. F. Curtiss, and M. P. Barnett, Phys. Fluids 4, 260 (1961).

E. Jouquet, J. d. Math. 1, 347 (1905), 2, 6 (1906). See also E. Jouquet, Mecanique des Explosifs (o. Doin et Fils, Paris, 1917).

J. G. Kirkwood and W. W. Wood, J. Chem. Phys. 22, 1915 (1954).

C. L. Mader, Los Alamos Scientific Laboratory Report LA-3297 (1965).

E. Mallard and H. L. LeChatelier, Compt. Rend. 93, 145 (1881).

H. D. Mallory, J. Appl. Phys. 38, 5302 (1967).

J. von Neumann, O.S.R.D. Report No. 549 (1942). Reprinted in Collected Works (The Macmillan Co., New York, 1963), Vol. 4, p. 203.

F. J. Petrone, Phys. Fluids 11, 1473 (1968).

G. L. Schott, Fourth Symposium (International) on Detonation (Office of Naval Research, Washington, D. C., 1965), p.67.

R. A. Strehlow, Combustion & Flame 12, 81 (1968).

B. V. Voitsekhovskii, V. V. Mitrofanov, and M. E. Topchian, Structure of a Detonation Front in Gases. (Izd-vo Sibirsk, Otdel. Akad. Nauk S.S.S.R., Novosibirsk, 1963). Translation: Wright-Patterson Air Force Base Report FTD-MT-64-527 (AD-633-281), Feb. 1966.

D. R. White. Phys. Fluids 4, 465 (1961).

W. W. Wood and Z. W. Salsburg, Phys. Fluids 3, 549 (1960).

W. W. Wood, Phys. Fluids 6, 1081 (1963).

Y. B. Zeldovich, Zh. Eksp. Teor. Fiz. 10, 542 (1940). [English Transl.: NACA Technical Memorandum 1261 (1950)].

TABLE I

	GAS $2H_2 + O_2$	LIQUID NITROMETHANE	SOLID PLASTIC-BONDED HMX
	p_o = 1 atm	ρ_o = 1.13 g/cc	ρ_o = 1.84 g/cc
D(m/s)	2850	6290	8790
p(kb)	.0186	141	362
ρ(g/cc)	.00090	1.65	2.47
ρ/ρ_o	1.77	1.46	1.34
T(°K)	3680	3400?	2500?
$M=D/c_o$	5.38	3.59	3.81

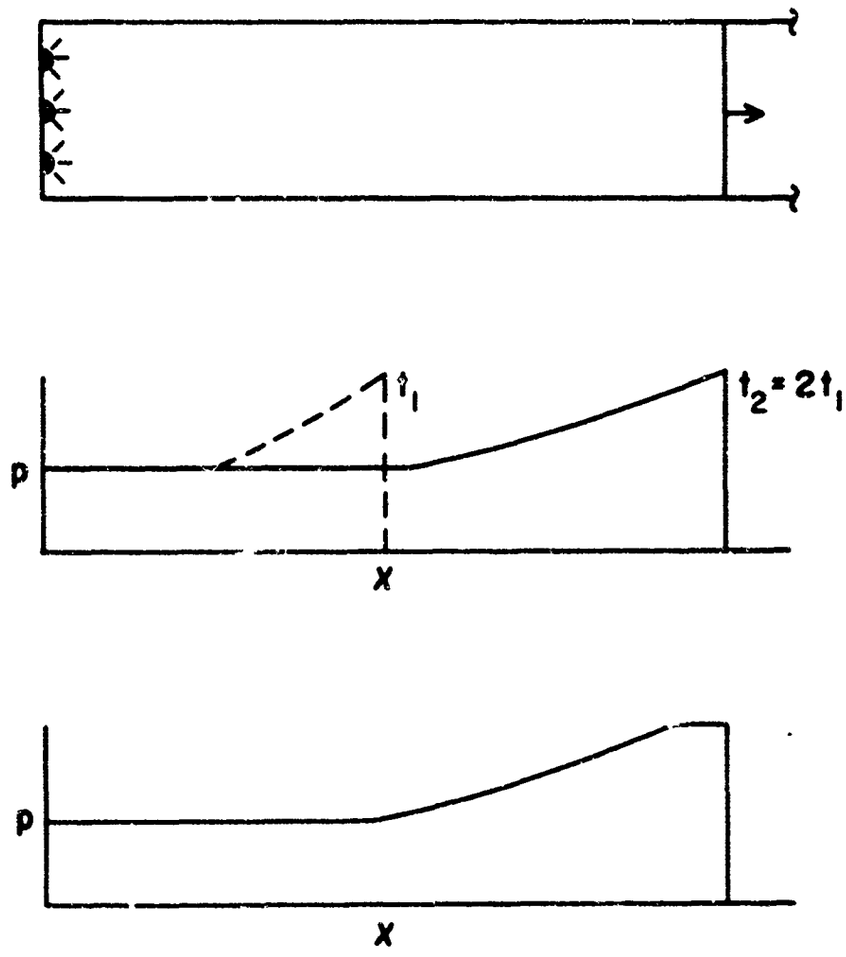

Figure 1. The flow behind a detonation initiated at the closed end of a tube.

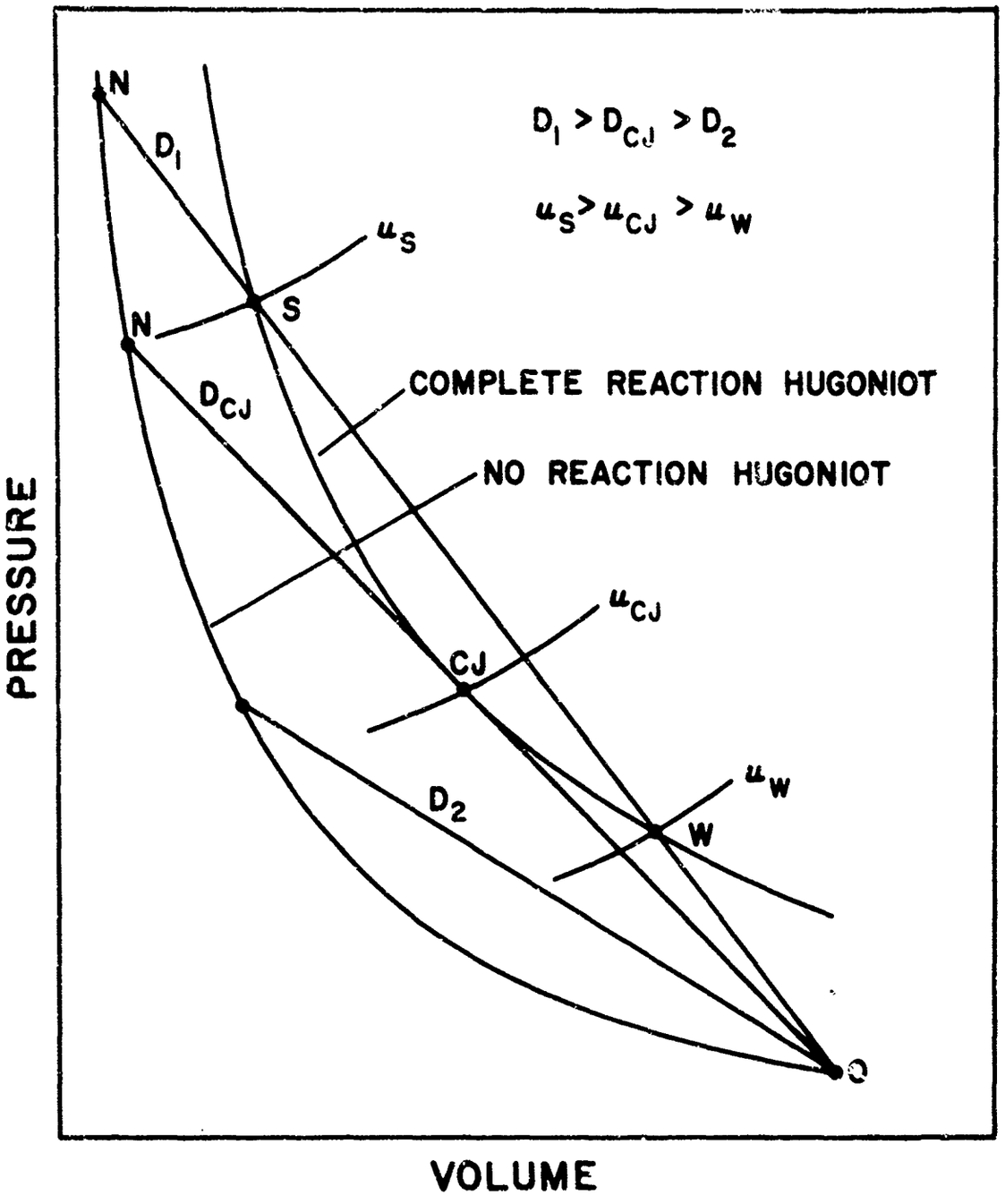

Figure 2. Curves of constant D and constant u and solutions of the Hugoniot equation in the p - v plane. Point 0 is the initial state.

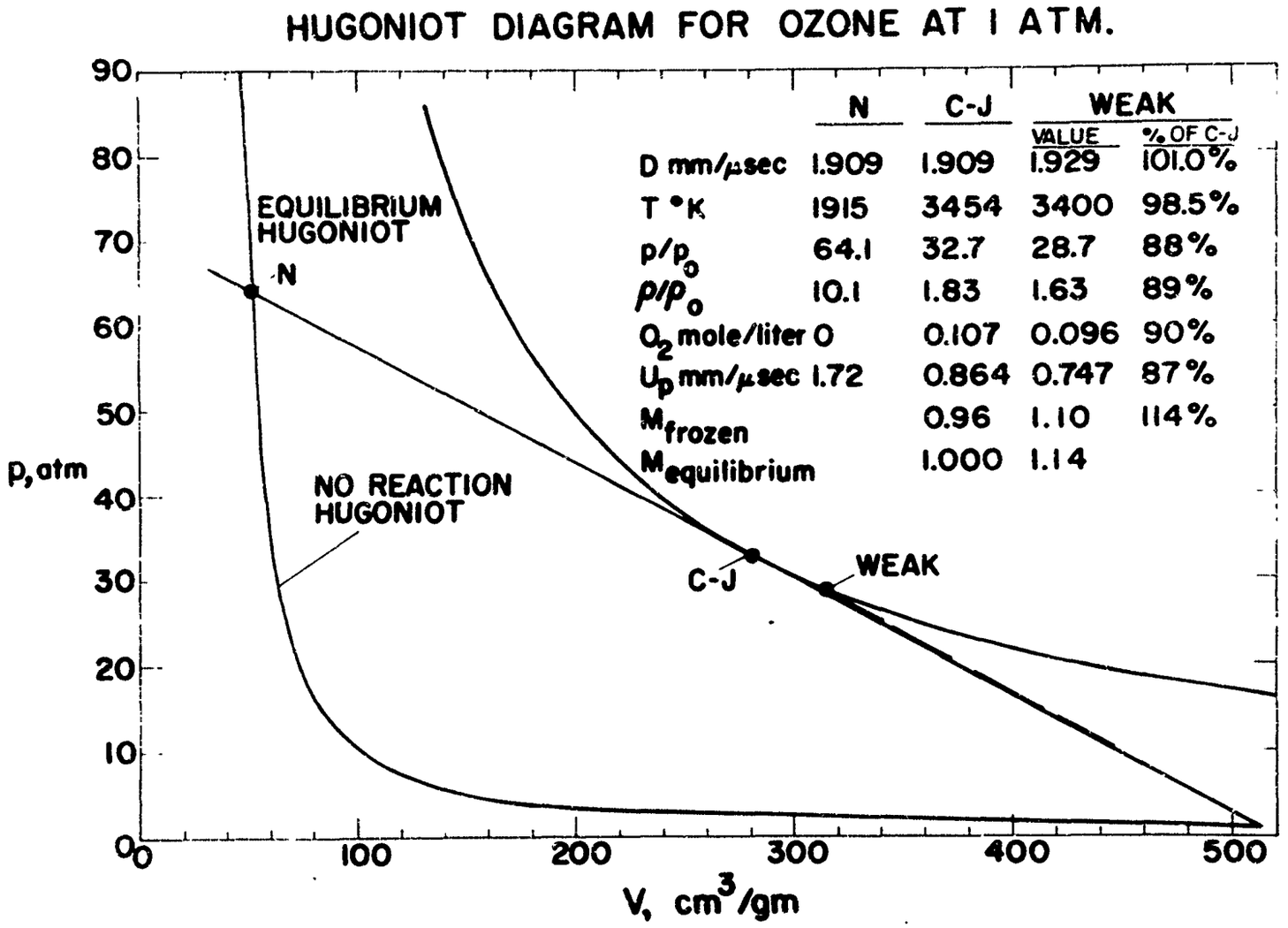

Figure 3. Example of a weak final state. Here Up is the material velocity and M is the local Mach number in the frame attached to the shock. The difference between frozen and equilibrium Mach numbers is not discussed here.

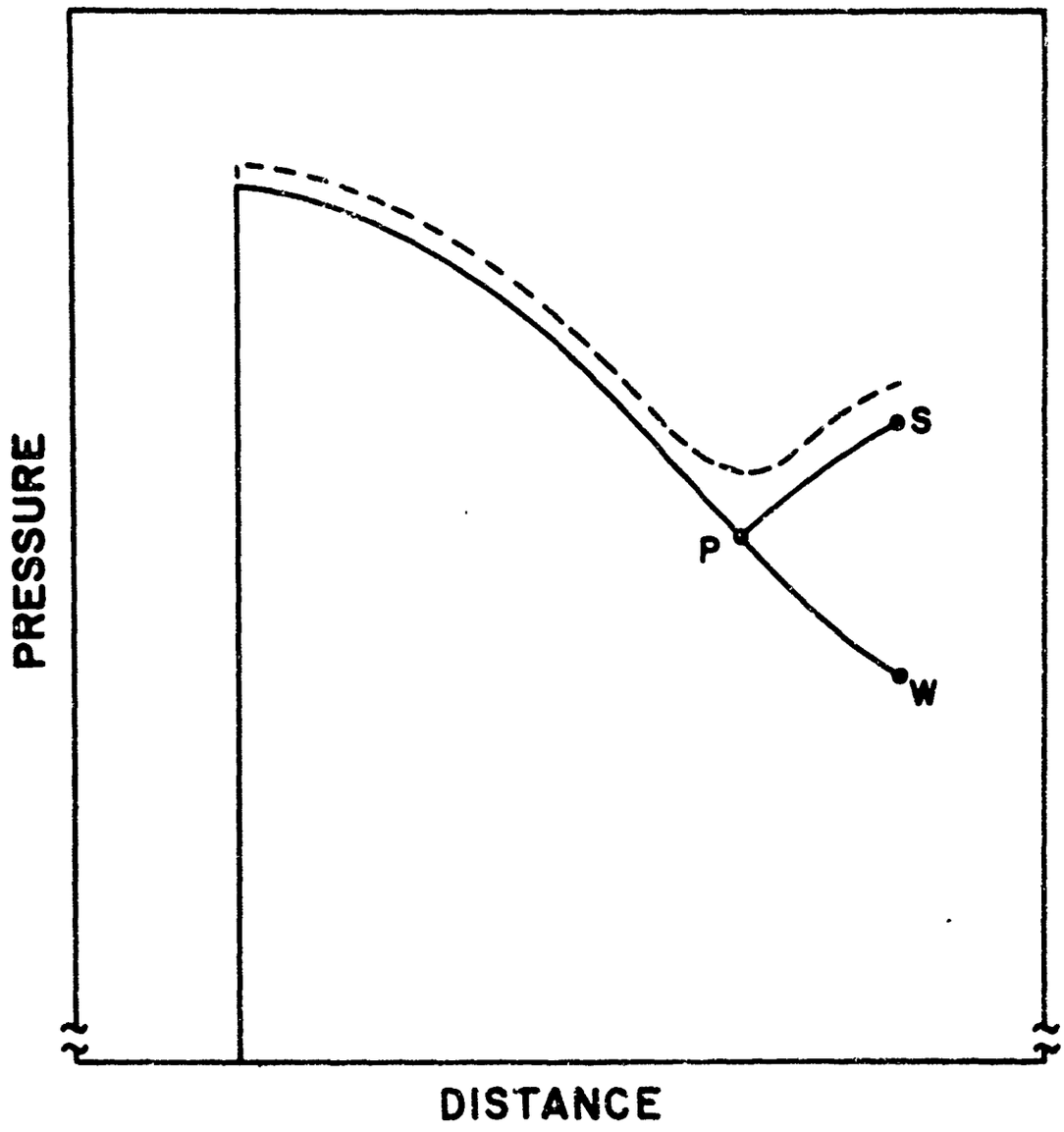

Figure 4. Diagram of steady-solution profiles for the eigenvalue case. The solid curve is the profile at the eigenvalue detonation velocity, and the dashed curve that for a slightly larger detonation velocity.

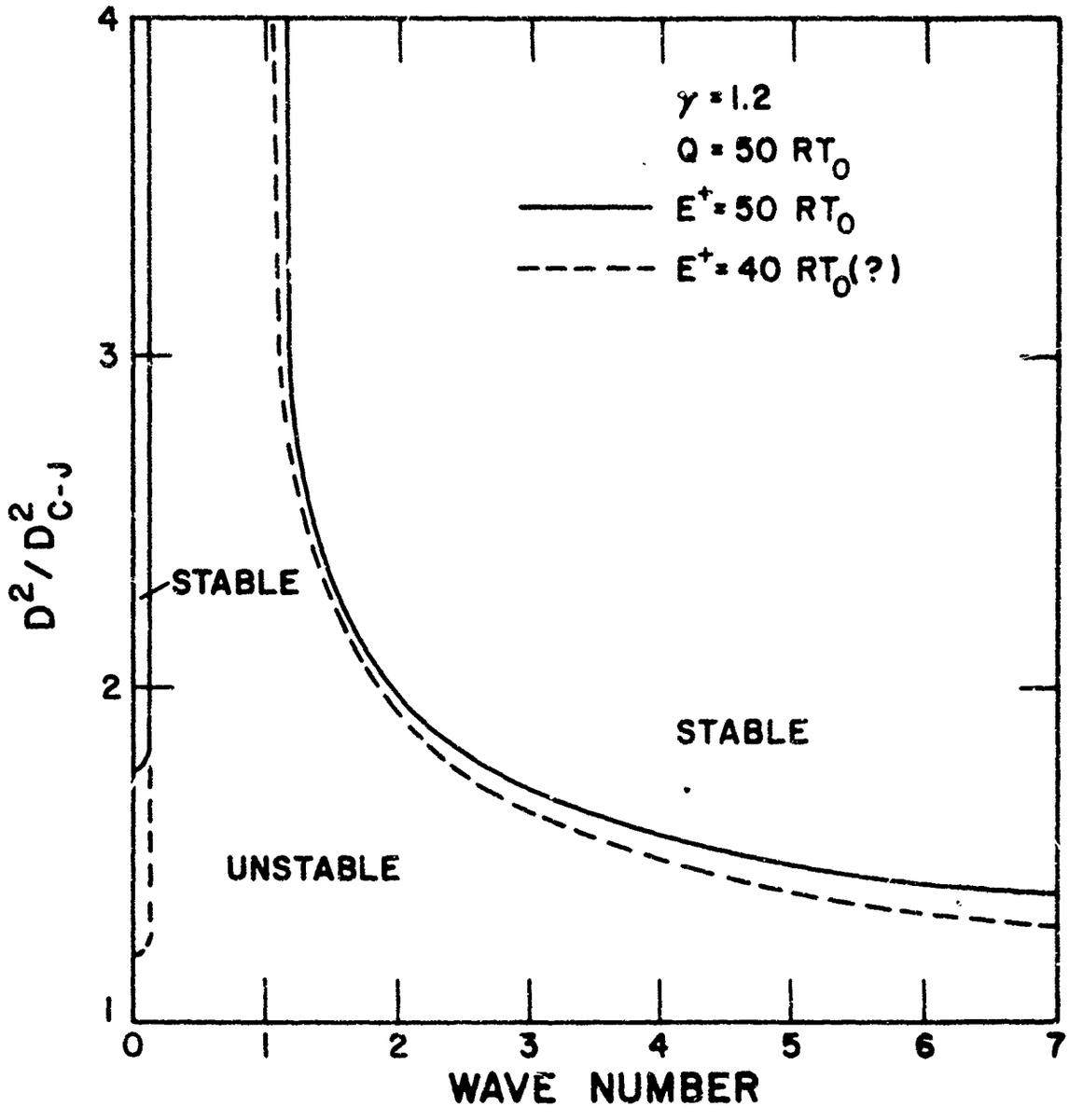

Figure 5. Stability of the steady one-dimensional solution to perturbations as a function of detonation velocity D and transverse (spatial) wave number of the perturbation. The wave number is in units of 2π divided by the distance from the shock to the point at which the reaction is half completed ($\lambda=1/2$) in the steady solution for the given value of D. Most of the $E^+=40RT_o$ curve is guessed from other results.

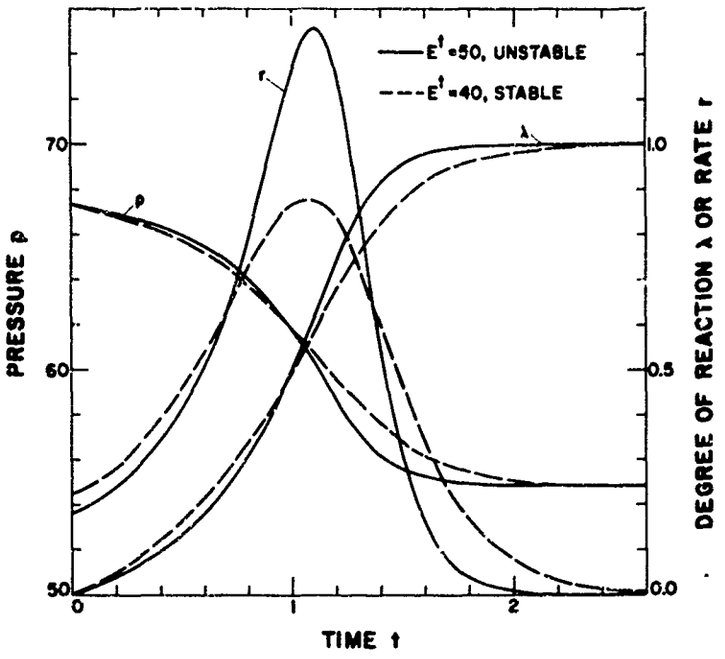

Figure 6. Steady solutions for the cases $\gamma=1.2$, $Q=50RT_o$, $D^2=1.6\ D^2_{CJ}$, $E^+=50RT_o$ (stable) and $E^+=40RT_o$ (unstable). The time origin and unit are such that the fluid element passes through the shock at t=0 and is half-reacted ($\lambda=1/2$) in a given steady solution at t=1. The pressure is in units of the initial pressure.

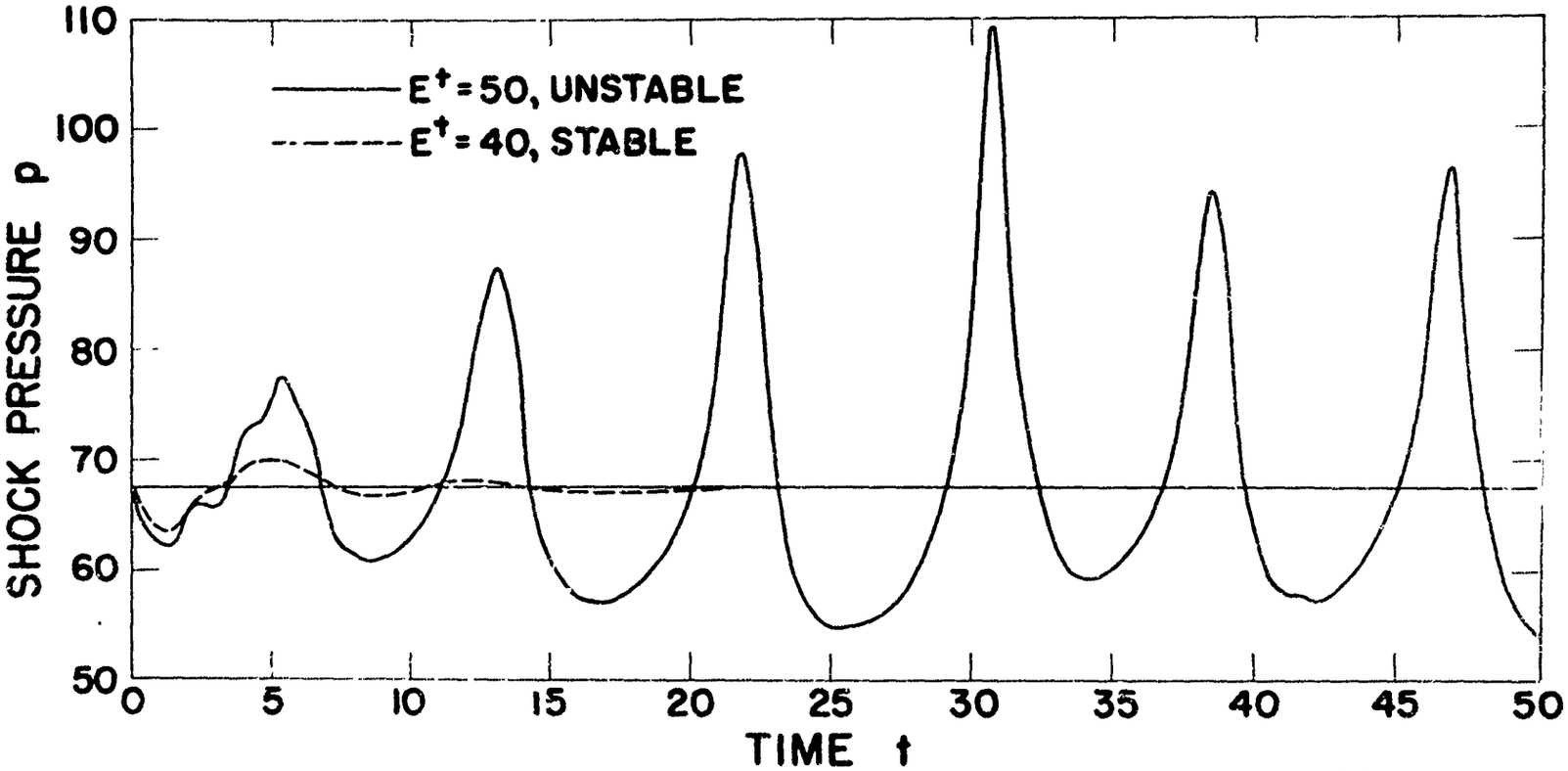

Figure 7. Shock pressure history for the detonations having the stable and unstable steady solutions of Fig. 5, driven by a piston with final constant velocity equal to that of the steady solutions. The unit of time is the steady-state half reaction time and the unit of pressure the initial pressure.

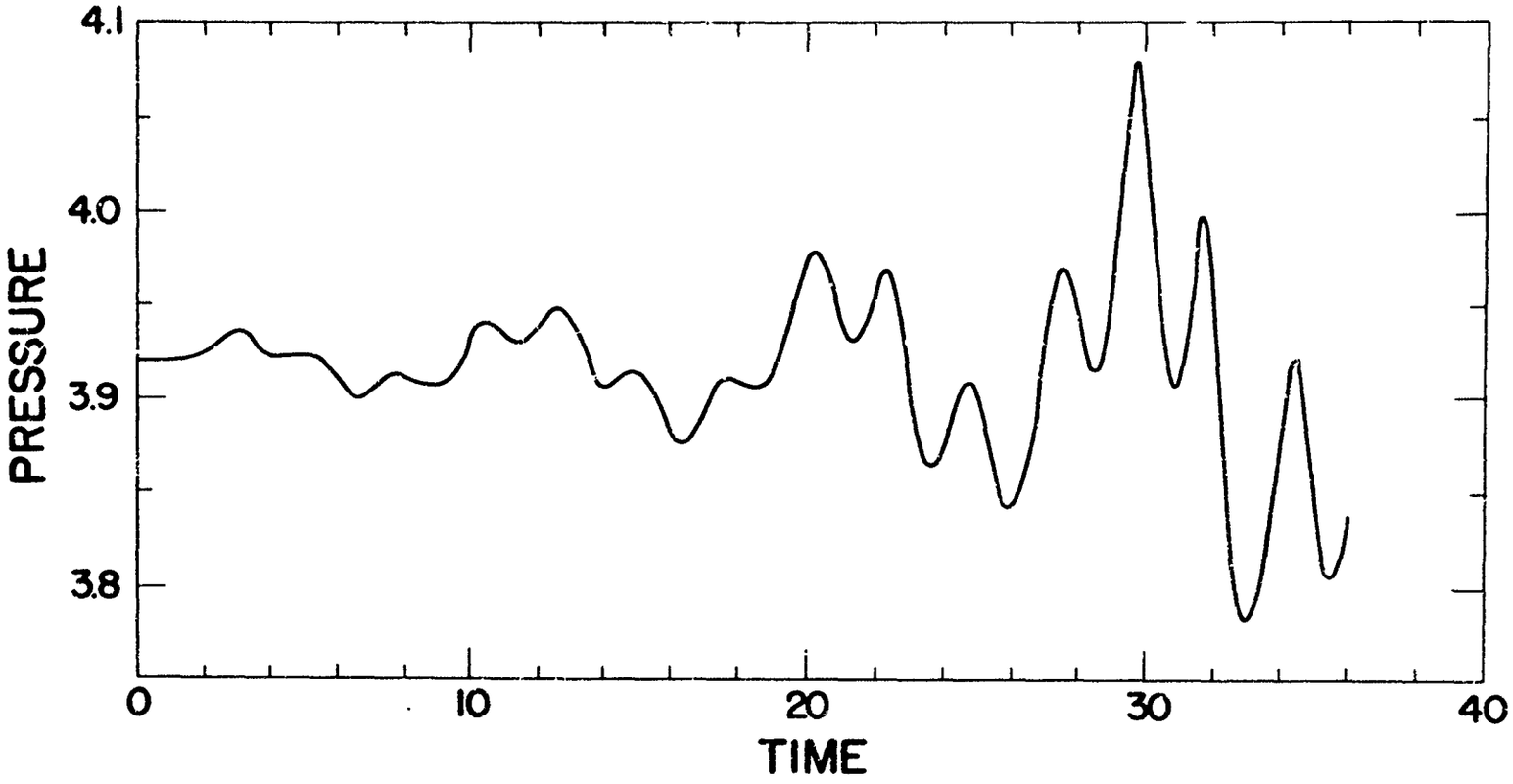

Figure 8. Shock pressure history for a detonation with small heat release: $\gamma=1.2$, $Q=RT_o$, $E^+=50RT_o$, and constant final piston velocity equal to that for the steady solution at $D^2=1.6D^2_{CJ}$.

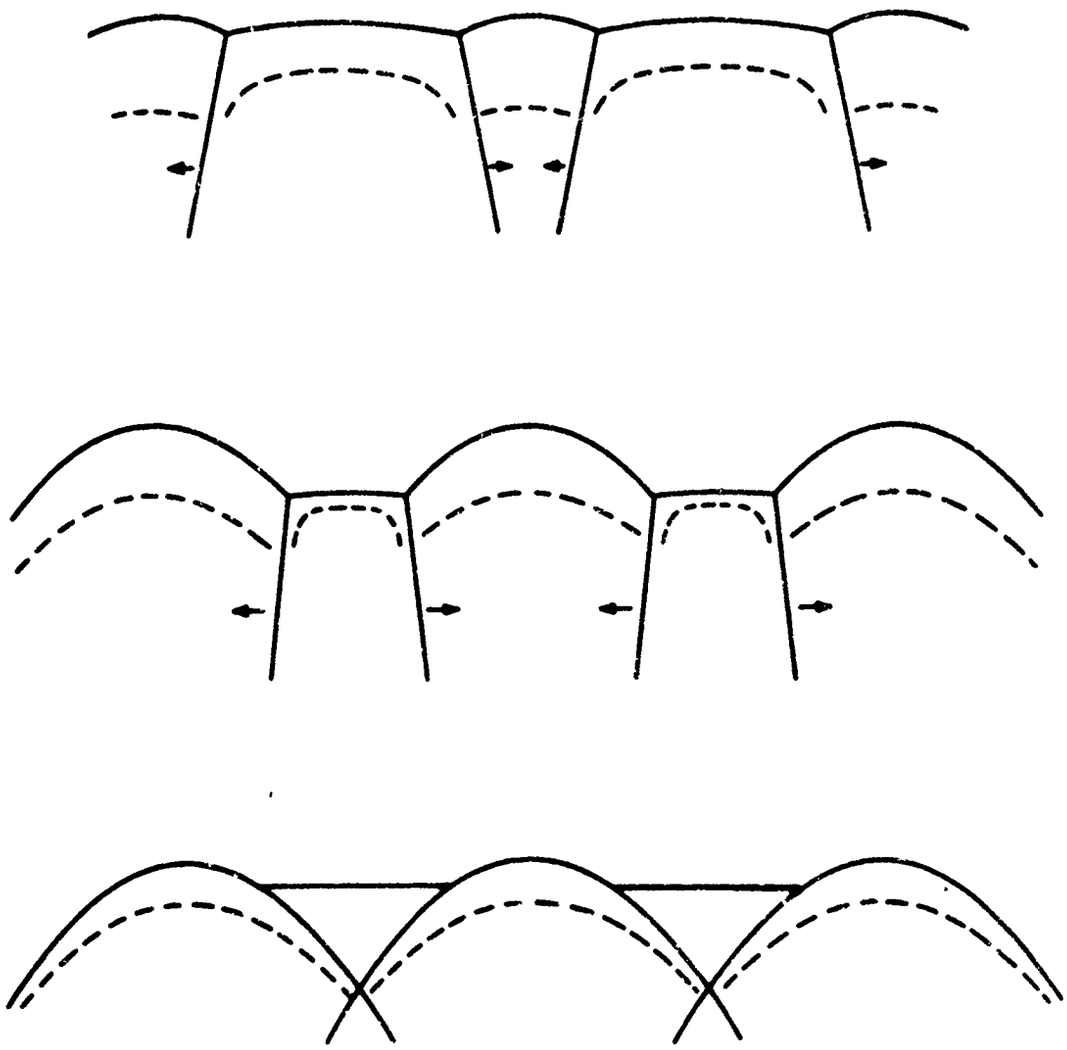

Figure 9. Development of front structure. The wave moves from bottom to top of the figure. The dashed lines indicate the end of the reaction zone.

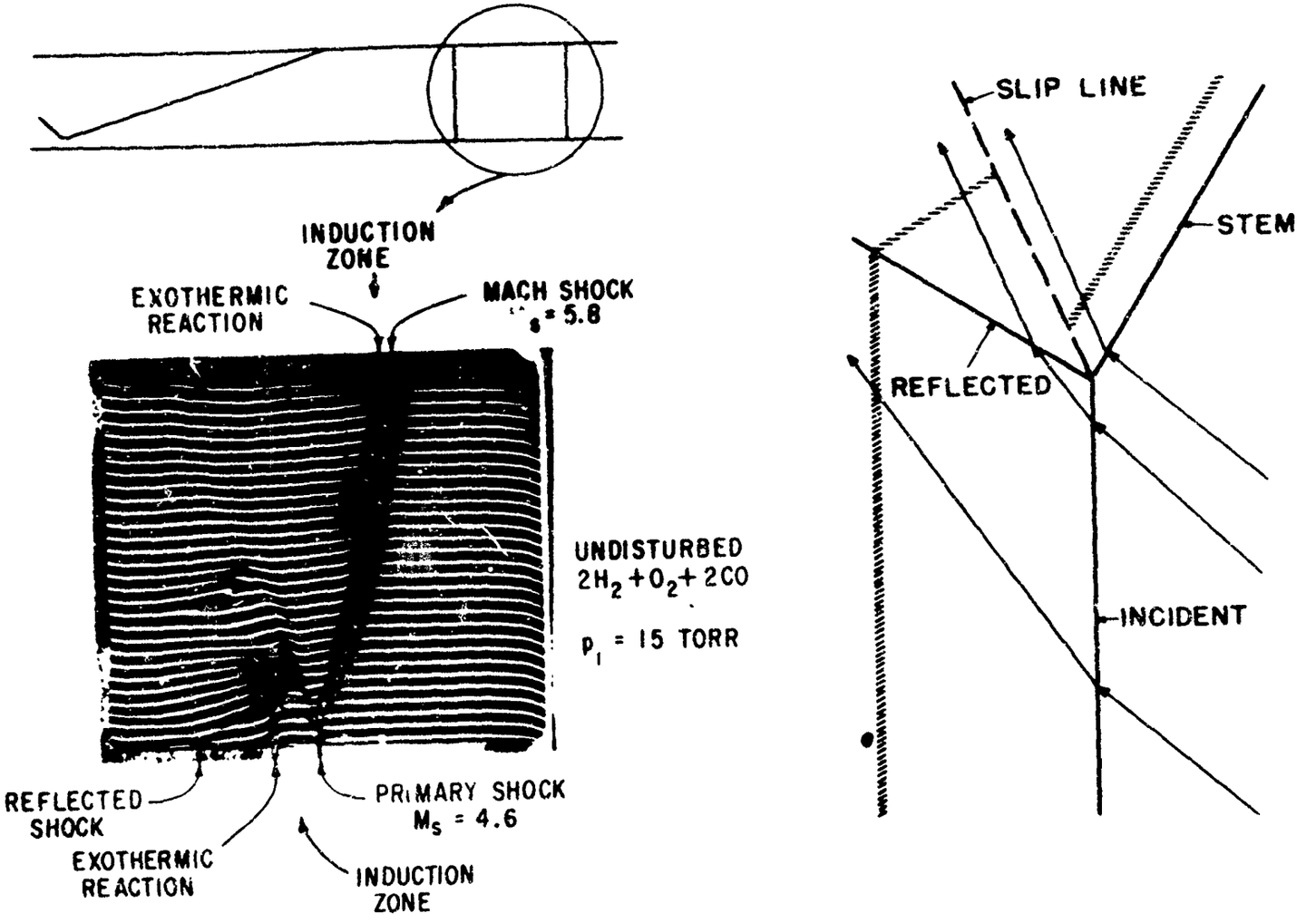

Figure 10. Mach reflection generated by passage of a one-dimensional detonation wave over a corner.

Unclassified

Security Classification

DOCUMENT CONTROL DATA - R & D

(Security classification of title, body of abstract and indexing annotation must be entered when the overall report is classified)

1. ORIGINATING ACTIVITY (Corporate author) U.S. Army Research Office-Durham Box CM, Duke Station Durham, North Carolina 27706	2a. REPORT SECURITY CLASSIFICATION Unclassified 2b. GROUP NA

3. REPORT TITLE

Proceedings of the Explosives Chemical Reactions Seminar

4. DESCRIPTIVE NOTES (Type of report and inclusive dates)

Technical Report

5. AUTHOR(S) (First name, middle initial, last name)

6. REPORT DATE 21-23 October 1968	7a. TOTAL NO. OF PAGES 254	7b. NO. OF REFS
8a. CONTRACT OR GRANT NO. b. PROJECT NO. c. d.	9a. ORIGINATOR'S REPORT NUMBER(S) ARO-D Report 70-4 9b. OTHER REPORT NO(S) (Any other numbers that may be assigned this report)	

10. DISTRIBUTION STATEMENT

This document has been approved for public release and sale; its distribution is unlimited

11. SUPPLEMENTARY NOTES None	12. SPONSORING MILITARY ACTIVITY USA Ballistic Research Laboratories Aberdeen Proving Ground, Md. 21005

13. ABSTRACT

This is a technical report describing the content of an Explosives Chemical Reactions Seminar. The feasibility of a more fundamental approach to the reaction rate characterization of detonation phenomena is explored.

14. KEY WORDS

explosives	chemical stabilization
explosions	wave propagation
detonation	dielectric properties
safety engineering	crystal lattices
organic compounds	argon
oxidizers	HMX
energy storage	shock waves
molecular beams	

END

DD FORM 1 NOV 68 1473 REPLACES DD FORM 1473, 1 JAN 64, WHICH IS OBSOLETE FOR ARMY USE.

Unclassified

Security Classification